BOSTON UNIVERSITY

SCHOOL OF MEDICINE

Dissertation

MASS SPECTROMETRY ANALYSIS OF PROTEIN/PEPTIDE *S*-PALMITOYLATION

by

YUHUAN JI

B.S., Harbin Medical University, 2005

M.S., Harbin Medical University, 2007

Submitted in partial fulfillment of the

requirements for the degree of

Doctor of Philosophy

2015

Approved by

First Reader _____

Cheng Lin, Ph.D.

Assistant Professor of Biochemistry

Second Reader _____

Markus M. Bachschmid, Ph.D.

Assistant Professor of Medicine

DEDICATION

I would like to dedicate this work to my parents and friends.

ACKNOWLEDGMENTS

I would like to express my sincere gratitude to my advisor Dr. Cheng Lin, not only for giving me the opportunity to work in his group but also for his enthusiasm in science which I can always learn from. I thank him for his guidance in using instruments, analyzing data, preparing presentations, and writing papers. He was always kind and patient to answer all of my questions, and willing to provide help whenever I got into trouble. Never could I accomplish what I have without his strong support.

I have been very fortunate to have collaborated with Dr. Markus M. Bachschmid during the past few years. Markus provided an immeasurable amount of support and guidance. Working with him was a great experience. He has inspired me in many ways and has always been the person with whom I could discuss experimental details.

My great thanks also go to Dr. Catherine E. Costello, Dr. Mark E. McComb, and Dr. Matthew A. Nugent. I thank them for serving on my thesis committee. Their valuable suggestions and great encouragement helped me to move forward smoothly during my graduate studies.

It was a great pleasure to work with my colleagues in the Center for Biomedical Mass Spectrometry. Their help contributed greatly to this thesis. My special thanks go to Dr. Nancy Leymaire, Dr. Deborah Leon, Dr. Yan Jiang, Yi Pu and John Haserick for their demonstrations on the operation of mass spectrometry instruments; Dr. Xiaobin Xu, Dr. Qi Wang, Dr. Yanyan Lu, Dr. Yu Huang, Dr. Yang Mao, Dr. Le Meng, and Chun Shao for inspiring discussions and suggestions. I would also like to thank Denise Neves and Erika Casavant for their administrative efforts.

I appreciate the help from my colleagues in the laboratory of Dr. Richard A. Cohen and Dr. Markus M. Bachschmid's. I thank Dr. Dagmar J. Haeussler and Dr. Joseph R. Burgoyne for providing biological samples and for teaching me how to perform many kinds of biochemistry experiments; Dr. Vikas Kumar for his help with data analysis; Dr. Kady Yao for great discussion in both mass spectrometry and biochemistry experiments; and Dr. Di Shao for her assistance with reagents and cell culture.

My deep appreciation goes to Dr. Elliott M. Ross who generously provided valuable virus strains, and my friend Minjing Liu who helped me with most work on the insect cell culture and protein overexpression. The research work from Chapter 5 and 6 could never have been accomplished without their help.

Lastly, I would like to thank my mom and dad for their endless love, comfort, and support.

MASS SPECTROMETRY ANALYSIS OF PROTEIN/PEPTIDE *S*-PALMITOYLATION

YUHUAN JI

Boston University School of Medicine, 2015

Major Professor: Cheng Lin, Ph.D., Assistant Professor of Biochemistry.

ABSTRACT

The dynamic *S*-palmitoylation regulates many intracellular events, including protein trafficking, anchoring, targeting, and protein-protein interactions. Direct detection of *S*-palmitoylation by conventional liquid chromatography-mass spectrometry (LC-MS) methods is challenging because of the tendency of palmitoyl loss during sample preparation and gas phase fragmentation. Additionally, the high hydrophobicity of the palmitoyl group can prevent proper elution of palmitoyl peptides from the commonly used C18 column. Here, we developed a comprehensive strategy tailored for *S*-palmitoyl detection using three palmitoyl peptide standards. We found that *S*-palmitoylation was largely preserved in neutral Tris buffer with tris(2-carboxyethyl)phosphine as the reducing agent and that various fragmentation methods provided complementary information for palmitoyl localization. Moreover, *S*-palmitoyl peptides were efficiently analyzed using a C4 column and the derivatization of free cysteine with a hydrophobic tag allowed relative quantification of palmitoyl peptides and their unmodified counterparts. We further discovered potential complications to *S*-palmitoylation analysis caused by the use of ProteaseMAX^{TM}, an MS-compatible detergent. The hydrophobic

degradation products of ProteaseMAX™ reacted with the free cysteine thiols, generating artifacts that mimic *S*-acylation and hydroxyfarnesylation. Another MS-compatible detergent, RapiGest™, did not produce such artifacts, and showed the ability to stabilize *S*-palmitoylation by preventing thioester hydrolysis and dithiothreitol-induced thioester cleavage. Moreover, we found that the palmitoyl peptide GC_{palm}LGNAK could undergo intermolecular palmitoyl migration from the cysteine to the peptide N-terminus or the lysine side chain during sample preparation, and this could lead to false discovery of *N*-palmitoylation. RapiGest™ inhibited such migration, and is thus recommended for *S*-palmitoyl sample preparation. We then applied the established method to analyze the regulator of G-protein signaling 4 (RGS4) which had been reported to undergo *S*-palmitoylation by radioactive labeling. It had also been reported that the *S*-palmitoylation state of RGS4 affects its GTPase activity. With LC-MS/MS analysis, we found that the addition of palmitate to the cell culture medium in metabolic labeling experiments could boost the level of *S*-palmitoylation, leading to false discovery of new *S*-palmitoylation site(s). We also noted discrepancies between the *S*-palmitoylation sites identified by radioactive labeling and by LC-MS/MS analysis. Further studies are needed to evaluate the reliability of *S*-palmitoyl detection by these two methods.

TABLE OF CONTENTS

TITLE PAGE i

READER'S APPROVAL PAGE ii

DEDICATION iii

ACKNOWLEDGMENTS iv

ABSTRACT vi

TABLE OF CONTENTS viii

LIST OF FIGURES xiv

LIST OF ABBREVIATIONS xxvi

Chapter 1: Introduction to Protein Palmitoylation 1

1.1 Mechanisms of Protein Palmitoylation 1

1.1.1 Non-Enzymatic and Enzymatic Palmitoylation 1

1.1.2 Palmitoyl Dynamics 8

1.1.3 Biological Roles of Protein Palmitoylation/Depalmitoylation 9

1.1.3.1 Membrane Association and Protein Trafficking 9

1.1.3.2 Protein Activity 12

1.1.3.3 Protein Targeting 13

1.1.3.4 Protein-Protein Interactions 14

1.1.3.5 Protein Stability 15
1.1.4 Protein Palmitoylation in Diseases 16
1.1.4.1 Palmitoylation and Oxidative Stress 16
1.1.4.2 Palmitoylation and Dysregulation of DHHC PATs 17
1.1.4.3 Palmitoylation and Dysfunction of Fatty Acid Synthase (FAS) 18
1.2 Traditional Methods to Investigate Protein Palmitoylation 19
1.2.1 Radioactive Labeling 19
1.2.2 Acyl-Biotinyl Exchange (ABE) Chemistry 21
1.2.3 Non-Radioactive Metabolic Labeling 24

Chapter 2: Introduction to Mass Spectrometry 27

2.1 Ion sources 27
2.1.1 Matrix-Assisted Laser Desorption/Ionization (MALDI) 28
2.1.2 Electrospray Ionization (ESI) 30
2.2 Mass Analyzers and Detectors 32
2.2.1 Time-of-Flight (TOF) 32
2.2.2 Quadrupole Mass Analyzer 35
2.2.3 Linear Quadrupole Ion Trap (LIT/LTQ) 39
2.2.4 Fourier Transform Ion Cyclotron Resonance (FTICR) 41
2.2.5 Orbitrap 44
2.3 Application of Mass Spectrometry to Proteomic Studies 47
2.3.1 Tandem Mass Spectrometry 48

2.3.1.1 Collision-Induced Dissociation (CID), including Higher Energy Dissociation (HCD) 50
2.3.1.2 Electron-Capture Dissociation (ECD) 53
2.3.1.3 Electron-Transfer Dissociation (ETD) 55
2.3.2 Sample Preparation Prior to Mass Spectrometry Analysis 56
2.3.2.1 Sample Enrichment 56
2.3.2.2 Sample Desalting 57
2.3.2.3 Sample Separation 57

Chapter 3: Direct Detection of *S*-Palmitoylation by Mass Spectrometry 61

3.1 Introduction 61
3.2 Experimental Section 63
3.2.1 Materials 63
3.2.2 Preparation of Palmitoyl Peptides 63
3.2.3 Stability Test of Palmitoyl Peptides 64
3.2.4 Preparation of IAM- and FIAM-labeled Peptides 65
3.2.5 HPLC Separation 65
3.2.6 LC-MS Quantification 66
3.2.7 Tandem MS Analyses 66
3.3 Results and Discussion 67
3.3.1 Stability of Palmitoyl Peptides 67
3.3.2 Analysis of Palmitoyl Peptides by RP-HPLC 75
3.3.3 Relative Quantification of Palmitoyl Peptides by On-Line LC-MS 78

3.3.4 Tandem MS Analysis of Palmitoyl Peptides 80

3.4 Conclusion 94

Chapter 4: *S*- to *N*-Palmitoyl Transfer during Proteomic Sample Preparation..... 96

4.1 Introduction..... 96

4.2 Experimental Section..... 98

4.2.1 Materials 98

4.2.2 Sample Preparation..... 99

4.2.3 Mass Spectrometry Analysis..... 99

4.2.4 UV Monitoring of S-Palmitoyl Peptides..... 100

4.3 Results and Discussion 100

4.3.1 Preparation of the S-Palmitoyl Peptide Standard $GC_{palm}LGNAK$..... 100

4.3.2 Intermolecular Palmitoyl Migration 102

4.3.3 The Effect of Detergent on Palmitoyl Migration..... 104

4.3.4 RapiGest^{TM}: an S-palmitoyl Stabilizer in Aqueous Solution..... 112

4.3.5 Tandem MS Analysis of Palmitoyl Peptide Isomers 114

4.4 Conclusion 127

Chapter 5: Surfactant-Induced Artifacts during Proteomic Sample Preparation..... 129

5.1 Introduction..... 129

5.2 Experimental Section..... 132

5.2.1 Materials 132

5.2.2 Overexpression and Purification of His-Tagged RGS4 from Sf9 Cells 133

5.2.3 In-Solution Proteolytic Digestion of His-Tagged RGS4 133
5.2.4 LC-MS/MS Analysis 134
5.2.5 MALDI-TOF MS Analysis of the Hydrophobic Peptides 135
5.3 Results and Discussion 136
5.3.1 Extraction of His-Tagged RGS4 from Sf9 Cells 136
5.3.2 Characterization of the Hydrophobic Peptides by MALDI-TOF MS Analysis 137
5.3.3 LC-MS/MS Analysis of Hydrophobic Peptides 141
5.3.4 Extent of ProteaseMAX™ -Induced Artifacts in Proteomic Sample Preparation 150
5.4 Conclusion 156
Chapter 6: Analysis of Lipid Modifications on RGS4 from Sf9 Cells 157
6.1 Introduction 157
6.2 Experimental Section 158
6.2.1 Materials 158
6.2.2 Sf9 Cell Culture, RGS4 Overexpression, and *in vivo* Metabolic Labeling with Palmitic Acid 159
6.2.3 *In vitro* Auto Palmitoylation of His-tagged RGS4 from Sf9 Cells 160
6.2.4 In-Solution Proteolytic Digestion of His-Tagged RGS4, Hydrophobic Peptide Enrichment, and MALDI-TOF Analysis 160
6.2.5 LC-MS/MS Analysis of the Enriched Hydrophobic Peptides 161
6.3 Results and Discussion 161

6.3.1 Production and Analysis of the Palmitoyl-RGS4 Standard 161

6.3.2 LC-MS/MS Analysis of *in vitro* Palmitoylated RGS4 and RGS4 Obtained from Sf9 Cell with or without Palmitate Labeling 167

6.3.3 Re-evaluation of the Previous Radioactive Labeling Results 169

6.4 Conclusion 176

Chapter 7: General Conclusion and Future Perspectives 177

7.1 General Conclusion 177

7.2 Future Perspectives 179

BIBLIOGRAPHY 181

CURRICULUM VITAE 204

LIST OF FIGURES

Figure 1.1 Proposed mechanisms of protein palmitoylation, adapted from reference [26]. (a) Spontaneous palmitoylation; (b) Palmitoylation via a palmitoyl-PAT intermediate; (c) Palmitoylation with the assistance of a transfer protein. 7

Figure 1.2 Schematic of palmitoylation-regulated cytosolic protein anchoring and trafficking, adapted from reference [55]. 11

Figure 1.3 Schematic of the ABE chemistry, adapted from reference [110]. 24

Figure 1.4 (a) Schematic of the detection of protein palmitoylation by metabolic labeling with 17-ODYA followed by click chemistry, adapted from reference [118]; (b) Click chemistry with copper(I)-catalyzed azide-alkyne [3 + 2] cycloaddition (CuAAC). 26

Figure 2.1 Schematic of the MALDI process, adapted from reference [122]. 29

Figure 2.2 Schematic of the proposed ESI mechanism, adapted from reference [128].... 31

Figure 2.3 Schematic of a MALDI-TOF/TOF instrument, adapted from reference [130]. 35

Figure 2.4 Schematic of a quadrupole mass spectrometer, adapted from reference [131]. 38

Figure 2.5 The stability diagrams of ions with different *m/z* values in the *U/V* space. 39

Figure 2.6 Schematic of a linear ion trap, adapted from reference [133]. 41

Figure 2.7 Schematic of a cubic ICR cell and the ion cyclotron motion. 42

Figure 2.8 Schematic of a solariX^{TM} Fourier transform ion cyclotron resonance mass spectrometer, adapted from the user manual (Bruker Daltonics). 44

Figure 2.9 The cutaway view of an Orbitrap mass spectrometer, adapted from reference [134]. 45

Figure 2.10 Schematic of an LTQ-Orbitrap Velos mass spectrometer, adapted from reference [135]. 46

Figure 2.11 Nomenclature of peptide backbone fragmentation, adapted from reference [137]. 49

Figure 2.12 The oxazolone pathway in the low energy CID process, adapted from reference [141]. 52

Figure 2.13 The mechanism proposed at Cornell, for ECD of protonated peptides, adapted from reference [149]. 55

Figure 3.1 Stability of the three palmitoyl peptide standards in 100 mM ABC buffer (pH 8.0), 50 mM Tris buffer (pH 7.4), and 50 mM AA buffer (pH 4.0) at 37 ^{o}C. 69

Figure 3.2 Plot of the pH value of several buffer solutions measured at various time points after preparation. All solutions were kept at 37 ^{o}C. 70

Figure 3.3 Stability of three palmitoyl peptides, as represented by the relative abundance of the palmitoyl peptides and their various depalmitoylated forms after 30 min or 60 min of incubation in Tris buffer (50 mM, pH 7.4) at 37 ^{o}C or at 55 ^{o}C, in the presence or absence of DTT or TCEP. 71

Figure 3.4 Stability of the three palmitoyl peptide standards in the presence of 1 mM and 10 mM DTT/TECP in 50 mM Tris buffer (pH 7.4). 72

Figure 3.5 Mechanisms for disulfide bond reduction by DTT (top) and by TCEP (bottom) 74

Figure 3.6 (a) Chromatogram of a mixture of three palmitoyl peptides and their IAM-labeled counterparts; (b) Chromatogram of a mixture of three palmitoyl peptides and their FIAM-labeled counterparts..... 77

Figure 3.7 Chemical structure of *N*-[(3-perfluorooctyl)propyl] iodoacetamide. 78

Figure 3.8 Relative quantification by UPLC-MS analysis on an LTQ-Orbitrap XL mass spectrometer. (a) The total ion chromatogram of a mixture of palmitoyl and FIAM-labeled peptides; (b), (c), and (d) the relative quantification calibration curves of the DFRIAFQELLC$_{FIAM}$LR and PDFRIAFQELLC$_{palm}$LR peptide pair, the MGC$_{FIAM}$VQC$_{FIAM}$KDKEA and MGC$_{palm}$VQC$_{palm}$KDKEA peptide pair, and the RAWC$_{FIAM}$QVAQKF and ARAW$_{palm}$C$_{palm}$QVAQKF peptide pair, respectively.... 80

Figure 3.9 Tandem MS spectra of PDFRIAFQELLC$_{palm}$LR: (a) CID on solariX, (b) CID on Orbitrap, (c) HCD on Orbitrap, (d) ECD on solariX, and (e) ETD on solariX. * indicates loss of $C_{16}H_{30}O$ (238.23 Da); § indicates loss of $C_{15}H_{31}COS^{\bullet}$ (271.21 Da). 86

Figure 3.10 Proposed mechanisms for formation of z^{*} and $z^{\S}$ ions in ECD..... 88

Figure 3.11 Tandem MS spectra of $MGC_{palm}VQC_{palm}KDKEA$: (a) CID on Orbitrap, (b) HCD on Orbitrap, (c) ECD on solariX, (d) ETD on Orbitrap. * indicates loss of $C_{16}H_{30}O$ (238.23 Da); § indicates loss of $C_{15}H_{31}COS^{\bullet}$ (271.21 Da)..... 92

Figure 3.12 Tandem MS spectra of $ARAW_{palm}C_{palm}QVAQKF$: (a) CID on Orbitrap, (b) HCD on Orbitrap, (c) ECD on solariX, (d) ETD on Orbitrap. * indicates loss of $C_{16}H_{30}O$ (238.23 Da); § indicates loss of $C_{15}H_{31}COS^{\bullet}$ (271.21 Da); # indicates loss of $C_{15}H_{31}CONC_8H_5$ (354.28 Da)..... 94

Figure 4.1 MALDI-TOF mass spectra of the peptide standard, GCLGNAK, (a) before and (b) after reaction with palmitoyl chloride in 100% TFA. (c) The MALDI-TOF mass spectrum of sample (b) after subsequent incubation with 500 mM HA/25 mM IAM..... 101

Figure 4.2 MALDI-TOF mass spectra of the palmitoyl peptide standard, $GC_{palm}LGNAK$, after incubation in (a) 50 mM ABC buffer (pH 8.0) or (b) 50 mM Tris (pH 7.4) at 37°C for 3 hr. 102

Figure 4.3 MALDI-TOF mass spectra of a mixture of GCpalmLGNAK and $GC_{IAM}LGNAK$ (a) before and (b) after incubation in ABC buffer (pH 8.0) at 37°C for 3 hr..... 103

Figure 4.4 The chemical structure of RapiGest^{TM}. 104

Figure 4.5 MALDI-TOF mass spectra of the palmitoyl peptide standard, GC_{palm}LGNAK, after incubation in (a) 50 mM ABC buffer (pH 8.0) /0.1% RapiGest^{TM} or in (b) 50 mM Tris buffer (pH 7.4) /0.1% RapiGest at 37°C for 3 hr..... 105

Figure 4.6 (a) The base peak chromatogram of GC_{palm}LGNAK after incubation in 50 mM Tris buffer (pH 7.4) at 37°C for 3 hr; (b-d) the EICs of various modified forms of GCLGNAK. Palmitoyl localization was achieved by tandem MS analysis, as illustrated in Figure 4.16. 107

Figure 4.7 (a) The base peak chromatogram of GC_{palm}LGNAK after incubation in 50 mM Tris buffer (pH 7.4) with 0.1% RapiGest^{TM} at 37°C for 3 hr; (b-d) the EICs of various modified forms of GCLGNAK. Palmitoyl localization was achieved by tandem MS analysis, as illustrated in Figure 4.16. 108

Figure 4.8 Comparison of the ion abundances of GC_{palm}LGNAK-derived peptides after a 3-hr incubation in 50 mM Tris (pH 7.4) in the absence or presence of 0.1% RapiGest^{TM}. Unpaired t test, standard deviation, n = 5, * $p < 0.05$, ** $p < 0.01$…. 111

Figure 4.9 The decay of UV absorbance at 230 nm of GC_{palm}LGNAK in 50 mM Tris (pH 7.4) buffer without (a) and with (b) 0.1% RapiGest^{TM} over a 3-hr incubation..... 112

Figure 4.10 Stability of the three palmitoyl peptide standards, as represented by the relative abundances of the palmitoyl peptides and their various depalmitoylated forms after 1-hr incubation in 50 mM Tris (pH 7.4), 50 mM Tris/10 mM DTT, and 50 mM Tris/0.1% RapiGest^{TM}/10 mM DTT. All experiments were performed at 37 °C. 113

Figure 4.11 Proposed mechanism for the stabilization of the thioester group by RapiGest^{TM}..... 114

Figure 4.12 Integrated EICs of the singly palmitoylated species [GCLGNAK+palm] obtained from the LC-MS analysis of the *S*-palmitoyl peptide standard $GC_{palm}LGNAK$ (a) before and (b) after a 3-hr incubation in 100 mM ABC (pH 8.0) buffer at 37°C followed by DTT reduction. (c) MS spectra of the three [GCLGNAK+palm] isomers. Note that each integrated EIC represents the sum of the singly (*m/z* 450.78) and doubly (*m/z* 900.56) charged species of [GCLGNAK+palm]. 116

Figure 4.13 CID spectra of (a) $GC_{palm}LGNAK$, (b) $GCLGNAK_{palm}$, and (c) $G_{palm}CLGNAK$..... 121

Figure 4.14 ETD spectra of (a) $GC_{palm}LGNAK$, (b) $GCLGNAK_{palm}$, and (c) $G_{palm}CLGNAK$. 122

Figure 4.15 Proposed mechanisms for (a) formation of *b*- and *y*- ions in CID; (b) formation of b_1+*palm* and y_6-*palm* ions from the peptide $GC_{palm}LGNAK$ in CID; and (c) formation of the $[M + 2H - C_{15}H_{31}COHS]^{+\bullet}$ ion from the peptide $GC_{palm}LGNAK$ by ETD. 125

Figure 4.16 CID spectra of (a) $GC_{palm}LGNAK_{palm}$, (b) $G_{palm}C_{palm}LGNAK$, and the disulfide-linked homo-dimers of (c) $GCLGNAK_{palm}$ and (d) $G_{palm}CLGNAK$. 127

Figure 5.1 Schematic of acid-induced decomposition of ProteaseMAX ™ 130

Figure 5.2 MALDI-TOF mass spectrum of the tryptic digest of the major band at 25 kDa in the SDS-PAGE of Ni-NTA purified proteins from the Sf9 cells overexpressed with His-tagged RGS4. Peptide mass fingerprinting showed a match of this band to RGS4 with a 73% sequence coverage (top). 137

Figure 5.3 MALDI-TOF mass spectra of RGS4-noRA (a) and its sequential eluents with 20% ACN/0.1% TFA (b), 40% ACN/0.1% TFA (c), and 60% ACN/0.1% TFA (d). 139

Figure 5.4 MALDI-TOF mass spectra of the hydrophobic peptides in the 40% ACN eluent (a) before and (b) after 1-h incubation with 10 mM DTT at 37 ^{o}C. X-modified peptides are labeled in blue, Y-modified peptides are labeled in red, and unmodified peptides are labeled in black. 140

Figure 5.5 The MALDI-TOF mass spectrum of the 40% ACN/0.1% TFA eluent of the RGS4-noRA digest following the HA treatment. 141

Figure 5.6 (a) The TIC of the RGS4-noRA sample; (b-d) the extracted ion chromatograms of the doubly charged tryptic peptide FYLDLTNPSSCGAEK and its X- and Y-modified forms. 143

Figure 5.7 The CID spectra of the doubly protonated peptides (a) FYLDLTNPSSCGAEK, (b) FYLDLTNPSSC$_X$GAEK, and (c) FYLDLTNPSSC$_Y$GAEK. 144

Figure 5.8 Sequence coverage maps and identified cysteine modifications obtained from the LC-MS/MS analysis of the tryptic digests of RGS-noRA (a) and RGS-RA (b). 146

Figure 5.9 Proposed mechanisms for the formation of (a) X- and (b) Y-modified peptides 148

Figure 5.10 Alternative pathways for the formation of X-modified peptides 149

Figure 5.11 The relative abundances of 9 cysteine-containing peptides with free thiol, X-, Y-, or carbamidomethyl modification in the RGS4-noRA and RGS4-RA digests. 153

Figure 5.12 (a-b) MALDI-TOF mass spectra of the peptide standard GCLGNAK after a 3-hr incubation at 37 ^{o}C in 50 mM ABC/0.05% ProteaseMAX ^{TM} without DTT and with 10 mM DTT, respectively. (c-d) MALDI-TOF mass spectra of sample (a) after subsequent incubation in 10 mM DTT at 37 ^{o}C for 1 h or in 1 M HA at room temperature for 1 h, respectively. 154

Figure 5.13 (a) The MALDI-TOF mass spectrum of the peptide standard GCLGNAK. (b-f) MALDI-TOF mass spectra of GCLGNAK after incubation in 50 mM ABC/0.05% ProteaseMAX ^{TM} at room temperature for 10 min (b), or at 37 ^{o}C for 30 min (c), 1 hr (d), 3 hr (e) and 5 hr (f). 155

Figure 6.1 The regulatory role of RGS4 in GPCR signaling, adapted from reference [239]. 157

Figure 6.2 MALDI-TOF mass spectra of tryptic digests of RGS4-palm-std (a) and its sequential eluents from the Poros R1 50 resin (b-d). 163

Figure 6.3 The TIC of the 60% ACN/0.1% TFA eluent of the RGS4-palm-std digest.. 164

Figure 6.4 Sequence coverage maps and identified palmitoylation sites obtained from the LC-MS/MS analysis of the tryptic digests of RGS4 pre-incubated with 1 mM palmitoyl-CoA (a), RGS4 from *in vivo* metabolic labeling (b), and RGS4 pre-incubated with 100 µM palmitoyl-CoA (c). 165

Figure 6.5 The CID spectra of GHHHHHHMC$_{palm}$K (a), GLAGLPASC$_{palm}$LR (b), and SEYSEENIDFWISC$_{palm}$EEYKK (c) extracted from the LC-MS/MS analysis of the RGS4-palm-std tryptic digest. 166

Figure 6.6 The CID spectra of NMLEPTITC$_{palm}$FDEAQKKIFNLMEK (a), and FYLDLTNPSSC$_{palm}$GAEK (b) extracted from the LC-MS/MS analysis of RGS4 from Sf9 cells treated with palmitate. 168

Figure 6.7 Localization of the palmitoylation site at Cys95 on RGS4, adapted from reference [61] 170

Figure 6.8 RGS4 palmitoylation map produced by radioactive labeling combined with the CNBr cleavage, based on the result from Figure 6.7. 171

Figure 6.9 Evaluation of the previous radioactive labeling results by LC-MS/MS. (a) Re-assignment of CNBr-derived fragments produced from RGS4-palm-in-vitro and RGS4-palm-in-vivo, (b) The CID spectrum of the tryptic peptide $NM_{ox}LEPTITC_{palm}FDEAQKKIFNLMEK$. 175

LIST OF ABBREVIATIONS

[^{125}I-IC16] palmitate	16-iodo-hexadecanoic acid
17-ODYA	17-octadecynoic acid
2D-PAGE	two-dimensional polyacrylamide gel electrophoresis
AA	ammonium acetate
ABC	ammonium bicarbonate
ABE	acyl-biotinyl exchange
ACBP	acyl-CoA binding protein
ACN	acetonitrile
ALS	acid-labile surfactant
AMPA	α-amino-3-hydroxy-5-methyl-4-isoxazolepropionic acid
APT	acyl-protein thioesterase
BK	big potassium
BPC	base peak chromatogram
CAD	collisionally activated dissociation
CE	capillary electrophoresis
CHCA	α-cyano-4-hydroxycinnamic acid
CI	chemical ionization
CID	collision-induced dissociation
CNBr	cyanogen bromide
CNS	central nervous system
CRD	cysteine-rich domain

CuAAC	copper(I)-catalyzed azide-alkyne [3+ 2] cycloaddition
DC	direct current
DHB	2,5-dihydroxy benzoic acid
DTT	dithiothreitol
ECD	electron-capture dissociation
EI	electron ionization
EIC	extracted ion chromatograms
eNOS	endothelial nitric oxide synthase
ER	endoplasmic reticulum
ERF	effect on Ras function
ESI	electrospray ionization
ETD	electron-transfer dissociation
FA	formic acid
FAS	fatty acid synthase
FFT	fast Fourier transformation
FIAM	*N*-[(3-perfluorooctyl)propyl] iodoacetamide
FTICR	Fourier transform ion cyclotron resonance
GAP	GTPase activating protein
GC	gas chromatography
GPCR	G-protein coupled receptor
GPI	glycophosphatidyl inositol
HA	hydroxylamine

HCD	higher-energy collisional dissociation
HIP	Huntington interacting protein
HMGCS	HMG-CoA synthase
HPLC	high-performance liquid chromatography
HTT	Huntington protein
IAM	iodoacetamide
IPA	isopropanol, isopropyl alcohol
LC	liquid chromatography
LIT/LTQ	linear quadrupole ion trap
m/z	mass-to-charge ratio
MALDI	matrix-assisted laser desorption/ionization
MBOAT	membrane-bound *O*-acyltransferase
MRM	multiple reaction monitoring
MS	mass spectrometry
MS/MS	tandem mass spectrometry
MudPIT	multi-dimensional protein identification technology
NEM	*N*-ethyl maleimide
PAT	protein acyl transferase
PKA	protein kinase A
PM	ProteaseMAX ™
PMF	peptide mass fingerprinting
ppm	parts-per-million

PPT	palmitoyl-protein thioesterase
PSD	postsynaptic density
PTM	post-translational modification
QqQ	triple quadrupole
Qq-TOF	quadrupole time-of-flight
RF	radio frequency
RG	RapiGest™
RGS	regulator of G-protein signaling
RGS4-noRA	RGS4 digests without reductive alkylation
RGS4-RA	RGS4 digests with reductive alkylation
ROS	reactive oxygen species
RP	reversed phase
SA	sinapinic acid
SCX	strong cation exchange
SDS-PAGE	sodium dodecyl sulfate polyacrylamide gel electrophoresis
Shh	sonic hedgehog
SILAC	stable isotope labeling by amino acids in cell culture
SPE	solid-phase extraction
SRM	selective reaction monitoring
TCEP	tris(2-carboxyethyl)phosphine
TFA	trifluoroacetic acid

THF	tetrahydrofuran
TIC	total ion chromatogram
TLC	thin layer chromatography
TOF	time-of-flight
Tris	tris(hydroxymethyl)aminomethane

Chapter 1: Introduction to Protein Palmitoylation

S-palmitoylation is a type of protein post-translational modification (PTM) resulting from the covalent attachment of a saturated sixteen-carbon acyl chain to a cysteine residue through a thioester linkage. It was first discovered on the virus glycoprotein E1/E2 in 1979 [1]. Later it was shown that *S*-palmitoylation is post-translational [2], dynamic [3], sensitive to hydroxylamine (HA) treatment [4], and is an ubiquitous modification occurring in viruses [5], plants [6], yeast [7, 8], and animal cells [9]. In the following decades, many proteins, including ion channels [10], receptors [11], small G proteins [12], secreted proteins [13], have been found to undergo palmitoylation *in vivo*. Unlike other lipid modifications (*e.g.* N-terminal myristoylation, prenylation, and glycophosphatidyl inositol (GPI)-linking), *S*-palmitoylation is readily reversible, owing to the labile nature of the thioester bond. Thus, *S*-palmitoylation, similar to phosphorylation, may vary in different intracellular environments and is subject to change upon regulation. Cycling between the palmitoylation and depalmitoylation states regulates several important intracellular events such as protein sorting, trafficking, anchoring, stability, and protein-protein interactions [14, 15]. This chapter reviews the mechanisms of *S*-palmitoylation and the methods for its characterization.

1.1 Mechanisms of Protein Palmitoylation

1.1.1 Non-Enzymatic and Enzymatic Palmitoylation

Investigation of the molecular mechanism of protein palmitoylation began with the identification of the palmitoyl donor. In 1984, by using pulse-chase radioactive

labeling followed by the analysis of the labeled lipids extracted from baby hamster kidney cells, Berger and Schmidt identified palmitoyl-CoA as the only potential acyl donor *in vivo* [16]. Later, a series of studies was performed, in which purified proteins that are known to undergo *in vivo* palmitoylation, such as rhodopsin, Gα, myelin P0, Yes, SNAP-25, were incubated *in vitro* with palmitoyl-CoA, under physiological conditions andthe results showed that palmitate could be incorporated into these proteins spontaneously [17-22]. Moreover, this *in vitro* palmitoylation appeared to target the same sites as those found *in vivo* [17, 21, 23]. It came as no surprise that *in vitro* palmitoylation could occur non-enzymatically, because the thioester bond in palmitoyl-CoA is highly activated and this makes the transfer an energetically favored process. By studying the reaction kinetics, Bharadwaj and Bizzozero showed that *in vitro* palmitoylation is a second-order reaction and proposed that it is the nucleophilic attack of the protein/peptide thiolates to the thioester bond in palmitoyl-CoA that initiates the transfer process (Figure 1.1a) [21, 24]. The pKa of the thiol group in a free cysteine is ~8.4. Thus, under physiological conditions (pH 7.4), the cysteine thiol group should exist primarily in the protonated form (R–SH), instead of in the reactive ionized thiolate form ($R–S^-$), and thus palmitoyl transfer should not be favored. However, the local environment surrounding each cysteine thiol group could significantly change its pKa. For example, the presence of positively charged amino acid residues such as histidine around the cysteine residue could stabilize the thiolate anion, thus making it more reactive [25]. Such a difference in the local environment may account for the selectivity of auto-palmitoylation to certain cysteine residues. Bharadwaj and Bizzozero also stated that the calculated activation

energy for the auto-acylation process could be significantly lower than that for enzymatic transacylation, and suggested that enzymatic palmitoylation may not play an important role *in vivo*. This hypothesis was supported by the lack of defined consensus sequences for palmitoylation and failure to identify a palmitoyl transferase in early days. However, the theory of non-enzymatic palmitoylation has also drawn sharp criticisms. The palmitoyl reaction performed in a test tube with buffers, proteins, and palmitoyl-CoA is a far too simple model to mimic the *in vivo* palmitoylation process. Since the spontaneous palmitoylation rate depends on the concentration of palmitoyl-CoA, one should take into consideration the various players affecting the level of *in vivo* palmitoyl-CoA. Indeed, the concentration of free palmitoyl-CoA in the cytoplasm is reported to be in the nanomolar range, much lower than expected, because most palmitoyl-CoA is bound to the acyl-CoA binding protein (ACBP) which is considered as the palmitoyl-CoA "buffer," thus sequestering its reactivity with thiolates [26, 27]. The importance of ACBP is further exemplified by the fact that the rate of *in vitro* auto-palmitoylation is attenuated by the addition of ACBP in a concentration-dependent manner [28, 29]. The addition of ACBP at the physiological concentration almost suppressed auto-palmitoylation to basal level (>95% inhibition). Finally, the rate of *in vitro* spontaneous palmitoylation, even in absence of ACBP, is much slower than the reported *in vivo* palmitoylation rate. Therefore, it is unlikely that spontaneous palmitoylation is the major mechanism for *in vivo* palmitoylation with fast turnover rate [28].

Historically, research on enzymatic palmitoylation began with the attempt to characterize "acyl transfer activity" by Berger and Schmidt in 1984 [30]. Based on the

results from a previous study, they postulated that the acylation reaction might occur in the endoplasmic reticulum (ER). Therefore, microsomes (mainly small ER particles reformed *in vitro*) were purified from various cell lines and incubated together with viral protein E1 and [^{14}C]palmitoyl-CoA. This incubation led to the addition of [^{14}C]palmitate to E1. However, the investigators reported that palmitoyl transfer was abolished if the microsomes were absent or had been pre-boiled (deactivated), and this suggested that something residing within the microsomes has the ability to acylate proteins, using palmitoyl-CoA as the palmitoyl donor. For nearly a decade, researchers were unable to purify an enzyme bearing such activity from the microsomes. Meanwhile, the discovery of auto-palmitoylation in several other proteins put the existence of palmitoyl transferases into question. Bartels and co-workers finally broke the dam by developing a yeast strain whose viability is dependent upon the palmitoylation of Ras2 [31]. Any gene mutation resulting in the failure of Ras2 palmitoylation will lead to the death of these yeast cells. Genetic screening identified two genes, *ERF2* and *ERF4* (*ERF*, effect on Ras function), as important players for Ras2 palmitoylation [7]. Further studies confirmed that the Erf2-Erf4 complex is a protein acyl transferase (PAT) and that it specifically palmitoylates Ras2 in yeast. Erf2 is a multi-pass membrane protein residing on the ER. It contains a motif of Asp-His-His-Cys (DHHC) in a cysteine-rich domain (DHHC-CRD) within the cytosolic loop between the transmembrane regions TM2 and TM3. The DHHC-CRD motif is critical for the enzyme activity; its mutation led to failure of Ras2 palmitoylation. Some researchers further proposed that the DHHC-CRD domain is the catalytic center of PAT [32]. Erf4 is a DHHC PAT-associated protein that plays an indispensable role in the

enzyme activity, probably because it prevents ubiquitin-mediated degradation of Erf2 and stabilizes the palmitoyl-Erf2 intermediate before the palmitoyl transfer [33]. Later, another yeast PAT and its corresponding substrate, Akr1p and Yck2p, were discovered and characterized [34]. Interestingly, Akr1p and Erf2 shared no homologous region except for the DHHC-CRD sequence. This finding conveyed the message that a protein containing the DHHC-CRD sequence might be a PAT candidate. A search against the GenBank database found 23 genes in mammalian cells that encode DHHC proteins, many of which showed authentic PAT activity; their substrate preference was studied by overexpressing each individual DHHC protein together with substrates of interest followed by the detection of palmitate incorporation [35].

With the identification of an increasing number of DHHC PATs, the notion that protein palmitoylation occurs enzymatically has been widely accepted. The research is now focused on the in-depth study of the mechanism by which PAT catalyzes the palmitoyl transfer reaction. No consensus exists to date and two different models have been proposed. In the first model (Figure 1.1b) [32, 36], PAT initially undergoes auto-palmitoylation in the presence of palmitoyl-CoA, forming a palmitoyl-PAT intermediate. In the second step, the substrate binds to the palmitoyl-PAT intermediate, leading to the transfer of palmitate to the substrate. By monitoring the release of CoA-SH and palmitate, Mitchell and co-workers found that the intermediate would undergo very fast palmitoyl turnover if it failed to meet its substrate. They also showed that the DHHC region is required for the formation of the intermediate, as well as for the palmitoyl transfer [32]. However, there was no direct evidence pinpointing the auto-palmitoylation site to the

cysteine residue in the DHHC region. The second proposed model (Figure 1.1c) was based on experimental results from Dietrich and co-workers [37]. They observed that Vac8 needs an equimolar amount of its palmitoyl transferase, Ykt6, to achieve sufficient palmitoylation *in vitro*, yet this observation does not conform to the classic catalytic reaction. In addition, Ykt6 binds to both palmitoyl-CoA and CoA-SH. It is possible that palmitoyl-CoA binds to Ykt6 through non-covalent interactions, with the CoA fitting into the binding pocket. The subsequent association of Ykt6 to its substrate brings the palmitoyl-CoA close to the targeted thiolate group, thus facilitating the palmitoyl transfer reaction. After the reaction, CoA-SH still binds to Ykt6 and sequesters its activity. The *in vivo* machinery to reactivate Ykt6 by releasing CoA-SH may regulate the palmitoylation process. Note that the two models presented here do not necessarily contradict one another, since they deal with different PATs. Furthermore, Ykt6 in the second model is not a classic protein palmitoyl transferase, as it does not contain the DHHC domain.

Another family of PATs, known as the MBOATs (membrane-bound-*O*-acyltransferase), have the ability to palmitoylate secreted proteins such as Sonic hedgehog, Spitz, and Wnt, via the irreversible amide linkage [38]. MBOAT-catalyzed palmitoyl transfer proceeds via a different mechanism from that catalyzed by the DHHC PATs as discussed above. Since the main focus of this thesis is *S*-palmitoylation, the detailed information on MBOAT PATs will not be reviewed here.

In summary, the discovery and characterization of various palmitoyl transferases and their substrates have undermined the notion of spontaneous *in vivo S*-palmitoylation. PATs are crucial and necessary for *S*-palmitoylation of many proteins. However, in

certain cellular environments, such as in mitochondria, where the free palmitoyl-CoA is present at a very high level, auto-palmitoylation can become the major pathway for *in vivo* palmitoylation.

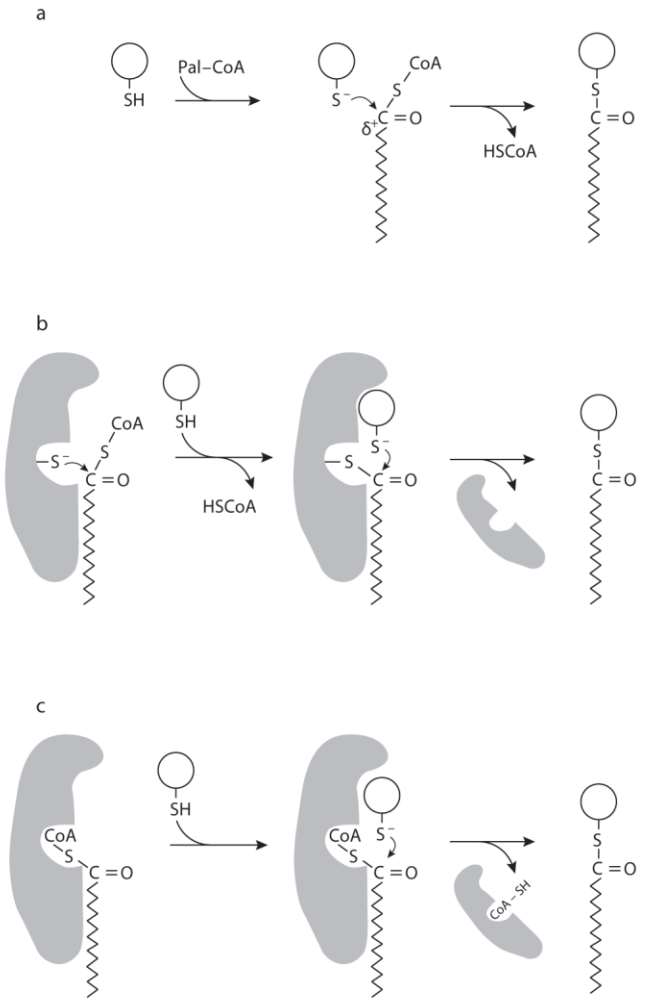

Figure 1.1 Proposed mechanisms of protein palmitoylation, adapted from reference [26]. (a) Spontaneous palmitoylation; (b) Palmitoylation via a palmitoyl-PAT intermediate; (c) Palmitoylation with the assistance of a transfer protein.

1.1.2 Palmitoyl Dynamics

Due to the labile nature of the thioester linkage, *S*-palmitoylation is a reversible and dynamic modification. A protein can go through several cycles of palmitoylation/depalmitoylation during its lifetime [39]. The regulation of palmitoyl turnover by stimulus or environmental change has been implicated in many studies. Wedegaertner and co-workers demonstrated that agonist activation of the β2-adrenergic receptor induces increased palmitate turnover on Gαs [40]. El-Husseini and co-workers showed that PSD-95 undergoes depalmitoylation in response to glutamate activation in neurons [41]. Robinson and co-workers found that bradykinin, a G protein-coupled receptor ligand, induces depalmitoylation of the endothelial nitric oxide synthase 3 (eNOS) [42]. Depalmitoylation is believed to be catalyzed by a palmitoyl thioesterase. To date, four thioesterases have been discovered: palmitoyl-protein thioesterase-1 (PPT1), palmitoyl-protein thioesterase-2 (PPT2), acyl-protein thioesterase-1 (APT1), and acyl-protein thioesterase-2 (APT2) [43]. PPT1 and PPT2 are lysosomal enzymes responsible for removal of *S*-palmitoylation from proteins which are taken up by the lysosome for degradation [44]. They are not involved in the regulation of the palmitoylation/ depalmitoylation cycle, because they only depalmitoylate proteins at the end of their lifetimes [13]. On the other hand, APT1 and APT2 are located in the cytosol, and they catalyze the depalmitoylation of membrane-associated cytosolic proteins, or membrane proteins bearing palmitoyl group at the cytoplasmic face. Their activity is subject to change in response to extracellular signals or other stimuli, making them important

factors in palmitoyl turnover. They have a variety of substrates including H-Ras, Gαs, GAP-43, and eNOS [12, 45]. Their biological roles are reviewed in the next section.

1.1.3 Biological Roles of Protein Palmitoylation/Depalmitoylation

Palmitoylation is involved in many intracellular events such as protein trafficking, anchoring, activity, stability, and protein-protein interaction. In this section, examples are given to illustrate the various roles of protein palmitoylation.

1.1.3.1 Membrane Association and Protein Trafficking

H-Ras Shuttling

H-Ras has been invoked as a classic model for palmitoylation-modulated protein anchoring/trafficking. H-Ras is a plasma membrane-associated GTPase that relays extracellular signaling to control cell proliferation, differentiation, invasion, and apoptosis. H-Ras has three cysteines near its C-terminus: Cys181, Cys184, and Cys186. The newly synthesized H-Ras located in the cytosol is first recognized by the protein farnesyl transferase through its C-terminal CAAX sequence. A farnesyl group is then added to C186 on the CAAX motif, followed by cleavage of AAX and methylation of the carboxyl group of C186 [46]. The farnesyl group increases the hydrophobicity of H-Ras and allows weak association of H-Ras with the Golgi. Although this association is reversible and not sufficient to tether H-Ras permanently to the Golgi, it increases the likelihood of H-Ras to present itself to the Golgi resident DHHC9 [47]. Subsequent palmitoylation on C181 and C184 by DHHC9 dramatically increases its hydrophobic interaction with the lipid bilayer, allowing H-Ras to associate stably with the Golgi

membrane. The mature H-Ras is then transported through trafficking vesicles to the plasma membrane, where it exerts its function in signal transduction [48]. Cleavage of the thioester linkage by APT results in the turnover of palmitoylation, leading to the shedding of H-Ras from the plasma membrane into the cytosol [49, 50]. H-Ras can be re-palmitoylated by interacting with DHHC9 on the Golgi surface. As a result, the palmitoylation/depalmitoylation process modulates the activity of H-Ras via its shuttling between different subcelluar compartments. A similar mechanism also applies to other membrane-associated signaling proteins including N-Ras [50], Gα [40], Lyn [51], eNOS [52], and others [53, 54]. Figure 1.2 shows a typical palmitoylation/depalmitoylation cycle that leads to the shuttling of proteins between the Golgi apparatus and the plasma membrane.

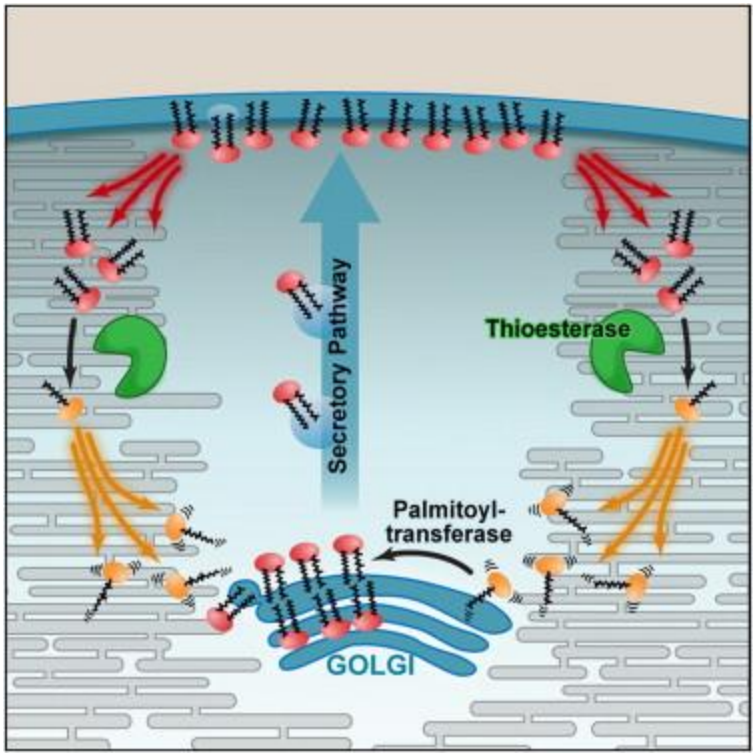

Figure 1.2 Schematic of palmitoylation-regulated cytosolic protein anchoring and trafficking, adapted from reference [55].

PSD-95-Mediated Protein Internalization in Response to Extracellular Stimuli

PSD-95 is a major component of the postsynaptic density (PSD) at glutamatergic synapses. It associates with the α-amino-3-hydroxy-5-methyl-4-isoxazolepropionic acid (AMPA) receptor through a trafficking protein, stargazin, and has been shown to be an important player in the translocation of the AMPA receptor. Stimulation of the AMPA receptor by glutamate results in depalmitoylation of PSD-95, in parallel with the internalization of the glutamate receptor AMPA. Pharmacological interruption of the palmitoylation/depalmitoylation cycle of PSD-95 results in a change in the number of

AMPA receptors at synapses, thereby attenuating the synaptic signaling. Therefore, it has been suggested that the AMPA stimulation leads to PSD-95 depalmitoylation, which in turn results in the internalization of the glutamate receptor AMPA, and serves as a feedback to deactivate the signaling pathway. It is not well understood how AMPA signaling affects the palmitoyl dynamics of PSD-95, but it has been postulated that activation of the glutamate receptor AMPA may lead to sconformational change on PSD-95, making it more accessible to APT [41].

1.1.3.2 Protein Activity

Ion Channels-Cross Talk between Palmitoylation and Other PTMs

Palmitoylation has been shown to be involved in the modulation of ion channels. Palmitoylation of ion channels occurs on intracellular loops or the N-/C- terminal cytoplasmic domains. These regions are implicated in protein disorders, suggesting possible involvement of palmitoylation in changing the protein conformation [10, 56]. Recent studies of big potassium (BK) channels are discussed below, as an example, to illustrate the modulation of protein activities by palmitoylation. The cytosolic C-terminus of BK channels contains both a palmitoylation site and a phosphorylation site. Palmitoylation promotes the association of the C-terminus to the plasma membrane, whereas phosphorylation, induced by protein kinase A (PKA), is responsible for inhibition of the BK channels' activity. Tian and co-workers found that phosphorylation by PKA leads to the dissociation of its C-terminus from the plasma membrane, presumably due to protein depalmitoylation, whereas mutation of the palmitoyl cysteine residue abolishes PKA-mediated inhibition of BK channels [57]. Although the details, as

to how the crosstalk between these two dynamic modifications occurs, remain unknown, it is clear that phosphorylation and palmitoylation together orchestrate the activities of the BK channels. It is possible that phosphorylation either blocks palmitoylation in the first place or facilitates the depalmitoylation process. Loss of its C-terminus anchor, in turn, results in global conformation change that shutx down the BK channels. Such an interplay of palmitoylation with other PTMs (phosphorylation, nitrosylation) has also been demonstrated to occur on several signaling proteins [58-60] and is reviewed in reference [15].

Regulator of the G-Protein Signaling (RGS) Family

Proteins of the RGS family, known as GTPase activating proteins (GAPs), can bind a G protein to activate its intrinsic GTPase that is responsible for switching off the G protein signaling. All RGS proteins contain a homologous domain named RGS-box, which is required for their GAP activity. Palmitoylation can occur on several family members, at the conserved cysteine residue located at RGS-box. *In vitro* studies showed that palmitoylation on the conserved cysteine results in decreased GAP activity of RGS4 and RGS10 [61], as compared to an increase in that of RGS16 [62].

1.1.3.3 Protein Targeting

Protein targeting to lipid rafts is another localization regulation mechanism besides protein trafficking. A lipid raft is a specialized functional plasma microdomain, known as a center of biological processes such as protein assembly and cell signaling. Because lipid rafts are rich in cholesterol as well as sphingolipids with a saturated fatty acyl side chain [63], proteins with very hydrophobic modifications tend to have an

affinity to lipid rafts that is higher than their attaraction to the surrounding bilayer. RGS16 has three potential palmitoylation sites (Cys2/Cys12, and Cys98). Interestingly, unlike H-Ras, RGS16 without palmitoylation can still be anchored and transported to the plasma membrane. However, mutation of Cys2/12, although not leading to the protein shedding from the membrane, makes RGS16 unable to localize to the lipid raft. Failure of the RGS16 targeting to lipid rafts prevents its further palmitoylation at Cys98 and leads to a decrease in its activity, suggesting the crucial role of palmitoylation in lipid raft targeting [62]. The essential role of palmitoylation for protein targeting to lipid rafts is also implicated in signaling proteins such as C81, LAT, and $\alpha_6\beta_4$ integrin, and has been reviewed in references [12, 64].

1.1.3.4 Protein-Protein Interactions

The involvement of palmitoylation in protein-protein interactions has been demonstrated by several studies. Yang and co-workers reported that mutation of cysteine residues that may be palmitoylated on CD151 abolished its association with CD9 and CD63 [65], leading to failure of the assembly of the signaling network in response to integrin stimulation [66]. A recent study by Yu and co-workers showed that the viral protein from the Hepatitis C Virus, NS4B, has two potential palmitoylation sites on its C-terminus, and that absence of palmitoylation on both sites significantly reduced binding of NS5A to NS4B [67]. Tu and Ross discovered that Gα undergoes depalmitoylation in response to the stimulation of β-adrenoreceptor. The depalmitoylated Gα had a higher affinity to RGS proteins and their association resulted in the deactivation of the β-adrenoreceptor-induced signaling pathway [68, 69]. Kostiuk and co-workers showed that

palmitoylation of mitochondrial HMG-CoA synthase (HMGCS2) promoted its association with PPARα, leading to the activation of transcription at the *Hmgcs2* gene [70].

1.1.3.5 Protein Stability

Recent studies on transmembrane protein adenosine receptor A1 [71], HIV receptor CCR5 [72], RSV glycoprotein [73], Tlg1 [74], showed that there isare positive correlations between palmitoylation and protein stability. Gao and co-workers investigated the palmitoyldeficient mutant of adenosine receptor A1, and found that the majority of the mutant A1 receptor underwent proteolysis, forming a 25-kDa receptor fragment whose turnover rate was much faster than that of the wild-type. They therefore concluded that palmitoylation can prevent protein degradation [71]. A more in-depth study by Valdez-Taubas and Pelham, using a different model, provided hints for a possible mechanism, although it may not be applicable to all cases. SNARE Tlg1 is a palmitoylated transmembrane protein, and its palmitoylation is catalyzed by Swf1, a member of the DHHC family in yeast. In the Swf1 mutant yeast, Tlg1 showed an abnormal intracellular distribution due to the loss of palmitoylation, and the unpalmitoylated Tlg1 could be recognized by Tul1, an E3 ubiquitin ligase, and marked for proteasomal degradation [74]. It is possible that palmitoylation on Tlg1 serves as a checkpoint in the process of protein quality control. Palmitoylation can modulate the protein conformation, and prevent Tul1 from accessing the ubiquitination site [14].

1.1.4 Protein Palmitoylation in Diseases

1.1.4.1 Palmitoylation and Oxidative Stress

Oxidative stress contributes to a number of human diseases, including neurodegenerative diseases, diabetes, cancers, and cardiovascular dysfunctions. The increased presence of reactive oxygen species (ROS), resulting from the incapability of the cell defense system against excess oxidants, is a hallmark of oxidative stress [75]. ROS can affect cell functions through modifications of lipids, proteins, and DNA, causing loss of the cell integrity, protein dysfunction, and genomic instability.

Several studies have demonstrated the regulatory role of oxidative stress in palmitoylation turnover and its involvement in pathological damage. Rodriguez-Capote and co-workers found that *in vitro* exposure of the surfactant protein SP-C to oxidants caused significant decrease in SP-C palmitoylation. Palmitoylation on SP-C is crucial for the formation of the lung surfactant film *in vivo*, and they suggested that the interplay between oxidants and palmitoylation may be one of the mechanisms for air pollution-induced lung diseases [76]. Parat and co-workers reported that treatment of endothelial cells with hydrogen peroxide remarkably decreased the incorporation of [^{3}H]]palmitate into caveolin-1 in a dose-dependent manner: 500 μM of hydrogen peroxide inhibited nearly 90% palmitoylation in caveolin-1 [77]. A similar effect was also observed by Clark and co-workers when they studied CD81 protein in the Jurkat cell line. They showed that, under oxidative stress, palmitoylation of CD81 was completely blocked, and this resulted in enhanced association of CD81 with 14-3-3 [78]. A more recent study by Burgoyne and co-workers showed that, under metabolic stress derived from the high

fat/high sugar treatment, bovine aortic endothelial cells suffered apoptosis coincident with a decrease in H-Ras palmitoylation, abnormal intracellular distribution of H-Ras, and reduced survival signaling from H-Ras. They further indicated that it was the intracellular oxidants that led to the failure of palmitoylation on H-Ras, rendering it incapable of relaying extracellular signals, and triggering apoptosis [79].

The mechanism by which oxidative stress inhibits protein palmitoylation is not fully understood. One explanation is that oxidants can modify reactive cysteine residues, therefore competing with protein palmitoylation [79]. It is also possible that oxidative stress-induced modifications on other amino acids may result in local or global changes in the protein structure, making them resistant to processing by PATs, or more susceptible to thioesterase cleavage by APTs.

1.1.4.2 Palmitoylation and Dysregulation of DHHC PATs

The biological importance of DHHC PATs, which have no known activities other than protein palmitoylation, has been demonstrated in several studies, illuminating the reasons for their significant correlation with neurological disorders (DHHC8, DHHC17)[80-82], osteoporosis (DHHC13)[83], cancers (DHHC2, DHHC9, DHHC11, DHHC14) [84-88], and other diseases [83, 89, 90]. For example, Yanai and co-workers discovered that, in Huntington disease, HIP14 (Huntington interacting protein 14, DHHC17) showed a decrease in interactions with its substrate, the mutant Huntington protein (HTT), leading to impaired palmitoylation. The unpalmitoylated HTT mutant can mislocalize, aggregate, and form inclusion bodies, which are apparently toxic to neurons [82]. Mukai and co-workers showed that the *Zdhhc8*-knockout mice developed a series of

behavioral abnormities which were similar to the symptoms in human schizophrenia [80]. A further genetic analysis demonstrated that there is a strong correlation between the risk of schizophrenia and the occurrence of different DHHC8 variants in the Han Chinese population [81]. Since many proteins are substrates of DHHC8 in neurons, failure of protein palmitoylation may lead to the development of mental disorders [80]. Yeste-Velasco and co-workers reported that DHHC14 is a tumor suppressor gene based on several observations: (1) there is a significant decrease in the expression of DHHC14 in clinical testicular germ cell tumor samples as well as tumor cell lines; (2) DHHC14 heterozygous deleted cells showed the ability to form larger colonies, whereas an increase in the expression of DHHC14 inhibited the xenograft tumor initiation; and (3) overexpression of DHHC14 resulted in apoptosis on tumor cell lines quantitatively [85]. Correlation of members of DHHC family to bladder cancer [86], colorectal cancer [87], and stomach cancer [88] has also been reported. In the future, it will be necessary to identify the downstream *S*-palmitoylation target of the DHHC family, to promote in-depth studies on the molecular mechanism of tumor initiation and progression [84].

1.1.4.3 Palmitoylation and Dysfunction of Fatty Acid Synthase (FAS)

FAS is the only enzyme catalyzing the *de novo* synthesis of palmitate using acetyl-CoA and malonyl-CoA as substrates [91]. The involvement of FAS in various physiological and pathological conditions (cancers, diabetes, hyperlipidemia, *etc*.) is very complex and has been reviewed [91-93]. However, FAS and protein palmitoylation had not been linked until 2008, when Fiorentino and co-workers found that overexpression of FASN in human prostate epithelial cells can lead to an increase of palmitoylation on

Wnt1. Palmitoylated Wnt1 subsequently activates the Wnt1/β-catenin pathway, which takes part in the development of prostate cancer [94]. Later, Wei and co-workers reported that specific knockdown of FAS from endothelial and hematopoietic cells in mice led to mild increase in blood pressure, consistent with a decrease in membrane-associated eNOS. A further *in vitro* study showed that FAS is physically associated with eNOS, and FAS-deficiency results in decreased the eNOS palmitoylation which is necessary for eNOS function [95]. Wei and co-workers also showed that FAS-deficiency in the intestine led to intestinal inflammation, because FAS is required to palmitoylate Mucin 2, an important intestinal barrier protein that has the ability to neutralize rotavirus [96].

1.2 Traditional Methods to Investigate Protein Palmitoylation

1.2.1 Radioactive Labeling

Detection of protein palmitoylation by radioactive labeling was first introduced by Schmidt and co-workers in 1979 [1]. In a typical experiment, the protein of interest is overexpressed by either virus infection or plasmid transfection of cultured cells. A subsequent incubation of the cells with tritiated palmitic acid, usually 9,10-[^{3}H] palmitic acid, is then performed. The tritiated palmitic acid can be utilized by the cells in the routine metabolic process to form radioactive palmitoyl-CoA, which is the acyl donor for protein palmitoylation [16]. Thus, proteins undergoing palmitoylation naturally can also incorporate the radioactive labeled palmitate. To achieve optimal labeling, it is important to tailor the incubation time specifically for the protein of interest, based on its synthesis rate and palmitoylation turnover speed [97]. After incubation, the protein of interest is enriched, subjected to sodium dodecyl sulfate polyacrylamide gel electrophoresis (SDS-

PAGE), exposed to X-ray films and detected by fluorography. Because tritium decay is a very slow process, the autoradiography exposure usually takes weeks or even months to complete, and this long exposure time is a main disadvantage of the radioactive labeling method. A few studies utilizing [^{125}I-IC16] palmitate (16-iodo-hexadecanoic acid) as an alternative label have also been reported [98-100]. The rationale to substitute the methyl group with an iodine atom is based on their similar volume. Compared to ^{3}H, ^{125}I is a high energy emitter and γ radiation emitted from ^{125}I can be detected by phosphor-imaging autoradiography with higher sensitivity and reduced exposure time.

Since *S*-palmitoylation is not the only fatty acylation that occurs *in vivo*, further linkage analysis is usually performed to distinguish among *S*-linked, *O*-linked, and *N*-linked fatty acylation. This can be achieved by treatment of the palmitoyl-labeled protein with HA [4], which is known to specifically cleave thioester linkages under neutral conditions [97]. Moreover, the released fatty acid can be further characterized by thin layer chromatography (TLC) or gas chromatography (GC) [1].

Besides palmitoyl detection, radioactive labeling can also be used to monitor *in vivo* palmitoyl turnover. The half-lives of palmitate modifications on proteins, including ankyrin [101], Gαi [102] α_{2A}-adrenergic receptor [103], H-Ras [104], and N-Ras [3], have been determined by pulse-chase experiments in which cells are labeled with 9,10-[^{3}H] palmitic acid for a short period of time (the pulse) followed by incubation with excess non-radioactive palmitate (the chase). The radioactive palmitate is incorporated into the protein during the pulse phase. If palmitoyl turnover occurs, the protein undergoes depalmitoylation, losing the radioactive palmitate, followed by re-

palmitoylation with non-radioactive palmitate during the chase phase. Through this process, palmitoyl turnover leads to a gradual decrease in the radioactive signal. Further studies showed that the half-life of palmitoylation measured by the pulse-chase assay is usually longer than the actual value, due to the complexity of fatty acid metabolism. An accurate measurement requires the analyst to account for [^{3}H] palmitate recycling during the chase phase [105].

As mentioned above, radioactive labeling enabled discovery of protein palmitoylation and this approach has been extensively used for the last three decades. It is a very sensitive and effective method for the absolute quantitation of protein palmitoylation. However, one must exercise particular care in the handling of the radioactive materials. The procedure is also tedious and time-consuming. Although the use of [^{125}I-IC16] palmitate can significantly shorten the exposure time, the method has never become popular as it is not commercially available. A serious limitation is that the radioactive labeling experiment only examines a single protein which is predicted to be palmitoylated. Moreover, the ratio of the palmitoylated protein versus its unpalmitoylated counterpart cannot be determined. Furthermore, this method is incapable of determining the palmitoylation site(s), unless mutations are made [106, 107], or antibodies that target regions of interest are used in conjunction with the enzymatic digestion [108].

1.2.2 Acyl-Biotinyl Exchange (ABE) Chemistry

In 2004, a novel method that utilizes a radioactive alkylation reagent to introduce the palmitoyl group by *in vitro* chemical reactions was described by Dridel and Green [109]. This method takes advantage of the specific cleavage of the *S*-palmitoyl group by

HA. In their study, free thiol groups generated by HA treatment were irreversibly blocked by ^{3}H-*N*-ethylmaleimide and this moiety was detected with autoradiography. The palmitoyl group modifications to all three proteins used in their study, the α7/5HT3A subunit, SNAP-25, and PSD-95, have been confirmed. These investigators also compared the results from their method to those obtained by traditional metabolic labeling with tritiated palmitate and claimed that it was much more sensitive. Moreover, they showed that tissue samples could also be analyzed by the newly developed method, demonstrating another advantage over the radioactive metabolic labeling method, which is almost exclusively applied to cultured cells. The authors also discussed the potential for thiol labeling by non-radioactive reagents, such as a fluorophore, chemiluminescent probe, or biotin. In particular, biotinylation of the HA-released thiol group would allow subsequent detection using streptavidin-horseradish peroxidase. This idea was later realized by Roth and coworkers, who developed the acyl-biotinyl exchange (ABE) chemistry and applied it to the detection of protein palmitoylation on a proteomic scale [8, 110]. Their multi-step method involved (Figure 1.3): (1) blocking of all free cysteine thiols with *N*-ethylmaleimide (NEM); (2) removal of the thioester-linked palmitoyl groups via hydroxylamine-induced hydrolysis; (3) labeling of the newly freed thiol groups with biotin-HPDP; (4) enrichment of biotinylated proteins with streptavidin-agarose beads. In-solution tryptic digestion was performed, and the resulting peptides were analyzed by integrated strong cation exchange/reversed phase high-performance liquid chromatography (SCX-RP-HPLC) coupled to a tandem mass spectrometer, a method commonly referred to as multi-dimensional protein identification technology

(MudPIT). The data were searched against a protein database using SEQUEST. Using this method, a total of 12 known and 35 novel palmitoyl proteins were identified in the yeast *Saccharomyces cerevisiae* [8]. This marked the first performance of large-scale profiling of protein palmitoylation (palmitoyl proteomics). was As indicated, one advantage of the ABE approach is the achievement of palmitoyl peptide/protein enrichment from complex samples, owing to the specific binding of biotin-HPDP with streptavidin-agarose beads followed by sample release from beads simply by disulfide bond reduction. Either a single targeted protein or total protein extracts can be analyzed by LC-MS analysis.

The lack of palmitoyl-specific antibodies has greatly impeded the study of protein palmitoylation in the past. The substitution of a palmitoyl group with a biotin tag, together with the availability of commercial anti-biotin antibodies, enables targeted palmitoyl detection by Western blotting. However, the ABE method involves multiple reactions and sample cleanup by triple precipitations in between each of the reaction steps and this may cause severe sample losses. As the authors themselves mentioned, false positives could arise due to incomplete blockage of free cysteines, and false negatives could occur due to inadequate thioester hydrolysis by hydroxylamine, or inefficient biotin-labeling. Further, palmitoylation is not the only form of thioester linkage, and the ABE method could lead to false assignments of palmitoylation when the cysteine is occupied by other types of acyl modification.

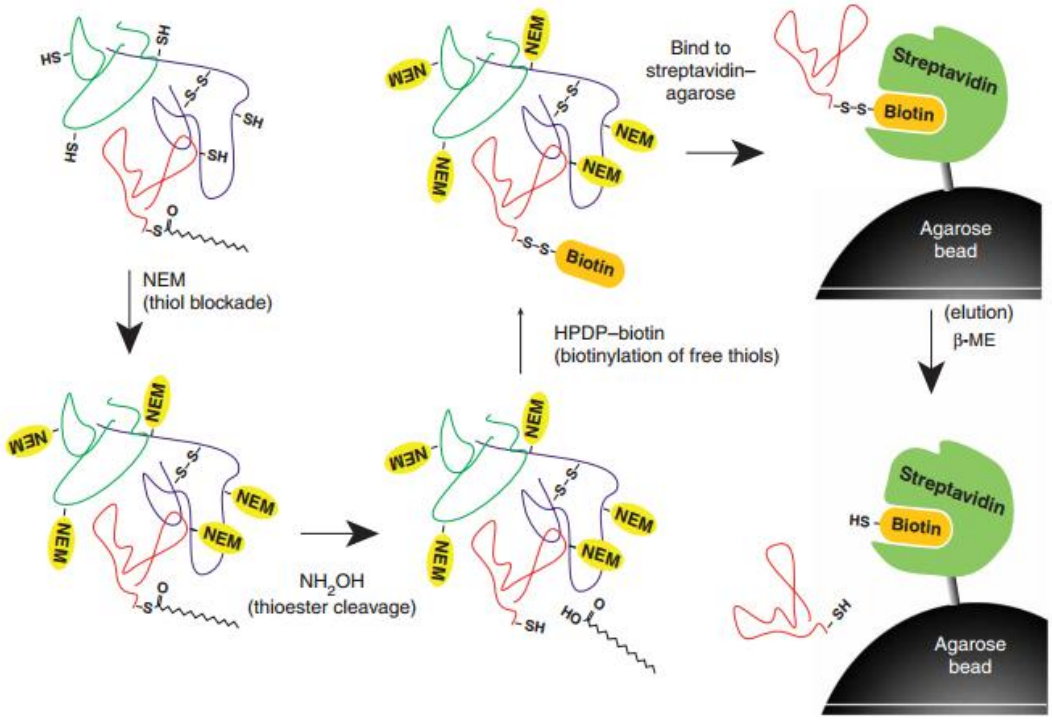

Figure 1.3 Schematic of the ABE chemistry, adapted from reference [110].

1.2.3 Non-Radioactive Metabolic Labeling

In 2009, Martin and Cravatt introduced an alternative approach for palmitoyl detection which utilizes endogenous labeling with the palmitic acid analogue, 17-octadecynoic acid (17-ODYA), and click chemistry [111]. Their method has shown great promise in palmitoyl proteomics using mammalian cell lines [112]. In that study, 17-ODYA was first incorporated into proteins undergoing *in vivo* palmitoylation in cultured cells. With Cu(I) catalysis, the alkyne group on 17-ODYA "clicked" with an azide which had been pre-linked to a reporter molecule. The reporter molecule, either biotin or

rhodamine, allowed the enrichment and detection of palmitoyl proteins, using either MS or non-MS methods (Figure 1.4). In conjunction with mass spectrometry, this approach was used for global profiling of palmitoyl proteins and more than one hundred palmitoyl proteins were identified from Jurkat T-cells [112]. Since it is a metabolic labeling method, a pulse-chase assay can be performed to examine palmitoyl turnover. When combined with the stable isotope labeling by amino acids in cell culture (SILAC) technique [113], differences in globe palmitoyl dynamics under various conditions can be monitored [114]. This approach involves fewer reaction steps compared to the ABE chemistry, resulting in a simpler sample preparation procedure and a significant reduction in sample losses. However, , it is difficult and costly to extend the use of such a metabolic labeling method to study palmitoylation in large organisms. Moreover, 17-ODYA is a potent inhibitor of cytochrome P450 ω-hydroxylase [115], which plays an important role in fatty acid metabolism [116]. The effect of 17-ODYA upon the palmitoyl machinery in living systems is still unclear. In addition, 17-ODYA undergoes degradation by the β-oxidation pathway [117], forming shorter acyl chain analogs which may target *N*-myristoylation sites leading to false discovery of "*S*-palmitoyl" proteins. Relative quantification of protein palmitoylation remains challenging, as the unpalmitoylated proteins are not retained. As discussed below, care must also be taken to minimize loss of palmitoyl groups during each reaction and sample cleanup step.

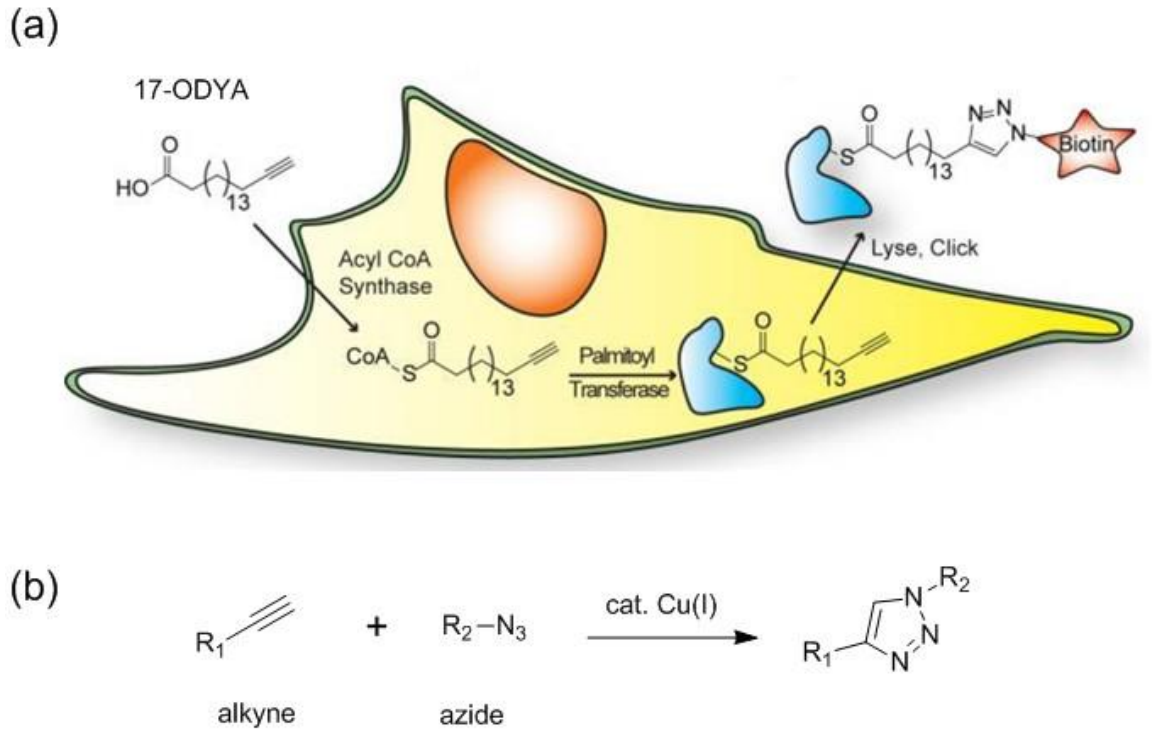

Figure 1.4 (a) Schematic of the detection of protein palmitoylation by metabolic labeling with 17-ODYA followed by click chemistry, adapted from reference [118]; (b) Click chemistry with copper(I)-catalyzed azide-alkyne [3 + 2] cycloaddition (CuAAC).

Chapter 2: Introduction to Mass Spectrometry

MS is an analytical chemistry technique that provides valuable structural information on analytes by measuring their mass-to-charge ratios (*m/z*). Because of its ability to analyze various types of molecules, ranging from biomolecules such as DNA/RNA, proteins, lipids, carbohydrates, and metabolites, to synthetic compounds/polymers, MS is playing an increasingly significant role in numerous fields such as molecular biology, materials science, environmental science, archaeology, drug discovery, and clinical diagnosis.

Modern MS instruments can be coupled to various separation devices, such as a GC, LC, or electrophoresis equipment, allowing the analysis of a complex mixture in a single run that yields rich information. A typical mass spectrometer consists of three main parts: an ion source, a mass analyzer, and a detector. Because MS measures the *m/z* value of analyte ions, a molecule of interest must first be ionized. The molecular ions are then separated based on their mass-to-charge ratios, and their signals are recorded as a function of scan time. Because of its high sensitivity, accuracy, and efficiency, MS is becoming an indispensable and reliable tool for proteomic studies [119]. In this chapter, the most commonly used MS instruments for analysis of proteins/peptides will be reviewed.

2.1 Ion sources

In early days, the application of MS to analyze proteins/peptides was a challenging and not completely achievable goal because there was no fully satisfactory ionization method. Proteins/peptides are large, nonvolatile, and thermally unstable

molecules, and it is difficult to volatilize them in order to utilize long-established ionization methods such as electron ionization (EI) and chemical ionization (CI) without extensive thermal degradation. For a long time, MS techniques were limited to the analysis of small molecules. Tthe emergence of soft ionization methods finally led to the wide-spread application of MS to analyze complex biomolecules and this laid the foundation for modern proteomic studies. Today, the two by far most important soft ionization methods are matrix-assisted laser desorption/ionization (MALDI) and electrospray ionization (ESI).

2.1.1 Matrix-Assisted Laser Desorption/Ionization (MALDI)

MALDI was first reported by Michael Karas and Franz Hillenkamp in 1987 [120]. Before positive-ion MALDI-MS analysis (Figure 2.1), the analyte is usually dissolved in an acidic solution and spotted together with excess matrix molecules on a steel plate. Solvent evaporation leads to the co-crystallization of the analyte with matrix molecules. The steel plate is then placed in vacuum and a pulsed laser,usually a nitrogen laser (337 nm) or the tripled frequency (355 nm) from a Nd:YAG laser for UV-MALDI, is used to irradiate the crystals, leading to the ablation of clusters of matrices with the analyte entrained within. Matrices are usually small molecules with a chromophore that can absorb at the laser wavelength (UV or IR), to assist the evaporation of analytes. The matrix can also serve as the proton donor to facilitate ionization of analytes [121]. The use of a high molar excess of matrix prevents analyte degradation caused by direct laser irradiation. Sinapinic acid (SA), 2,5-dihydroxy benzoic acid (DHB), and α-cyano-4-

hydroxycinnamic acid (CHCA) are the most commonly used matrices for UV-MALDI-MS analysis of proteins and peptides.

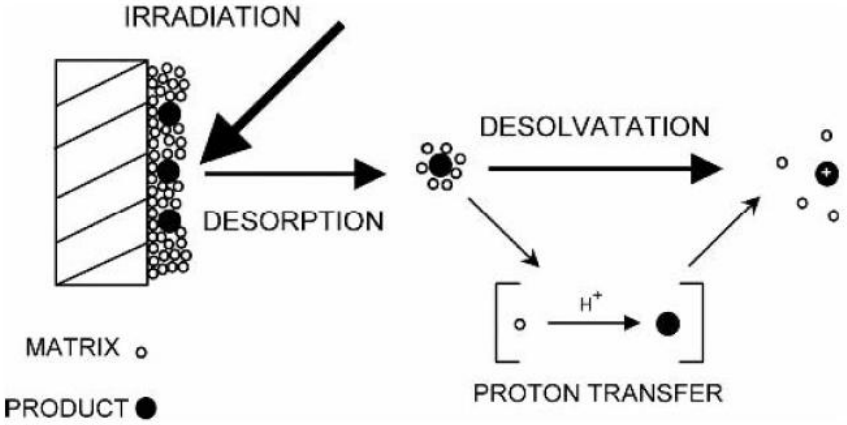

Figure 2.1 Schematic of the MALDI process, adapted from reference [122].

Besides its reputation as a soft ionization technique, the reasons for the wide use of MALDI-MS for protein/peptide analysis include several other advantages. As described above, sample preparation is simple. MALDI has a fairly high salt/contaminant tolerance, and thus, in most cases, good results can be obtained with minimal purification,. For high-throughput analysis, thousands of laser shots can be applied during a burst in a very short time. The peptides in a tryptic digest are predominantly detected as singly charged ions in MALDI mass spectrometry, and this simplifies the spectral interpretation. As a pulsed ionization source, MALDI can be easily coupled to fast Time-of-Flight (TOF) mass spectrometers. MALDI-TOF MS analysis has been extensively used in peptide mass fingerprinting [123] due to its high throughput and easily interpretable spectra. However, the MALDI-MS technique may suffer from poor

reproducibility due to shot-to-shot signal variation, and this can undermine its potential use in quantitative studies, unless internal standards are included. It is difficult to couple online separation to a MALDI source, but offline deposition of chromatographic fractions onto a MALDI plate is straightforward.

2.1.2 Electrospray Ionization (ESI)

Like MALDI, ESI is a widely-used soft ionization technique for modern mass spectrometry analysis, first introduced into the worldwide community by the Nobel Prize winner John Fenn [124, 125]; a parallel development took place in Russia [126]. ESI allows the direct transfer of analytes from solution into the gas phase under atmospheric pressure. Figure 2.2 illustrates the most widely accepted ESI mechanism. The sample solution is loaded to a syringe or capillary, to which a high voltage is applied. The electric field pushes the solution forward, forming a Taylor cone at the end of the tip. Charged droplets continuously bud from the Taylor cone when the electrostatic force overcomes the surface tension. Utilization of a nebulizer gas in this step can facilitate the formation of a fine mist of charged droplets. Charged droplets then undergo evaporation, usually with the assistance of a flow of bath gas as well as a heated transfer capillary, during their travel to the analyzer inlet, leading to shrinkage of droplets and increase in their surface charge density. The larger droplets break apart to form smaller droplets in a process termed Coulomb fission, when the surface tension of the shrinking droplets can no longer withstand the increased charge repulsion at the Rayleigh limit. This solvent evaporation/Coulomb fission cycle repeats until each droplet carries a single analyte

molecule within, from which the naked, charged analyte is produced by further evaporation of solvent molecules [127, 128].

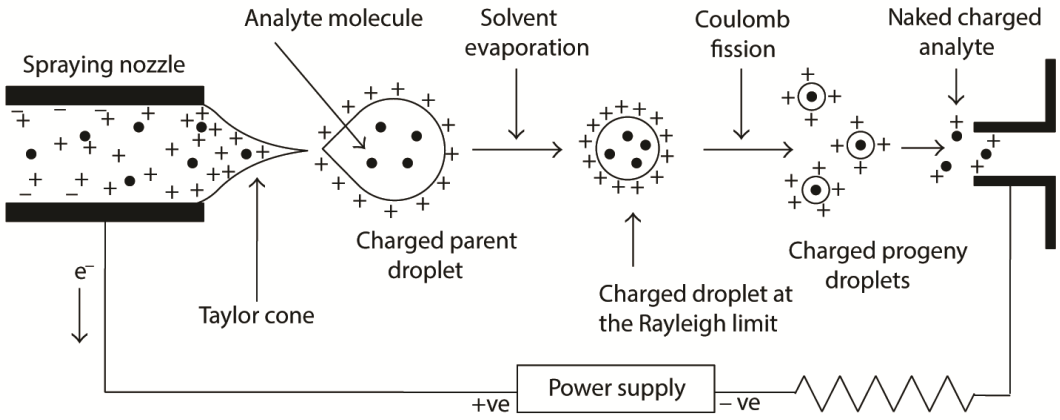

Figure 2.2 Schematic of the proposed ESI mechanism, adapted from reference [128].

ESI offers several advantages over other ionization techniques. First and foremost, since analytes are ionized and transferred to the gas phase from a continuously flowing solution, ESI can be coupled to online HPLC or capillary electrophoresis (CE), allowing the qualitative and quantitative analysis of complex samples with high sensitivity and reproducibility. Second, ESI often produces ions with multiple charges, and this significantly extends the upper mass detection limit of mass spectrometers, a property which is particularly useful for mass analyzers with limited *m/z* ranges. Third, because the desolvation process during ESI consumes energy, analytes can be efficiently cooled and only a small amount of energy is deposited to the analyte ions before mass analysis. Thus, ESI is an even softer ionization technique than MALDI, and more easily capable of preserving non-covalent interactions. However, ESI often requires extra

sample cleanup steps, because ESI does not work well with samples containing salts, detergents or other contaminants, and even a small amount of impurity may lead to significant reduction (or complete suppression) of the analyte signal.

2.2 Mass Analyzers and Detectors

A mass analyzer measures the mass-to-charge ratios of ions and is the central part of the mass spectrometer. Transmission efficiency, mass resolution, and mass accuracy are the key parameters for the performance of a mass analyzer. Transmission efficiency corresponds to the percentage of ions that actually reach the detector from the ion source. Transmission efficiency affects the instrument sensitivity, a parameter referring to the minimum sample amount required to produce detectable MS signals; high sensitivity is especially important for analyzing low-abundance samples. Mass resolution or mass resolving power describes the ability of a mass analyzer to distinguish ions with closely separated *m/z* values and can be calculated as the ratio of the *m/z* of a peak divided by its width, usually determined at the half maximum height. The absolute mass accuracy is the difference between the experimental and theoretical *m/z* values, and it is often expressed in a relative term as the ratio of the mass measurement error to the theoretical mass in parts-per-million (ppm). High mass accuracy (low mass measurement error) is crucial for confident identification.

2.2.1 Time-of-Flight (TOF)

As its name indicates, a time-of-flight mass analyzer determines the *m/z* value of an ion by measuring its transit time from the ion source to the detector. A TOF analyzer

requires a pulsed ion beam, and thus it is usually coupled with a MALDI ion source, but it can also be coupled with an ESI source via orthogonal ion injection, as implemented in Q-o-TOF and FT MS instruments. The MALDI-TOF MS is one of the most commonly used MS instruments, due to its low cost, ease of sample preparation, user friendly operation, and relatively high sensitivity and mass resolution. In a MALDI-TOF MS measurement, a burst of ions extracted from the MALDI plate are accelerated by a static electric field and all ions carrying the same charge (*z*) will gain the same kinetic energy (E_k), which is expressed as:

$$E_k = \frac{1}{2}mv^2 = zeV \qquad \text{Eqn. 2.1}$$

where *m* and *z* are the mass and charge of the ion, respectively, *v* is the velocity of the ion as it exits the ion source, *e* is the elemental charge, and *V* is the accelerating potential. After acceleration, all ions traverse a field-free flight tube in vacuum to reach the detector. Assuming the length of the tube is *L*, the flight time of an ion can be calculated as:

$$t = \frac{L}{v} \qquad \text{Eqn. 2.2}$$

Combining the Equations 2.1 and 2.2 yields:

$$t^2 = \frac{L^2}{2eV} \times \frac{m}{z} \qquad \text{Eqn. 2.3}$$

The equations above outline the principle of operation for a TOF mass analyzer: ions with a higher *m/z* travel with a lower velocity and thus more slowly than ions with a lower *m/z*, so they take a longer time to reach the detector. For a given accelerating

potential (V) and distance of flight (L), the *m/z* value of an ion scales quadratically with its time of flight [122].

The linear MALDI-TOF MS design, as described above, suffers from its poor mass resolution because ions produced from a MALDI source have different initial velocities as well as a certain degree of temporal and spatial distributions, and therefore ions with same *m/z* do not all arrive at the detector simultaneously; this leads to peak broadening. Two techniques have been widely implemented in modern MALDI-TOF instruments to improve the mass resolution: pulsed-delayed extraction and the reflectron geometry. Figure 2.3 illustrates the schematic of a MALDI-TOF/TOF instrument with pulsed-delayed extraction and a reflectron. The pulsed-delayed extraction is accomplished by two-stage ion acceleration. The extraction voltage (U_e) is applied to the sample plate following a short time delay (usually several hundred nanoseconds) after ions are produced by the pulsed laser desorption/ionization. The underlying principle is that slower ions will not travel as far from the sample plate during the delay, and, when the extraction voltage is applied, they will stay in the extraction electric field longer and obtain more kinetic energy. When the delay time and accelerating voltage are properly chosen, ions with a lower initial velocity will emerge from the extraction field with a slightly higher final velocity, allowing them to catch up, at the detector, with ions with a higher initial velocity. The optimal extraction voltage is mass-dependent and linear to the *m/z* of ions being focused [129]; the user has to adjust the voltage and delay time in order to optimize the results. Use of a reflectron, rather than a simple linear flight tube, is another strategy to compensate for the initial kinetic energy spread of ions. A reflectron is

an electrostatic device that sits between two stages of the flight tube that can be physically the same but traversed in opposite directions. It acts as an ion mirror that creates a retarding electric field where ions can be deflected and sent into the second stage of the flight tube. Ions that enter the reflectron are subjected to deceleration by the electric field. Their velocities will eventually reach zero, at which point ions begin to move in the opposite direction and regain the lost kinetic energy before they are expelled from the reflectron. Ions with higher kinetic energies penetrate more deeply into the retarding field and spend more time in the reflectron than ions with lower kinetic energy, thus compensating for a shorter flight time outside of the reflectron, and leading to improved mass resolution.

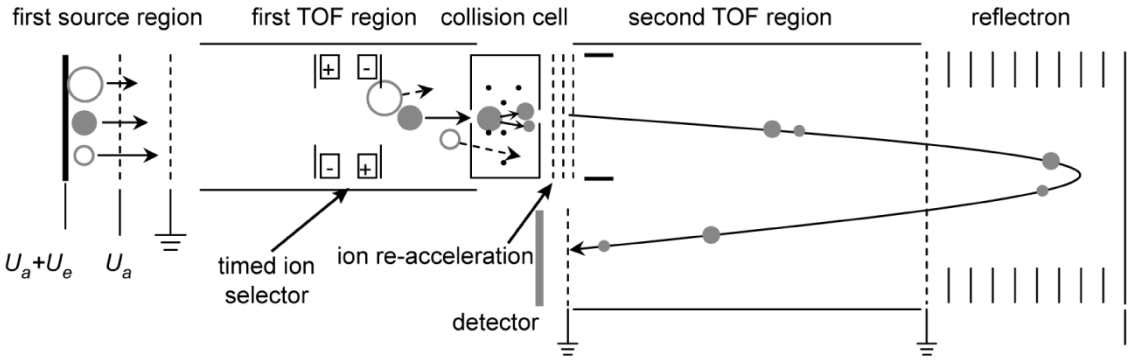

Figure 2.3 Schematic of a MALDI-TOF/TOF instrument, adapted from reference [130].

2.2.2 Quadrupole Mass Analyzer

A quadrupole mass analyzer consists of four parallel metal rods that are symmetrically assembled around the z axis (Figure 2.4). In order for ions to reach the detector, they must have stable trajectories inside the quadrupole. A quadrupole is

operated in such a way that opposite potentials ($\emptyset_0$ and -$\emptyset_0$) are applied to the two pairs of opposing rods to create a quadrupolar electric field:

$$\emptyset_0 = +(U + Vcos\ \omega t)\ \ and\ \ -\emptyset_0 = -(U + Vcos\ \omega t) \qquad \text{Eqn. 2.4}$$

where *U* is direct current (DC) voltage, *V* is radio frequency (RF) voltage oscillating at a frequency of ω, and *t* is the time. Whereas the quadrupolar field contains no z-component, allowing ions to traverse the quadrupole unhindered, ion motion in the x and y directions is very complex and governed by the oscillating electric field. The ion trajectory must remain bound in both the x and y directions in order for ions to travel through the quadrupole without striking the rods. Figure 2.5 shows the stability diagram for an ion and depicts the first stability region in the *U/V* space where ion motion is confined in both x and y directions. The stability regions of ions with different *m/z* values have the same shape, but their dimensions scale linearly with the ion *m/z* value. During a scanning event, *U* and *V* are successively increased, at a fixed ratio along the operating line, allowing the sequential transfer and detection of ions with increasingly higher *m/z* values. The *U/V* ratio is a user-defined value that controls the resolving power of the quadrupole mass analyzer: a higher *U/V* ratio leads to a higher resolving power. However, achieving the highest resolving power also comes at the price of reduced ion transmission efficiency (sensitivity) and scan speed (throughput), and one must make a compromise to obtain the best result, based on the objectives of the experiment.

A quadrupole can function not only as a mass filter but also as an ion guide. By setting the proper *U* and *V* values, only ions with the selected *m/z* value can be transmitted through the quadrupole, while ions with other *m/z* values will have unstable

trajectories and strike the rods. When operated in the RF-only mode (U = 0), a quadrupole allows all ions above a certain *m/z* cutoff to pass though, turning it into an ion guide or an ion focusing device. A triple quadrupole mass spectrometer (QqQ), consisting of three quadrupoles (Q1, q2, and Q3), as its name suggests, is a good example to illustrate the versatility of quadrupole instruments. While Q1 and Q3 are mass analyzers, q2 operates exclusively in the RF-only mode, serving as an ion transfer device and collision cell. A triple quadrupole instrument may be operated under several modes, depending on whether Q1 and Q3 operate in the scanning mode or as mass filters. In the MS/MS mode, also known as the product ion scanning mode, Q1 works as a mass filter, transmitting ions of interest to q2, where they are subjected to dissociation, usually collision-induced dissociation (CID). All fragment ions and the remaining precursor ions are subsequently focused and guided into Q3, where they are mass analyzed, thus providing detailed structural information on the precursor ion. Another common operating mode for a triple quadrupole instrument is the selective reaction monitoring (SRM) or multiple reaction monitoring (MRM) mode, where Q1 is tuned to transmit a selected precursor ion of interest and Q3 is tuned to transmit a specific fragment ion from that precursor ion. The SRM mode monitors a specific "transition" of a compound rather than its mass alone, which leads to improved confidence and S/N ratio in the monitoring of a preselected component, especially in complex samples.

Quadrupole mass analyzers are widely used because they are inexpensive, easy to build and operate. They are characterized by their high transmission efficiency and fast scan rate. A quadrupole mass analyzer has a mass range up to around *m/z* 4000 (though

often lower), and can be used to analyze large highly charged biomolecules when coupled to an ESI source. However, the mass resolution of quadrupole mass analyzers is typically low, up to a few thousand at best.

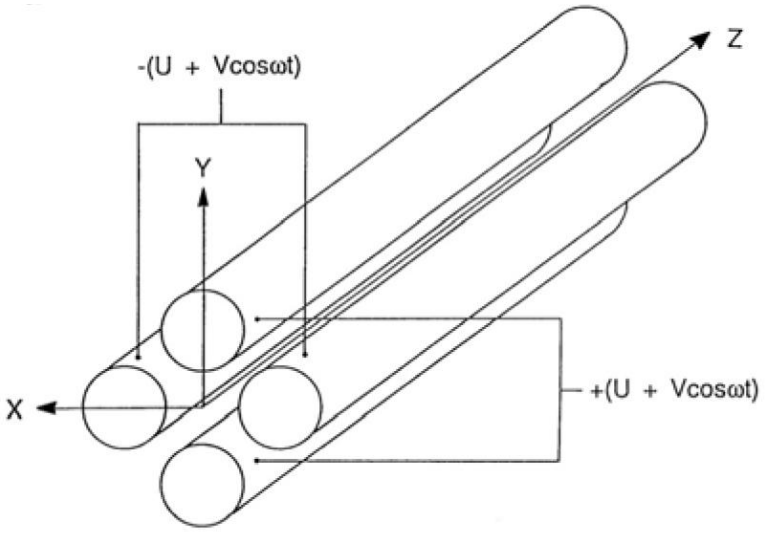

Figure 2.4 Schematic of a quadrupole mass spectrometer, adapted from reference [131].

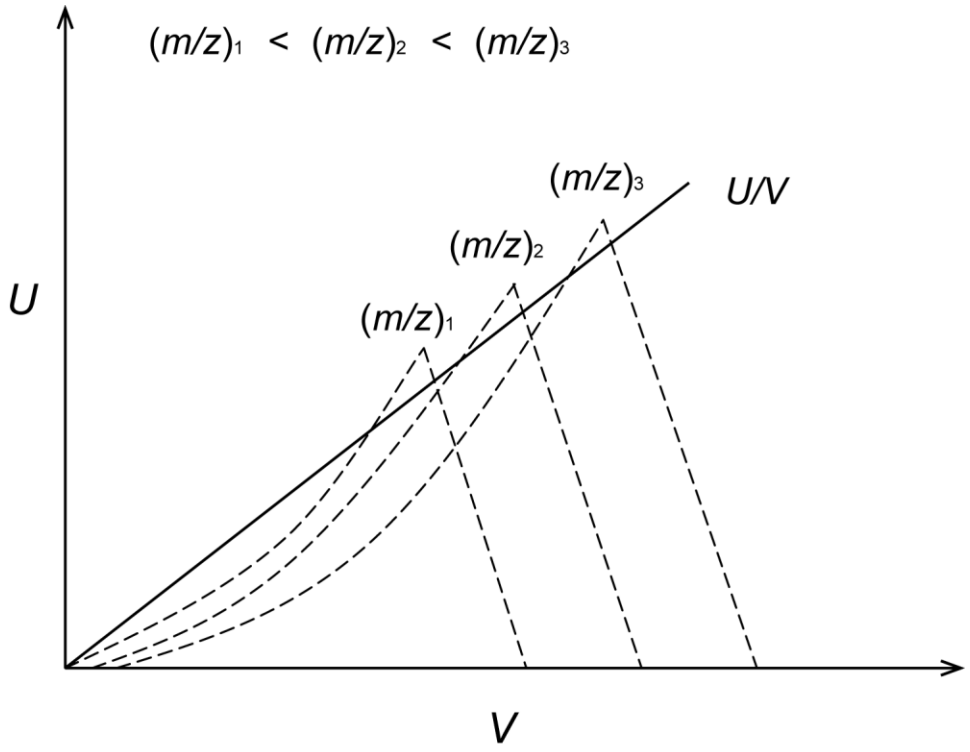

Figure 2.5 The stability diagrams of ions with different *m/z* values in the *U/V* space.

2.2.3 Linear Quadrupole Ion Trap (LIT/LTQ)

A linear ion trap (LIT) is a mass analyzer built with three sets of RF-only quadrupoles arranged in a linear configuration (Figure 2.6). A differential RF potential is applied to all three sets of quadrupoles to trap the ions along the x and y directions (or radially), whereas a DC potential is superimposed on the two end quadrupoles to confine ion motion along the z direction (or axially). During an MS scan cycle, a packet of ions is first injected into the LIT and trapped there. A gas such as helium is commonly used to cool down the ions without introducing fragmentation, and focus them to the center of the LIT. The amplitude of the main RF potential, *V*, is then ramped up, which moves the ions out of their stability regions, and ejects the ions radially, from low *m/z* ions to high *m/z*

ions. An auxiliary alternate current (AC) voltage at a fixed frequency is often applied to the x-rods during the main RF ramp to facilitate rapid resonant ejection of the ions, which not only improves the scanning speed and mass resolution, but also increases the upper mass detection limit. Besides functioning as a mass analyzer, an LIT can also be used to perform CID experiments. During an MS/MS event, ions with a specific *m/z* value are isolated by applying resonance ejection voltage to x-rods at the secular frequencies of all ions except for the ion of interest, and this leads to the ejection of all unwanted ions from the trap. The ions selected as precursors are then excited by collision with the neutral gas molecules inside the trap to produce fragment ions. Note that there is a trade-off between the extent of fragmentation and the observation of low mass product ions, as a higher energy deposition in the precursor ions requires the main RF to operate at a higher amplitude, and this unfortunately leads to an increase in the low-mass cutoff of the LIT and the loss of low mass fragment ions from the trap.

As described above, LIT is an ion trapping device. Precursor ion isolation, fragmentation, and analysis of product ions can be conducted sequentially in one place in the LIT, whereas precursor and product ion analyses are performed in two physically separated mass analyzers in other tandem instruments, *e.g.*, triple quadrupole instruments. Consequently, it is possible to perform multi-stage tandem MS analysis (known as an MS^n experiment) in an LIT. An LIT also has a large ion trapping capacity and space charge effect that is reduced compared to a 3D ion trap [132]. An LIT can either serve as a stand-alone mass spectrometer, or be combined with another mass analyzer to form a hybrid MS instrument such as the LTQ-Orbitrap.

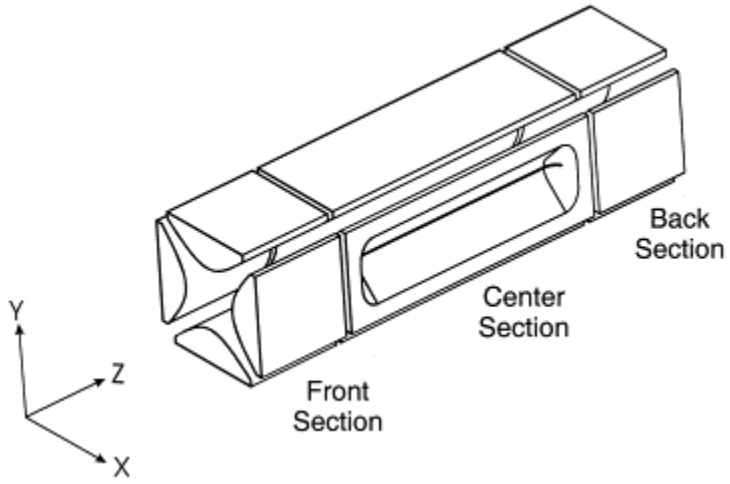

Figure 2.6 Schematic of a linear ion trap, adapted from reference [133].

2.2.4 Fourier Transform Ion Cyclotron Resonance (FTICR)

The major components of an FTICR mass analyzer are a magnet and three pairs of electrodes which form an ICR cell. An ICR cell uses the combination of a homogeneous magnetic field and an inhomogeneous electric field to trap the ions. For a cubic ICR cell (Figure 2.7), two pairs of electrode plates, placed in parallel with the magnetic field and oriented along the z axis, are used for ion excitation and detection, respectively, and a third pair of plates (trapping plates), positioned perpendicular to the z axis, are responsible for the axial ion confinement. An ion in a homogenous magnetic field experiences a Lorentz force ($F = qv \otimes B$) which is perpendicular to its velocity, *v*, and the direction of the magnetic field, *B*. The Lorentz force is always normal to the direction of the ion motion, leading to the cyclotron motion of an ion about the z axis.

The cyclotron frequency of an ion in a constant magnetic field is inversely proportional to its mass-to-charge ratio, as described by the equation below:

$$f_c = \frac{qB}{2\pi m} \qquad \text{Eqn. 2.5}$$

where f_c is the cyclotron frequency, q is the ion charge, B is the strength of magnetic field, and m is ion mass. Therefore the mass-to-charge ratio of an ion can be determined by measuring its cyclotron frequency [122].

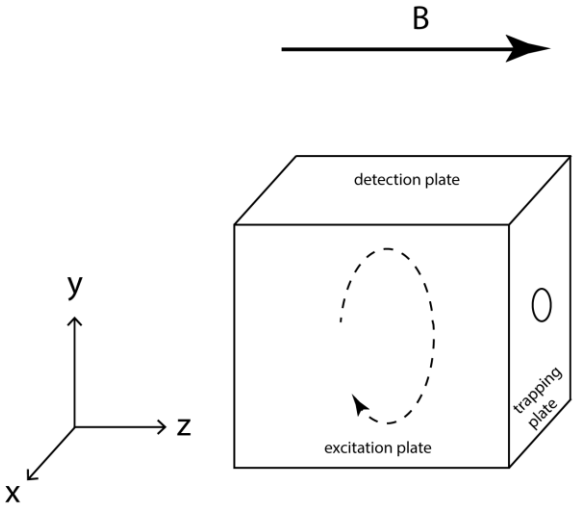

Figure 2.7 Schematic of a cubic ICR cell and the ion cyclotron motion.

In a typical FTICR MS experiment, ions are injected into the ICR cell with low kinetic energy, so that they can be trapped with a low electric potential applied to the trapping plates. Trapped ions undergo cyclotron motion in the center of the ICR cell, but their signals cannot be detected because the thermal cyclotron radii are too small for the ions to produce a measurable signal, and, more importantly, the initial cyclotron motions of ions are out of phase and thus the small signals produced by their incoherent ion

motions would cancel out. A frequency-sweeping RF voltage which contains the cyclotron frequencies of ions with a wide range of *m/z* values, is applied to the excitation plates, bringing all ions to larger orbits in coherent motion. The cyclotron motions of the excited ions induce alternating currents at the detector plate (known as image currents) which are subsequently amplified and recorded as a time domain transient [134]. Fast Fourier Transform (FFT) of the transient is then performed to generate a frequency domain spectrum that can be subsequently converted into a mass spectrum via mass calibration.

Although the ICR mass analyzer is operated in a pulsed mode, it can be easily coupled to a continuous ion source by gated ion trapping. Commercial FTICR instruments are often coupled to an external ion isolation and storage device. Figure 2.8 illustrates the schematic of the solariX Qh-FTICR, a hybrid MS instrument built by Bruker Daltonics. It contains a dual MALDI/ESI source, two ion funnels, a negative chemical ionization (nCI) source, a split octopole, a mass selecting quadrupole, a collision cell, an ion transfer guide, and an ICR cell. Briefly, ions are focused and transferred to the first quadrupole (Q) where ions of interest can be isolated and guided to the collision cell. The ions of interest can be accumulated in the collision cell, and they may undergo CID or electron transfer dissociation (ETD) in this cell. From there, ions are transferred into the ICR cell for mass analysis or tandem MS analysis. Unlike the RF-only ion trap, an ICR cell offers a unique capability in that the magnetic field can efficiently confine the radial electron motion, allowing the performance of electron capture dissociation (ECD), a soft fragmentation method that can retain labile PTMs. In

addition, an FTICR mass analyzer offers superior mass resolving power and mass accuracy, making it well suited for *de novo* sequencing and top-down analysis.

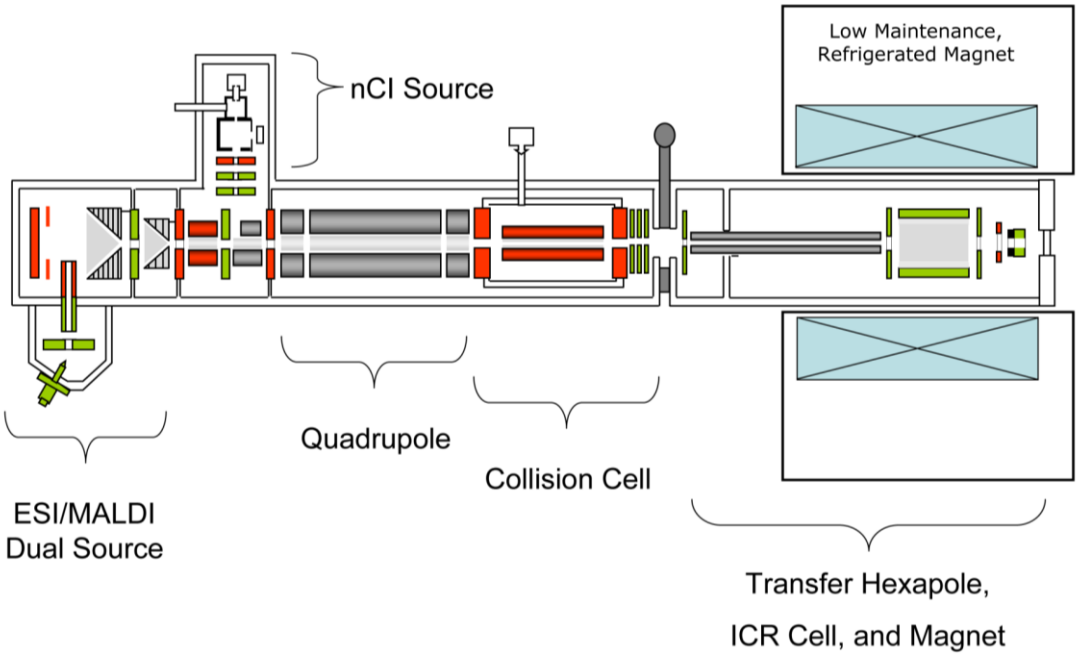

Figure 2.8 Schematic of a solariX^{TM} Fourier transform ion cyclotron resonance mass spectrometer, adapted from the user manual (Bruker Daltonics).

2.2.5 Orbitrap

An Orbitrap is an electrostatic ion trap with a spindle-like inner electrode and a barrel-like outer electrode which is split in the middle (Figure 2.9). Ion trajectories inside an Orbitrap consist of three periodic motions: rotation around the z axis, radial oscillation, and axial oscillation along the z axis. Whereas the rotational frequency (ω_φ) and the radial oscillation frequency (ω_r) are affected by the initial ion velocity and position, the

axial oscillation frequency (ω_z) only depends on the *m/z* values of the ions and the instrument parameters as shown in the equation below:

$$\omega_z = \sqrt{\frac{k}{m/z}} \qquad \text{Eqn. 2.6}$$

where *k* is the field curvature. Thus, ions with the same *m/z* form a packet and oscillate harmonically along the z direction in the shape of a thin ring around the inner electrode, and this motion produces a small alternating image current between the two halves of the outer electrode, the frequency of which can be obtained by performing FFT on the recorded transient, and thereafter used to generate the mass spectrum.

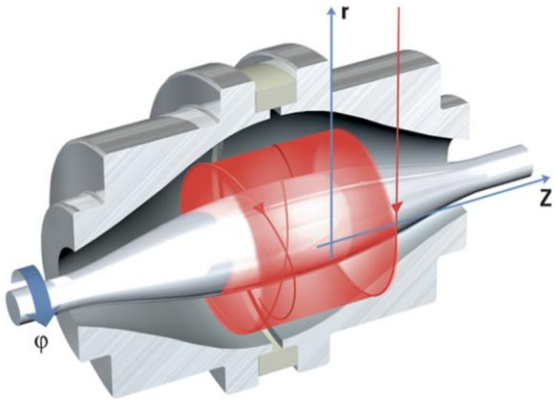

Figure 2.9 The cutaway view of an Orbitrap mass spectrometer, adapted from reference [134].

The Orbitrap has become the mass analyzer most frequently employed in proteomic studies, owing to its high sensitivity, very high mass resolving power and accuracy, and wide mass range. Figure 2.10 illustrates the schematic of a commercially available

Orbitrap instrument, known as the LTQ-Orbitrap Velos™ hybrid mass spectrometer. It is made up of an ESI source, a series of ion transfer optics, a dual pressure LTQ/LIT, a C-trap, an Orbitrap, and a higher-energy collisional dissociation (HCD) collision cell. Ions pass through a series of ion lenses and multipoles, that are operated with stepwise decreasing pressures, to the LTQ where they can be stored, isolated, and fragmented. The resulting ions can either be ejected radially for LTQ detection, or injected axially into the C trap. The C trap is a curved linear quadrupole ion trap which cools the ions and focuses them within a small volume, then injects them tangentially ,, into the Orbitrap, as a tight packet. The inner electrode potential is then increased, and the ion packets are squeezed to the center of the electrode and begin coherent axial oscillations at various frequencies according to their *m/z* values. The Orbitrap can also receive ions produced in the HCD collision cell, an octopole device where precursor ions can undergo higher energy fragmentation. The Orbitrap does not suffer from the low mass cutoff issue that is encountered in an LTQ and is thus suitable for detection of low molecular weight reporter ions and immonium ions.

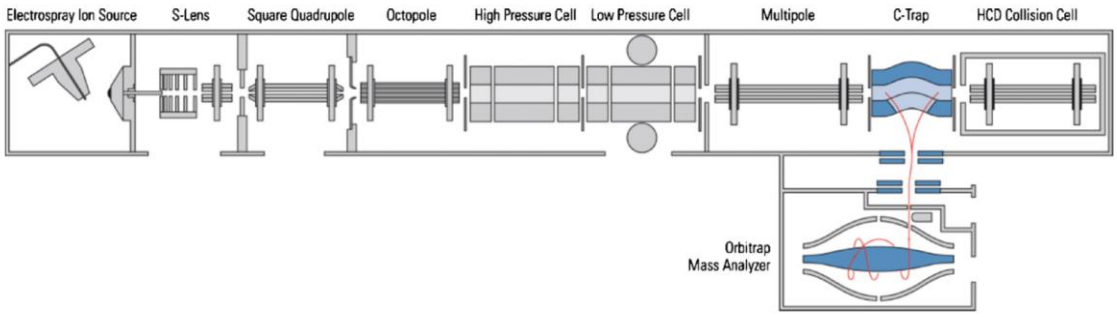

Figure 2.10 Schematic of an LTQ-Orbitrap Velos mass spectrometer, adapted from reference [135].

2.3 Application of Mass Spectrometry to Proteomic Studies

MS is the enabling technique for modern proteomic studies, due to its high efficiency, sensitivity, and accuracy. It is widely used for protein sequence determination, quantification, characterization of PTMs, study of protein-protein interactions, among other tasks. The success of MS-based proteomics stems from the in-depth development of protein/peptide preparation/separation techniques, ionization methods, gas-phase fragmentation methods, spectral interpretation and bioinformatics software and relevant databases. Bottom-up proteomics, which involves proteolytic digestion, is by far the most widely-used approach for MS-based proteomics. In a bottom-up proteomics experiment, the total complement of proteins from the biological samples, either tissues or cell pellets, are first extracted with a lysis buffer, usually in combination with sonication and/or homogenization. Proteolytic digestion of proteins of interest (or total proteins) is then performed either in-gel or in-solution, usually by trypsin, leading to the conversion of proteins into peptide fragments that are subsequently analyzed by mass spectrometry. In an approach commonly referred to as the peptide mass fingerprinting (PMF), the set of peptide masses obtained from the MS measurement can be compared to predicted sets generated by *in silico* digestion of proteins in a database, to deduce the presence of certain proteins. However, it is very likely that one peptide mass can be assigned to multiple sequences in the database, potentially leading to erroneous identifications even when multiple highly accurate peptide masses are used. In order to improve the confidence of peptide assignments, peptides of interest can be isolated and subjected to

tandem MS (MS/MS) analysis, whereby each selected peptide is fragmented to produce pieces that can be used to deduce the peptide sequence. In contrast to the bottom-up analysis, top-down proteomics is a method used to analyze proteins without enzymatic digestion or chemical cleavage. Intact proteins are sent directly into the mass spectrometer where their masses can be determined and their fragments can be generated in the gas phase to deduce the protein sequence and to identify PTMs. These two approaches can be used independently, or in parallel. Regardless of the method of choice, tandem MS analysis has become an integral part of confident protein sequencing. Moreover, tandem MS analysis also plays an important role in isotope-coded affinity tag (ICAT)- and tandem mass tag (TMT)-based protein quantification. The next section reviews the tandem MS methods that are widely used in protein analysis.

2.3.1 Tandem Mass Spectrometry

Proteins and peptides are linear biopolymers made up from the 20 naturally occurring amino acids as the building blocks which are linked by amide bonds, as illustrated in Figure 2.11. There are three types of chemical bonds along the backbone of proteins/peptides: the Cα-C(carbonyl) bond, the amide bond, and the N-Cα bond. Cleavage of these bonds gives rise to three pairs of fragment ions which are classified into two categories [136]: N-terminal fragments which are defined as *a*-, *b*-, and *c*-type ions, and C-terminal fragments which are labeled as *x*-, *y*-, and *z*-type ions (Figure 2.11). Only those fragments that retain at least one charge can be detected. Backbone fragments are essential for determining the protein/peptide sequence. The mass difference between two adjacent fragment ions of the same type can be used to assign the amino acid

increment that differentiates these two fragments. In principle, the full sequence can be deduced *de novo* if all inter-residue cleavages are observed. In practice, even the reconstruction of a partial sequence (or a sequence tag) can significantly improve the confidence of assignment. Besides the backbone fragment ions, tandem MS analysis may also produce other types of ions, such as satellite (backbone plus side chain cleavage) ions (*d*-, *v*-, and *w*- ions), immonium ions, and internal fragment ions; these ions, although adding complexity to the tandem mass spectra, may also provide valuable information for sequencing.

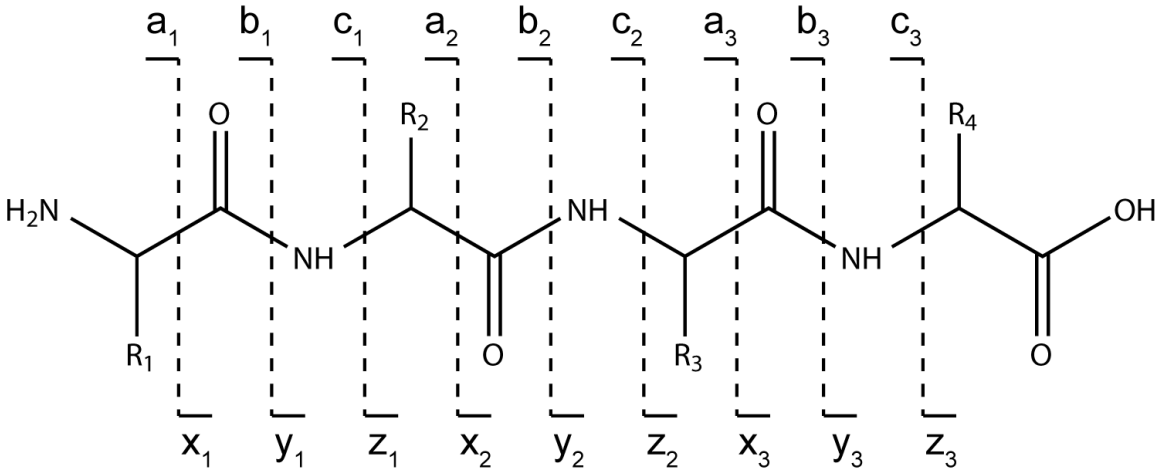

Figure 2.11 Nomenclature of peptide backbone fragmentation, adapted from reference [137].

2.3.1.1 Collision-Induced Dissociation (CID), including Higher Energy Dissociation (HCD)

CID, also known as collisionally activated dissociation (CAD), is a widely used tandem MS technique to dissociate protein/peptide ions in the gas phase. During the CID process, ions collide with neutral gas molecules (*e.g.* He, N_2, or Ar) and a portion of the translational energy is converted to internal energy, leading to the decomposition of the activated ions, producing mainly *b*- and *y*- ions. CID can be further classified into three categories based on the magnitude of the collisional energy, which influences the rate and extent of energy deposit [138]:

High-Energy CID (Fast Activation)

High-energy CID is usually performed on a magnetic/electric sector or TOF/TOF instrument. Ions are accelerated to gain several kilo-electron volts (keV) of kinetic energy as they enter the collision cell. In addition, the gas (usually He) pressure in the collision cell is adjusted to a level at which only a single or a few (< five) collision(s) take place during the ion's residence time there. The collision event (or the ion activation event) occurs within a very short time frame (several microseconds), due to the high kinetic energy of the ions and the low gas density. It is believed that protonated proteins/peptides are activated by high-energy CID mainly fragment via charge-remote pathways, because the energy deposition to the ions is sufficiently high. Besides producing *b*- and *y*- type ions as seen in other types of CID experiments, high-energy CID can also generate fragment ions that exhibit side chain losses, which are especially useful for differentiation of isomeric residues, *e.g.*, leucine and isoleucine [139].

Low-Energy CID (Slow Activation)

CID experiments performed in RF-only quadrupole or other multipole devices are characterized by a collision energy of less than 100 eV, and are commonly referred to as low-energy CID. The gas pressure is optimized to allow precursor ions to collide with the gas molecules multiple times (up to a few hundred times), with a small amount of energy being deposited into the ions during each collision event. The longer activation time in low-energy CID (usually varying from hundreds of microseconds to a few milliseconds) significantly improves the fragmentation efficiency. The other advantage of using a multipole device as the collision cell is that fragment ions can be focused after collision. Instead of direct amide bond cleavage, which requires a high energy input, the backbone cleavage of protonated proteins/peptides in low-energy CID is believed to be triggered by mobile protons and to follow a charge-directed fragmentation pathway [140]. In the mobile proton model, the energy deposited in the ions facilitates the transfer of a proton from basic residues such as the guanidine group on arginine, or the amino group on lysine or the peptide N-terminus, to the backbone amide nitrogen or carbonyl oxygen. The protonation of the amide nitrogen or carbonyl oxygen not only weakens the amide bond, but also increases the electrophilicity of the corresponding amide carbon. Backbone cleavage is subsequently initiated by the nucleophilic attack of the oxygen from the N-terminal neighboring amide bond to the amide carbon atom, forming an oxazolone *b* ion and a *y*-ion (Figure 2.12) [140, 141]. Commercial instruments utilizing low-energy CID include triple-quadrupole (QqQ), quadrupole time-of-flight (Q-TOF), and hybrid FTICR mass spectrometers. It needs to be pointed out that the HCD that takes place in the

octopole collision cell, at the far end of the C-trap in the LTQ-Orbitrap and Q-Exactive instruments, falls into upper energy range of this category and may produce side-chain as well as backbone cleavages.

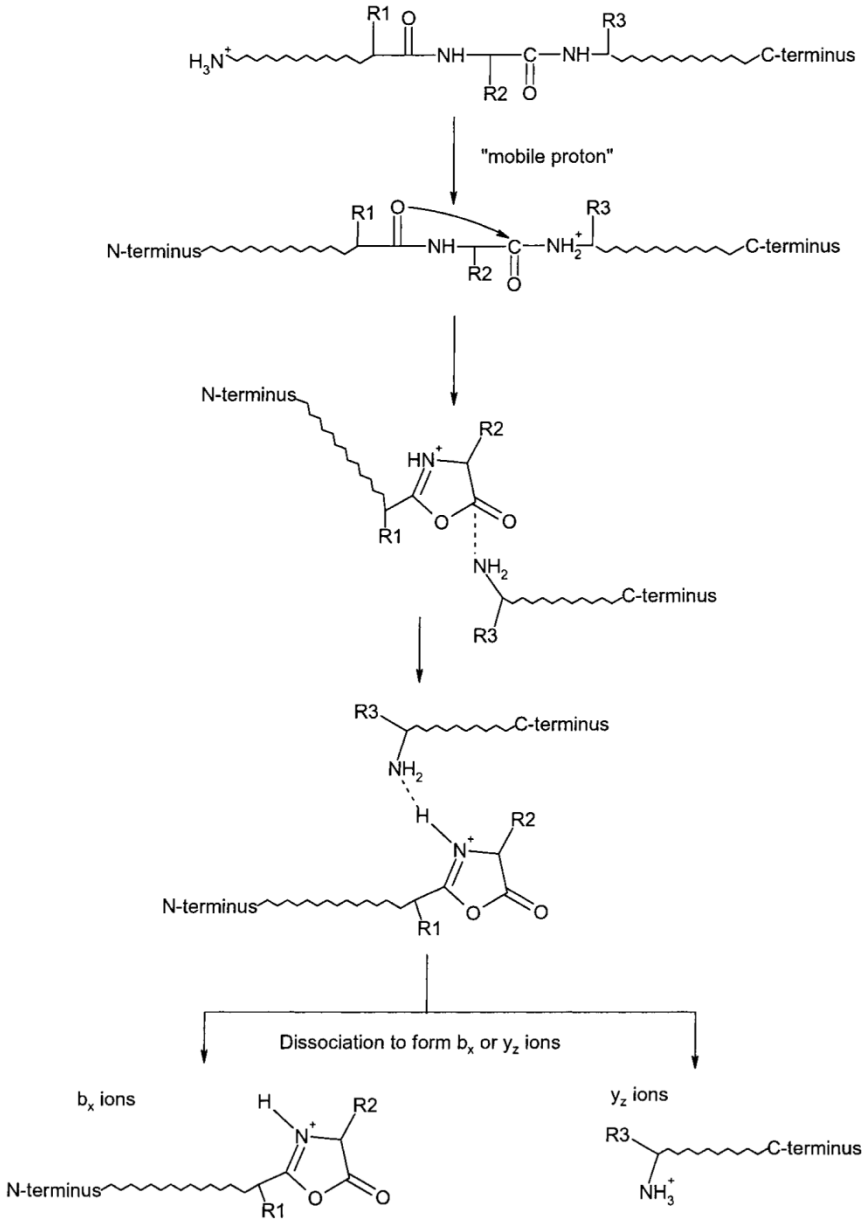

Figure 2.12 The oxazolone pathway in the low energy CID process, adapted from reference [141].

Ion-Trap CID (Very Slow Activation, Slow Heating)

CID performed in ion trap instruments such as LIT, QIT, and the ICR cell takes advantage of the ion residence time inside the trap that is longer than in collision cells. Ions are resonantly excited to gain only a few eV of kinetic energy, and this allows multiple collisions to take place during a very long time window (tens to hundreds of milliseconds). Ion activation is also accompanied by deactivation processes such as collisional cooling and/or IR emission [132]. Consequently, the ion internal energy is built up slowly and can achieve extremely high dissociation efficiency. Such a slow heating method is known to be able to efficiently dissociate high mass ions [142]. However, because ion-trap CID is a slow heating method, it preferentially breaks the weakest bond in a molecule, and is not well-suited for characterization of labile modifications. Further, as mentioned before, detection of the products from low-energy CID performed in a quadrupole ion trap (LIT or QIT) is limited by the low-mass cutoff issue.

2.3.1.2 Electron-Capture Dissociation (ECD)

ECD is another fragmentation method that can induce efficient dissociation of proteins and peptides. It was first introduced by McLafferty and Zubarev in 1998 [143]. In ECD, multiply charged protein or peptide ions are irradiated by low-energy electrons (< 0.2 eV) which can be captured at a protonated site. The electron capture is an exothermic process resulting in the release of ~6 eV of recombination energy. Instead of undergoing internal energy randomization, the released energy is used locally to induce

peptide backbone cleavages via a nonergodic process. The classic ECD fragmentation mechanism (also known as the Cornell mechanism) proposed by Zubarev is illustrated in Figure 2.13. The addition of an electron to a protonated amine group ($R\text{-}NH_3^+$) produces an odd electron species ($R\text{-}NH_3^{\bullet}$). An $H^{\bullet}$ can dissociate from $R\text{-}NH_3^{\bullet}$ and migrate to an amide carbonyl group which has a higher $H^{\bullet}$ affinity than the amine group. The resulting carbon-centered aminoketyl radical intermediate induces $N\text{-}C_{\alpha}$ cleavage to produce *c*- and *z*-type ions[144]. Compared to CID, ECD has the advantage of being able to generate extensive backbone cleavages while preserving the types of labile PTMs (*e.g.* phosphorylation and glycosylation) that are often lost during CID. In addition, disulfide bond cleavage is favored by the ECD process, presumably because of the higher hydrogen affinity of the sulfhydryl group ($H^{\bullet}$ affinity: sulfhydryl group > amide carbonyl group > amino group) [145]. Moreover, isomeric amino acid residues, *e.g.*,aspartic and isoaspartic acids, can be distinguished by ECD through secondary, radical-induced side chain cleavage [146].

The nonergodic premise in the Cornell mechanism was later challenged by the Utah-Washington mechanism which maintains that electron capture can occur directly at a backbone amide site, with sufficient Coulomb stabilization. The subject of ECD mechanism(s) has been extensively reviewed [147, 148], and will not be discussed further here. Despite its many advantages, the use of ECD has been limited because its implementation is largely restricted to expensive FTICR instruments. Additionally, ECD is only applicable to multiply charged precursor ions, and its dissociation efficiency is relatively low. Finally, it is important to recognize that CID and ECD are complementary

methods, and thus it is desirable to combine the information obtained from both, whenever possible.

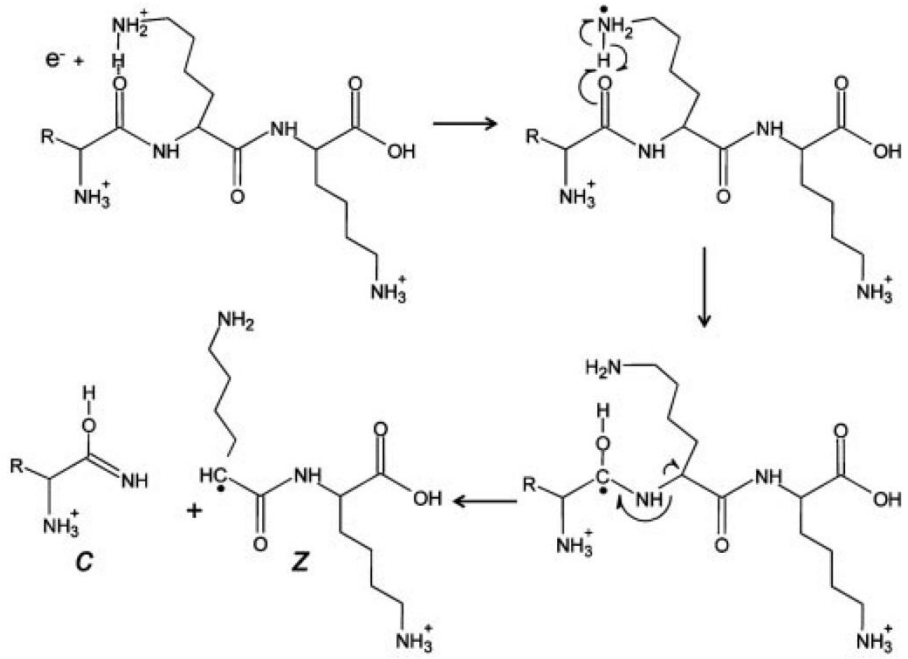

Figure 2.13 The mechanism proposed at Cornell, for ECD of protonated peptides, adapted from reference [149].

2.3.1.3 Electron-Transfer Dissociation (ETD)

ETD is an ECD-like fragmentation method introduced by Hunt and co-workers in 2004 [149]. Instead of relying on direct electron capture, the ETD process originates via electrons transferred from reagent anion radicals to multiply charged analyte cations. ETD shares many features with ECD, including the extensive backbone cleavage, production of *c*- and *z*-type ions, and preservation of labile PTMs. A major advantage of

ETD over ECD is that ETD can be performed in low cost instruments such as LITs and QITs. Thus, ETD has quickly been widely implemented in proteomics research. ETD appears to be a more gentle fragmentation process than ECD, due to its smaller energy deposit and the presence of collisional cooling in ion trap instruments, and thus even the most labile PTMs such as sulfation can be preserved during ETD.

2.3.2 Sample Preparation Prior to Mass Spectrometry Analysis

In parallel with their development of better MS instrumentation and novel fragmentation techniques, researchers have also exerted a great deal of effort to optimize the protocols for sample preparation prior to MS analysis. A poorly prepared sample not only leads to failure of MS detection, but can also be deleterious to the mass spectrometer hardware. Whereas there is no universal sample preparation strategy, the protocols need to be tailored case by case based on the sample type and quantity, experimental goals, and the detection method. Successful proteomic sample preparation can be time-consuming and may involve (but is not limited to) the optimization of protein extraction, proteolysis, enrichment, separation, and desalting. Generally speaking, the common goal here is to efficiently reduce the sample complexity and remove impurities, albeit without causing appreciable sample losses.

2.3.2.1 Sample Enrichment

Successful MS analysis of targeted proteins or the whole proteome relies on the efficient enrichment of the protein(s) of interest, especially for low-abundance proteins. Enrichment can be performed at either the protein or the peptide level. For example, the

targeted protein can be affinity purified using a specific antibody. In order to facilitate the purification, as well as to increase the abundance of the target protein, the protein under investigation can be (over)expressed with affinity tag(s) such as the His-tag, Flag-tag, or GST-tag, so that it can be later pulled down by corresponding resins. Meanwhile, enrichment at the peptide level is often used for PTM studies. A successful example is phosphoproteomics, where the total protein extract is often first digested into peptides followed by the enrichment of phosphopeptides by immobilized metal chromatography [150].

2.3.2.2 Sample Desalting

Buffer salts and other additives such as detergents are usually not compatible with MS analysis and have to be removed from the analyte solution, as these impurities can be ionized so easily that their presence will significantly suppress the signal of analyte molecules. Additionally, additive-analyte clusters may be formed, spreading the analyte signal into many peaks, which not only reduces the intensities of individual signals but also complicates spectral interpretation. Commonly used desalting techniques include dialysis, centrifugal filtration, and solid-phase extraction (SPE).

2.3.2.3 Sample Separation

The total protein mixture extracted from biological samples is usually too complex to be analyzed directly by MS. The MS instrument has a limited dynamic range and low-abundance proteins may not be efficiently ionized and will be difficult to identify in a complex mass spectrum dominated by ions from high-abundance proteins.

Additionally, there is a serious issue caused by the overlap of ions with similar *m/z* values in complex samples. Reduction of the sample complexity is a demanding but important task for successful proteomics analyses. Improved separation before the MS analysis lowers the interferences among analytes and increases the information content in the resulting mass spectra. In the early days of proteomics, protein separation for MS analysis was mainly gel-based. With this approach, protein mixtures are subjected to either one-dimensional separation by SDS-PAGE or two-dimensional polyacrylamide gel electrophoresis (2D-PAGE) which separates proteins based on both their molecular weights and/or isoelectric points. A gel spot containing the protein of interest is excised and subjected to a series of treatments including reductive alkylation, proteolytic digestion, peptide extraction, and desalting. The masses of the resulting peptides can be measured by MALDI-TOF MS. By combining the MS database search result with the protein isoelectric point and molecular weight information from the 2D-PAGE, the protein sequence can be determined. Gel-based protein separation is still widely used today because it separates proteins well, is simple to perform, and can easily remove impurities [151].

More recently, HPLC has become increasingly widely used. HPLC is a type of gel-free separation technique tightly linked to MS analyses. A modern HPLC instrument typically consists of a sample injector, a mobile phase (solvent gradient system), a stationary phase (usually densely packed column), a degasser, solvent pumps, a UV detector, and a fraction collector. An analyte mixture is first dissolved in the mobile phase and introduced into HPLC through the sample injector. The mobile phase is pushed

by the pumps through the system, bringing the analyte to the analytical column where different components in the mixture can be separated. After components elute from the column, they are detected at the detector, recorded as peaks in a chromatogram. Eluting analytes can be collected by a fraction collector for later analysis. The degasser is placed prior to the pump to remove air pockets in the mobile phase, leading to better chromatographic baselines. Optimization of the HPLC conditions is a delicate and time-consuming task. In order to obtain a desirable chromatogram, several parameters need to be optimized, including the mobile phase composition/pH/flow rate, the column material/dimensions/temperature, the sample concentration/solubility, and the injection volume.

The commonly used stationary phases for separation of proteins and peptides are the reversed phase (RP) materials, typically with alkyl chains (C4, C8, or C18) covalently bonded to a silica resin. RP-HPLC separates analytes based on their hydrophobicity. The mobile phase of RP-HPLC consists of an aqueous solution (water) and an organic modifier (*e.g.* acetonitrile, methanol). The sample is initially loaded into the system with a high percentage of the aqueous solution. The analytes can adsorb to the surface of the stationary phase though hydrophobic interaction. Addition of the organic modifier leads to partition of the analytes between the mobile phase and the stationary phase and the analytes will elute from the stationary phase into mobile phase when a critical organic concentration is reached. The separation is achieved by gradually increasing the concentration of the organic modifier: molecules with higher hydrophobicity bind to the stationary phase more tightly, so that a higher percentage of organic modifier is needed to

elute them out, leading to a longer retention in the column. A major advantage of RP-HPLC is that its mobile phase is compatible with the ESI source, and by scaling down the flow rate to nL/min level, RP-HPLC, as a single phase or the last dimension of multidimensional separation [152], can be coupled directly to a mass spectrometer equipped with an ESI source. In addition, the column for online-HPLC analysis is usually packed with smaller particles (1.7 μm vs. the traditionally used 5 μm), significantly boosting the separation speed with superior resolution and sensitivity [153]. Generally, a trapping column can be mounted before the analytical column to enable online desalting and sample enrichment. The coupling of HPLC to MS is the cornerstone for shotgun proteomics, enabling global proteome analysis in a single run while generating a huge amount of structural data [152].

Chapter 3: Direct Detection of *S*-Palmitoylation by Mass Spectrometry

3.1 Introduction

It is often desirable to perform MS analysis of protein PTMs in their native form, as it does not require laborious reactions, such as derivatization, metabolic labeling, or click chemistry, and minimizes artifacts during sample preparation. There are few ambiguities: the type of modifications and their locations can be determined with high confidence by tandem MS analysis. When coupled with modern separation techniques, very complex samples can be analyzed and both qualitative and quantitative information can be obtained in a single experiment. However, direct PTM analysis can also be a very difficult task. The barriers for successful detection of PTM may include its low abundance or ionization efficiency, instability and potential loss during MS and MS/MS analyses. Various strategies to overcome these barriers have been developed and are still an active research area. To date, MS-based methods have been extensively applied to the studies of many types of PTMs, including phosphorylation [154], acetylation [155], deamidation [156], ubiquitination [157], among others [158, 159]. MS has become an increasingly powerful and indispensable tool for everyday PTM analysis in proteomic studies.

Direct detection of *S*-palmitoylation by MS has also been reported [160-165]. This usually starts with the purification of the proteins of interest, followed by a classic bottom-up proteomic sample preparation involving reduction, alkylation, tryptic digestion either in-gel or in-solution, and sample cleanup. MS analysis, typically using a MALDI-

TOF or a MALDI-TOF/TOF instrument, can then be performed for palmitoyl peptide identification. This seemingly straightforward method has never become widely adopted, and no follow-up study with advanced instrumentation has been reported. Most researchers still choose the laborious ABE chemistry or metabolic labeling over this simple approach, because of the difficulties for direct palmitoyl detection.

Although the approach described above has shown some success on the discovery of novel palmitoylation sites in some proteins, it is not always applicable to other proteins, especially those with a low degree of palmitoylation. Quantification could also be problematic, as complete or partial palmitoyl loss may occur during sample preparation, because of the labile thioester linkage. In particular, controversy exists over the stability of palmitoylation when dithiothreitol (DTT) is used as the reducing agent [68, 165, 166]. The effect of other experimental factors, such as buffer salts, temperature, and the presence of detergents, on the palmitoyl stability has not been investigated. Additionally, palmitoyl groups may be lost, through prompt or metastable fragmentation, during tandem MS analysis, leading to uncertainty in palmitoylation site determination. Finally, the large difference in the hydrophobicity of the palmitoylated and unpalmitoylated peptides makes relative quantification a challenging task. All these uncertainties and difficulties have greatly impeded palmitoyl analysis, and necessitate the development of a universal protocol tailored for direct detection of *S*-palmitoylation.

In this section, we will present a comprehensive strategy for direct detection of *S*-palmitoylation by MS. The stability of palmitoylation in several palmitoyl peptide standards under various experimental conditions was investigated in order to establish a

sample preparation protocol that retains palmitoylation for MS analysis. The potential of a derivatization strategy for relative quantification of palmitoyl peptides and their unmodified counterparts was also explored. Lastly, the fragmentation behavior of palmitoyl peptides under several dissociation modes was studied to evaluate their applicability for characterization of palmitoyl peptides.

3.2 Experimental Section

3.2.1 Materials

Cysteine-containing synthetic peptide standards, PDFRIAFQELLCLR, MGCVQCKDKEA, and ARAWCQVAQKF were acquired from AnaSpec (San Jose, CA). Palmitoyl chloride, Tris(2-carboxyethyl)phosphine (TCEP), DTT, tetrahydrofuran (THF), ammonium bicarbonate (ABC), ammonium acetate (AA), and tris(hydroxymethyl)aminomethane (Tris) were purchased from Sigma-Aldrich (St. Louis, MO). Trifluoroacetic acid (TFA), formic acid (FA), iodoacetamide (IAM), and micro BCA (bicinchoninic acid assay) protein assay kits were purchased from Pierce (Rockford, IL, USA). *N*-[(3-perfluorooctyl)propyl] iodoacetamide (FIAM) was obtained from Fluorous Technologies Inc. (Pittsburgh, PA). The MALDI matrix DHB was obtained from Bruker Daltonics (Billerica, MA). Acetonitrile (ACN) and isopropanol (IPA) were obtained from Burdick and Jackson (Muskegon, MI).

3.2.2 Preparation of Palmitoyl Peptides

The palmitoylation reaction was performed as previously reported [167] with some modifications. Each peptide standard (200 μg) was allowed to react with 1 μL of

palmitoyl chloride in 10 μL of 100% TFA for 10 min at room temperature. The resulting mixture was dried under a nitrogen flow. Purification of the products was performed on an Agilent 1200 series HPLC system (Agilent Technologies, Santa Clara, CA) using a Vydac 214ms5215 column (C4, 5 μm, 300 Å, 2.1 mm ID x 150 mm). Mobile phase A consisted of 95:5 water/ACN with 0.1% TFA and mobile phase B consisted of 85:10:5 ACN/IPA/water with 0.1% TFA. The sample was suspended in 400 μL of 30% B (singly palmitoylated peptides) or 40% B (doubly palmitoylated peptides), sonicated for 1 min, centrifuged for 10 min at 21,000 RCF (relative centrifugal force). The supernatant was collected and centrifuged for another 10 min before HPLC injection. A linear gradient of 30−100% B (singly palmitoylated peptides) or 40-100% B (doubly palmitoylated peptides) over 20 min was employed with a flow rate of 0.3 mL/min. UV detection was performed at 214 nm. The palmitoyl peptide fractions were collected, aliquoted, and dried. The amount of palmitoyl peptide in each aliquot was determined by a micro BCA protein assay kit. Aliquots were frozen at -80 °C for later use.

3.2.3 Stability Test of Palmitoyl Peptides

Aliquots of HPLC-purified palmitoyl peptides were incubated in 100 mM ABC (pH 8.0), 50 mM Tris (pH 7.4), or 50 mM AA buffer (pH 4.0), with or without the presence of DTT or TCEP in different concentrations, at either 37 ^{o}C or 55 ^{o}C. At several time points, a 0.5-μL aliquot was taken and diluted in 5 μL of 50% ACN/0.1% TFA. A portion of diluted sample (0.5 μL) was co-crystallized with 0.5 μL of DHB (10 μg/μL in 50% ACN/0.1% TFA) on a steel MALDI target plate, and later analyzed on either a Reflex IV MALDI-TOF mass spectrometer (Bruker Daltonics, Billerica, MA) or an

ultrafleXtreme MALDI-TOF/TOF mass spectrometer (Bruker Daltonics, Billerica, MA) with 25~50% laser power. A typical MALDI-TOF mass spectrum was acquired by signal averaging over 4000 laser shots from a Smartbeam-II^{TM} Nd:YAG laser operating at 355 nm and a repetition rate of 2 kHz. The MALDI-TOF mass spectra were analyzed using the FlexAnalysis 3.4 software.

3.2.4 Preparation of IAM- and FIAM-labeled Peptides

Alkylation with IAM was performed according to the manufacturer's protocol. FIAM-labeling was performed following the protocol as described previously [168] with slight modifications. The peptide standard was first dissolved in 50 mM Tris buffer (pH 7.4) with 0.5 mM TCEP and kept at 37 °C for 30 min; the resulting solution was incubated with equal amount of 10 mM FIAM dissolved in THF at 37 °C for 30 min in the dark. The mixture was dried under a nitrogen flow. Purification was performed using a linear gradient of 30−100% B over 20 min at a flow rate of 0.3 mL/min. The amount of IAM- and FIAM-labeled peptides in each fraction was determined using a micro BCA protein assay kit. Aliquots were frozen at -80 °C for later use.

3.2.5 HPLC Separation

The HPLC behavior of IAM-labeled, FIAM-labeled and palmitoyl peptides was investigated on an Agilent 1200 series HPLC system using a Vydac 214ms5215 column with the solvent system as described above. The samples were introduced at 20% B and analyzed with a linear gradient of 20−100% B over 20 min at a flow rate of 0.3 mL/min.

Peaks were detected by the UV absorption at 214 nm, and fractions were collected and analyzed by MALDI-TOF MS for identification.

3.2.6 LC-MS Quantification

Quantification was achieved by LC-MS on an LTQ-Orbitrap XL instrument (Thermo Fisher Scientific, San Jose, CA) equipped with a nanoACQUITY UPLC (Waters, Milford, MA) and a Triversa Nanomate system (Advion Biosystems, Inc., Ithaca, NY). A nanoACQUITY BEH300 C4 column from Waters (1.7 µm, 150 µm ID x 100 mm) was used for separation. Mobile phase A consisted of 95:5 water/ACN with 0.1% FA and mobile phase B consisted of 95:5 ACN/water with 0.1% FA. Palmitoyl peptides and FIAM-labeled peptides were combined at different ratios and introduced at 40% B with a flow rate of 0.5 µL/min. The gradient was held at 40% B for 20 min, followed by a ramp to 100% B over 30 min. It was then held at 100% B for 5 min, followed by a ramp to 40% B over 2 min, and was maintained at 40% B for 23 min for column re-equilibration. All mass spectra were acquired in the Orbitrap and analyzed by the Xcalibur software.

3.2.7 Tandem MS Analyses

Off-line tandem MS analyses were performed on a 12-T solariX hybrid Qh-FTICR mass spectrometer (Bruker Daltonics, Bremen, Germany). HPLC-purified palmitoyl peptides were dissolved in 50:50 water/ACN with 0.1% FA to a concentration of 1 pmol/µL and directly infused into the mass spectrometer. Precursor ions of interest were isolated by the front-end quadrupole and fragmented by different dissociation

methods. Collision-induced dissociation (CID) was performed with the collision voltage set to 7 to 20 V; electron capture dissociation (ECD) was achieved with irradiation of ~1.5-eV electrons from an indirectly heated cathode dispenser for 50 ms; electron transfer dissociation (ETD) was performed with a 400-ms reagent accumulation and a 50 to 100-ms reaction time. A 1-s transient was acquired for each scan and each spectrum was the result of summing 100 transients. Fluoranthene anions were used as the reagent for ETD.

On-line LC-MS/MS analyses were performed on the LTQ-Orbitrap XL mass spectrometer. Data-dependent acquisition was performed by switching between one MS scan (r = 60,000 at m/z 400) and three MS/MS events (r = 7,500). The three most abundant ions with charge state ≥ 2 were isolated with a window of ± 3 m/z for CID, high-energy CID (HCD), and ETD (with fluoranthene anions). The normalized collision energy was set at 35% for CID, and 30% for HCD. ETD reaction time was set at 80 ms with supplemental activation set at 15.

3.3 Results and Discussion

3.3.1 Stability of Palmitoyl Peptides

Synthetic peptides PDFRIAFQELLCLR, MGCVQCKDKEA, and ARAWCQVAQKF were chosen as model systems because their sequences contain palmitoylation motifs from proteins that are known to undergo *in vivo* palmitoylation: beta-2 adrenergic receptor [106], tyrosine-protein kinase Fyn [169], and glutamate decarboxylase 2 [170], respectively. The chosen sequences do not contain serine, threonine, or tyrosine residues, which are targets of *O*-palmitoylation that could

complicate the analysis. The *in vitro* palmitoylation was performed in 100% TFA, under which condition all basic groups, including the N-terminal amine and the side chains of the lysine and arginine residues, were protonated and not palmitoylated. Tandem MS analysis showed that palmitoylation occurred at the cysteine and tryptophan residues, producing PDFRIAFQELLC$_{palm}$LR, MGC$_{palm}$VQC$_{palm}$KDKEA, and ARAW$_{palm}$C$_{palm}$QVAQKF. The stability of palmitoylation in various buffers was investigated by incubating HPLC-purified palmitoyl peptides at 37 ^{o}C for 1 hr, 3 hr, 6 hr, and 16 hr. The MALDI-TOF mass spectra (Figure 3.1) show that 6-hr incubation of MGC$_{palm}$VQC$_{palm}$KDKEA in the standard tryptic digestion buffer (100 mM ABC, pH 8.0) at 37 ^{o}C already led to significant palmitoyl loss, whereas all three palmitoyl peptides were stable after overnight incubation in either the neutral buffer (50 mM Tris, pH 7.4) or the acidic buffer (50 mM AA, pH 4.0). Further investigation revealed that even incubation in the pH 7.4 ABC buffer resulted in complete depalmitoylation within 16 hr, and this was attributed to the gradual pH increase of the solution containing the ABC buffer (Figure 3.2), presumably because CO_2 is more volatile than NH_3. Since most proteases used in proteomics research attain their highest enzymatic activities at or near physiological pH, Tris buffer was used in the following studies.

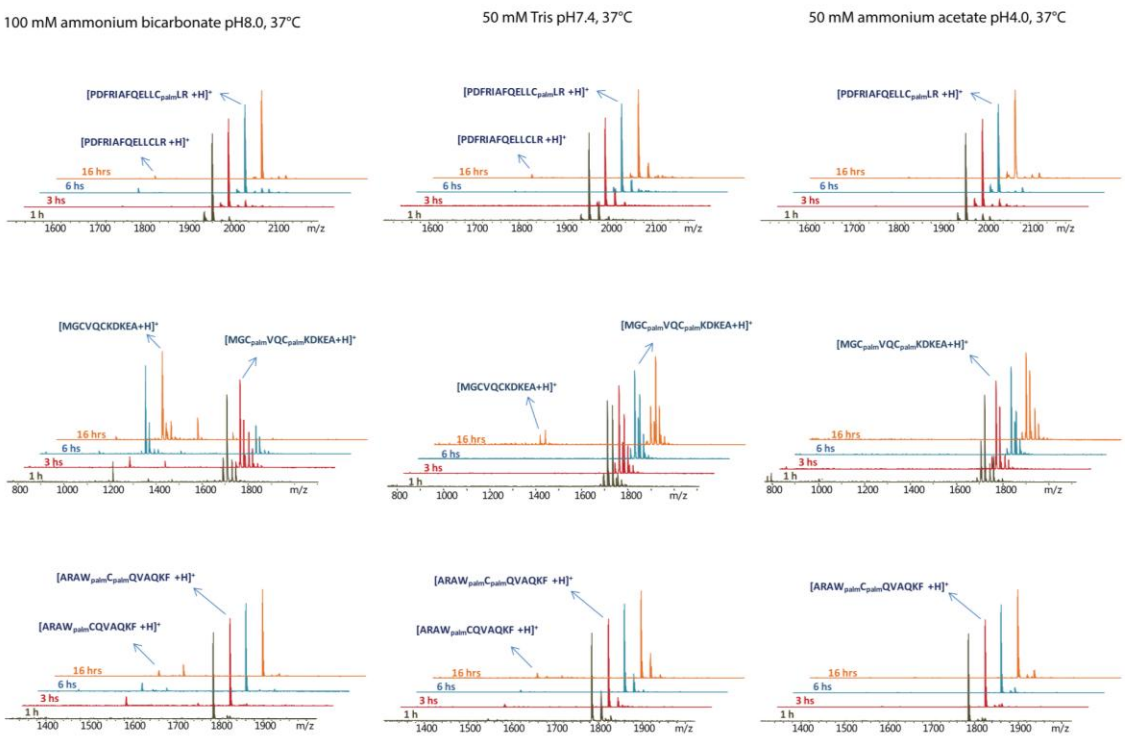

Figure 3.1 Stability of the three palmitoyl peptide standards in 100 mM ABC buffer (pH 8.0), 50 mM Tris buffer (pH 7.4), and 50 mM AA buffer (pH 4.0) at 37 ^{o}C.

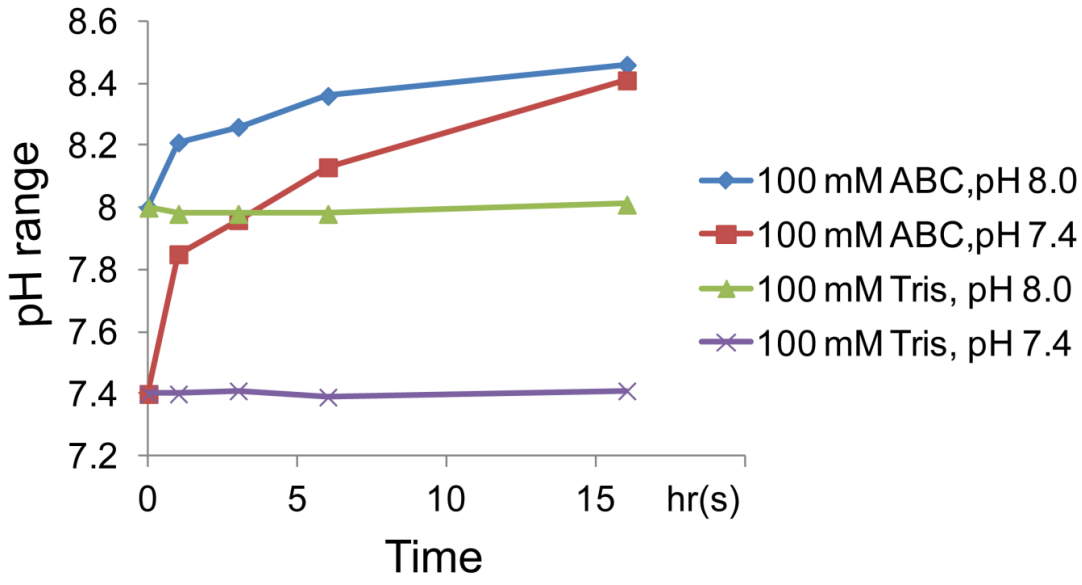

Figure 3.2 Plot of the pH value of several buffer solutions measured at various time points after preparation. All solutions were kept at 37 ^{o}C.

To test the effect of the reducing agents on the palmitoyl stability, palmitoyl peptide standards were incubated in Tris buffer in the presence of DTT or TCEP at 37 ^{o}C or at 55 ^{o}C for 30 min and 1 hr. The results are summarized in Figures 3.3 and 3.4, which show the relative abundances of the palmitoyl peptides and their depalmitoylated forms as a function of the incubation time and temperature, with DTT or TCEP. DTT, a reducing agent commonly used for reduction of disulfide bonds and other reversible oxidative modifications of cysteines, accelerated the depalmitoylation process for all three peptides, but the other widely-used reducing reagent, TCEP, did not cause appreciable loss of palmitoylation. Further, the depalmitoylation rate was significantly

increased at higher temperature, as one would expect for any reaction with an activation barrier.

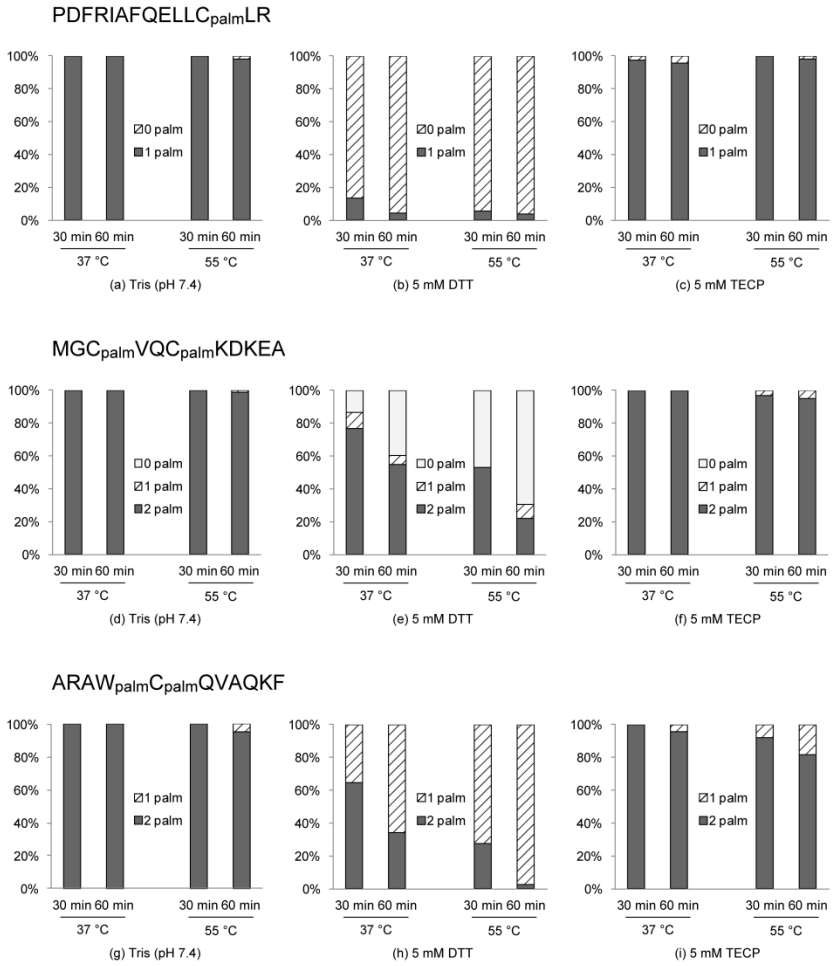

Figure 3.3 Stability of three palmitoyl peptides, as represented by the relative abundance of the palmitoyl peptides and their various depalmitoylated forms after 30 min or 60 min of incubation in Tris buffer (50 mM, pH 7.4) at 37 ^{o}C or at 55 ^{o}C, in the presence or absence of DTT or TCEP.

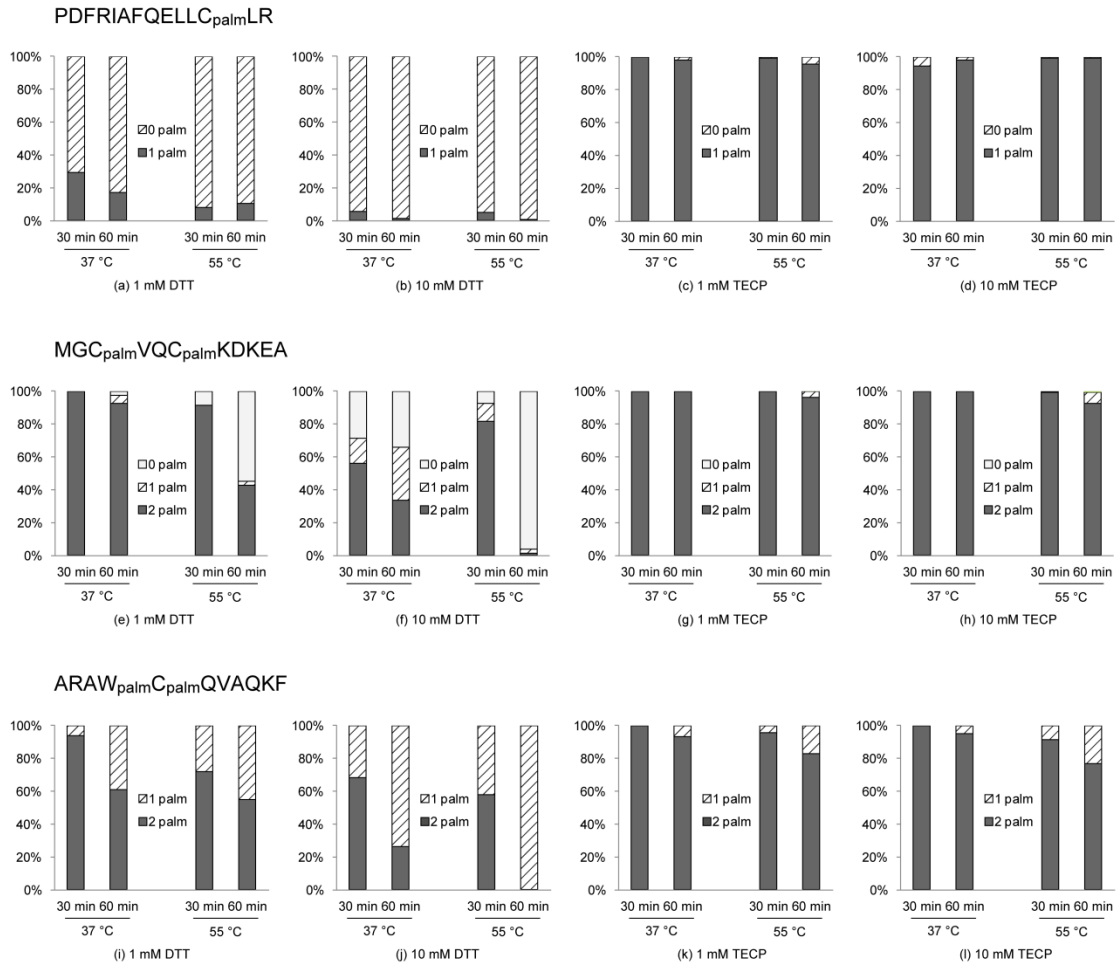

Figure 3.4 Stability of the three palmitoyl peptide standards in the presence of 1 mM and 10 mM DTT/TECP in 50 mM Tris buffer (pH 7.4).

The mechanisms for disulfide bond reduction by DTT and by TCEP are illustrated in Figure 3.5. For DTT, disulfide reduction proceeds *via* sequential thiol-disulfide exchange reactions, where one of the two disulfide sulfur atoms is attacked by a thiolate group of DTT, releasing one cysteine residue and creating a mixed disulfide species; the subsequent nucleophilic attack by the remaining thiolate of DTT releases the other

cysteine and forms cyclic oxidized DTT. Although thiol-disulfide exchanges are reversible, disulfide bond reduction by DTT is quite unidirectional, as the byproduct, the oxidized DTT, is highly stable due to its 6-membered ring structure. DTT is reactive only at pH >7 since the negatively charged thiolate is the only reactive form. Furthermore, DTT must be used in at least 20-fold molar excess to the disulfide bond to ensure complete reduction [171]. However, thiolate is a strong nucleophile that can also attack the carbonyl of the thioester linkage in *S*-palmitoylated peptides, resulting in disruption of the palmitoylation, as observed here.

The reactive group on TCEP is the free electron pair on the phosphine group, which can attack the disulfide bond, releasing one cysteine and forming an intermediate phosphorus-sulfur linkage. The subsequent nucleophilic attack to the positively charged phosphorus by the oxygen of a water molecule releases the second cysteine, and forms a phosphine oxide. This reaction is irreversible because of the formation of a strong phosphorus-oxygen double bond in the oxidized TCEP [172] and proceeds at nearly stoichiometric ratio. TCEP is a potent reducing agent, and works under a broad pH range since phosphine is a very weak base and retains its nucleophilic character even in acidic solutions. In addition, phosphine does not react with a thioester, making TCEP an ideal reducing agent for studying *S*-palmitoylation.

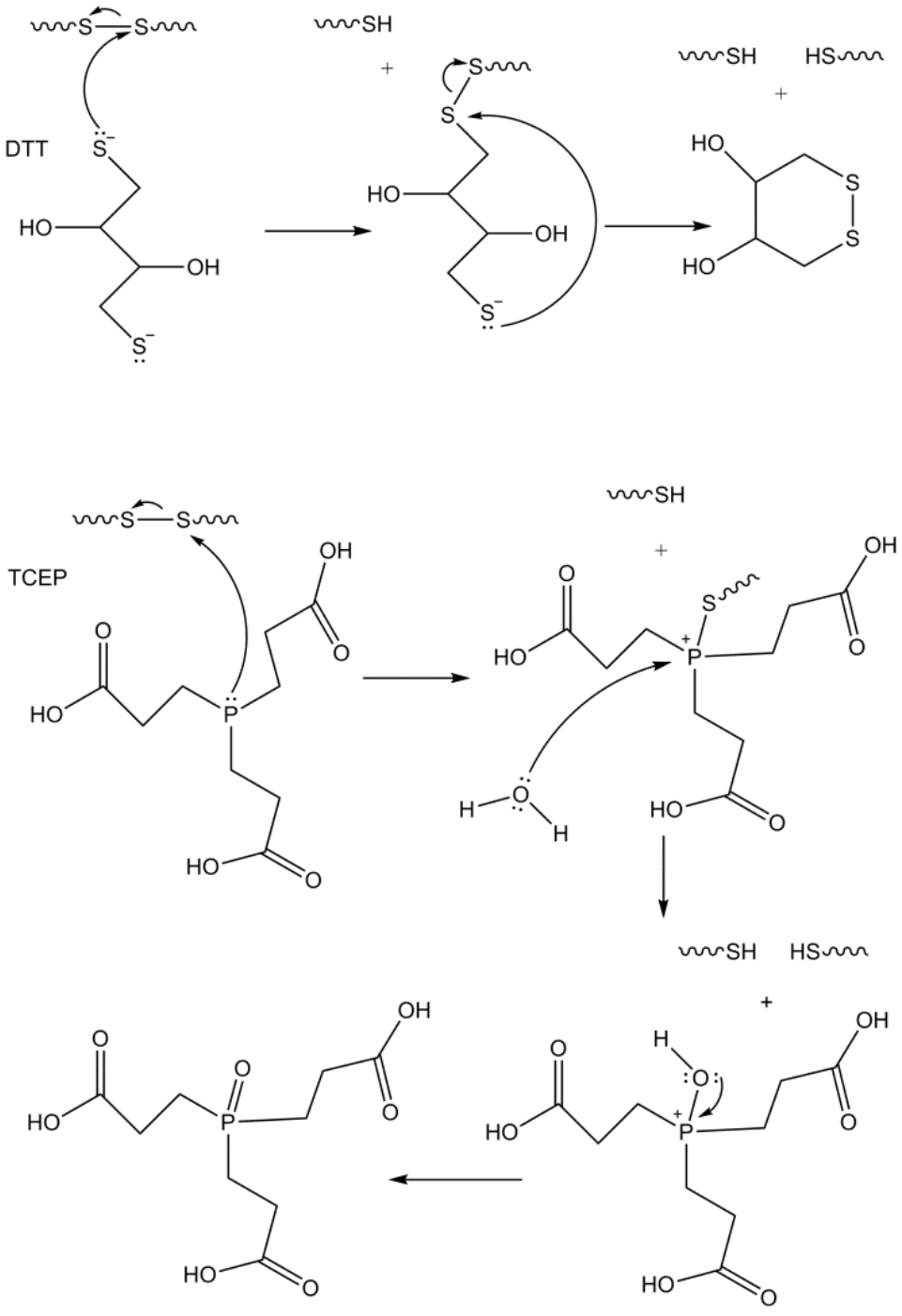

Figure 3.5 Mechanisms for disulfide bond reduction by DTT (top) and by TCEP (bottom).

3.3.2 Analysis of Palmitoyl Peptides by RP-HPLC

Several HPLC methods have been developed to analyze very hydrophobic peptides [173] and peptides with lipid modifications [174, 175]. Due to their dramatic difference in hydrophobicity, it is challenging to analyze palmitoyl peptides and their unmodified counterparts in a single HPLC run. While it is possible to analyze lipid modified peptides on a C18 column, it requires the use of strong organic solvent systems. For example, Gustafsson *et al.* reported that SP-C, a 35-residue palmitoyl peptide, can be separated on a C18 column by using 60~75% methanol/ethanol as the initial solvent followed by elution with isopropanol [175], under which conditions most unmodified peptides cannot be retained. Meanwhile, C4 columns retain palmitoyl peptides through weaker interactions, allowing separation and elution of palmitoyl peptides using mild organic solvents such as acetonitrile. However, C4 columns are not suitable for analysis of unmodified peptides which are usually not retained. Figure 3.6a shows the chromatogram of a mixture of the three palmitoyl peptide standards and their IAM-labeled counterparts, acquired on a C4 column with the gradient program shown in the inset. Although all three palmitoyl peptides were retained and well separated; two of the three IAM-labeled peptides flowed through with the initial solvent. One way to overcome this difficulty is to increase the hydrophobicity of unmodified peptides through derivatization. FIAM, with its structure shown in Figure 3.7, is a cysteine alkylation reagent with a hydrophobic perfluoroalkyl moiety, that our laboratory has demonstrated to be useful for enrichment of native cysteine-containing peptides and the RP-HPLC analysis of the mixtures of these products with their irreversibly modified analogs [168].

For the quantitative studies undertaken herein, we rationalized that this selective hydrophobic FIAM labeling of the cysteine thiol group in the unmodified peptides would allow them to be analyzed simultaneously with the palmitoyl peptides. Figure 3.6b shows the chromatogram of a mixture of the palmitoyl peptides and their FIAM-labeled counterparts, acquired on a C4 column using the same gradient program as shown in Figure 3.6a. All six peptides were retained on the C4 column in the initial phase, and were well resolved by gradient elution with mild organic solvent.

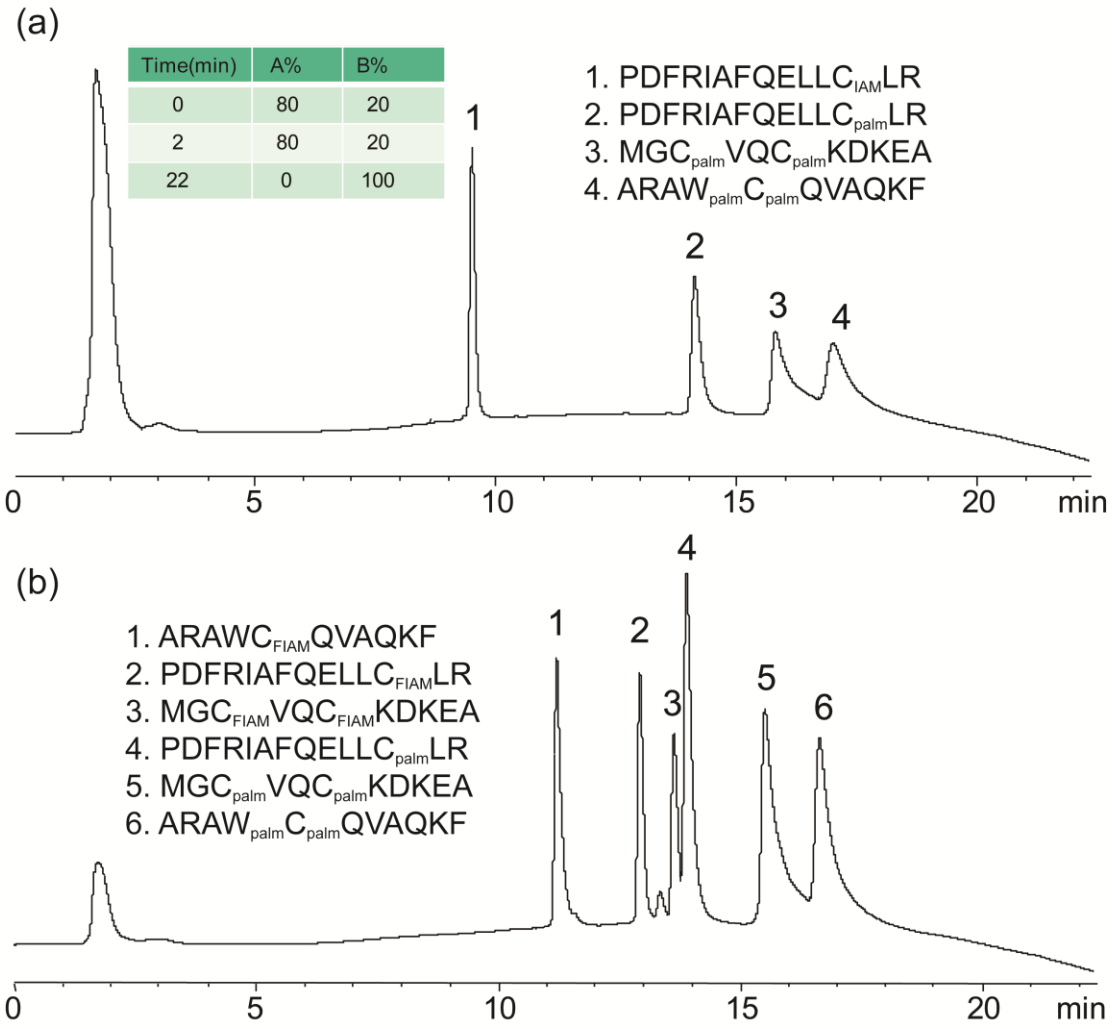

Figure 3.6 (a) Chromatogram of a mixture of three palmitoyl peptides and their IAM-labeled counterparts; (b) Chromatogram of a mixture of three palmitoyl peptides and their FIAM-labeled counterparts.

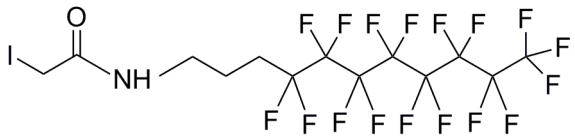

Figure 3.7 Chemical structure of *N*-[(3-perfluorooctyl)propyl] iodoacetamide.

3.3.3 Relative Quantification of Palmitoyl Peptides by On-Line LC-MS

Site-specific quantification of protein palmitoylation can be achieved by utilizing either the ABE chemistry or metabolic labeling. However, these methods are not suitable for relative quantification of palmitoyl peptides with respect to their unpalmitoylated forms, as the unpalmitoylated peptides are usually not retained under the HPLC conditions employed. As demonstrated above, with FIAM-labeling, all the cysteine-containing peptides, both with and without palmitoylation, can be analyzed in a single LC run. Here, an on-line LC-MS study of palmitoyl and FIAM-derivatized peptide mixtures was performed on an LTQ-Orbitrap XL mass spectrometer using an in-house built C4 column to explore the potential of using extracted ion chromatograms (EICs) for the relative quantification of peptide palmitoylation.

Figure 3.8a shows the total ion chromatogram (TIC) of a mixture of palmitoyl and FIAM-labeled peptide standards containing equal amounts of each peptide. The six peptides were well separated from one another and eluted between 50% and 90% B. Note that the differences in the peak areas observed for these peptides likely results from differences in their ionization efficiencies. LC-MS analyses were then performed on mixtures of these peptides at seven different ratios (FIAM/palm = 10:1, 5:1, 2:1, 1:1, 1:2, 1:5, and 1:10). The ion abundance of each peptide was calculated as the sum of the

charge-state normalized integrated peak areas of all observed charge states in their respective EICs using the Xcalibur Quan browser. The calibration curve for relative quantification was generated by plotting the ratio of the calculated ion abundance as a function of the ratio of the amount of peptides injected. As shown in Figures 3.8b-d, for all three pairs of palmitoyl and FIAM-labeled peptides, a satisfying linear correlation exists between these two ratios, thus establishing the validity of relative quantification based on the integrated EIC peak areas of the palmitoyl and FIAM-derivatized peptides. It is important to note that all samples must be analyzed under the same LC conditions as those used to generate the calibration curve. A change in the column, solvent system, and/or gradient program would lead to changes in the solvent composition during elution of peptides of interest, and consequently, their ionization efficiencies.

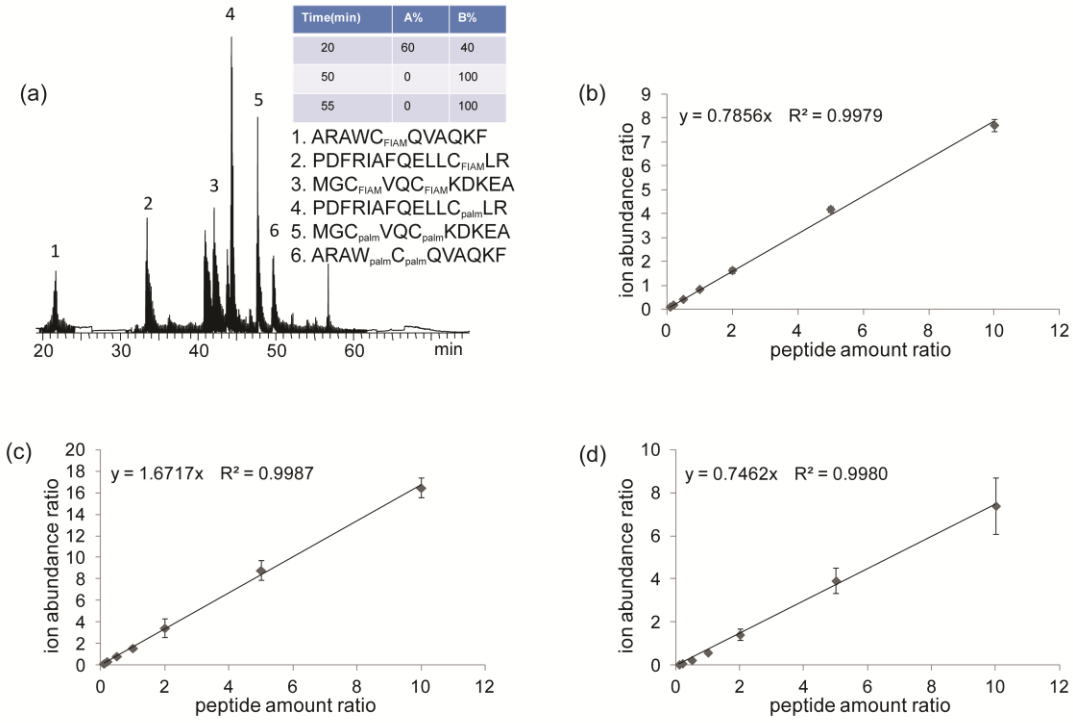

Figure 3.8 Relative quantification by UPLC-MS analysis on an LTQ-Orbitrap XL mass spectrometer. (a) The total ion chromatogram of a mixture of palmitoyl and FIAM-labeled peptides; (b), (c), and (d) the relative quantification calibration curves of the DFRIAFQELLC$_{FIAM}$LR and PDFRIAFQELLC$_{palm}$LR peptide pair, the MGC$_{FIAM}$VQC$_{FIAM}$KDKEA and MGC$_{palm}$VQC$_{palm}$KDKEA peptide pair, and the RAWC$_{FIAM}$QVAQKF and ARAW$_{palm}$C$_{palm}$QVAQKF peptide pair, respectively.

3.3.4 Tandem MS Analysis of Palmitoyl Peptides

Tandem mass spectrometry is a powerful tool for identification and localization of PTMs, and has been applied to characterize lipid-modified peptides [168] [176-178]. In

general, the thioether linkage is stable under low-energy CID conditions, as illustrated by the retention of the perfluoroalkyl group in most CID fragment ions from the FIAM-labeled peptides [168]. Hoffman and Kast reported a CID study of peptides with various lipid modifications, including *N*-myristoylation, farnesylation, and *S*-palmitoylation [176]. Whereas *N*-myristoylation was fairly stable under CID, *S*-palmitoylation was labile upon collisional activation, producing abundant $b - 238$ ions as the result of the thioester bond breakage either before or after the backbone amide cleavage. On the other hand, labile modifications are often preserved under ECD, which is considered non-ergodic and directional towards the backbone *N*-C_α bond cleavage. Guan studied the CID and ECD fragmentation behaviors of ghrelin [177], a peptide with *O*-acylation, and found that ECD produced far more extensive backbone fragmentation without breaking the ester bond, while the ester-linked octanoyl group was lost in many CID fragments. Kaczorowska *et al.* recently studied the CID and ECD fragmentation behaviors of *S*-dipalmitoylated peptides, and found that both CID and ECD could provide structural information on the peptide sequence and the modification [178]. However, in the *S*-dipalmitoylated peptides reported in that study, the palmitoyl groups were not directly attached to the cysteine thiol group, but were connected *via* ester linkages to a glycerol, which was linked to the cysteine via a thioether bond. Since the thioester linkage is more labile than the ester linkage, we felt that it would be important to study the fragmentation behaviors of *S*-acylated peptides under different dissociation conditions. A systematic investigation of the fragmentation behaviors of *S*-palmitoyl peptides was performed here with CID, ECD, and ETD as the dissociation modes. Tandem mass spectra were acquired either on-line on

the LTQ-Orbitrap instrument (CID, HCD, and ETD), or off-line on the hybrid Qh-FTICR instrument (CID, ECD, and ETD). Representative tandem mass spectra of the three palmitoyl peptide standards and their corresponding cleavage maps are shown in Figures 3.9, 3.11, and 3.12, respectively.

For the triply charged peptide, PDFRIAFQELLC$_{palm}$LR, low-energy CID spectra acquired on both instruments provided complete inter-residue cleavage coverage, generating abundant *b*- and *y*-type ions, as well as a few *a*-ions (Figure 3.9a, b). Some *y*-ions, labeled with an asterisk (*y**), were also observed with loss of the palmitoyl group ($C_{16}H_{30}O$, 238.23 Da). In general, *y** ions were in much lower abundance than normal *y*-ions, and should not have a significant impact on palmitoylation site determination. Similar sequence coverage was obtained by HCD (Figure 3.9c). However, with its higher energy input, HCD also resulted in increased palmitoyl losses from many *y*-ions. Nonetheless, the palmitoylation site could still be localized to the cysteine residue based on the presence of a high-abundance y_3 ion with the palmitoyl group attached (*m/z* 629.44) and absence of any smaller palmitoyl group-carrying *y*-ions.

The ECD spectrum (Figure 3.9d) of the same precursor ion was characterized by extensive *c*- and *z*- ion series, providing complete inter-residue cleavage coverage. Surprisingly, ECD also produced many *z* ions with loss of a palmitoyl group, labeled as z^* ions, some of which were in very high abundance. Considering that insignificant palmitoyl loss was observed in the CID spectra of this peptide, formation of these z^* ions was unlikely an ergodic process. It has been previously reported that the alpha carbon radical formed upon N-C_α bond cleavage in ECD can initiate further backbone and/or

side-chain cleavages, with or without radical migration [179-181]. Figure 3.10a illustrates a possible mechanism for the z^* ion formation, in which the backbone alpha carbon radical abstracts a hydrogen from the alpha carbon of the palmitoyl group, and the subsequent radical-induced alpha cleavage releases a tetradecylketene ($C_{16}H_{30}O$, 238.23), leaving the radical on the sulfur atom of the cysteine residue. Palmitoyl loss here was driven by the stability of the sulfur-centered radical formed, whereas in the case of *O*-acylation, no acyl loss was observed because it would have required the unfavorable formation of an oxygen-centered radical [177]. The ECD spectrum also contains another series of ions, labeled as $z^{\S}$ ions, which correspond to *z* ions with partial loss of the cysteine side-chain ($C_{15}H_{31}COS^{\bullet}$, 271.21 Da). The $z^{\S}$ ions were likely formed as the result of radical induced alpha cleavage following radical migration to the alpha carbon of the cysteine residue (Figure 3.10b). Loss of the $C_{15}H_{31}COS^{\bullet}$ group was so energetically favored, once the radical was formed at the alpha carbon of the cysteine residue, that neither the z_3 nor the z_3^* ion was observed in the ECD spectrum. The N-C_α bond cleavage N-terminal to the palmitoylated cysteine residue was always followed by the partial cysteine side chain loss, leading to the formation of an abundant $z_3^{\S}$ ion. Overall, we found that ECD generated too many site-nonspecific side chain loss product ions as a result of radical migration to be useful for palmitoylation site determination.

Similar to ECD, ETD of the triply charged PDFRIAFQELLC_{palm}LR precursor also produced extensive *c*- and *z*- ion series, with complete inter-residue cleavage coverage. However, unlike ECD, no palmitoyl loss was observed in any of the *z* ions formed. Moreover, only one $z^{\S}$ ion was detected: a $z_3^{\S}$ ion. Note that the $z_3^{\S}$ ion is

essentially the w_3 ion, and its formation did not require radical migration. It appears that radical migration was suppressed in ETD, either due to its lower energy input, or because of radical stabilization by collisional cooling. The palmitoylation site could be confidently assigned to the cysteine residue based on the mass difference between the c_{11} and c_{12} ions. The absence of the z_3 ion and the presence of the w_3 ion provided additional evidence for cysteine palmitoylation.

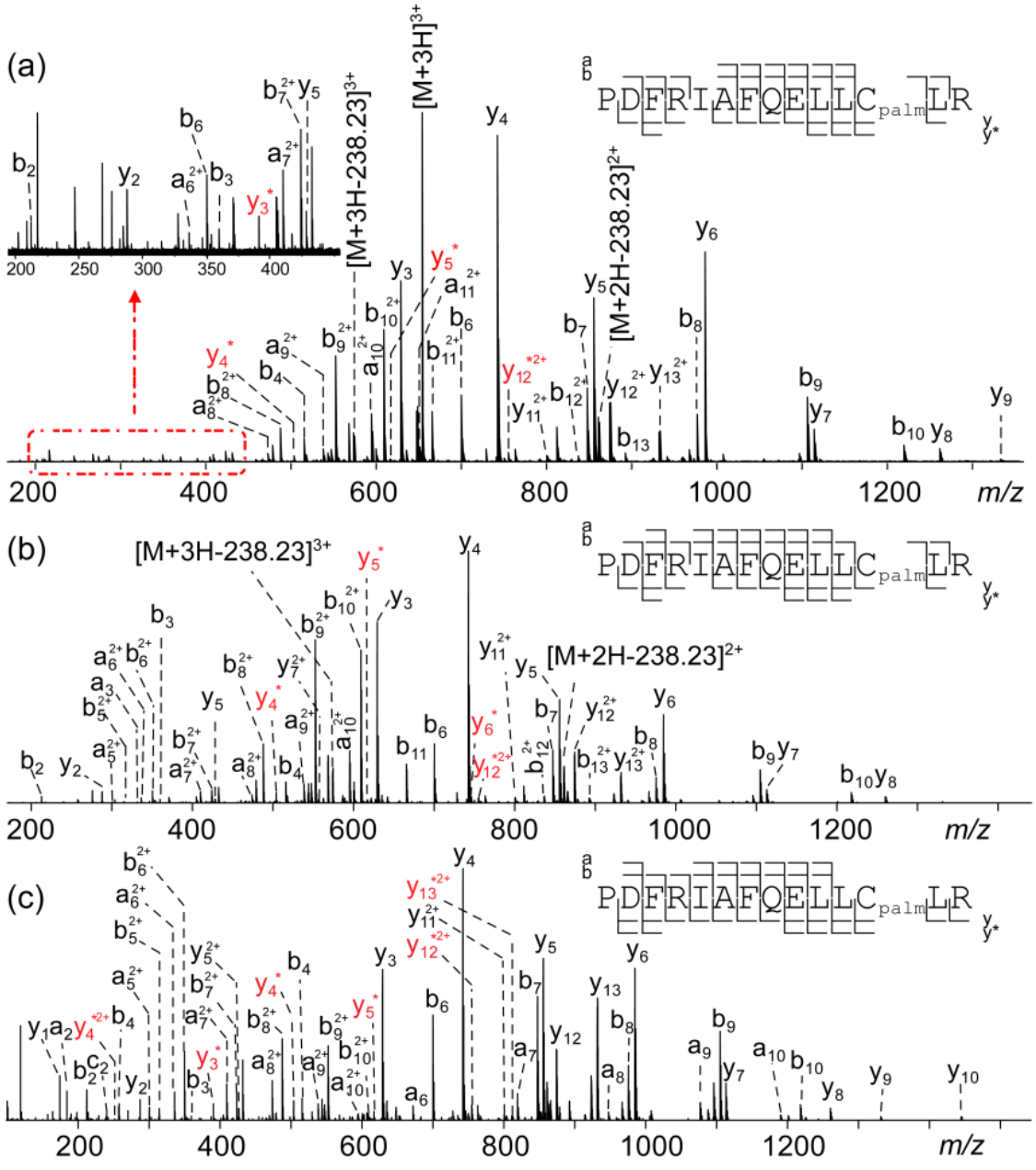
(a)
(b)
(c)
PDFRIAFQELLCpalmLR
[M+3H]3+
[M+3H-238.23]3+
[M+2H-238.23]2+
m/z

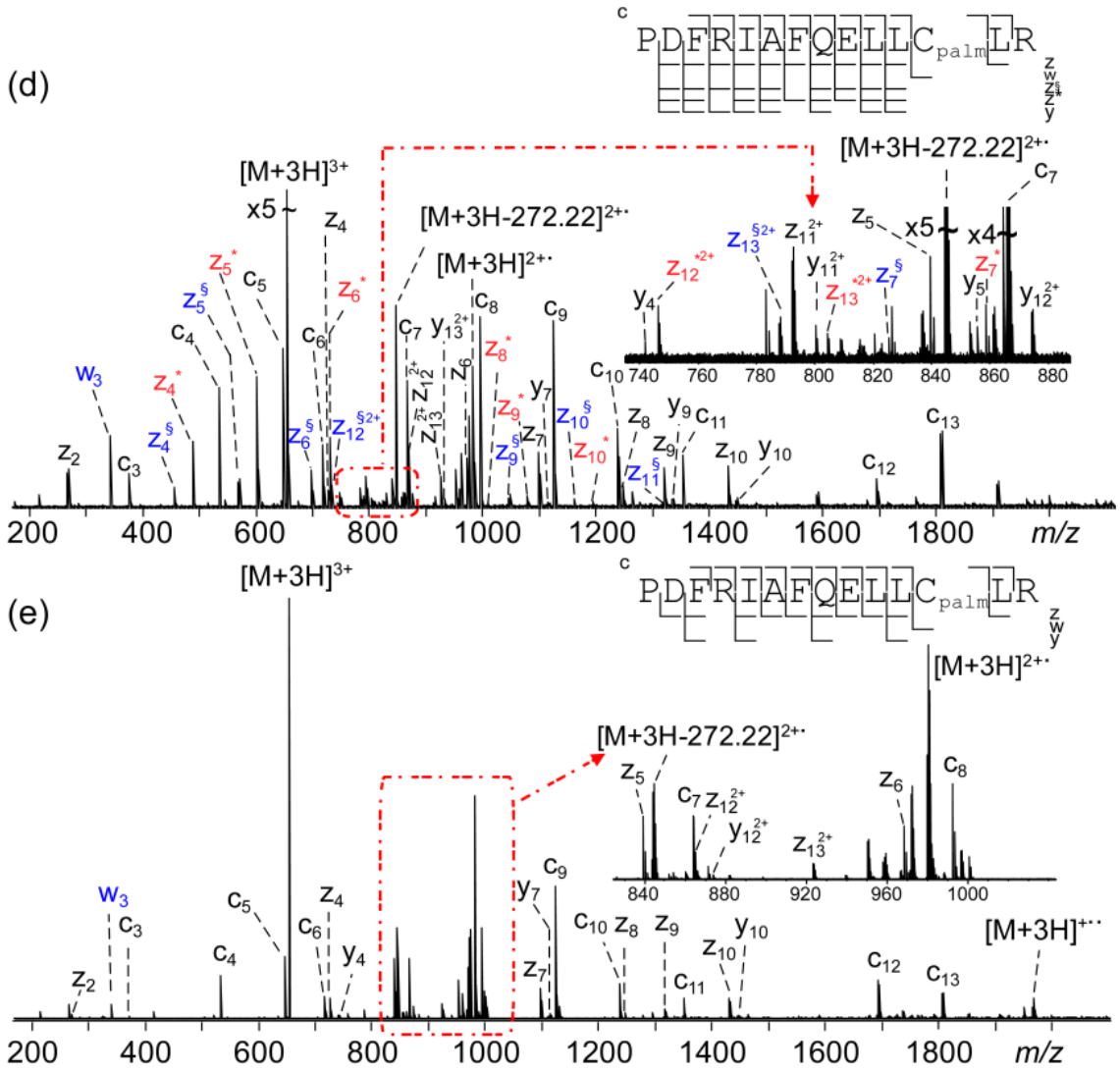

Figure 3.9 Tandem MS spectra of PDFRIAFQELLC$_{palm}$LR: (a) CID on solariX, (b) CID on Orbitrap, (c) HCD on Orbitrap, (d) ECD on solariX, and (e) ETD on solariX. * indicates loss of $C_{16}H_{30}O$ (238.23 Da); § indicates loss of $C_{15}H_{31}COS^{\bullet}$ (271.21 Da).

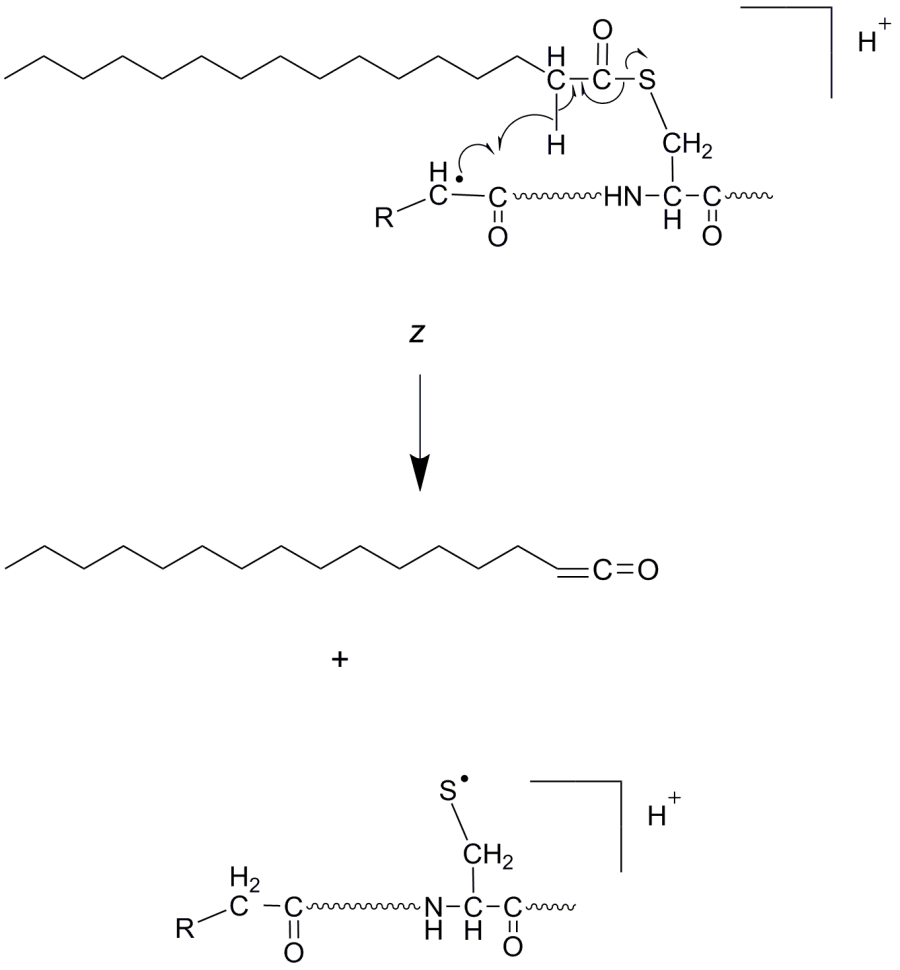

z-238.23 (z)*

(a)

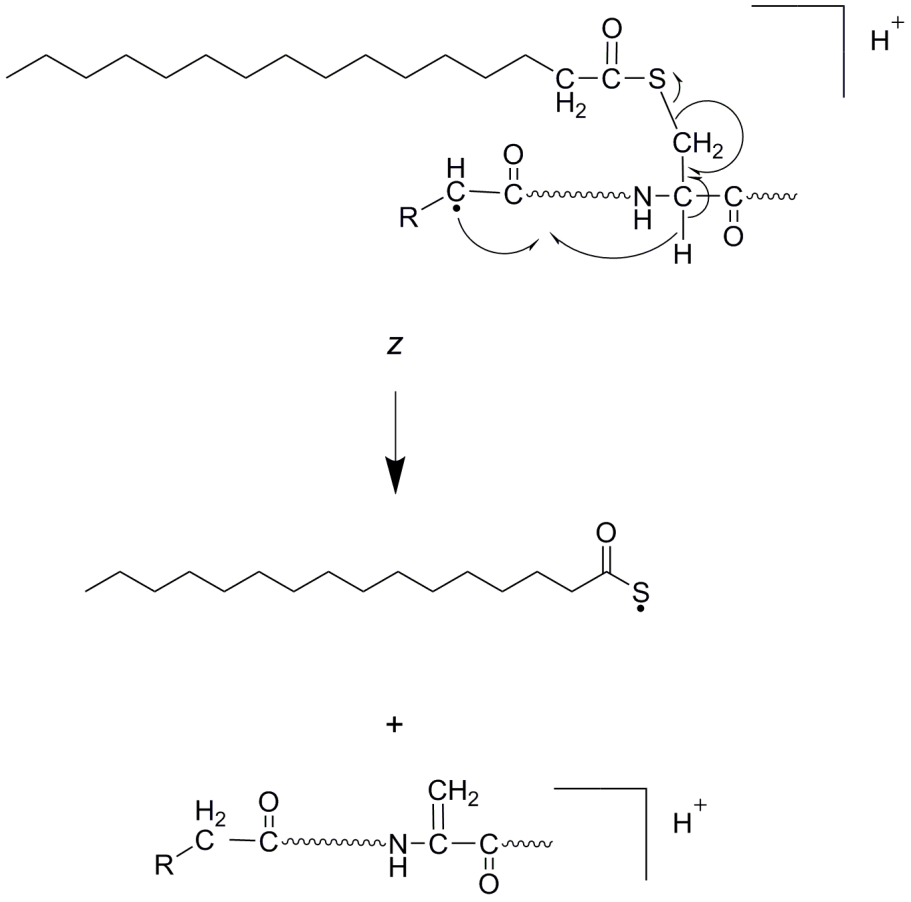

Figure 3.10 Proposed mechanisms for formation of z^{*} and $z^{\S}$ ions in ECD.

The tandem MS fragmentation behavior of the doubly palmitoylated peptide, $MGC_{palm}VQC_{palm}KDKEA$, was similar to that of the $PDFRIAFQELLC_{palm}LR$ peptide,

but also showed some distinct differences. For the triply charged $MGC_{palm}VQC_{palm}KDKEA$ precursor ion, low-energy CID (Figure 3.11a) produced only a limited number of *b*- and *y*- type ions, and the palmitoylation site at the second cysteine residue could not be determined because no backbone cleavage at either side of that cysteine residue was observed. Although its HCD spectrum (Figure 3.11b) was more informative, and provided 100% cleavage coverage, most palmitoyl-containing fragment ions also underwent extensive palmitoyl loss during the fragmentation process, including some with loss of two palmitoyl groups, *e.g.* the y_{10}^{**} ion, thus preventing reliable palmitoylation site localization. For this peptide, unlike in the previous case, ECD (Figure 3.11c) produced complete cleavage coverage with minimum palmitoyl loss. Note that the $PDFRIAFQELLC_{palm}LR$ peptide contains polar residues (D, E, and R) near both termini, allowing it to adopt a folded gas-phase conformation, in which the palmitoyl-cysteine residue was close to several potential backbone cleavage sites. Upon the N-C_α bond cleavage by ECD, the radical could migrate from the initial C_α position to the spatially adjacent palmitoyl-cysteine residue even if it was distant in sequence, initiating further side chain losses and formation of $z^{\S}$ and z^{*} ions. Such spatial proximity may not be present in the $MGC_{palm}VQC_{palm}KDKEA$ peptide, because all of its polar residues (K, D, and E) were located on one side of the palmitoyl-cysteine residues, and the two bulky hydrophobic palmitoyl-cysteine side chains further prevented formation of a compact structure. Consequently, radical migration was not prevalent here, resulting in only two low-abundance $z_7^{\S}$ and $z_8^{\S}$ ions. As in the previous case, *z* ions with an N-terminal cysteine, z_6 and z_9, were not observed; instead, cleavages N-terminal to the two cysteine

residues led to the formation of the $z_6^{\S}$ (w_6) and $z_9^{\S}$ (w_9) ions, which could be used to confirm the two cysteine palmitoylation sites. The ETD spectrum of $MGC_{palm}VQC_{palm}KDKEA$ (Figure 3.11d) was very similar to its ECD spectrum, containing a complete series of N-C_α bond cleavages, with no palmitoyl loss. Partial cysteine side chain loss was only observed for *z* ions with an N-terminal cysteine. Interestingly, two *c* ions with partial cysteine side chain loss, $c_9^{\S}$ and $c_{10}^{\S}$, were also observed. As *c* ions are even electron species, radical migration was unlikely to play a role here. Since both $c_9^{\S}$ and $c_{10}^{\S}$ ions were singly charged ions produced from triply charged precursor ions with all three potential protonation sites residing within the first nine residues, these two ions were likely formed as a result of two electron transfer processes, with one accounting for the cysteine side chain loss, and the other leading to the backbone N-C_α bond cleavage.

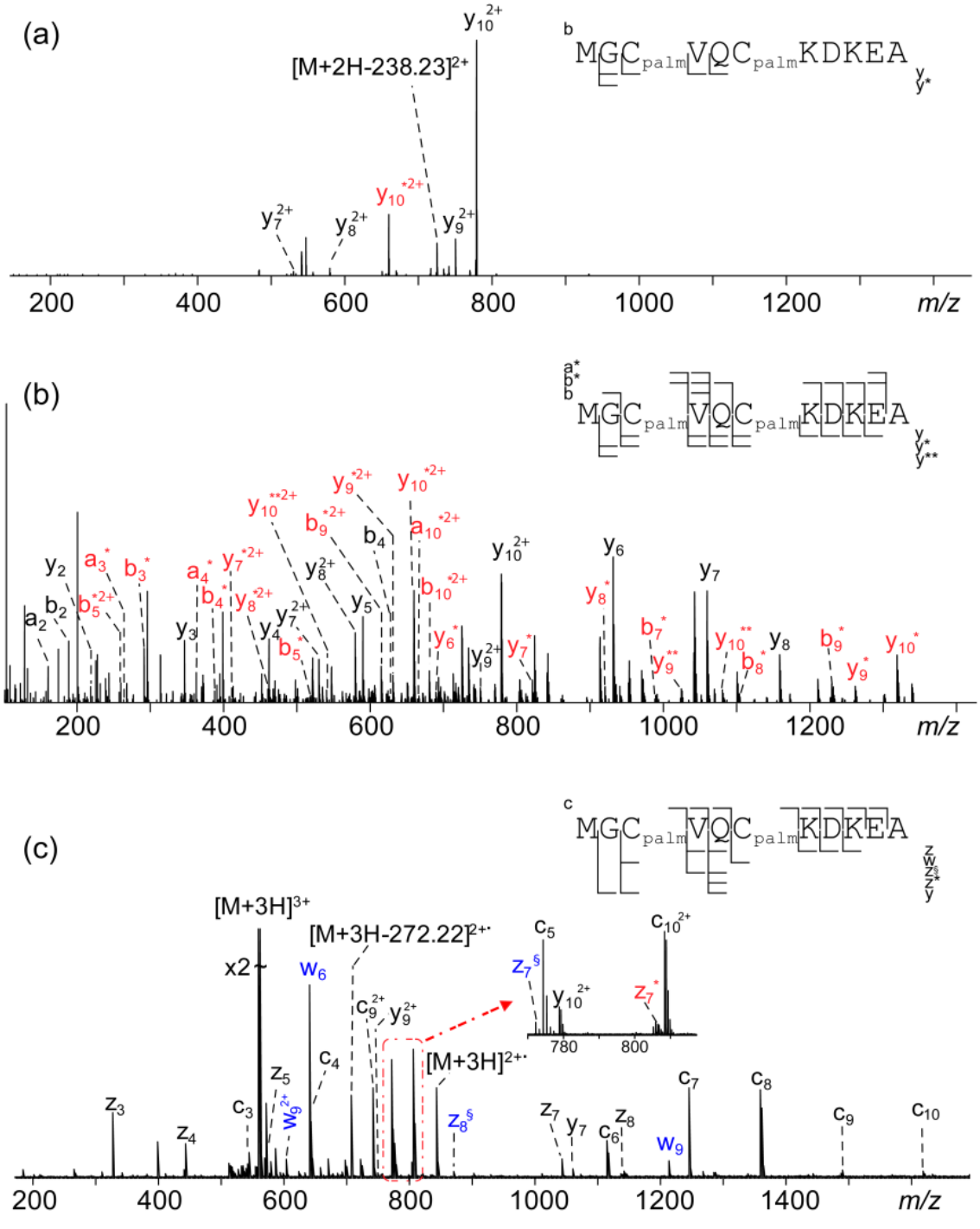
(a)
[M+2H-238.23]2+
MGCpalmVQCpalmKDKEA
200
400
600
800
1000
1200
m/z
(b)
MGCpalmVQCpalmKDKEA
200
400
600
800
1000
1200
m/z
(c)
MGCpalmVQCpalmKDKEA
[M+3H]3+
[M+3H-272.22]2+·
x2
[M+3H]2+·
780
800
200
400
600
800
1000
1200
1400
m/z

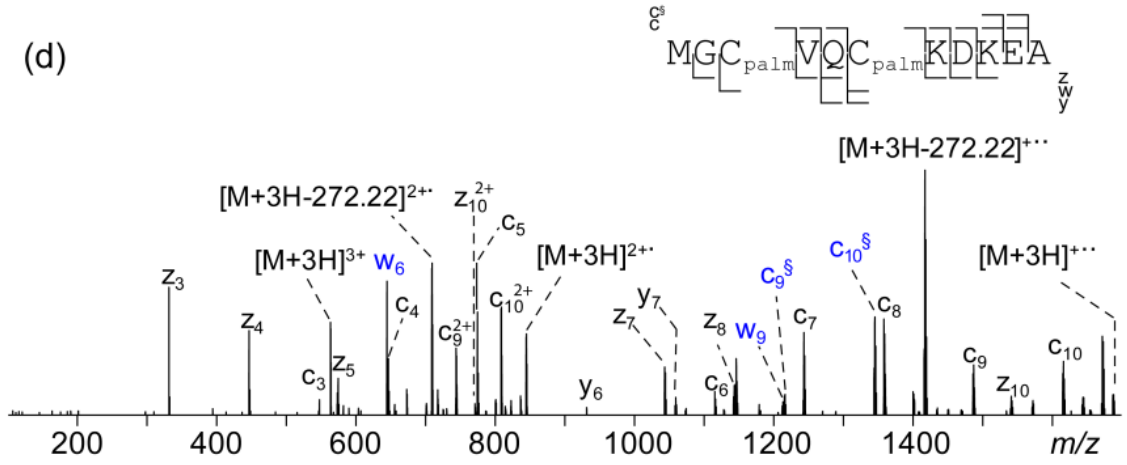

Figure 3.11 Tandem MS spectra of MGC$_{palm}$VQC$_{palm}$KDKEA: (a) CID on Orbitrap, (b) HCD on Orbitrap, (c) ECD on solariX, (d) ETD on Orbitrap. * indicates loss of $C_{16}H_{30}O$ (238.23 Da); § indicates loss of $C_{15}H_{31}COS^{\bullet}$ (271.21 Da).

The general features of the tandem mass spectra (Figure 3.12) of the triply charged peptide, ARAW$_{palm}$C$_{palm}$QVAQKF, resemble those of the other two peptides. Abundant palmitoyl losses were observed in its low-energy CID (Figure 3.12a) and HCD spectra (Figure S3b). For ECD (Figure 3.12c), in addition to the palmitoyl loss and cysteine side chain loss, abundant tryptophan side chain loss remote from the ECD cleavage site was observed, in agreement with findings from a previous study.[182] Again, the ETD spectrum (Figure 3.12d) was the most informative with minimal secondary side chain losses, except for the characteristic cysteine side chain loss at the cysteine cleavage site.

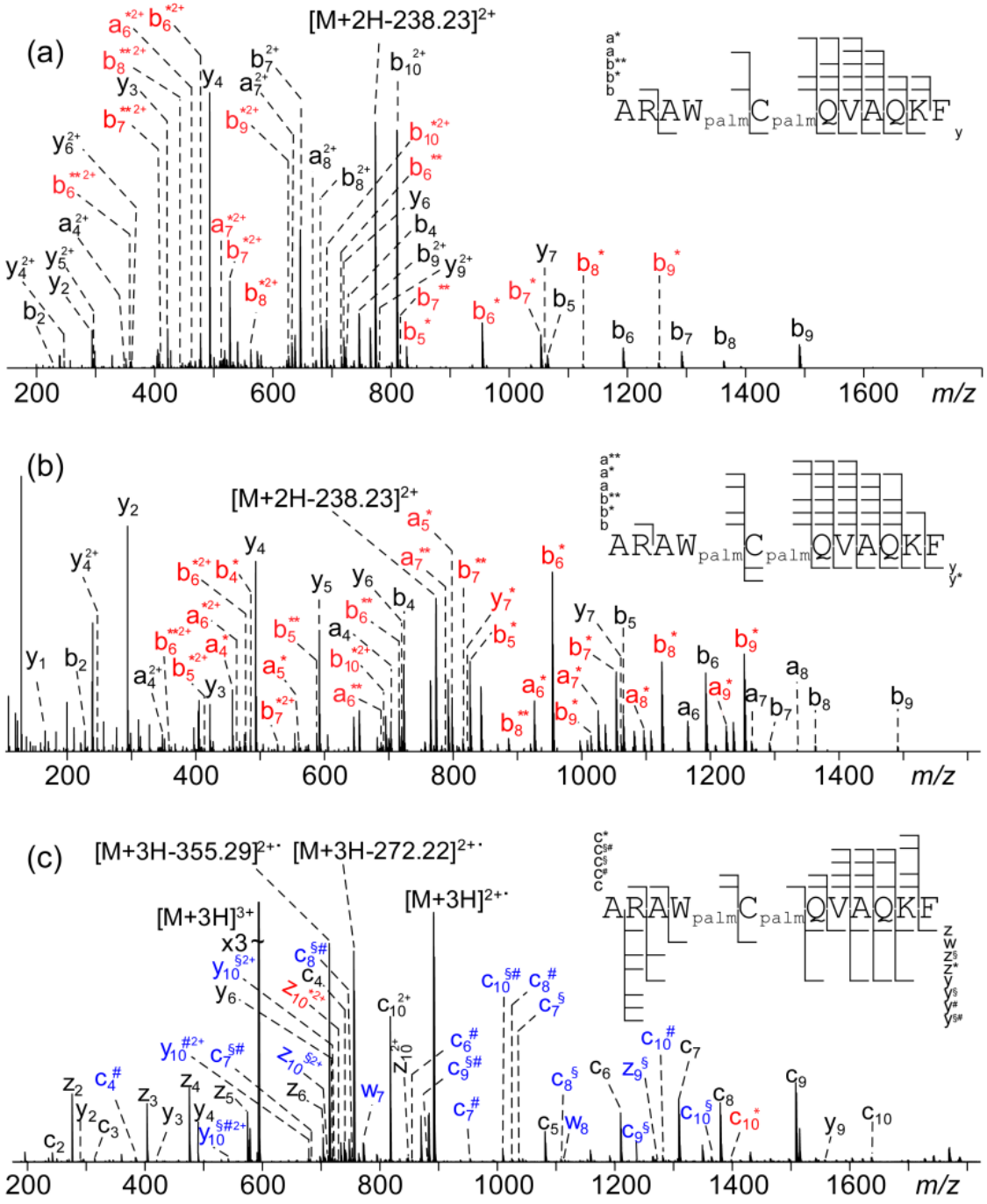
(a)
[M+2H-238.23]2+
ARAWpalmCpalmQVAQKF
200
400
600
800
1000
1200
1400
1600
m/z
(b)
[M+2H-238.23]2+
ARAWpalmCpalmQVAQKF
200
400
600
800
1000
1200
1400
m/z
(c)
[M+3H-355.29]2+·
[M+3H-272.22]2+·
[M+3H]2+·
[M+3H]3+
x3
ARAWpalmCpalmQVAQKF
200
400
600
800
1000
1200
1400
1600
m/z

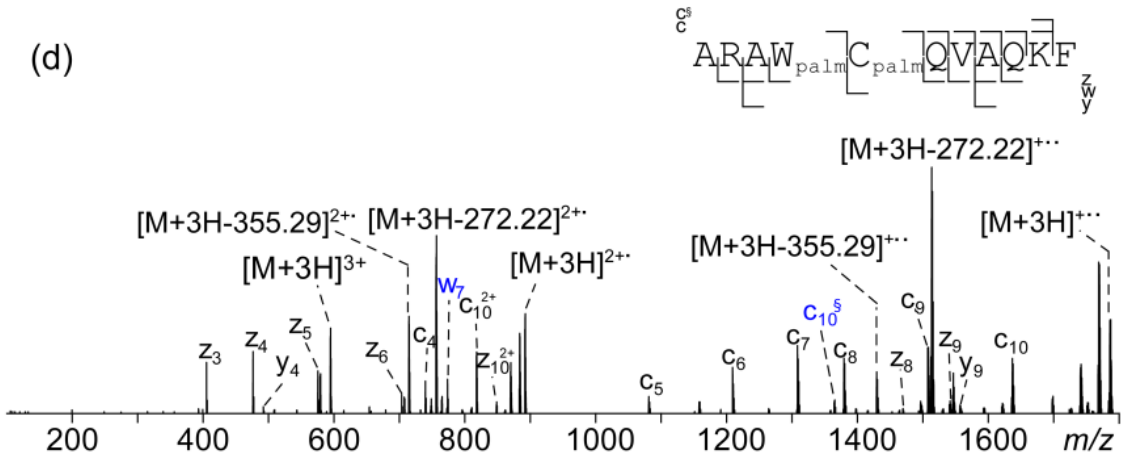

Figure 3.12 Tandem MS spectra of $ARAW_{palm}C_{palm}QVAQKF$: (a) CID on Orbitrap, (b) HCD on Orbitrap, (c) ECD on solariX, (d) ETD on Orbitrap. * indicates loss of $C_{16}H_{30}O$ (238.23 Da); § indicates loss of $C_{15}H_{31}COS^{\bullet}$ (271.21 Da); # indicates loss of $C_{15}H_{31}CONC_8H_5$ (354.28 Da).

3.4 Conclusion

S-palmitoylation is a labile modification both in solution and in the gas phase. In order to minimize palmitoyl loss during proteomic sample preparation, it is recommended that palmitoyl (and other acylated) proteins and peptides be processed under neutral or slightly acidic conditions and at room temperature. Use of DTT should be avoided; instead, TCEP is the preferred disulfide reducing agent for palmitoyl protein analysis. The drastic difference in hydrophobicity between palmitoyl peptides and their unpalmitoylated forms can be reduced by derivatization of free cysteine residues with a perfluoroalkyl tag, enabling relative quantification of palmitoylation by LC-MS. CID of

S-palmitoylated peptides can lead to facile loss of palmitoyl groups, whereas ECD can result in extensive radical migration and secondary side chain loss driven by the formation of stable sulfur-centered radicals. ETD appeared to be the best fragmentation method for tandem MS analysis of palmitoyl peptides because it produced extensive backbone fragmentation with minimum palmitoyl loss. In summary, this study presents a comprehensive strategy, including sample preparation, LC-MS and tandem MS analysis, for direct detection and quantification of *S*-palmitoyl peptides.

Chapter 4: *S*- to *N*-Palmitoyl Transfer during Proteomic Sample Preparation

4.1 Introduction

Besides *S*-palmitoylation, a less common form, *N*-palmitoylation, has also been reported, and this involves palmitoyl attachment to the lysine side chain [175, 183-185] or the protein N-terminus [186-190]. Unlike *S*-palmitoylation, *N*-palmitoylation is irreversible and not regulated. The biological functions of *N*-palmitoylation are not well understood, but are believed to derive primarily from its interaction with lipid bilayers. Olsen and Andersen suggested that palmitoylation at the lysine (or tyrosine/threonine) residue of the R peptide of the Moloney murine leukemia virus could play a role in controlling the conformational change of the p15E transmembrane protein and regulating the viral budding process [183]. Hackett *et al.* reported that adenylyl cyclase toxin, a virulence factor responsible for forming hemolytic channels and catalyzing the conversion of ATP to 3',5'-cyclic AMP in host cells, underwent palmitoylation at lysine 983 in the wild-type Bordetella pertussis stain. In contrast, the cyaC-deficient mutant strain lacking the acyltransferase showed no toxin or hemolytic activity, signifying the importance of lysine palmitoylation for membrane insertion and delivery of the catalytic domain [184]. *In vivo* N-terminal palmitoylation was first detected in human sonic hedgehog (Shh) [186], an extracellular signaling protein that is a key regulator for cell proliferation and differentiation during embryonic development [191]. For Shh, palmitoylation on its N-terminal cysteine is required for its normal distribution and for inducing cell signaling [187, 188]. Another secreted ligand, Spitz, was also found to undergo N-terminal palmitoylation, and this could restrict its diffusion to allow proper local signaling [189].

Recently, Kleuss *et al.* reported that the α-subunit of the heterotrimeric G protein ($G\alpha_s$) is palmitoylated on its N-terminal glycine (Gly2) [190], in addition to its well-known *S*-palmitoylation site at Cys3 [108]. Gly2-palmitoylation appeared to lead to more efficient stimulation of particulate adenylyl cyclases, and this was attributed to its preferential membrane localization. Localization of the palmitoylation site to Gly2 was confirmed by the observation of a palmitoylated b_1 ion in the CID spectrum of the tryptic peptide $^{2}G_{palm}C_{IAM}LGNSK^{8}$.

The mechanism for *N*-palmitoylation is still under debate. It was originally suggested that N-terminal palmitoylation of Shh is a two-step process involving intramolecular *S*→*N* palmitoyl transfer after the initial palmitoyl attachment to the cysteine sulfhydryl group [186]. Consistent with this, Gly2-palmitoylation was not observed in the Cys3 mutants of the $G\alpha_s$ protein. Later, however, Buglino *et al.* showed that hedgehog acyltransferase (Hhat) could directly catalyze palmitoyl attachment to the N-terminal amino group of Shh without a thioester intermediate [192]. Interestingly, the three proteins with N-terminal palmitoylation reported to date all contain a cysteine residue either at the N-terminus (Shh, and Spitz), or next to the N-terminus ($G\alpha_s$). It is unclear whether such proximity of a cysteine residue to the N-terminus is a required motif for the acyltransferase activity, or the evolutionary result to facilitate intramolecular palmitoyl transfer.

Although no explicit studies on *S*→*N* palmitoyl migration in peptides have been reported to date, *S*→*N* acyl transfer in small model systems has been extensively studied [193-196]. For the series $CH_3COS(CH_2)_nNH_3^+$, at pH < 7, acetyl transfer from sulfur to

nitrogen was observed when n = 2 or 3, but not for $n \geq 4$ [193]. *S→N* acyl transfer has also been utilized in protein synthesis by native chemical ligation (NCL) [197]. NCL works effectively when the C-terminal peptide segment of the protein contains a cysteine residue at its N-terminus, thus enabling intramolecular transacylation via an entropically favored five-membered ring intermediate [198]. Similarly, rapid *O→N* acyl transfer was observed only when the esterified serine residue was present at the N-terminus [199]. The rate of transacylation increases with increasing pH. At pH 8, intramolecular acyl transfer via larger ring intermediates could also take place [193]. As protein characterization often involves sample processing in neutral or slightly basic solutions, it is important to investigate whether *S→N* palmitoyl migration could occur during sample preparation, even when the cysteine residue is not at the N-terminus, and whether this would lead to erroneous reporting of *in vivo N*-palmitoylation.

In this study, an analogue of the N-terminal tryptic peptide from the protein $G\alpha_s$, GCLGNAK, was chosen as the model system to test the palmitoyl migration hypothesis. The serine[7] residue was replaced by an alanine residue to avoid potential interference from *O*-palmitoylation.

4.2 Experimental Section

4.2.1 Materials

Synthetic peptide GCLGNAK was acquired from AnaSpec (San Jose, CA). Palmitoyl chloride, DTT, and ABC were purchased from Sigma-Aldrich (St. Louis, MO). TFA, FA, and IAM were purchased from Pierce (Rockford, IL, USA). RapiGest^{TM} was

obtained from Waters (Milford, MA). DHB was obtained from Bruker Daltonics (Billerica, MA). ACN and IPA were obtained from Burdick and Jackson (Muskegon, MI).

4.2.2 Sample Preparation

Palmitoyl peptide standard $GC_{palm}LGNAK$ was produced by incubating GCLGNAK with excess palmitoyl chloride in TFA, followed by C4-RP-HPLC purification on an Agilent 1200 series HPLC system (Agilent Technologies, Santa Clara, CA) as described previously [200]. The incubation typically took place in either 100 mM ABC buffer (pH 8.0) or 50 mM Tris (pH 7.4) at 37 °C for 3 hr with or without 0.1% RapiGest^{TM}. The resultant peptides were diluted, co-crystallized with DHB, and analyzed on an ultrafleXtreme MALDI-TOF/TOF instrument (Bruker Daltonics, Billerica, MA). A typical MALDI-TOF mass spectrum was acquired by signal averaging over 4000 laser shots from a Smartbeam-II^{TM} Nd:YAG laser operating at 355 nm and a repetition rate of 2 kHz. Alternatively, the resultant peptides were desalted by POROS R1 50 and subjected to LC-MS/MS analysis.

4.2.3 Mass Spectrometry Analysis

Online HPLC-MS/MS was performed on an LTQ-Orbitrap XL instrument (Thermo Fisher Scientific, San Jose, CA) equipped with a nanoAcquity UPLC (Waters, Milford, MA) mounted with a BEH300 C4 column (150 µm ID x 10 mm, 1.7 µm, Waters). Mobile phase A consisted of 5:95 ACN/water with 0.1% FA and mobile phase B consisted of 95:5 ACN/water with 0.1% FA. Samples were loaded to C4-UPLC with

equal amount at 20% B at a flow rate of 0.5 µL/min. The gradient was held at 20% B for 15 min, followed by a ramp to 100% B over 40 min and then held at 100% B for 5 min. It was then ramped to 20% B over 2 min, and held at 20% B for 25 min for column re-equilibration. Data dependent acquisition was performed by switching between the MS scan (r = 60,000) and MS/MS events (r = 30,000) with an inclusion list of peptides of interest. The isolation window was ±3 *m/z*. The normalized collision energy was set at 35% for CID. ETD reaction time was set at 80 ms with supplemental activation set at 15.

4.2.4 UV Monitoring of S-Palmitoyl Peptides

The kinetics of de-*S*-palmitoylation due to thioester hydrolysis or *S*→*N* palmitoyl migration was studied by monitoring the UV absorption of the thioester functional group at λ = 230 nm, measured by an Agilent Cary 60 UV-Vis spectrophotometer (Agilent Technologies, Santa Clara, CA). The UV-Vis absorption of the palmitoyl peptide standard GC_{palm}LGNAK was monitored for 3 hr following its incubation in 50 mM Tris (pH 7.4) buffer with or without the presence of 0.1% RapiGest^{TM} at 37°C.

4.3 Results and Discussion

4.3.1 Preparation of the S-Palmitoyl Peptide Standard GC_{palm}LGNAK

Reliable investigation of the *S*→*N* palmitoyl migration requires the use of a pure *S*-palmitoyl peptide standard. *In vitro* palmitoylation with palmitoyl chloride in TFA should produce only *S*- and *O*-palmitoylation, but not *N*-palmitoylation, since the amino and guanidino groups would be protonated in an acidic solution and lose their nucleophilic property. Incubation of the peptide standard, GCLGNAK, with palmitoyl

chloride in TFA produced a singly palmitoylated peptide, $(GCLGNAK)_{palm}$, as evidenced by the 238.23-Da mass shift in its MALDI-TOF mass spectrum (Figure 4.1a, b). HA/IAM treatment of the HPLC-purified peptide $(GCLGNAK)_{palm}$ led to complete palmitoyl loss (Figure 4.1c), suggesting that all palmitoyl peptides existed in the form of $GC_{palm}LGNAK$, where the palmitoyl group was connected to the cysteine residue via a thioester linkage, as HA should selectively remove *S*-palmitoylation [68, 201] but not *N*-palmitoylation [202].

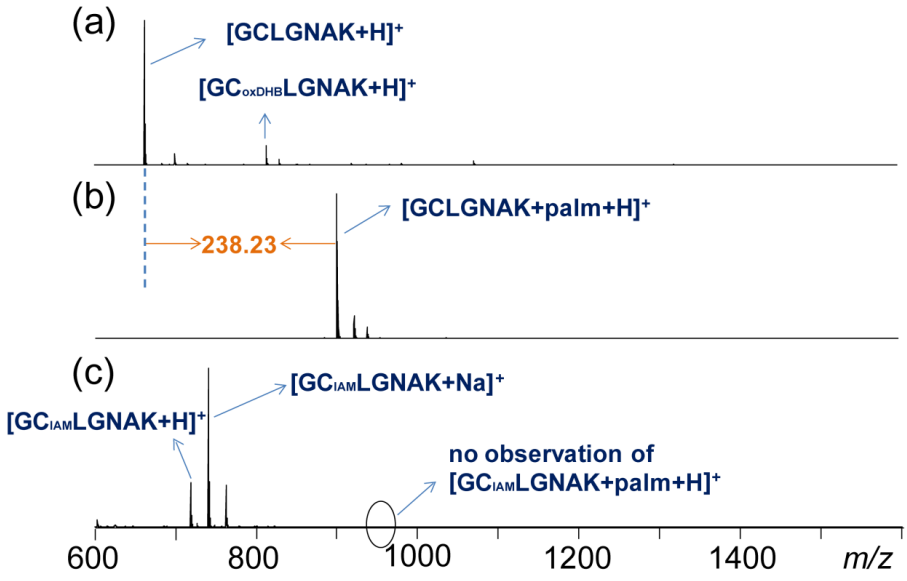

Figure 4.1 MALDI-TOF mass spectra of the peptide standard, GCLGNAK, (a) before and (b) after reaction with palmitoyl chloride in 100% TFA. (c) The MALDI-TOF mass spectrum of sample (b) after subsequent incubation with 500 mM HA/25 mM IAM.

4.3.2 Intermolecular Palmitoyl Migration

After a 3-hr incubation at 37 °C in either 100 mM ABC buffer (pH 8.0) or 50 mM Tris buffer (pH 7.4), $GC_{palm}LGNAK$ gave rise to a mixture of peptides, containing zero, one, or two palmitoyl groups, respectively (Figure 4.2). The presence of a doubly palmitoylated peptide is indicative of the occurrence of *in vitro* palmitoyl transfer between two palmitoyl peptides.

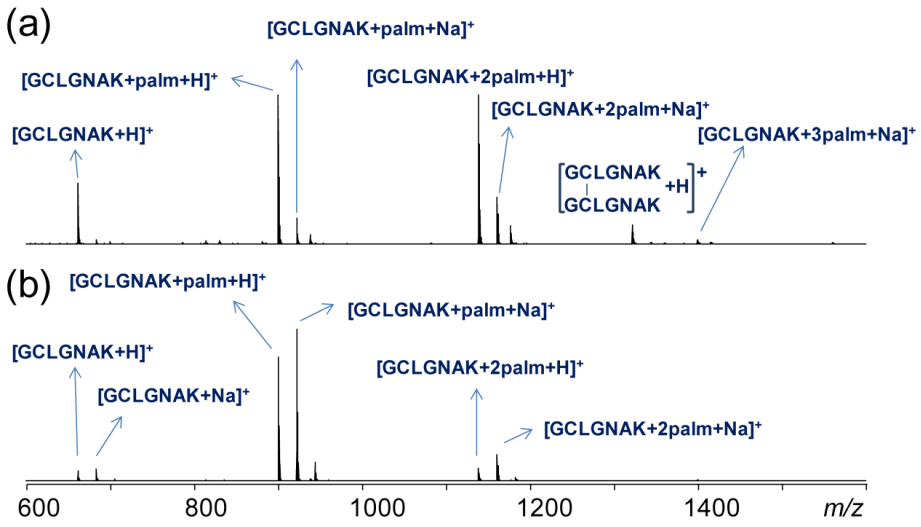

Figure 4.2 MALDI-TOF mass spectra of the palmitoyl peptide standard, $GC_{palm}LGNAK$, after incubation in (a) 50 mM ABC buffer (pH 8.0) or (b) 50 mM Tris (pH 7.4) at 37°C for 3 hr.

In neutral or slightly basic solutions, hydrolysis of *S*-palmitoyl peptides should produce primarily palmitate ions (pKa of palmitic acid is 4.78) which are not reactive towards amino groups. Thus, intermolecular *S*→*N* palmitoyl transfer must have occurred

directly between two palmitoyl peptides without palmitoyl release into the solution, and this would require that the palmitoyl group on one peptide be in the vicinity of the amino group on the other peptide. In support of this hypothesis, a 3-hr co-incubation of the peptides $GC_{palm}LGNAK$ and $GC_{IAM}LGNAK$ in the 100 mM ABC buffer at 37 °C led to intermolecular palmitoyl transfer only between two palmitoyl peptides, but not from a palmitoyl peptide to an IAM-labeled peptide, as no $(GC_{IAM}LGNAK)_{palm}$ peptide was observed (Figure 4.3). This preference may be attributed to the aggregation of palmitoyl peptides in aqueous solutions because of the hydrophobic interaction between their palmitoyl groups. Such interaction was lacking between an IAM-labeled peptide and a palmitoyl peptide.

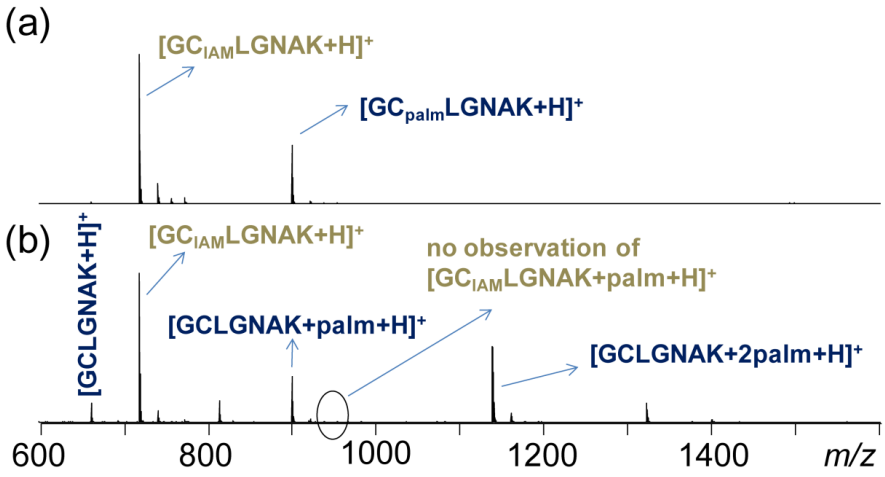

Figure 4.3 MALDI-TOF mass spectra of a mixture of GCpalmLGNAK and $GC_{IAM}LGNAK$ (a) before and (b) after incubation in ABC buffer (pH 8.0) at 37°C for 3 hr.

4.3.3 The Effect of Detergent on Palmitoyl Migration

If the intermolecular *S*→*N* palmitoyl migration was facilitated by the aggregation of palmitoyl peptides, it could be suppressed by disrupting their hydrophobic interaction. To test this hypothesis, $GC_{palm}LGNAK$ was incubated in either 100 mM ABC buffer (pH 8.0) or 50 mM Tris buffer (pH 7.4) with 0.1% RapiGest™ (structure shown in Figure 4.4), an MS-compatible detergent commonly used to solubilize proteins and to prevent protein/peptide aggregation. The MALDI mass spectrum remained largely unchanged after 3 hr of incubation at 37 °C, although a very low level of doubly palmitoylated peptide was observed (Figure 4.5). Therefore, it seems that RapiGest™ significantly reduced the intermolecular palmitoyl transfer.

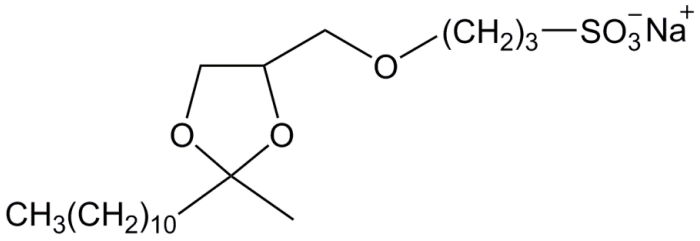

Figure 4.4 The chemical structure of RapiGest™.

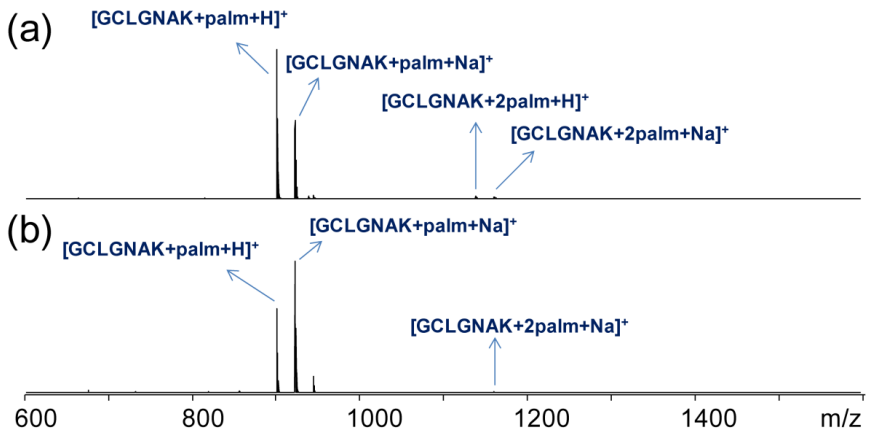

Figure 4.5 MALDI-TOF mass spectra of the palmitoyl peptide standard, $GC_{palm}LGNAK$, after incubation in (a) 50 mM ABC buffer (pH 8.0) /0.1% RapiGest^{TM} or in (b) 50 mM Tris buffer (pH 7.4) /0.1% RapiGest at 37°C for 3 hr.

Though the MALDI-TOF MS analysis provided solid evidence for the occurance of intermolecular palmitoyl migration, it was unable to determine whether the palmitoyl group was transferred to the peptide N-terminus or the lysine side chain. Neither did it suggest whether intramolecular migration took place since it is not possible to differentiate among the three palmitoyl peptides, $GC_{palm}LGNAK$, $G_{palm}CLGNAK$, and $GCLGNAK_{palm}$ based only on their *m/z* values. LC-MS/MS analysis was then performed in order to distinguish and determine the relative abundances of various palmitoyl peptide isomers, since separation of isomeric palmitoyl peptides by reversed phase HPLC has been previously reported [199], and tandem MS analysis would provide information for palmitoyl localization. All samples were analyzed by online-C4-UPLC-MS/MS analysis

on an LTQ-Orbitrap XL instrument with equal sample loading amounts. Figure 4.6 and 4.7 show the base peak chromatogram (BPC) and the extracted ion chromatograms (EICs) of various forms of peptides identified after a 3-hr incubation of $GC_{palm}LGNAK$ in 50 mM Tris (pH 7.4) without and with 0.1% RapiGest^{TM}. The palmitoylation sites on various peptides were determined based on their tandem mass spectra (Figure 4.16) and will be discussed later. Note that the depalmitoylated peptide, GCLGNAK, observed in the MALDI-TOF mass spectra was not detected by LC-MS/MS, because it was very hydrophilic and had been removed during the desalting step. EIC of $[GCLGNAK+palm+2H]^{2+}$ (*m/z* 450.7830) contains a single peak (Figures 4.6b, 4.7b), and it is assigned as $GC_{palm}LGNAK$ base on the similarity of its retention time (RT = 40.8 min) and fragmentation pattern to those of the $GC_{palm}LGNAK$ standard (Figure 4.13a). Meanwhile, EIC of $[GCLGNAK+2palm+2H]^{2+}$ (*m/z* 569.8978) (Figures 4.6c, 4.7c) contains two peaks with baseline separation and these two isomers are later identified as $GC_{palm}LGNAK_{palm}$ (RT = 51.9 min) and $G_{palm}C_{palm}LGNAK$ (RT = 53.2 min) (Figures 4.6c, 4.12a-b). Another pair of isomeric peptides (*m/z* 899.5509) were also observed in very low abundance, and they correspond to the disulfide-bonded homo-dimer of $GCLGNAK_{palm}$ (RT = 47.25 min) and of $G_{palm}CLGNAK$ (RT = 47.76 min) (Figures 4.6d, 4.7d). These dimers were not observed in the MALDI-TOF mass spectra.

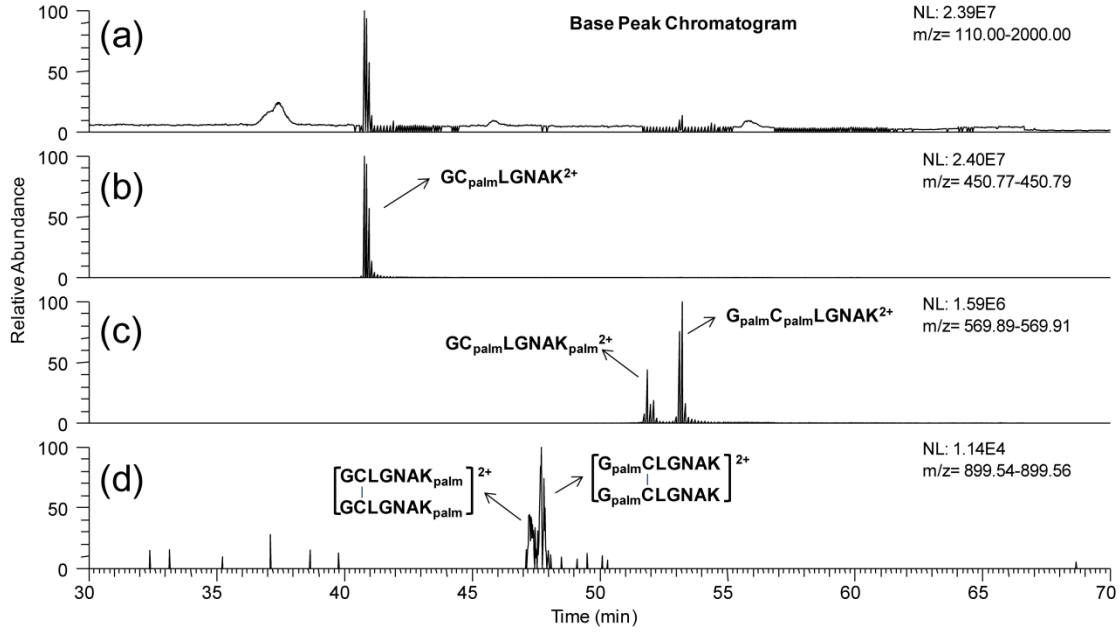

Figure 4.6 (a) The base peak chromatogram of $GC_{palm}LGNAK$ after incubation in 50 mM Tris buffer (pH 7.4) at 37°C for 3 hr; (b-d) the EICs of various modified forms of GCLGNAK. Palmitoyl localization was achieved by tandem MS analysis, as illustrated in Figure 4.16.

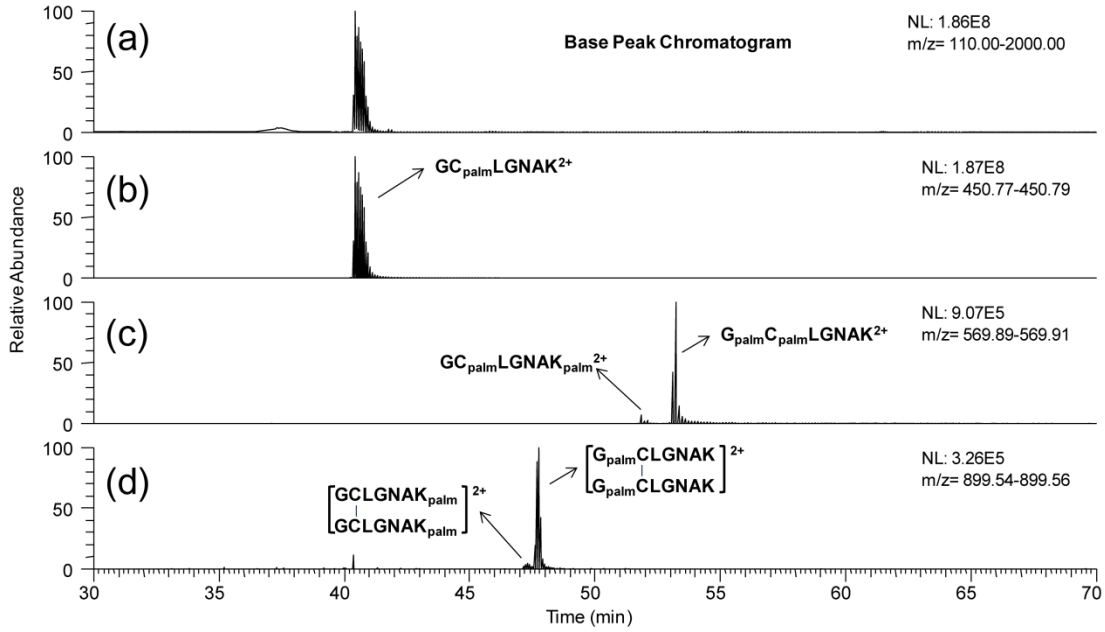

Figure 4.7 (a) The base peak chromatogram of $GC_{palm}LGNAK$ after incubation in 50 mM Tris buffer (pH 7.4) with 0.1% RapiGest^{TM} at 37°C for 3 hr; (b-d) the EICs of various modified forms of GCLGNAK. Palmitoyl localization was achieved by tandem MS analysis, as illustrated in Figure 4.16.

We further evaluated the effect of RapiGest^{TM} on *S*→*N* palmitoyl migration by comparing the relative abundances of the various peptides that resulted from incubation of $GC_{palm}LGNAK$ in the Tris and Tris-RapiGest^{TM} buffers from the LC-MS/MS data. The absolute ion abundance of each peptide was measured as the sum of the charge-state normalized integrated peak areas of all observed charge states in their respective EICs and is presented in a bar graph (Figure 4.8). Each data set was derived from five experimental repeats with the same loading amount. The average ion abundance of each

peptide and its relative ratio between the two incubation conditions are presented in Table 4.1. Addition of RapiGest^{TM} led to a significant decrease in the level of $GC_{palm}LGNAK_{palm}$ and $G_{palm}C_{palm}LGNAK$, and an increase in the level of disulfide-bonded homo-dimers, especially the $G_{palm}CLGNAK$ dimer. This is understandable, as the hydrophobic palmitoyl group can be effectively solvated by the RapiGest^{TM} micelle, and this should inhibit intermolecular palmitoyl migration and may facilitate intramolecular palmitoyl migration. If so, the N-terminal amino group should be the preferred target site for intramolecular palmitoyl migration due to its proximity to the cysteine residue, which explains the preference for the formation of the $G_{palm}CLGNAK$ dimer. It is, however, not possible to determine the percentage of the $GC_{palm}LGNAK$ peptides that underwent inter- or intra-molecular palmitoyl migration based on the LC-MS/MS result, since the resultant peptides have different ionization efficiencies.

The thioester group has a very strong UV absorption at 230 nm with an extinction coefficient (ε) of 4300 M^{-1} cm^{-1} compared to that of the amide group (ε = 122 M^{-1} cm^{-1}) [195]. Thus, the change in the *S*-palmitoyl content (*c*) under various incubation conditions can be studied by monitoring the UV absorbance (*A*) at 230 nm, according to the Lambert-Beer law: $A = \varepsilon cL$, where L is the light path length. Figure 4.9a shows that the UV absorbance of $GC_{palm}LGNAK$ was reduced by nearly half when incubated in 50 mM Tris buffer (pH 7.4) for 3 hr, indicating a significant loss of *S*-palmitoylation. This is in stark contrast to the previous observation that the *S*-palmitoyl group in several palmitoyl peptide standards was stable in neutral Tris buffer. However, the *S*-palmitoyl loss in $GC_{palm}LGNAK$ can be greatly slowed by addition of RapiGest^{TM} to the incubation

buffer, by an estimate of 510 fold (Figure 4.9b). Meanwhile, the LC-MS/MS result showed that addition of RapiGest^{TM} led to an abundance decrease of the two doubly palmitoylated peptides, $GC_{palm}LGNAK_{palm}$ and $G_{palm}C_{palm}LGNAK$, presumably the intermolecular palmitoyl migration products, by only 28-fold and 5-fold, respectively (Table 1). Thus, the thioester decay in the Tris-only buffer should mainly result from the thioester hydrolysis rather than from the intermolecular palmitoyl migration.

Table 4.1 The average ion abundances of the peptides resulting from incubation in Tris and Tris-RapiGest^{TM} and their relative ratios.

Peptide Sequence	**Average Ion Abundance**		**Abundance Ratio**
	Tris	Tris-RapiGest^{TM}	Tris /Tris-RapiGest^{TM}
$GC_{palm}LGNAK$	916255313	10680552362	0.09
$GC_{palm}LGNAK_{palm}$	52499259	1875914	27.99
$G_{palm}C_{palm}LGNAK$	339175845	68210171	4.97
$GCLGNAK_{palm}$ (dimer)	229817	519292	0.44
$G_{palm}CLGNAK$ (dimer)	349611	3655364	0.10

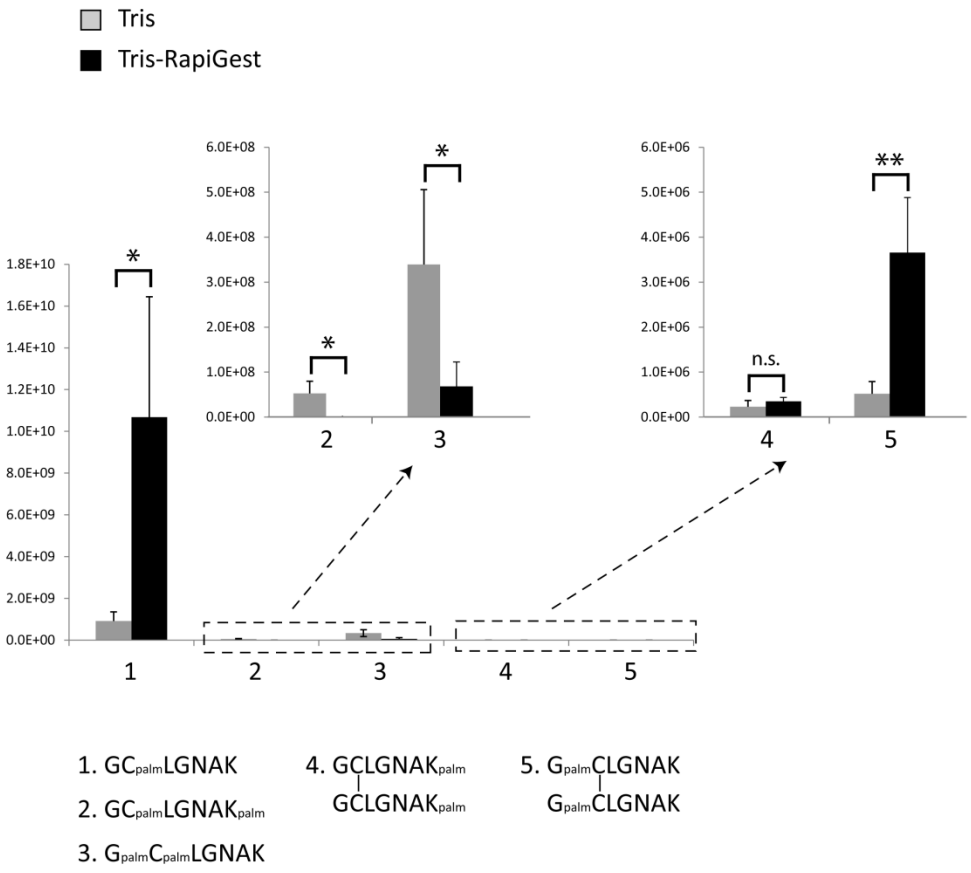

Figure 4.8 Comparison of the ion abundances of $GC_{palm}LGNAK$-derived peptides after a 3-hr incubation in 50 mM Tris (pH 7.4) in the absence or presence of 0.1% RapiGest^{TM}. Unpaired t test, standard deviation, n = 5, * $p < 0.05$, ** $p < 0.01$.

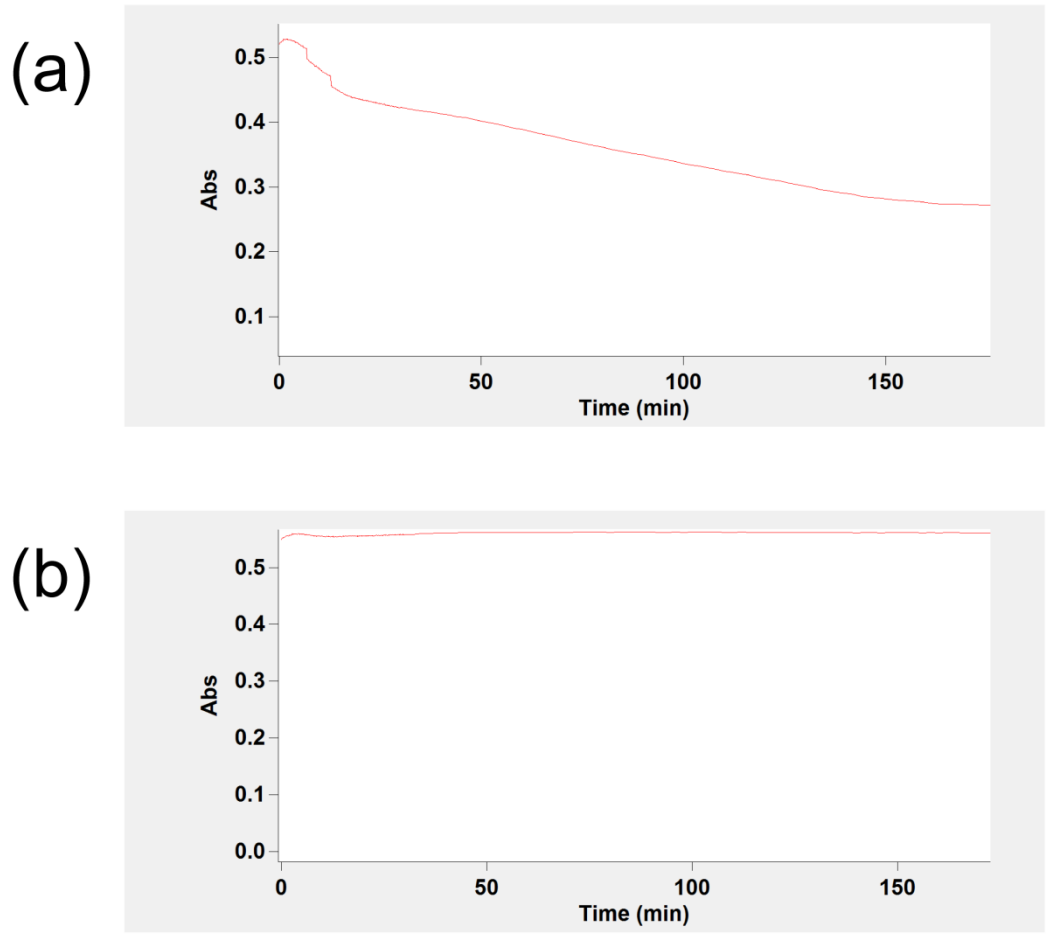

Figure 4.9 The decay of UV absorbance at 230 nm of GC_{palm}LGNAK in 50 mM Tris (pH 7.4) buffer without (a) and with (b) 0.1% RapiGest^{TM} over a 3-hr incubation.

4.3.4 RapiGest^{TM}: an S-palmitoyl Stabilizer in Aqueous Solution

The stabilizing effect of RapiGest^{TM} upon *S*-palmitoylation was further investigated by incubating the three previously studied palmitoyl peptide standards in the presence of DTT. All three palmitoyl peptides underwent severe palmitoyl loss when

DTT was added to the neutral Tris buffer, whereas addition of RapiGest^{TM} greatly decelerated the DTT-induced depalmitoylation process in all cases as shown in Figure 4.10. We suggest that the hydrophobic alkyl chain of the palmitoyl group can either insert into the RapiGest^{TM} micelle or aggregate with the RapiGest^{TM} molecules, and such interaction would shield the thioester group from the nucleophilic attack by water or DTT, thus stabilizing the *S*-palmitoylation. (Figure 4.11)

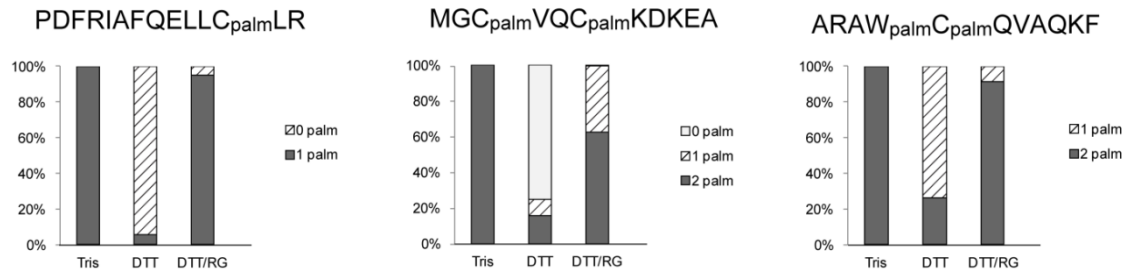

Figure 4.10 Stability of the three palmitoyl peptide standards, as represented by the relative abundances of the palmitoyl peptides and their various depalmitoylated forms after 1-hr incubation in 50 mM Tris (pH 7.4), 50 mM Tris/10 mM DTT, and 50 mM Tris/0.1% RapiGest^{TM}/10 mM DTT. All experiments were performed at 37 °C.

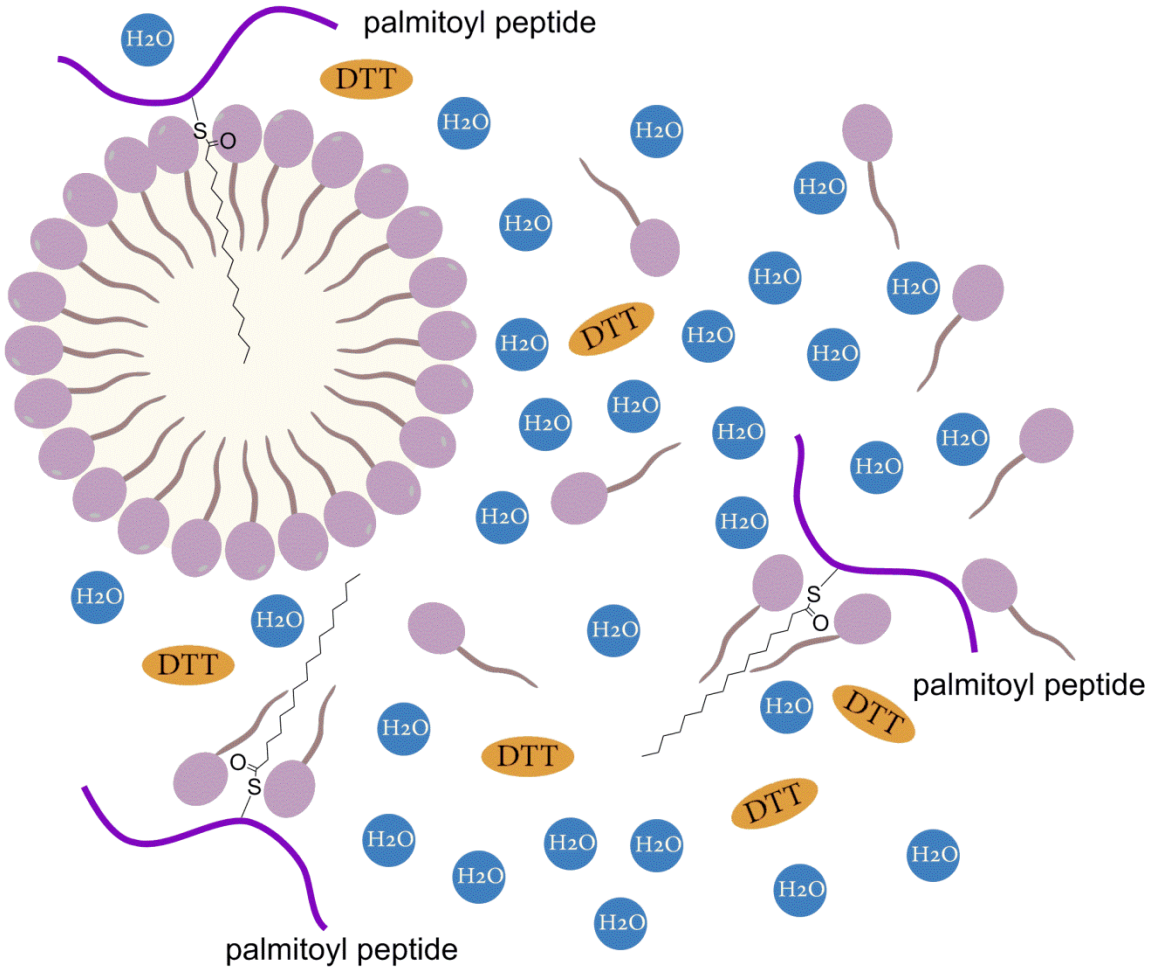

Figure 4.11 Proposed mechanism for the stabilization of the thioester group by RapiGest™.

4.3.5 Tandem MS Analysis of Palmitoyl Peptide Isomers

In proteomic studies, tandem MS is often used for characterization of PTMs, for which successful PTM localization requires PTM retention at its original site. For labile PTMs, such as sulfation and *O*-glycosylation, CID can lead to facile side-chain group loss, thus preventing accurate PTM localization. Additionally, PTM relocation has been

observed during CID of phosphotyrosine-containing peptide monoanions [203], although another study suggested that such relocation of the phosphate group was minimal during CID of both tryptic and Lys-N generated peptide cations [204].

Here, we first investigated the LC-MS/MS behaviors of three singly palmitoylated peptide isomers [GCLGNAK+palm]. The EIC of the *S*-palmitoyl peptide standard GC_{palm}LGNAK contained a single peak (Figure 4.12a), with the doubly charged ions as the dominant species in its mass spectrum (Figure 4.12c). Incubation in 100 mM ABC (pH 8.0) followed by DTT treatment produced three peaks in the EIC for the singly palmitoylated species (Figure 4.12b). The isomer with the shortest retention time was identified as GC_{palm}LGNAK based on its similar retention time, ionization pattern and CID/ETD spectra as the *S*-palmitoyl peptide standard (Figures 4.13a, 4.14a). The isomer with the intermediate retention time was assigned as $GCLGNAK_{palm}$ based on the observation of a series of palmitoylated *y*/*z* ions in its CID/ETD spectra (Figures 4.13b, 4.14b). The isomer with the longest retention time was assigned as G_{palm}CLGNAK based on the presence of a series of palmitoylated *b*/*c* ions (Figures 4.13c, 4.14c) in its CID/ETD spectra. Noticeably, $GCLGNAK_{palm}$ and G_{palm}CLGNAK produced doubly charged precursor ions in much lower abundance than GC_{palm}LGNAK (Figure 4.12c), as expected when one of the two favored protonation sites was occupied by the transferred palmitoyl group.

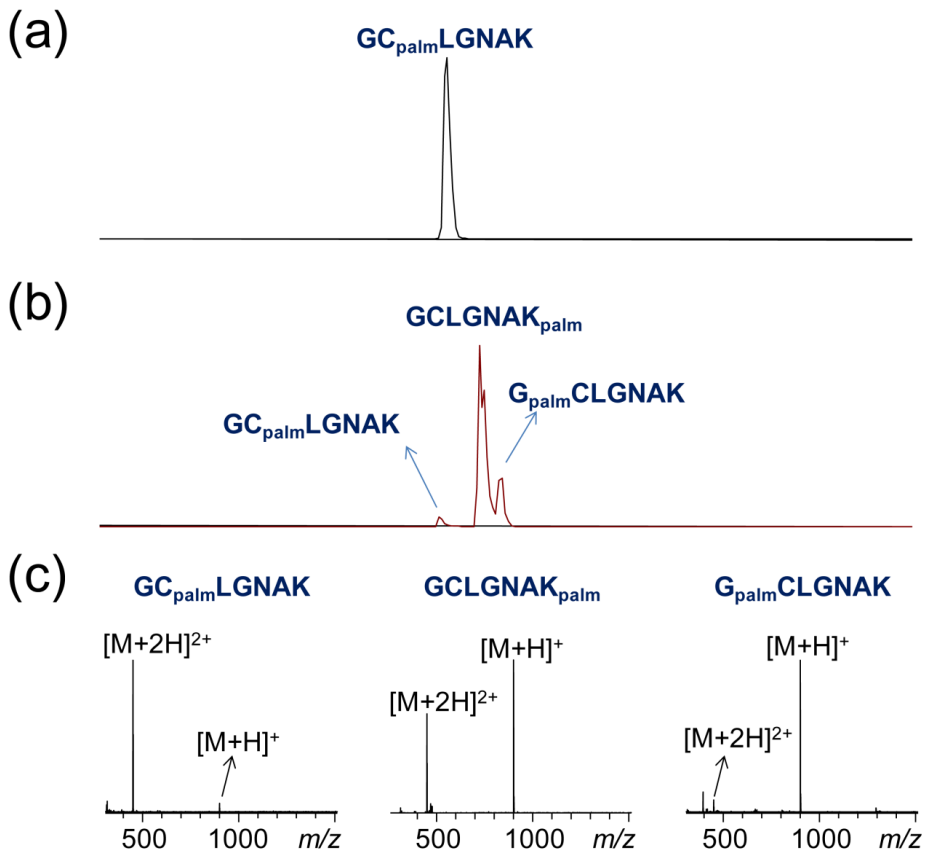

Figure 4.12 Integrated EICs of the singly palmitoylated species [GCLGNAK+palm] obtained from the LC-MS analysis of the *S*-palmitoyl peptide standard $GC_{palm}LGNAK$ (a) before and (b) after a 3-hr incubation in 100 mM ABC (pH 8.0) buffer at 37°C followed by DTT reduction. (c) MS spectra of the three [GCLGNAK+palm] isomers. Note that each integrated EIC represents the sum of the singly (*m/z* 450.78) and doubly (*m/z* 900.56) charged species of [GCLGNAK+palm].

As expected, the CID spectrum of the *S*-palmitoyl peptide standard GC_{palm}LGNAK (Figure 4.13a) was characterized by a series of palmitoylated *b* ions (b_2-b_6) and y ions without palmitoylation (y_1, y_2, y_4, and y_5). Surprisingly, a palmitoylated a_1, a palmitoylated b_1, and an unpalmitoylated y_6 ion were also observed in relatively high abundance, although they were supposed to be the diagnostic ions for palmitoylation at the N-terminus. The presence of these ions suggests the occurrence of palmitoyl migration from the cysteine residue to the peptide N-terminus during the CID process. For peptide ions, the formation of *b*- and *y*- ions during CID is usually initiated by the proton migration from a charged basic site (*e.g.* the amino group at the N-terminus) to an amide group along the peptide backbone. Protonation at a backbone amide not only weakens the amide bond, but also increases the electrophilicity of the amide carbon, which is subsequently attacked by the oxygen from its N-terminal neighboring carbonyl group followed by chemical rearrangement to produce an oxazolone *b* ion and its complementary *y* ion (Figure 4.15a). The b_1 ion cannot be produced via the oxazolone pathway in the absence of carbonyl oxygen on the N-terminal side of the first amide group along the peptide backbone. For the peptide GC_{palm}LGNAK, however, the carbonyl group of the cysteine thioester may be nucleophilically attacked by the N-terminal nitrogen during CID, leading to the transfer of the palmitoyl group from the cysteine thiol to the amine at the N-terminus. After migration, the carbonyl oxygen from the palmitoyl group can attack the N-terminal amide carbon to produce a palmitoylated b_1 ion and its complementary unpalmitoylated y_6 ion (Figure 4.15b). Because of the palmitoyl migration, CID of GC_{palm}LGNAK generated the same *b*- and *y*-ion series as that of

G_{palm}CLGNAK, but with different ion abundances. A major difference between the CID spectra of these two peptides is the presence of a $[M + H - 238.23]^+$ ion in the GC_{palm}LGNAK spectrum but not in that of G_{palm}CLGNAK. The 238.23 Da loss from the precursor ion corresponds to the loss of a palmitoyl group ($C_{16}H_{30}O$), which is diagnostic to *S*-palmitoyl peptides, as reported previously [200]. Meanwhile, Hoffman and Kast reported that no neutral loss of a myristoyl group was observed in CID of the doubly charged GAPVPYPDPLEPR with a myristoyl group covalently attached to its N-terminus through the amide linkage which is the same linkage as the N-terminal palmitoylation in G_{palm}CLGNAK studied here [176]. Moreover, in the CID spectrum of $GCLGNAK_{palm}$ (Figure 4.13b), the palmitoyl group was also retained on the precursor ion and all fragment ions, further indicating that the amide-linked N-palmitoylation is stable under CID and that the presence or absence of $[M+H-238.23]^+$ could be used for the differentiation of *S*- and *N*- palmitoyl peptide isomers.

The lysine palmitoylation in $GCLGNAK_{palm}$ could also be identified by ETD based on the observation of several palmitoylated *z*-ions (Figure 4.14b). However, it was challenging to use ETD for differentiation of GC_{palm}LGNAK (Figure 4.14a) and G_{palm}CLGNAK (Figure 4.14c). ETD produced the same backbone fragments from these two isomers, as the potential diagnostic c_1 fragments had too low abundance to be efficiently charged. The other potential diagnostic ion, the palmitoylated z_6 ion from GC_{palm}LGNAK, underwent efficient side chain loss, producing the same w_6 ions (*m/z* 556.31) as that of G_{palm}CLGNAK. However, different from G_{palm}CLGNAK (Figure 4.14c), the ETD spectrum of GC_{palm}LGNAK (Figure 4.14a) contains two peaks assigned

as $[M + 2H - C_{15}H_{31}COHS]^{+\bullet}$ (*m/z* 629.35) and $[M + 2H - NH_3]^{+\bullet}$ (*m/z* 844.54). The neutral loss of $C_{15}H_{31}COHS$ from the precursor ion was commonly observed in ECD and ETD of *S*-palmitoyl peptides [200], and may be produced by electron transfer to the protonated carbonyl of the thioester linkage followed by the radical-induced alpha cleavage (Figure 4.15c). The NH_3 loss from the charge-reduced precursor ion is very common in ECD/ETD, and generally does not provide any information for peptide sequencing. However, as the NH_3 loss often originates from the N-terminal amine, the absence of NH_3 loss could suggest the presence of the N-terminal modification [205].

As was the case for the singly palmitoylated peptide isomers, it is also possible to identify the doubly palmitoylated isomers [GCLGNAK+2palm] (*m/z* 569.8978) based on their fragmentation behaviors. A 3-hr incubation of $GC_{palm}LGNAK$ in the Tris or Tris/RapiGest^{TM} buffer produced two doubly palmitoylated isomers (Figures 4.6c, 4.7c). The CID spectrum of the isomer that eluted first (RT = 51.9 min) (Figure 4.16a) was characterized by a series of *y* ions with a palmitoyl group (y_1, y_2, y_4, and y_5), indicating that the C-terminal lysine was one of the palmitoylation sites. Meanwhile, the presence of $[M + H - 238.23]^+$ indicated that the second palmitoyl group was attached to the cysteine residue. Thus, the first isomer could be identified as $GC_{palm}LGNAK_{palm}$. The doubly palmitoylated isomer that eluted later (RT = 53.2 min) was similarly identified as $G_{palm}C_{palm}LGNAK$ based on the observation of the $[M + H - 238.23]^+$ ion and a series of *b* ions carrying two palmitoyl groups ($b_{2\text{-}6}$) (Figure 4.16b). The CID spectra of the two disulfide-bonded dimers (Figures 4.6d, 4.7d) are shown in Figure 4.16c-d, and they could be identified as the homo-dimer of $GCLGNAK_{palm}$ (RT = 47.25 min) and $G_{palm}CLGNAK$

(RT = 47.76 min), based on the characteristic palmitoylated *y*-ions and *b*-ions, respectively.

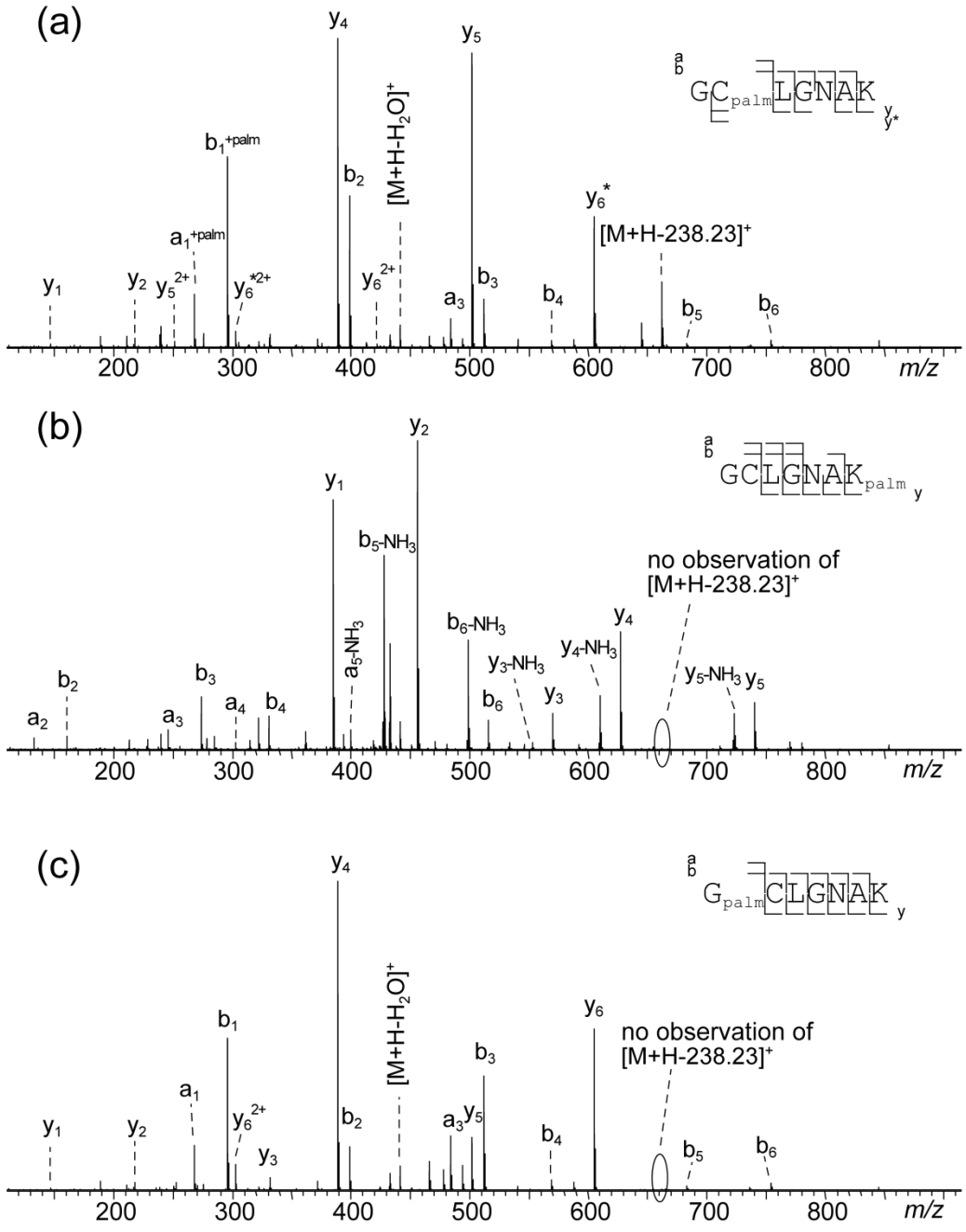

Figure 4.13 CID spectra of (a) $GC_{palm}LGNAK$, (b) $GCLGNAK_{palm}$, and (c) $G_{palm}CLGNAK$.

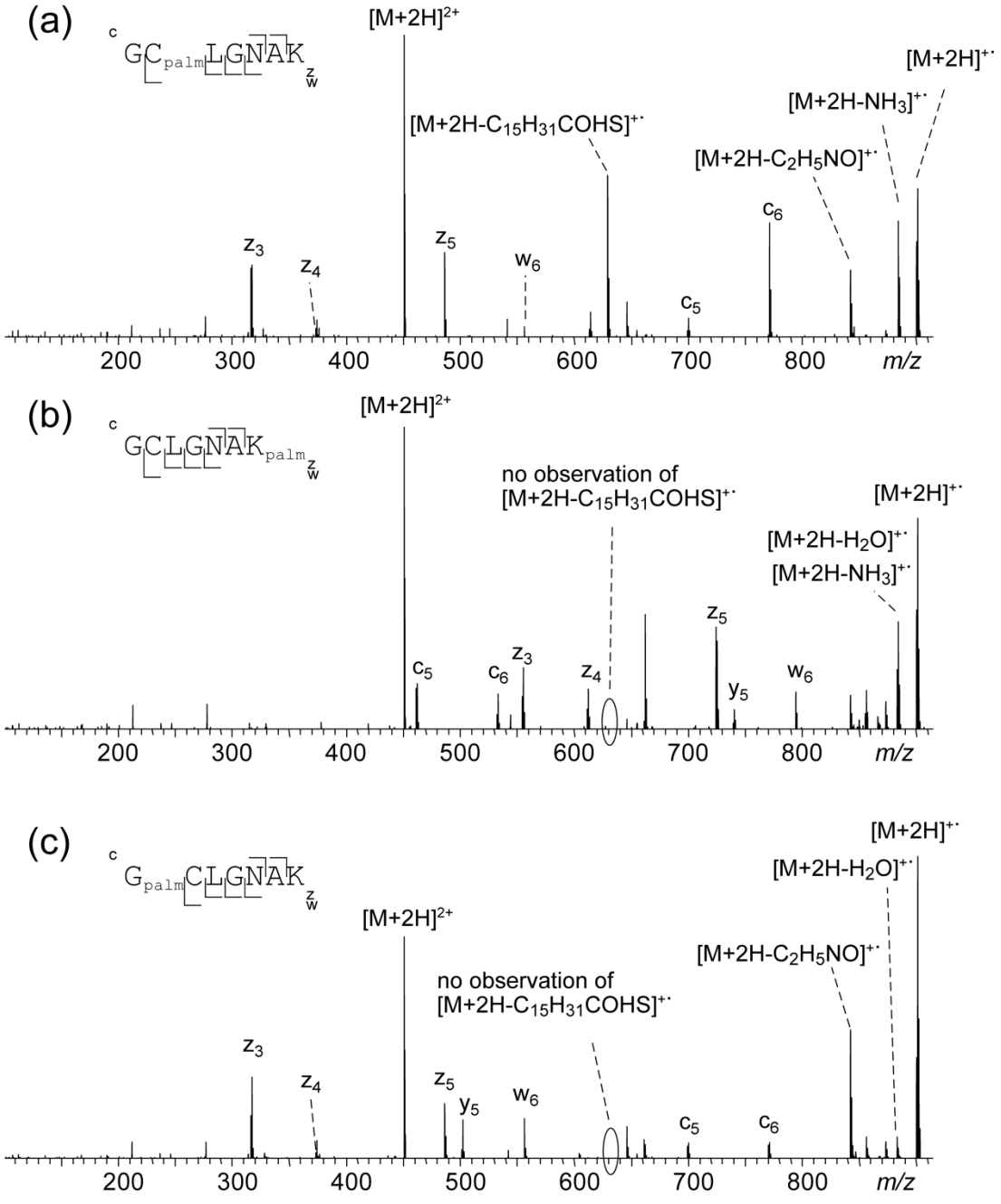

Figure 4.14 ETD spectra of (a) $GC_{palm}LGNAK$, (b) $GCLGNAK_{palm}$, and (c) $G_{palm}CLGNAK$.

(a)

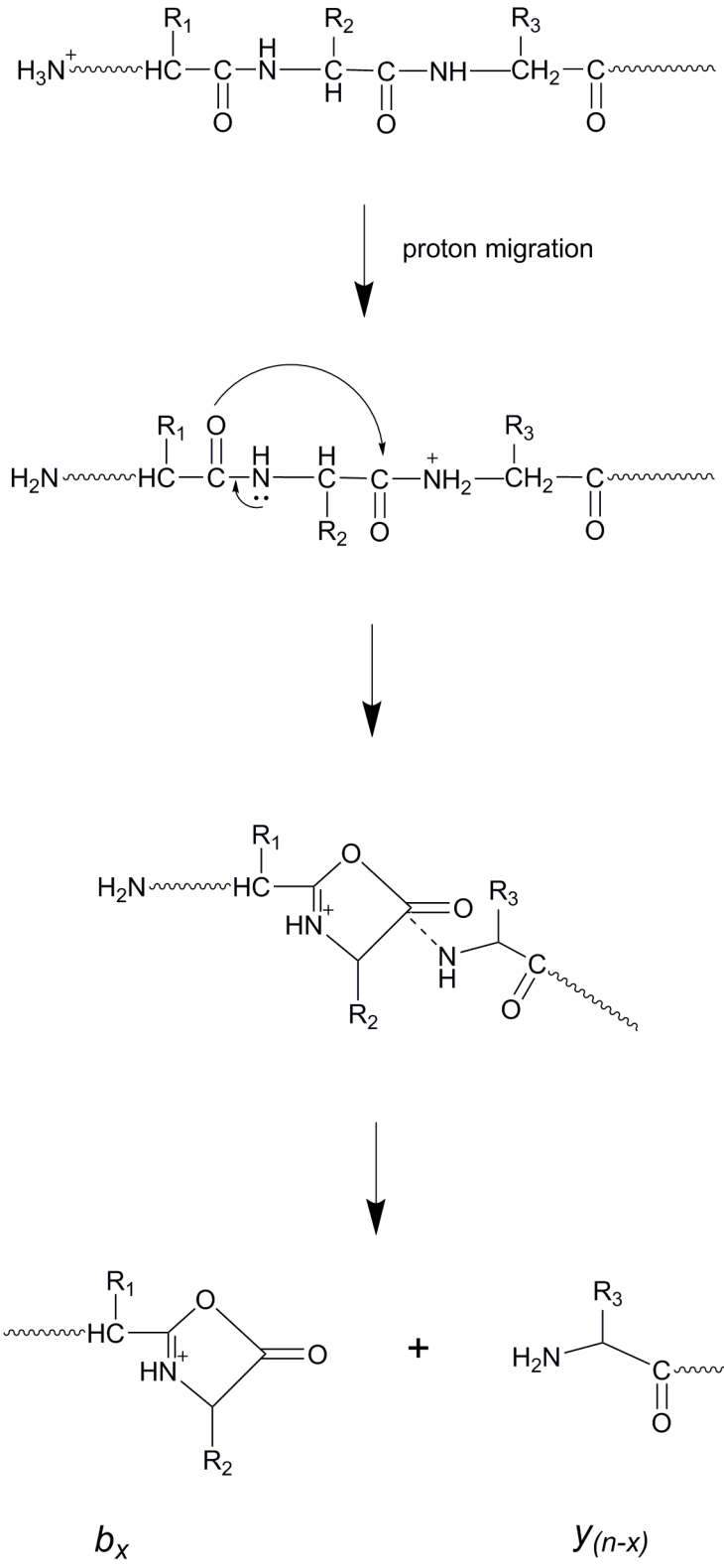

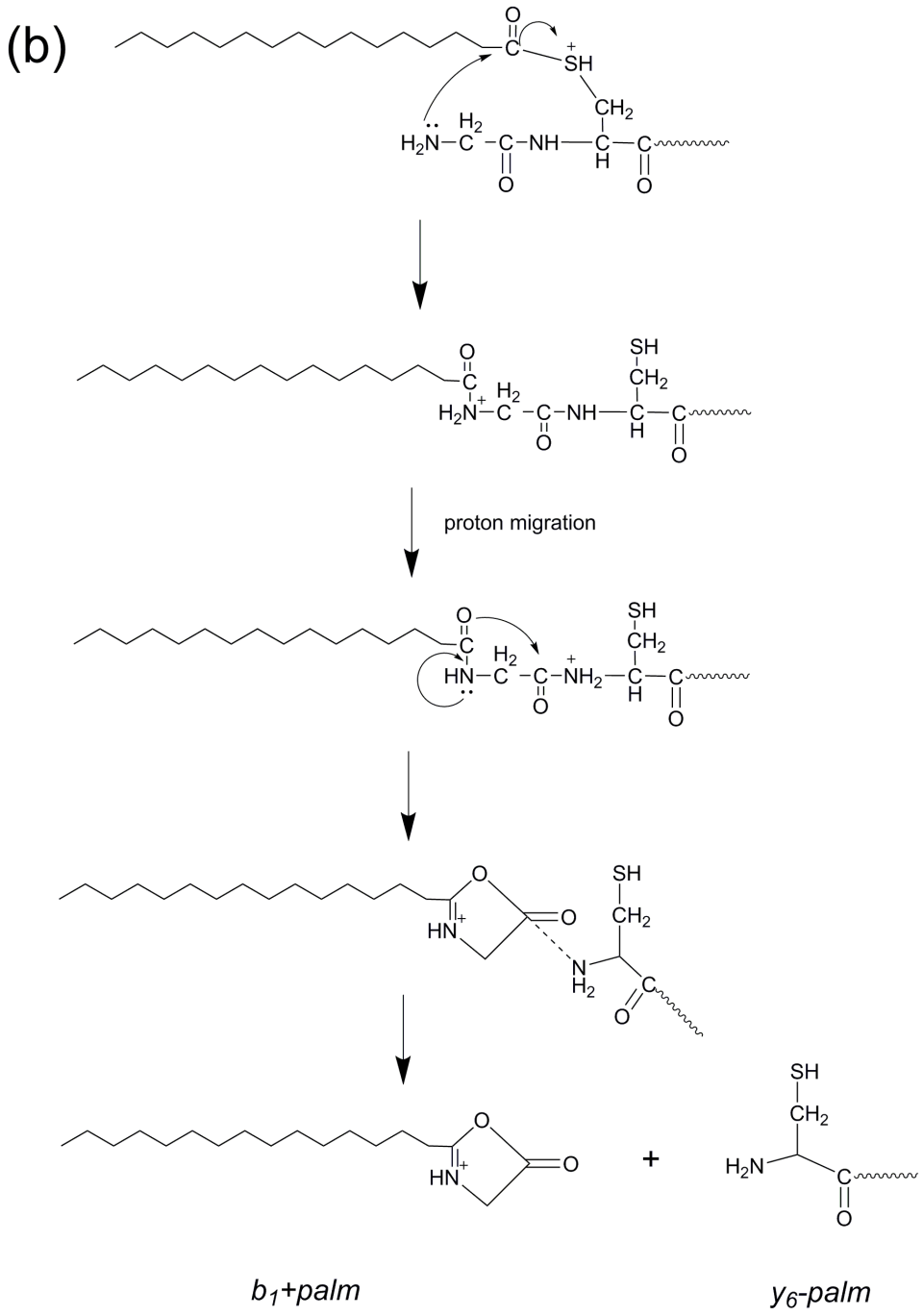
(b)
proton migration
+
b_1+palm
y_6-palm

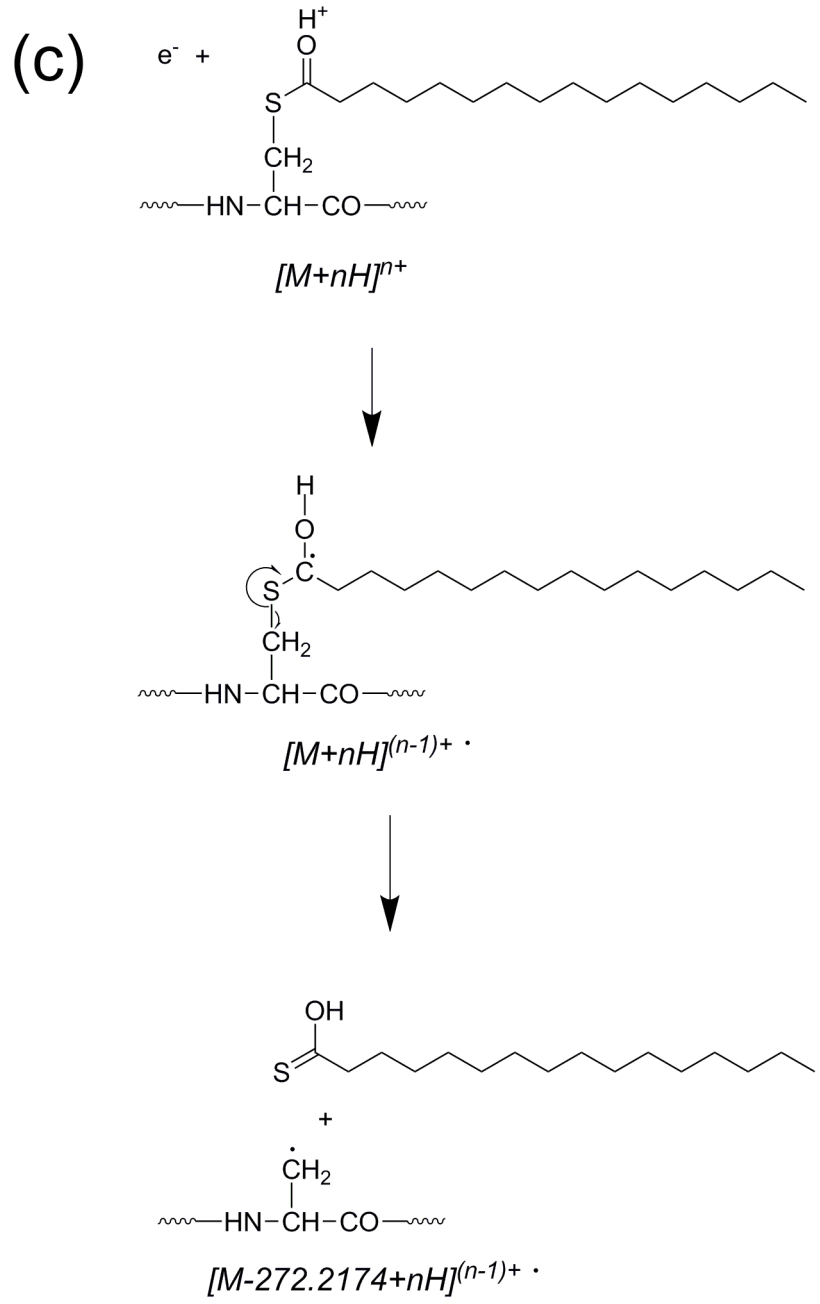

Figure 4.15 Proposed mechanisms for (a) formation of *b*- and *y*- ions in CID; (b) formation of b_1+*palm* and y_6-*palm* ions from the peptide $GC_{palm}LGNAK$ in CID; and (c) formation of the $[M + 2H - C_{15}H_{31}COHS]^{+\bullet}$ ion from the peptide $GC_{palm}LGNAK$ by ETD.

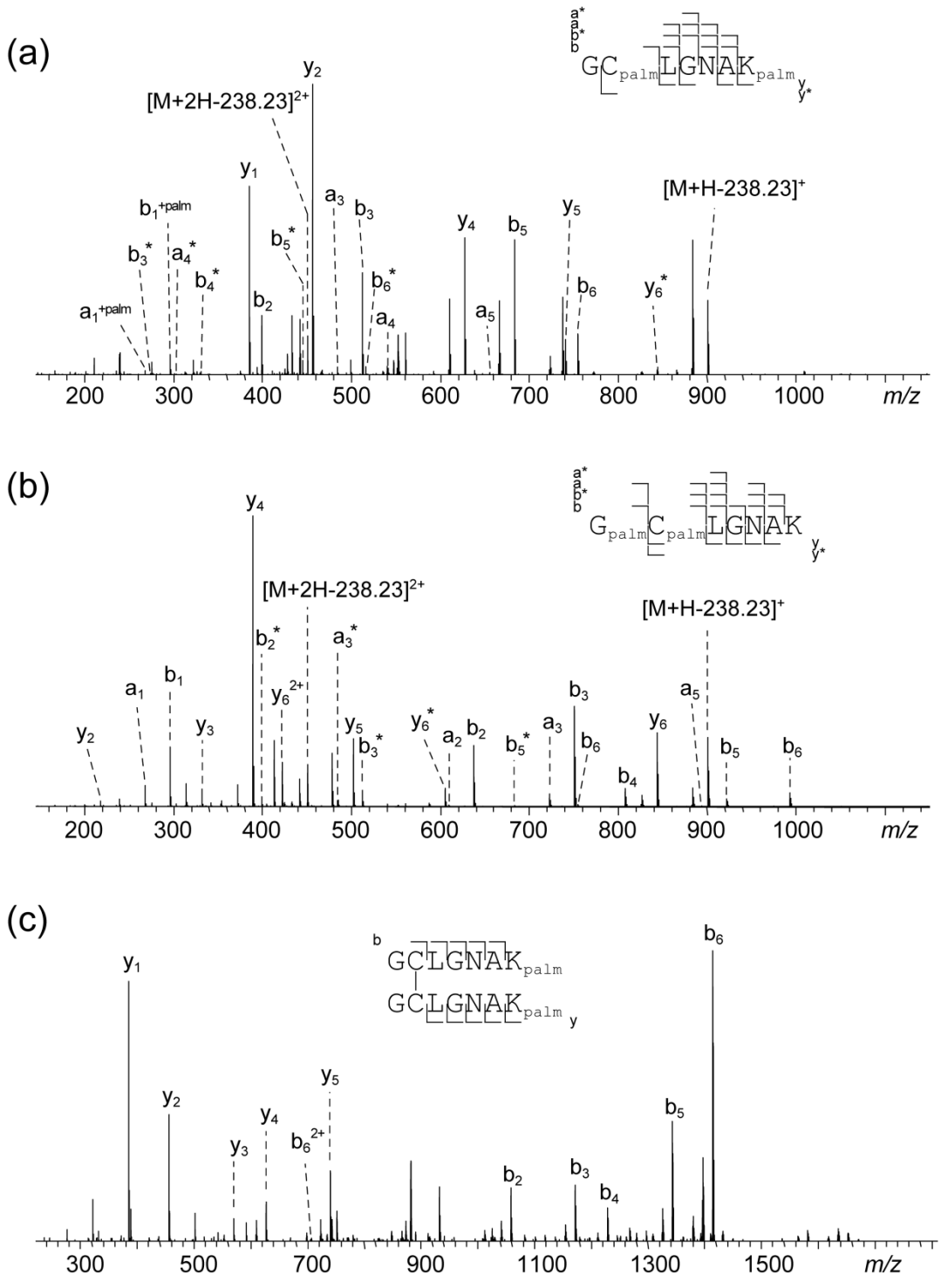
(a)
GC palm LGNAK palm
[M+2H-238.23]2+
[M+H-238.23]+
(b)
G palm C palm LGNAK
[M+2H-238.23]2+
[M+H-238.23]+
(c)
GCLGNAK palm
GCLGNAK palm
m/z

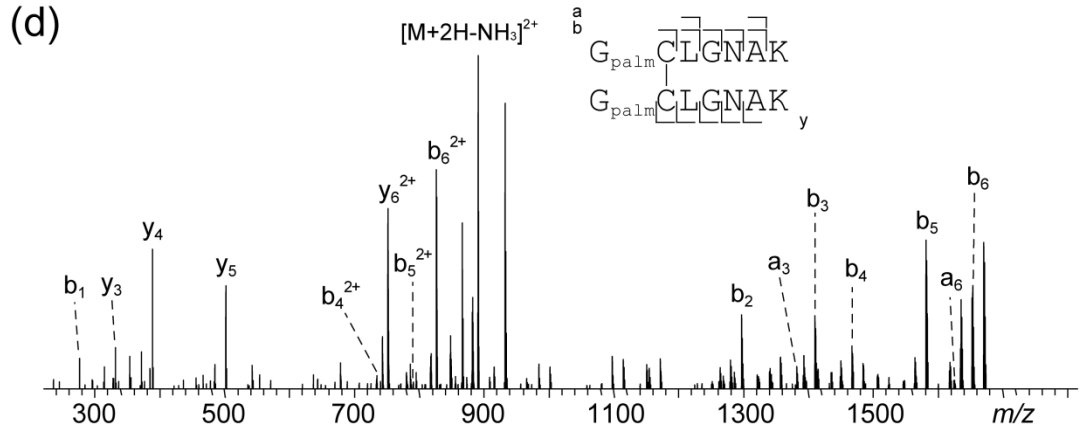

Figure 4.16 CID spectra of (a) $GC_{palm}LGNAK_{palm}$, (b) $G_{palm}C_{palm}LGNAK$, and the disulfide-linked homo-dimers of (c) $GCLGNAK_{palm}$ and (d) $G_{palm}CLGNAK$.

4.4 Conclusion

Here, using the *S*-palmitoyl peptide standard, $GC_{palm}LGNAK$, as the model system, we observed palmitoyl migration from the cysteine residue to either the peptide N-terminus or the lysine side chain during incubation in both neutral (Tris, pH 7.4) and slightly basic buffers (ABC, pH 8.0) commonly used for proteomic sample preparation. Moreover, the thioester of $GC_{palm}LGNAK$ underwent extensive hydrolysis, even in the neutral Tris buffer, which had previously been reported to preserve the *S*-palmitoylation on other palmitoyl peptide standards. It was found that addition of the MS-compatible detergent RapiGest^{TM} at suggested concentration could significantly inhibit thioester hydrolysis, DTT-induced thioester cleavage, and intermolecular *S*→*N* palmitoyl migration. Although the use of detergent may slightly facilitate intramolecular migration,

it should not be a major concern for the palmitoylation site localization, since the inter- and intra-molecular migration processes are both fairly slow. Therefore, RapiGest^{TM} is recommended during palmitoyl protein/peptide sample preparation. The palmitoylation site(s) in various palmitoyl peptide isomers can be generally determined by tandem MS analysis. However, complications may arise due to the gas-phase transfer of the palmitoyl group from the cysteine residue to the peptide N-terminus during CID, which may lead to false identification of *N*-palmitoylation. One must be careful with sample preparation and interpretation of tandem mass spectra for identification of *N*-palmitoylation.

Chapter 5: Surfactant-Induced Artifacts during Proteomic Sample Preparation

5.1 Introduction

Bottom-up proteomics is a MS-based methodology for protein identification and quantification, and for characterization of PTMs [206-210]. In bottom-up proteomics, MS is often used in conjunction with chromatographic separation to analyze peptides generated by enzymatic digestion of proteins. The success of a bottom-up proteomics experiment hinges upon attaining high sequence coverages, and this requires optimized sample preparation prior to MS analysis. A typical sample preparation procedure involves protein solubilization, disulfide reduction, enzymatic digestion, and sample cleanup. Detergents are often used to solubilize and denature proteins to improve their accessibility to enzymatic digestion, thereby producing more peptide fragments, especially for hydrophobic proteins. However, many detergents interfere with LC separation and MS analysis, and must be removed after digestion. Recently, several acid labile surfactants (ALS's) have been designed for proteomic sample preparation [211-213]. As its name suggests, an ALS degrades in acidic conditions, and its degradation products can be readily eliminated before subsequent LC-MS analysis. Figure 5.1 illustrates the decomposition pathway of a widely used ALS, sodium 3-((1-(furan-2-yl)undecyloxy)carbonylamino)propane-1-sulfonate, marketed by Promega under the trade name of ProteaseMAX ^{TM} (PM) [213]. The hydrophilic head of PM is connected to its hydrophobic alkyl tail through a labile furanyl carbamate group. Hydrolysis of PM produces a hydrophilic zwitterionic species (3-aminopropane-1-sulfonic acid) and a lipophilic compound (1-(furan-2-yl)undecan-1-ol), both of which can be easily removed,

by RP-SPE and by centrifugation, respectively. Unlike other ALSs, PM hydrolyzes under weakly basic conditions, *e.g.*, over the course of tryptic digestion (pH 8.0, 37 °C), thus eliminating the need for buffer acidification after digestion. Moreover, the hydrophobic degradation product of PM helps to improve the recovery of peptides by preventing their adsorption to plastic during and after digestion. These advantages over other ALSs would seem to make PM the favored surfactant for LC-MS analysis.

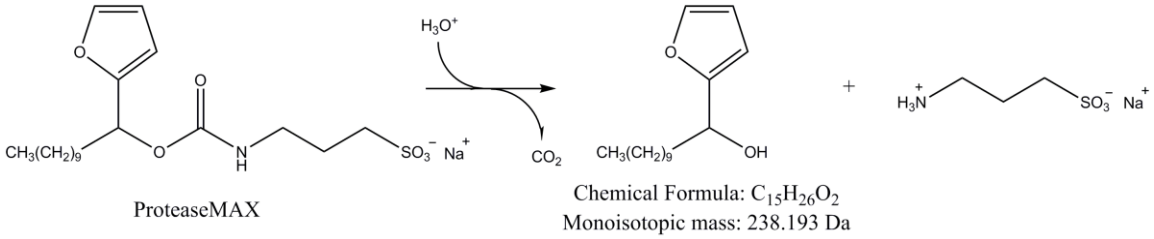

Figure 5.1 Schematic of acid-induced decomposition of ProteaseMAX ™

A major confounding factor in MS-based PTM analysis is the introduction of artifacts during sample preparation, especially in bottom-up proteomics, which requires additional sample processing steps associated with proteolysis [214-216]. Artifacts may be produced simply because of the prolonged sample incubation in various buffer solutions. A common artifact in bottom-up proteomics is asparagine deamidation in the tryptic digestion buffer, and its conversion to an aspartate may be mistaken as *in vivo* deamidation [217] or misinterpreted as a marker for newly released *N*-linked glycosylation sites following PNGase F digestion [218]. Sample exposure to ambient oxygen species may also lead to a variety of oxidative modifications that are difficult to differentiate from *in vivo* oxidative PTMs [219-221]. Moreover, the presence of

chaotropic, reducing, or alkylating reagents, detergents and other chemicals can cause additional modifications that complicate the spectral interpretation. For example, the unpolymerized acrylamide in polyacrylamide gels can react with a free sulfhydryl group to form a cysteinyl-*S*-propionamide adduct [222-224]. Cyanate, which is a degradation product from urea, can react with the amino and sulfhydryl groups to produce *in vitro* carbamylation [225, 226]. Some chemical modifications may be mistaken as *in vivo* PTMs, as highlighted in two recent studies. Thibault and co-workers showed that the common silver-staining procedure could introduce artifactual sulfation on serine, threonine and tyrosine residues, and this may be misinterpreted as *in vivo* sulfation or as phosphorylation if only low-mass accuracy data are available [227]. Mann and co-workers showed that lysine residues could be covalently modified by two acetamide molecules when iodoacetamide was used as the alkylating reagent [228]. The resultant 114.0429-Da mass shift is the same as that caused by the diglycyl modification from the ubiquitin remnant after trypsin digestion, and this could lead to erroneous reporting of ubiquitination sites.

The work presented here was prompted by our recent study on the lipid modifications of RGS4 from insect cells. RGS4 is a member of the family of GTPase activating proteins which are responsible for switching off the G protein signaling pathway. It was previously reported that RGS4 contains three potential *S*-palmitoylation sites at Cys95 and Cys2/Cys12 residues, as determined by a radioactive labeling experiment and site mutation [61]. We have recently shown that with optimized sample preparation, MS can be used for direct detection of *S*-palmitoylation [200]. The MALDI-

TOF MS analysis of the RGS4 tryptic digest revealed the presence of two types of hydrophobic modifications, which were initially assigned as *S*-palmitoylation and hydroxyfarnesylation based on their mass shifts and response to the HA treatment. However, these two modifications were found to be ubiquitously present in all cysteine residues, a characteristic of *in vitro* modifications. The present study aims to understand the origin of these modifications and to evaluate whether they could be problematic for PTM analysis.

5.2 Experimental Section

5.2.1 Materials

Tris, ABC, DTT, HA, and CHAPS were purchased from Sigma-Aldrich (St. Louis, MO). TFA, FA, IAM, and the micro BCA protein assay kit were acquired from Pierce (Rockford, IL, USA). DHB was obtained from Bruker Daltonics (Billerica, MA). ACN was obtained from Burdick and Jackson (Muskegon, MI). PM and Trypsin Gold™ were purchased from Promega (Madison, WI). RapiGest™ (RG) was acquired from Waters (Milford, MA). Ni-NTA Magnetic Agarose Beads were obtained from Qiagen (Valencia, CA). C18 ZipTip and 10K MWCO centrifuge filter were acquired from Millipore (Billerica, MA). POROS R1 50 was obtained from Applied Biosystem (Foster City, CA). Insect cell culture medium Sf-900™ II SFM was purchased from Invitrogen (Carlsbad, CA). Complete EDTA-free protease inhibitor cocktail tablets were acquired from Roche (Indianapolis, IN). The RGS4 baculovirus was generously provided by Prof. Elliott M. Ross at the University of Texas Southwestern Medical Center.

5.2.2 Overexpression and Purification of His-Tagged RGS4 from Sf9 Cells

Sf9 cells were maintained in the Sf-900™ II SFM media. His-tagged RGS4 was overexpressed by infection of the Sf9 cells with baculovirus. Cells were harvested after the 24-h infection and washed with PBS twice. The cell pellets were resuspended in 10 volumes of lysis buffer (300 mM NaCl, 25 mM sucrose, 0.5% CHAPS in 1x PBS supplemented with the protease inhibitor cocktail), sonicated, and kept on ice for 30 min. The cell debris was removed by centrifugation at 21,000 x *g* for 20 min at 4 °C. The affinity purification of His-tagged RGS4 was performed by incubation of the resultant cell extract with Ni-NTA magnetic agarose beads followed by elution against 250 mM imidazole in the lysis buffer according to the QIAexpressionist protocol [228]. The amount of protein was determined by the BCA protein assay. A small portion of the purified proteins was separated by SDS-PAGE, digested by trypsin according to the PM in-gel digestion protocol [229], and analyzed by an ultrafleXtreme MALDI-TOF/TOF mass spectrometer (Bruker Daltonics, Billerica, MA) for protein ID. A typical MALDI-TOF mass spectrum was acquired by signal averaging over 4000 laser shots from a Smartbeam-II™ Nd:YAG laser operating at 355 nm and a repetition rate of 2 kHz. The rest of the protein mixture was aliquoted and stored at -80 °C for later use.

5.2.3 In-Solution Proteolytic Digestion of His-Tagged RGS4

In-solution tryptic digestion was performed following the PM in-solution digestion protocol [230]. Briefly, a 50-µg aliquot of purified His-tagged RGS4 protein was precipitated with 4 volumes of cold acetone. The protein pellet was solubilized by adding 20 µL of ABC buffer (50 mM, pH 8.0) containing 0.2% PM, and vortexing for

15~20 min. Another 71 µL of ABC buffer was then added to the resultant protein solution. Reductive alkylation was performed by addition of 1 µL of DTT (500 mM) and incubation at 56 °C for 20 min, followed by addition of 3 µL of IAM (500 mM) and incubation at room temperature for 15 min in the dark. Digestion was performed by addition of 1 µL of PM (1%) and 4 µL of trypsin (0.5 µg/µL) and incubation at 37 °C for 3 hr. For tryptic digestion without reductive alkylation, 50 µg of purified His-tagged RGS4 was buffer exchanged against 100 µL of Tris (50 mM, pH 7.4)/0.05% PM solution through a 10K MWCO centrifuge filter, followed by addition of 2 µg of trypsin and incubation at 37 °C for 3 hr. In both cases, the resultant digests were incubated with 0.5% TFA at room temperature for 10 min to hydrolyze PM and to deactivate trypsin. The insoluble PM degradation product was removed by centrifugation at 16,000 x *g* for 10 min. The digests were aliquoted, dried and stored at -80 °C for later use.

5.2.4 LC-MS/MS Analysis

RGS4 digests with (RGS4-RA) or without reductive alkylation (RGS4-noRA) were desalted by C18 ZipTip. Briefly, samples were loaded onto C18 ZipTip pipette tips in 5% ACN/0.1% TFA, eluted with 90% ACN/0.1% TFA after 5 washes with 5% ACN/0.1% TFA, dried down, and re-dissolved in 5% ACN/0.1% FA. LC-MS/MS analyses were performed on an LTQ-Orbitrap XL instrument (Thermo Fisher Scientific, San Jose, CA) equipped with a nanoAcquity UPLC (Waters, Milford, MA) and a Triversa Nanomate system (Advion Biosystems, Inc., Ithaca, NY). Mobile phase A consisted of 99:1 water/ACN with 0.1% FA and mobile phase B consisted of 1:99 water/ACN with 0.1% FA. Samples were loaded onto a Waters Symmetry trapping column (C18, 5 µm,

0.18 mm ID x 20 mm) at a flow rate of 4 µL/min and washed with 95% A for 4 min. Separation was performed on a Waters BEH130 analytical column (C18, 1.7 µm, 0.15 mm ID x 100 mm) at a flow rate of 0.5 µl/min. The gradient was held at 5% B for 3 min, increased to 95% B over 90 min, and kept at 95% B for 9 min. It was then ramped to 98% B in 1 min, kept at 98% B for 4 min, and ramped down to 5% B over 3 min followed by column re-equilibration at 5% B for 15 min. The MS event cycle consists of one MS scan (r = 60,000 at m/z 400) and three data-dependent MS/MS scans (r = 7,500), where the three most abundant ions with charge state ≥ 2 were selected with an isolation window of ±3 m/z for CID tandem MS analysis with the normalized collision energy set at 35%. The MS data were processed manually using the Proteome Discoverer software (Thermo Fisher Scientific, San Jose, CA).

5.2.5 MALDI-TOF MS Analysis of the Hydrophobic Peptides

Hydrophobic peptides were enriched using the homemade RP-SPE tips packed with the POROS R1 50 resin. An aliquot of RGS4-noRA was dissolved in 5% ACN/0.1% TFA and loaded onto the POROS R1 50 tip. After 3 washes with 5% ACN/0.1% TFA, the sample was sequentially eluted with 20% ACN/0.1% TFA, 40% ACN/0.1% TFA, and 60% ACN/0.1% TFA. A small portion of the RGS4-noRA digest and each of its three fractions were crystallized with DHB (10 µg/µL in 40% ACN/0.1% TFA) and analyzed on an ultrafleXtreme MALDI-TOF/TOF mass spectrometer (Bruker Daltonics, Billerica, MA). Additional aliquots of the 40% ACN eluent which contains the majority of the hydrophobic peptides were dried down and incubated either in the 50 mM ABC buffer containing 10 mM DTT at 37 °C for 1 h, or in 1 M HA (pH 7.4) at room temperature for

1 h. The resulting peptides were also analyzed on the ultrafleXtreme instrument. The spectra were analyzed with the FlexAnalysis 3.4 software.

5.3 Results and Discussion

5.3.1 Extraction of His-Tagged RGS4 from Sf9 Cells

SDS-PAGE of the purified proteins showed a major band at ~25 kDa (> 90% purity, Figure 5.2). This band was excised and subjected to reductive alkylation, in-gel digestion, and MALDI-TOF MS analysis. Peptide mass fingerprinting showed a match of the 25-kDa band to RGS4 with 73% sequence coverage by tryptic digestion, indicating the successful overexpression and purification of RGS4.

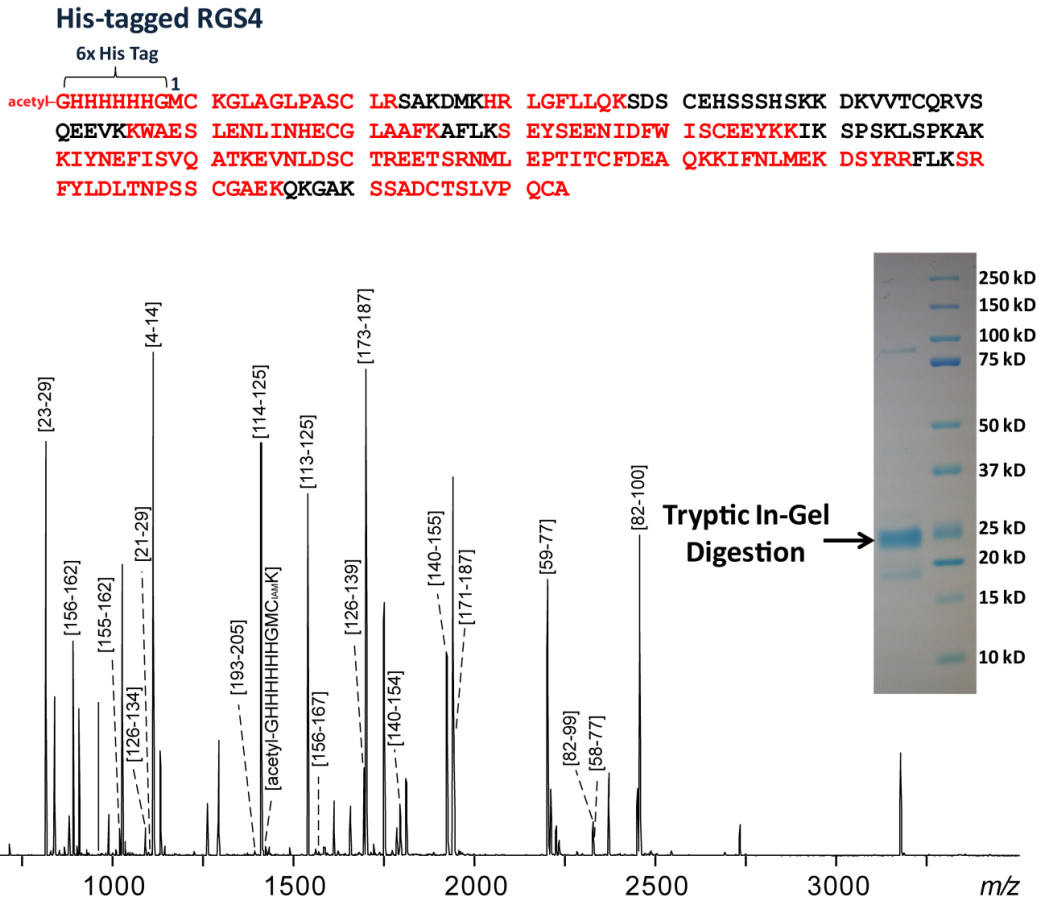

Figure 5.2 MALDI-TOF mass spectrum of the tryptic digest of the major band at 25 kDa in the SDS-PAGE of Ni-NTA purified proteins from the Sf9 cells overexpressed with His-tagged RGS4. Peptide mass fingerprinting showed a match of this band to RGS4 with a 73% sequence coverage (top).

5.3.2 Characterization of the Hydrophobic Peptides by MALDI-TOF MS Analysis

Although the in-gel tryptic digest of RGS4-RA covered 9 out of 11 cysteine residues, including all three reported *in vivo* palmitoylation sites, no palmitoyl peptide

was observed. The absence of palmitoyl peptides could be due to their low abundances and/or facile palmitoyl loss during sample preparation or MS analysis. It was recently shown that *S*-palmitoylation is unstable in the regular ABC-containing tryptic digestion buffer, and that the presence of DTT greatly accelerates the depalmitoylation process [200]. Here, following the protocol suggested by our previous study, in-solution tryptic digestion of purified RGS4 was performed in the neutral Tris buffer (50 mM, pH 7.4) with PM (0.05%) added to the digestion buffer to prevent protein aggregation and adsorption of hydrophobic peptides to onto plastic surfaces. Since there is no disulfide bond in RGS4, the reductive alkylation step was skipped to minimize potential palmitoyl loss. Enrichment of the hydrophobic peptides was achieved by stepwise elution as described in the experimental section.

The MALDI-TOF mass spectra of RGS4-noRA and its digestion products (Figure 5.3) showed that nearly all peptides were recovered in the 20% and 40% ACN elution buffers, with rough separation of the more hydrophilic peptides into the 20% ACN/0.1% TFA eluent and the hydrophobic peptides into the 40% ACN/0.1% TFA eluent. The majority of the hydrophobic peptides contained either modification X (238.19 Da) or modification Y (220.18 Da) (Figure 5.4a). To further determine the linkage of these modifications, the 40% ACN eluent was subjected to either DTT or HA treatment, and the MALDI-TOF mass spectra of the DTT- and HA-treated sample are shown in Figure 5.4b and Figure 5.5, respectively. Incubation with DTT or HA resulted in the loss of modification X from all X-modified peptides, whereas modification Y was resistant to the DTT and HA treatments. HA cleavage is considered specific to the thioester linkage

and has been commonly used to distinguish *S*-acylation from other cysteine modifications. Because modification X resulted in a mass shift close to that caused by palmitoylation (238.230 Da), and was similarly susceptible to the DTT and HA treatments, it seemed reasonable to assign it as *S*-palmitoylation. Meanwhile, modification Y was tentatively assigned as hydroxyfarnesylation (220.183 Da) due to their comparable mass shift and similar resistance to the DTT and HA treatments.

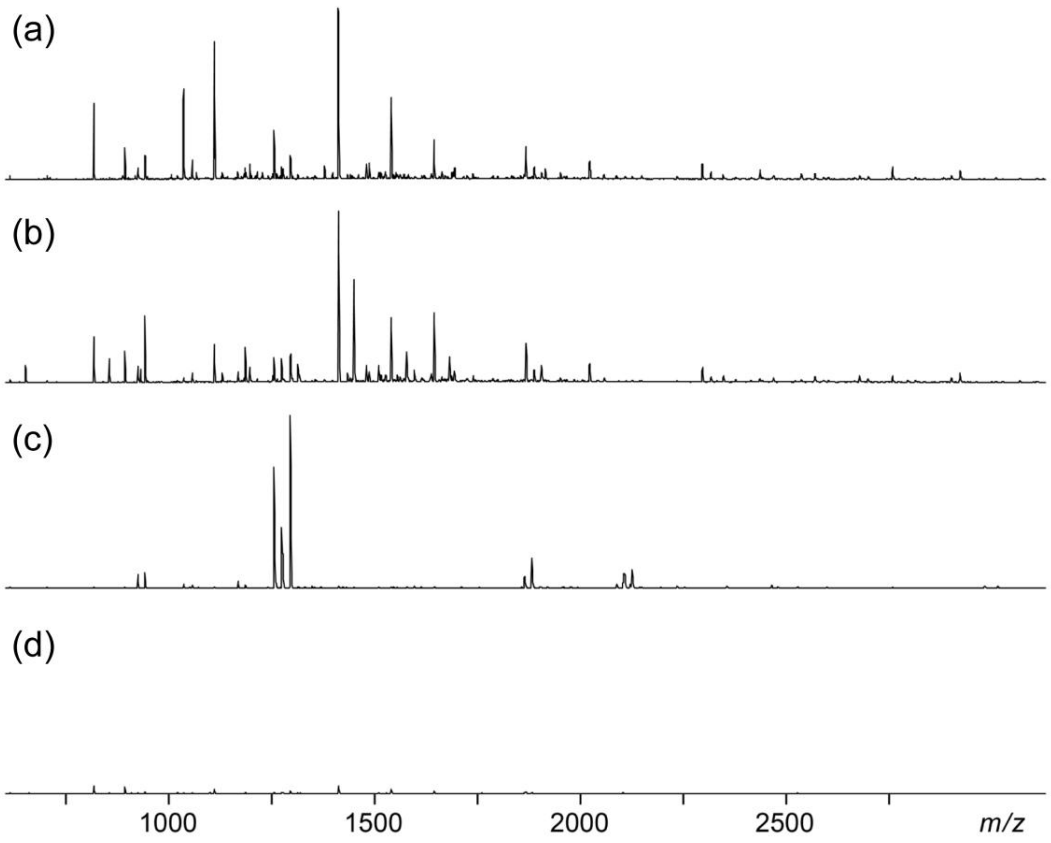

Figure 5.3 MALDI-TOF mass spectra of RGS4-noRA (a) and its sequential eluents with 20% ACN/0.1% TFA (b), 40% ACN/0.1% TFA (c), and 60% ACN/0.1% TFA (d).

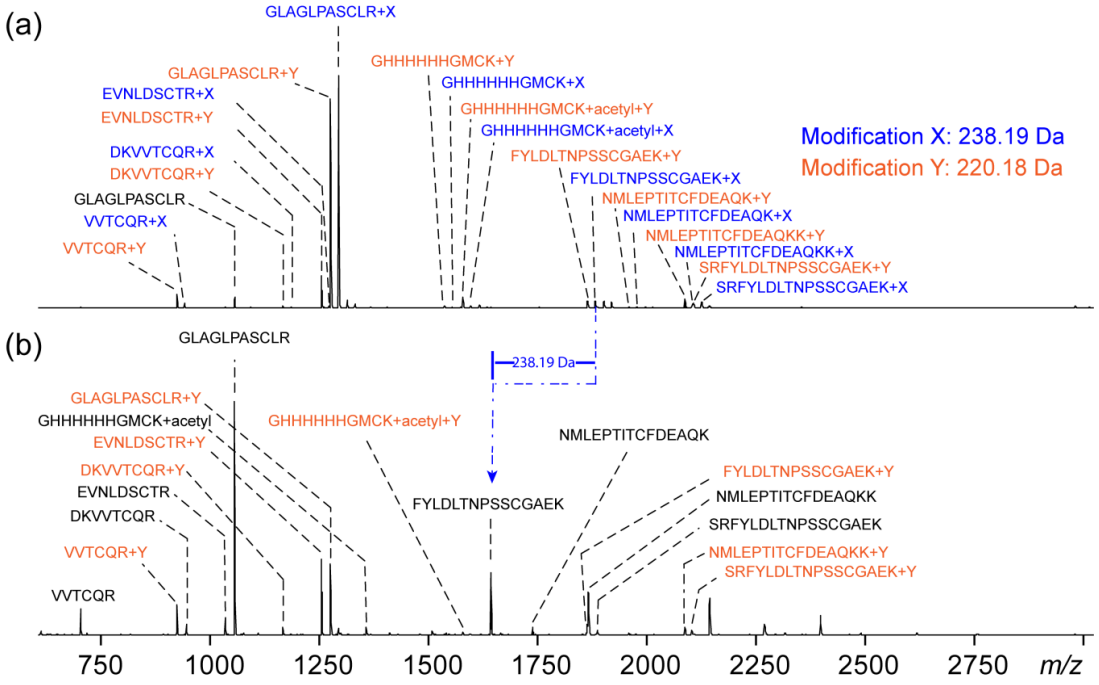

Figure 5.4 MALDI-TOF mass spectra of the hydrophobic peptides in the 40% ACN eluent (a) before and (b) after 1-h incubation with 10 mM DTT at 37 ^{o}C. X-modified peptides are labeled in blue, Y-modified peptides are labeled in red, and unmodified peptides are labeled in black.

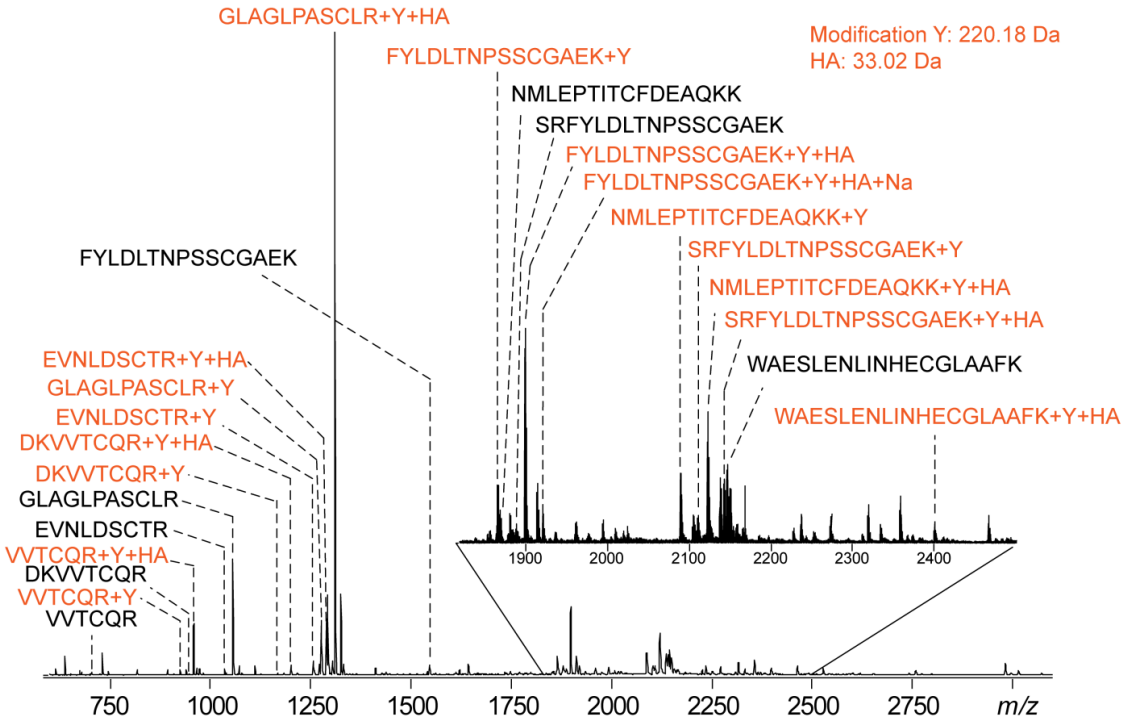

Figure 5.5 The MALDI-TOF mass spectrum of the 40% ACN/0.1% TFA eluent of the RGS4-noRA digest following the HA treatment.

5.3.3 LC-MS/MS Analysis of Hydrophobic Peptides

To further determine the modification site(s), the tryptic digest of RGS4-noRA was analyzed by LC-MS/MS on an LTQ-Orbitrap instrument. Figure 5.6a shows the TIC of the 3-hr tryptic digest of RGS4 analyzed on a nano-C18-UPLC column using the gradient program described in the experimental section. Most unmodified peptides were eluted within 35 min, whereas the modified peptides were eluted after 35 min, presumably due to their increased hydrophobicity. Like the MALDI-TOF MS analysis,

LC-MS/MS analysis also revealed two types of modifications on these hydrophobic peptides. Figures 5.6b-d and 5.7 show the extracted ion chromatograms and the CID tandem mass spectra of a tryptic peptide and its two modified counterparts from RGS4-noRA. The peptide eluted at 31.3 min (*m/z* 822.8834, Figure 5.6b) was identified as FYLDLTNPSSCGAEK ($[M + 2H]^{2+}$, *m/z* 822.8823) based on its accurate mass and CID spectrum (Figure 5.7a). This peptide was also detected in the X- and Y-modified forms. The CID spectrum of the X-modified peptide FYLDLTNPSSC$_X$GAEK ($[M + 2H]^{2+}$, *m/z* 941.9805, R.T. = 48.2 min, Figure 5.6c) is shown in Figure 5.7b. Modification X can be localized to the cysteine residue based on the mass difference between the y_4 and y_5 ions ($\Delta m = m_{Cys} + 238.196$). Similar to *S*-acylation, modification X appeared to be labile under CID, as evidenced by the presence of a high-abundance $[M – X + 2H]^{2+}$ ion and several *y* – X ions (labeled as y^* ions) in the CID spectrum. However, despite having the same nominal mass as palmitoylation and sharing similar chemical and physical properties as *S*-acylation, modification X cannot be assigned as *S*-palmitoylation, as such an assignment would have a mass error that significantly exceeds the range acceptable for an Orbitrap measurement. The CID spectrum of the Y-modified peptide FYLDLTNPSSC$_Y$GAEK ($[M + 2H]^{2+}$, *m/z* = 932.9744, R.T. = 48.5 min, Figure 5.6d) is shown in Figure 5.7c. The mass difference between the y_4 and y_5 ions as well as that between the b_{11} and b_{11} ions ($\Delta m = m_{Cys} + 220.184$) indicates that modification Y also occurred at the cysteine residue. Consistent with the MALDI-TOF MS result, the accurate mass of modification Y also matches that of hydroxyfarnesylation.

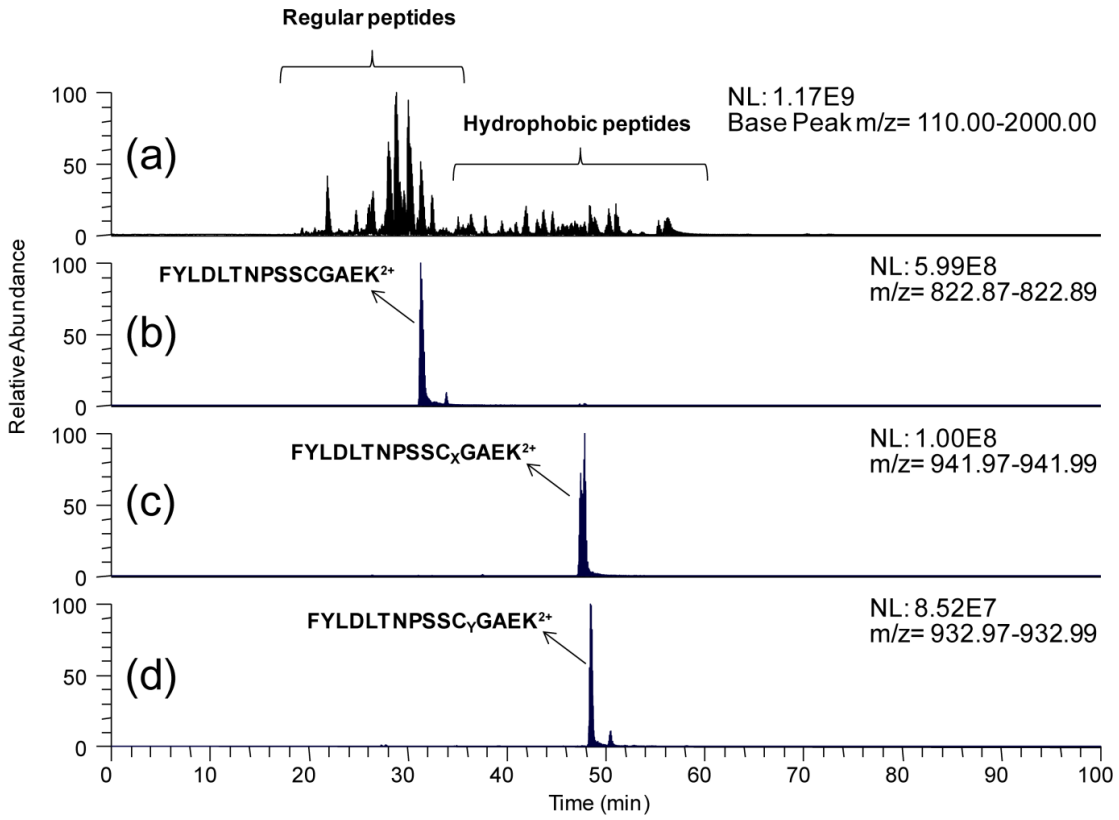

Figure 5.6 (a) The TIC of the RGS4-noRA sample; (b-d) the extracted ion chromatograms of the doubly charged tryptic peptide FYLDLTNPSSCGAEK and its X- and Y-modified forms.

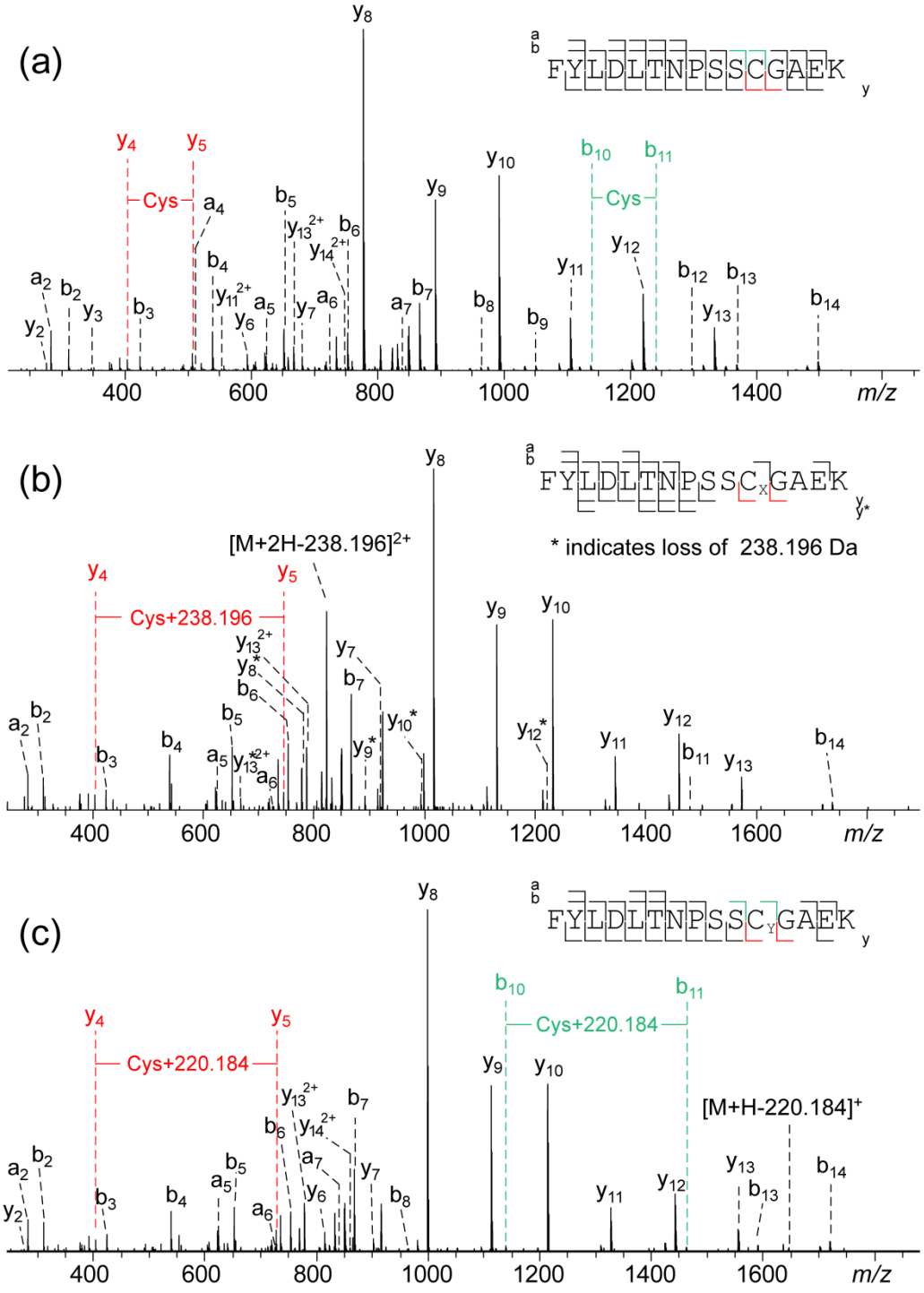

Figure 5.7 The CID spectra of the doubly protonated peptides (a) FYLDLTNPSSCGAEK, (b) FYLDLTNPSSC$_X$GAEK, and (c) FYLDLTNPSSC$_Y$GAEK.

Although the MS analysis positively identified two types of cysteine modifications here, neither modification has been reported on RGS4, and modification X does not match any known PTM in the Unimod database. X and Y appeared to be universal modifications, with either or both occurring on all eleven cysteine residues on RGS4 (Figure 5.8a). Such non-specificity is a hallmark of *in vitro* modifications. Moreover, the accurate mass of modification X matches that of the hydrophobic degradation product of PM, and the mass difference between modifications X and Y suggested that Y may be simply formed from X via loss of a water molecule. To further investigate the origin of these modifications, the tryptic digestion was performed in the Tris buffer without PM, but with the addition of a different ALS, RapiGest^{TM}. LC-MS/MS analysis of the RGS4 digest in RapiGest^{TM} (data not shown) showed no evidence of peptides carrying either modification X or Y, suggesting that these modifications were ProteaseMAX ^{TM}-induced artifacts.

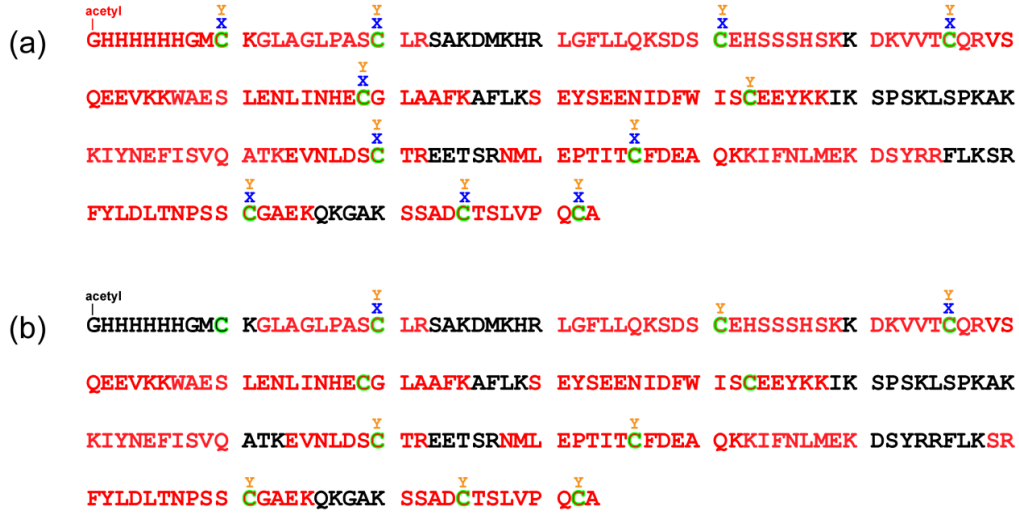

Figure 5.8 Sequence coverage maps and identified cysteine modifications obtained from the LC-MS/MS analysis of the tryptic digests of RGS-noRA (a) and RGS-RA (b).

Figure 5.9a illustrates a possible mechanism for formation of X-modified peptides. In an aqueous solution, the hydrophobic degradation product of PM, **1**, exists in equilibrium with its various protonated forms. The C5-protonated species can be represented by several resonance structures, **2a-2c**, among which the oxonium cation, **2c**, is the preferred structure, with all atoms having octets of electrons. The C4 position in **2c** may be attacked by the sulfhydryl group on the cysteine residue via 1,4-nucleophilic conjugate addition, forming the X-modified peptide, **3**. The cysteine sidechain can also be attached to other positions on the furanyl ring, depending on the original proton attachment site. For example, C2 protonation would lead to C3 substitution (Figure 5.10a). In general, protonation at α positions (C2, C5) is favored over protonation at β positions (C3, C4), as it results in more extensive charge delocalization. Further, a β-

protonated furan can only undergo 1,2-addition, and the resultant thioketal or thioacetal product is not as stable as the thioether (Figure 5.10b, c). It is important to note that, regardless of the cysteine attachment site, the aromaticity of the furanyl ring is gone in the X-modified peptide, and this may contribute to the shift of equilibrium towards loss of modification X, especially in the presence of HA or DTT due to their competitive binding to the oxonium. Meanwhile, formation of Y-modified peptides may proceed via a mechanism shown in Figure 5.9b, in which protonation of the hydroxyl group in **1** is followed by water loss. The resultant oxonium ion, **4**, may be attacked by the cysteine thiol via 1,6-nucleophilic conjugate addition to form the Y-modified peptide, **5**. In structure **5**, the aromatic furanyl ring is regenerated and modification Y is connected to the cysteine residue via a stable thioether linkage. Consequently, modification Y is more stable, and resistant to HA- and DTT-induced cleavages. Further chemical analysis is needed to validate the structure of X- and Y-modifications.

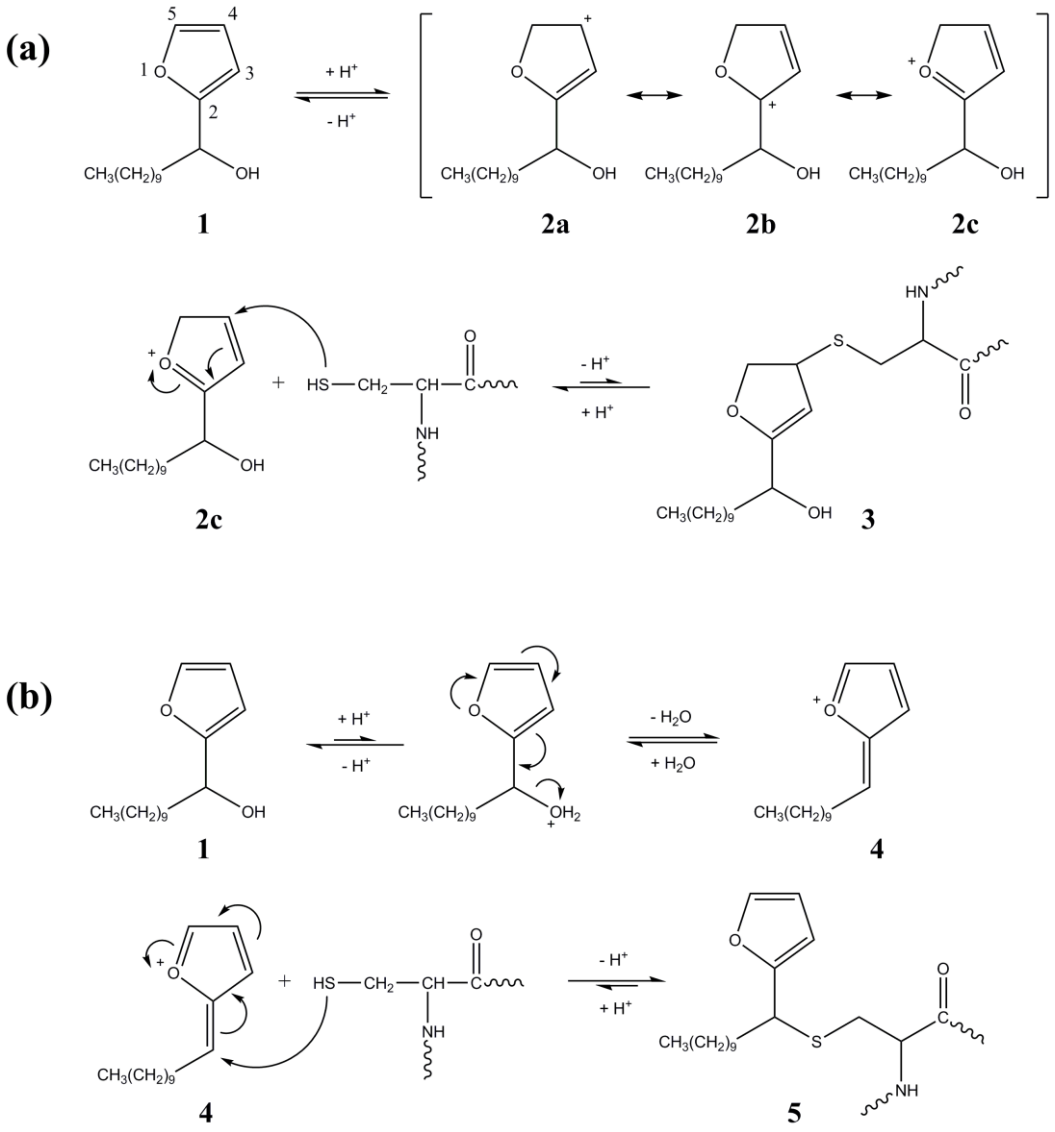

Figure 5.9 Proposed mechanisms for the formation of (a) X- and (b) Y-modified peptides

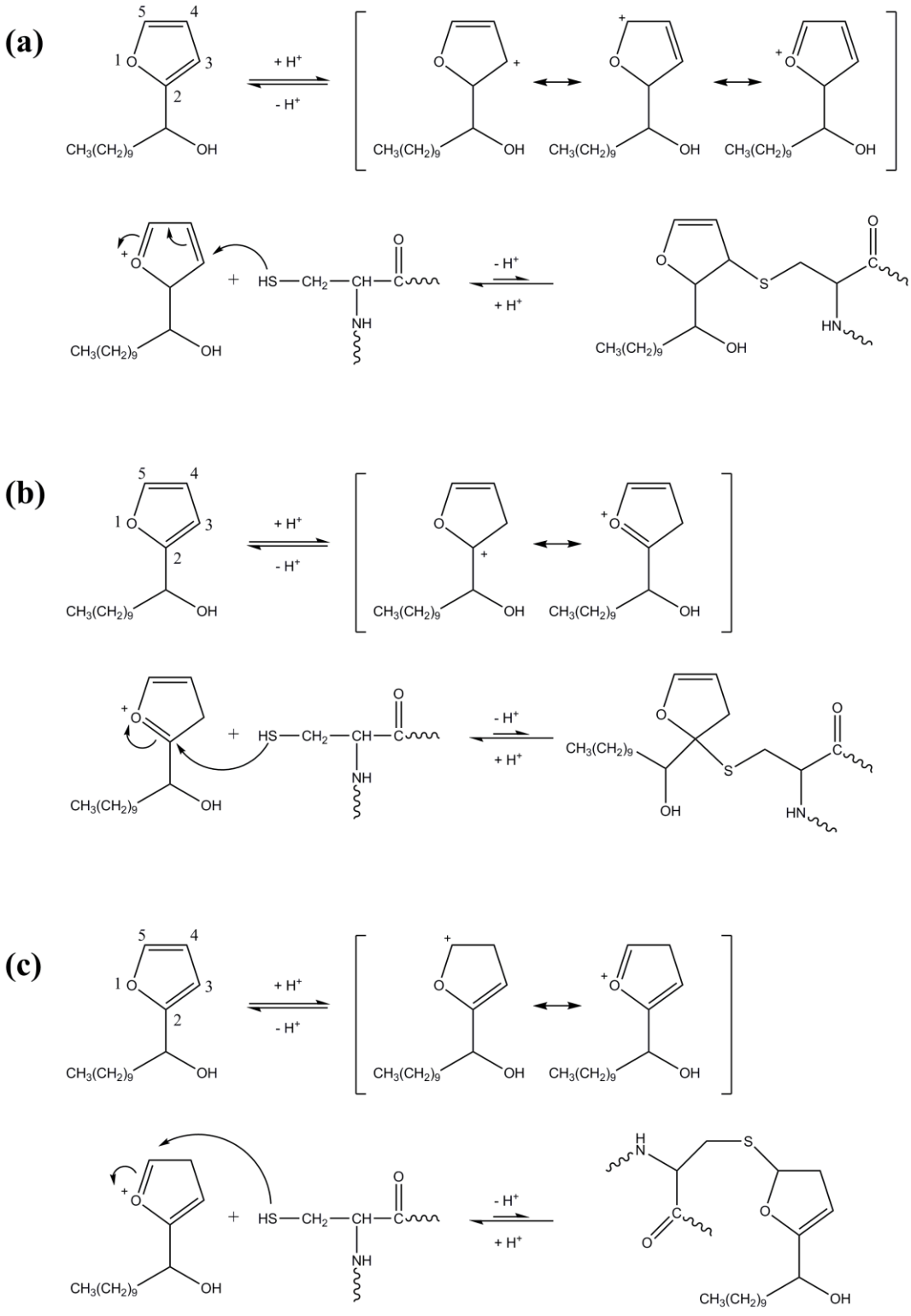

Figure 5.10 Alternative pathways for the formation of X-modified peptides

5.3.4 Extent of ProteaseMAX ™ -Induced Artifacts in Proteomic Sample Preparation

Given the wide use of ProteaseMAX ™ in proteomics studies, it is necessary to investigate the extent of PM-induced artifacts in proteomic sample preparation. The analysis so far has been focused on the RGS4-noRA sample, where the reductive alkylation step was omitted to minimize potential loss of *S*-palmitoylation. However, reductive alkylation is commonly used in MS-based proteomic analysis, and since the reducing reagent DTT has a profound effect on modification X, an accurate account of the extent of PM-induced artifacts should be obtained following the routine sample preparation protocol. Figure 5.8b shows the modification map of RGS4-RA from the LC-MS/MS analysis of its tryptic digest. Even with reductive alkylation, modification X was still detected on 2 cysteine residues and modification Y on 7 cysteine residues. The effect of reductive alkylation can be evaluated by comparing the relative abundance of X- and Y-modified peptides from the RGS4-noRA and RGS4-RA samples. To compensate for the variation in the sample loading amount, electrospray current, and other factors, the native reference peptide method [231] was adopted for ion abundance normalization among different samples. Here, the tryptic peptide LGFLLQK from RGS4 was chosen as the internal reference, since it does not contain any missed cleavage or residue that is prone to *in vitro* modifications. The peak area of the extracted ion chromatograms of the reference peptide and peptides of interest in all observed charge states was measured manually in the Xcalibur Quan browser, and the normalized peptide abundance was

calculated as the ratio of the integrated peak area of the peptide of interest to that of the internal reference peptide.

The relative abundances of 9 cysteine-containing peptides with free thiol, X-, Y-, or carbamidomethyl modification in the RGS4-noRA and RGS4-RA samples are summarized in Figure 5.11. In the RGS4-noRA sample, the extent of X- and Y-modifications varied substantially from peptide to peptide, possibly influenced by the location of the cysteine residue and the pKa value of its thiol group. Not surprisingly, with reductive alkylation, modification X was either undetectable or significantly diminished in abundance because of its vulnerability to the DTT treatment. The observation of a small amount of X-modified peptides, $VVTC_XR$ and $GLAGLPASC_XLR$, could be due to incomplete alkylation that allowed addition of X to the residual free thiol during the subsequent digestion step. Additionally, the hydrophobic X-groups may have been buried inside PM micelles and protected against the DTT cleavage. In contrast, in the sample prepared for the MALDI-TOF MS analysis (Figure 5.4), complete removal of modification X by DTT was achieved because PM was eliminated by hydrolysis under acidic condition prior to the DTT treatment.

The level of modification Y was also reduced in the RGS4-RA digest despite its apparent resistance to the DTT treatment (Figure 5.4). This could be due to the competing reaction of DTT with the hydrophobic PM degradation product. Consistent with this hypothesis, co-incubation of a cysteine-containing peptide standard GCLGNAK with PM and DTT for 3 hr produced negligible amounts of modifications X and Y (Figure 5.12b). On the other hand, the Y-modified peptide remained an abundant product when DTT or

HA was added after it had already been formed during the 3-h incubation with PM (Figure 5.12c, d). Similarly, many Y-modified peptides were detected in the RGS4-RA sample, and they were presumably formed during the protein solubilization step before the addition of DTT. A time-course study on these PM-induced modifications revealed that Y-modification was a slow process, with its level gradually increasing over a span of 5 hr, whereas X-modification was much faster, reaching a high level within 10 minutes. The level of X-modification dropped substantially at later time points, possibly due to its reversible nature and competition from the irreversible Y-modification (Figure 5.13). It appears that reductive alkylation can largely eliminate X-modification and significantly reduce the level of Y-modifications, provided that there is not much delay between the addition of PM and the addition of DTT. In an actual proteomic experiment, however, the rate of these modifications will likely vary depending on the accessibility of the cysteine residue and its local environment. The RGS4-RA study showed that these artifacts will remain a tangible problem even with a short solubilization period (Figure 5.11). It is recommended to revise the ProteaseMAX ^{TM} digestion protocol to minimize the impact of these artifacts.

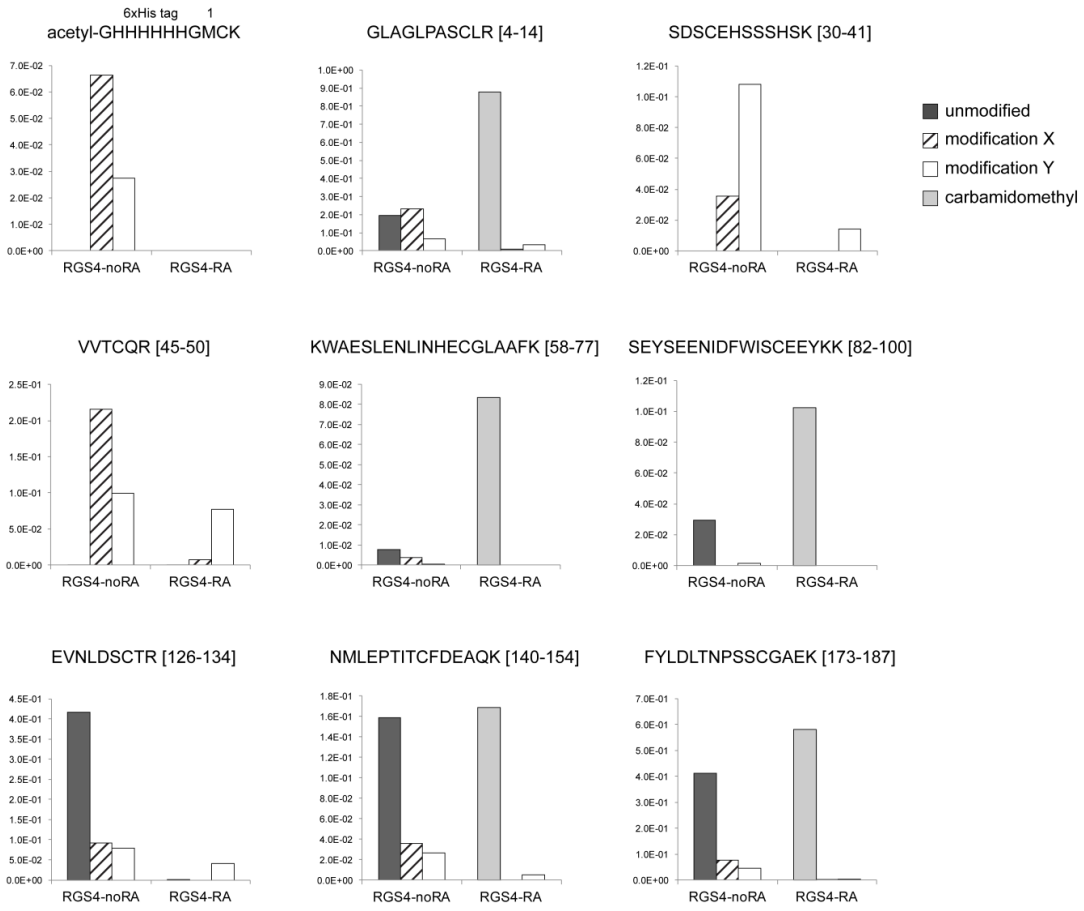

Figure 5.11 The relative abundances of 9 cysteine-containing peptides with free thiol, X-, Y-, or carbamidomethyl modification in the RGS4-noRA and RGS4-RA digests.

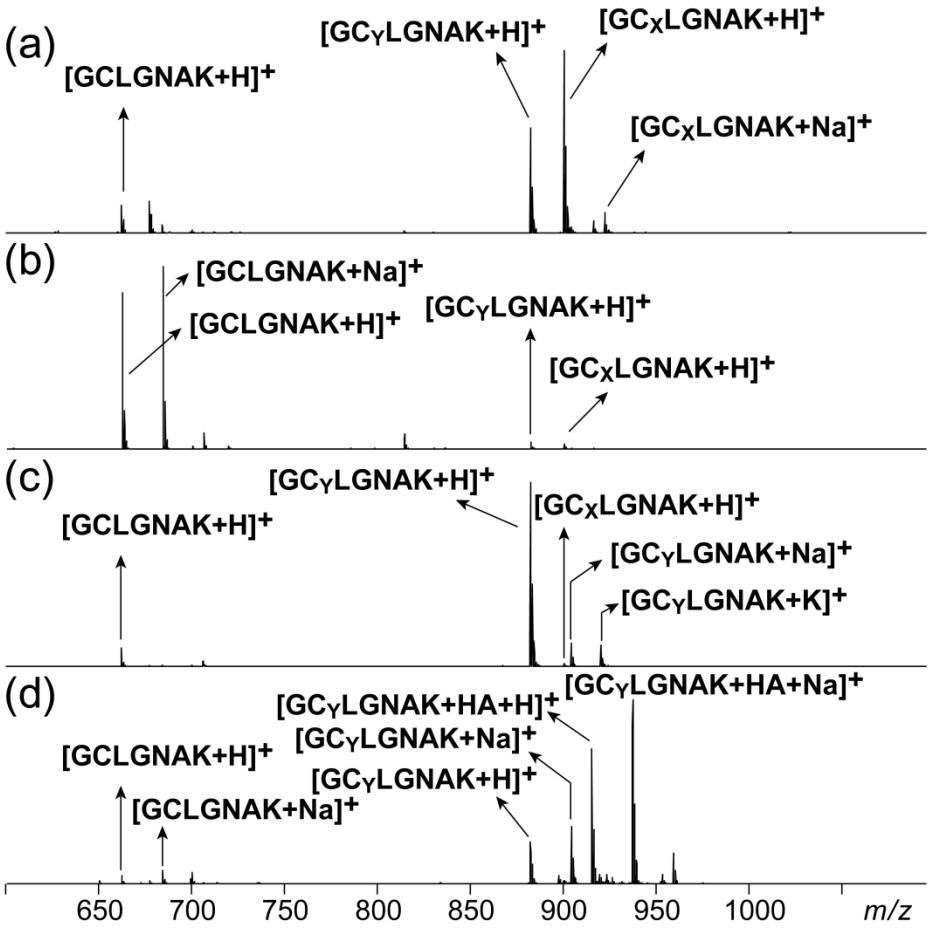

Figure 5.12 (a-b) MALDI-TOF mass spectra of the peptide standard GCLGNAK after a 3-hr incubation at 37 ^{o}C in 50 mM ABC/0.05% ProteaseMAX™ without DTT and with 10 mM DTT, respectively. (c-d) MALDI-TOF mass spectra of sample (a) after subsequent incubation in 10 mM DTT at 37 ^{o}C for 1 h or in 1 M HA at room temperature for 1 h, respectively.

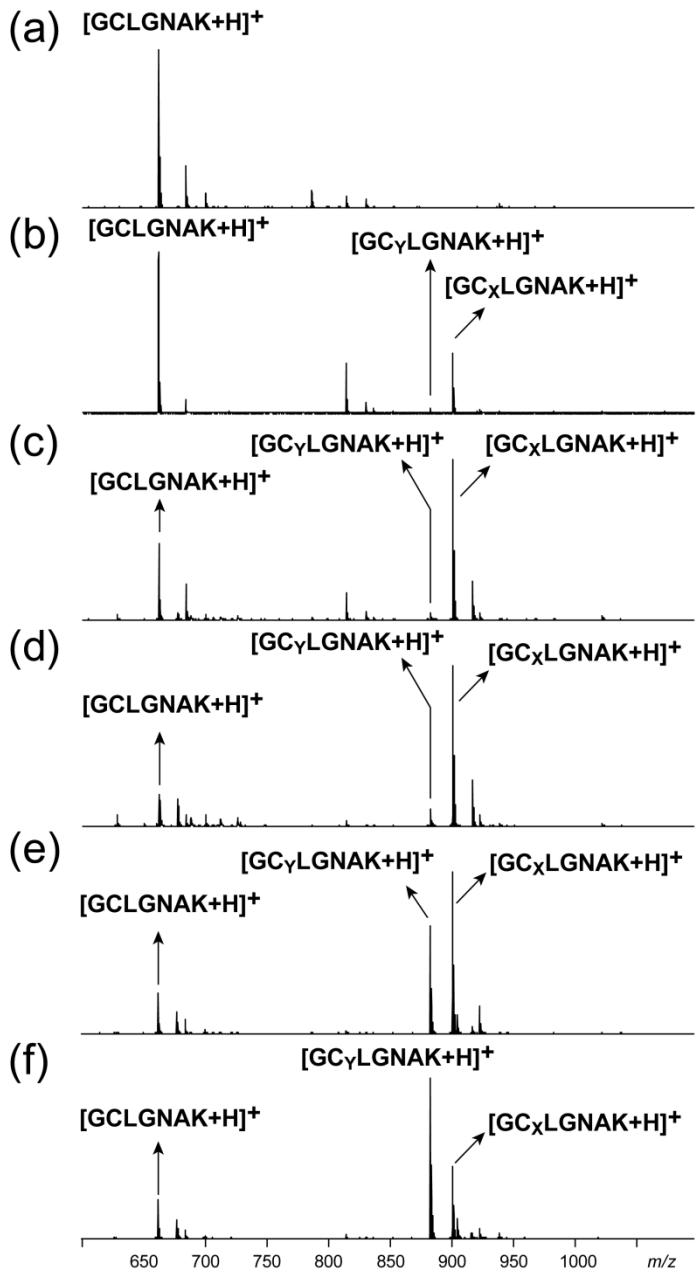

Figure 5.13 (a) The MALDI-TOF mass spectrum of the peptide standard GCLGNAK. (b-f) MALDI-TOF mass spectra of GCLGNAK after incubation in 50 mM ABC/0.05% ProteaseMAX™ at room temperature for 10 min (b), or at 37 ^{o}C for 30 min (c), 1 hr (d), 3 hr (e) and 5 hr (f).

5.4 Conclusion

The present study shows that two types of *in vitro* cysteine modifications (X and Y) can occur during routine proteomic sample preparation involving ProteaseMAX™. Modification X has the same nominal mass and similar chemical and physical properties as *S*-palmitoylation, including its gas-phase fragmentation behavior under CID, and this could lead to false reporting of *in vivo* palmitoylation, especially when a low-mass accuracy MS instrument is used. Modification Y has the same elemental composition as hydroxyfarnesylation, likely via the same thioester linkage, making it extremely difficult to differentiate these two modifications by chemical reactions or mass spectrometry. Although the level of PM-induced modifications can be substantially reduced by performing reductive alkylation immediately after a short solubilization period, addition of DTT also causes undesirable loss of *in vivo S*-acylation. Thus, one should be cautious with the use of ProteaseMAX ™ in proteomic sample preparation, especially when studying lipid modifications of proteins. In addition, the current study also calls for an investigation on the impact of these PM-induced artifacts on the accuracy of quantitative analysis of various cysteine modifications because they too, target the cysteine thiol group.

Chapter 6: Analysis of Lipid Modifications on RGS4 from Sf9 Cells

6.1 Introduction

RGS4 is a GTPase-activating protein that belongs to the RGS family. It facilitates the intrinsic GTPase of the Gα protein, accelerating the hydrolysis of GTP to GDP and thus bringing the Gα protein to its inactive form to switch off the G-protein coupled receptor (GPCRs) signaling (Figure 6.1). RGS4 is widely distributed in the central nervous system (CNS) [232]. By modulating the $G\alpha_{i/o}$ and $G\alpha_{q}$ activities [233], RGS4 regulates a number of neurotransmitter signals, such as dopamine [234], metabotropic glutamate [235], and serotonin receptor signaling [236]. Previous studies showed that RGS4-deficient mice have sensorimotor deficits [237], whereas a decrease in RGS4 expression has been linked to human schizophrenic disorders [238], suggesting an important role of RGS4 in CNS.

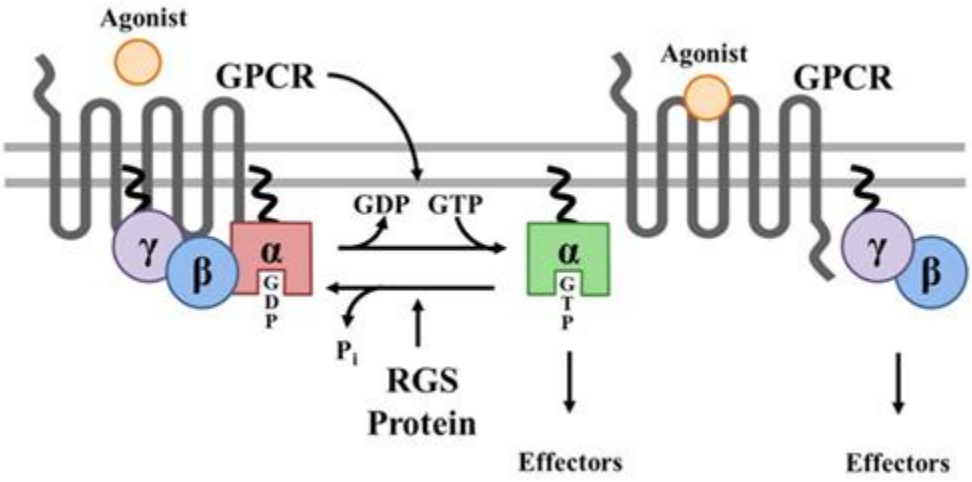

Figure 6.1 The regulatory role of RGS4 in GPCR signaling, adapted from reference [239].

Three potential palmitoylation sites (Cys2/Cys12 and Cys95) have been reported by Tu and co-workers [61]. In their study, His-tagged-RGS4 (rat) was first overexpressed in Sf9 cells by baculovirus infection. In order to detect palmitoylation, *in vivo* radioactive labeling was performed by incubation of Sf9 cells with [^{3}H] palmitate. His-tagged-RGS4 was then purified, subject to SDS-PAGE, and exposed to autoradiography film for detection. *In vitro* labeling of purified RGS4 with radioactive palmitoyl-CoA was also performed as supportive evidence for *in vivo* RGS4 palmitoylation. Palmitoylation sites were subsequently localized to Cys2/Cys12 and Cys95 by cyanogen bromide (CNBr) cleavage combined with site mutation. They further noticed that palmitoylation on Cys2/Cys12 is required for Cys95 palmitoylation, since mutation of Cys2 and Cys12 eliminated all palmitoylation on RGS4 both *in vivo* and *in vitro*.

As a robust and sensitive technique, mass spectrometry has been widely used for PTM characterizations. In this chapter, we will present an application of our established method to the analysis of biological samples. RGS4, a protein known to undergo *in vivo* palmitoylation, was chosen as the model system, so that we could validate our recently developed direct MS detection method and compare its performance with other methods.

6.2 Experimental Section

6.2.1 Materials

Tris, Na-Hepes, palmitate, dimethyl sulfoxide (DMSO), BSA, and CHAPS were purchased from Sigma-Aldrich (St. Louis, MO). FA was acquired from Pierce (Rockford, IL, USA). DHB was obtained from Bruker Daltonics (Billerica, MA). ACN was obtained from Burdick and Jackson (Muskegon, MI). Trypsin Gold^{TM} was purchased from

Promega (Madison, WI). RG was acquired from Waters (Milford, MA). Ni-NTA Magnetic Agarose Beads were obtained from Qiagen (Valencia, CA). The 10K MWCO centrifuge filters were acquired from Millipore (Billerica, MA). POROS R1 50 was obtained from Applied Biosystems (Foster City, CA). Insect cell culture medium Sf-900™ II SFM was purchased from Invitrogen (Carlsbad, CA). Complete EDTA-free protease inhibitor cocktail tablets were acquired from Roche (Indianapolis, IN). The RGS4 baculovirus was generously provided by Prof. Ross at the University of Texas Southwestern Medical Center.

6.2.2 Sf9 Cell Culture, RGS4 Overexpression, and *in vivo* Metabolic Labeling with Palmitic Acid

Overexpression of His-tagged RGS4 in Sf9 cell culture has been described in the last chapter. For *in vivo* metabolic labeling, palmitic acid (2 mM in stock) was prepared by gradually adding 400 mM palmitic acid (in DMSO) into 6.7% BSA/Sf-900™ II SFM media, heating at 57 ^{o}C until well dissolved. The resulting solution was subjected to sterile filtering and stored at -20 ^{o}C for later use. The labeling solution was made by diluting the palmitic acid stock solution to 30 μM with Sf-900™ II SFM media. Sf9 cells were first infected with RGS4 virus for 24 hr. Cells were gently spun down, resuspended and incubated with the labeling solution for 1 hr. Cells with or without metabolic labeling were harvested and subjected to lysis buffer. His-tagged RGS4 was purified, quantified, aliquoted, and stored at 80 °C as previously described.

6.2.3 *In vitro* Auto Palmitoylation of His-tagged RGS4 from Sf9 Cells

Sf9 cells overexpressing His-tagged RGS4 were harvested and resuspended in lysis buffer. His-tagged RGS4 was pulled down from the whole cell lysate by using Ni-NTA magnetic agarose beads. On-bead palmitoylation was performed by incubating His-tagged RGS4-beads with either 1 mM or 100 µM palmitoyl-CoA in 50 mM NaHepes (Ph7.8), 0.1% RapiGest^{TM}, 100 µM DTT at 30 ^{o}C for 3 hr [61]. The beads were washed with 50 mM NaHepes (pH 7.8), 0.1% RapiGest^{TM} for 3 times followed by incubation with 250 mM imidazole to elute His-tagged RGS4. The eluent was aliquoted and stored at -80 °C for later use.

6.2.4 In-Solution Proteolytic Digestion of His-Tagged RGS4, Hydrophobic Peptide Enrichment, and MALDI-TOF Analysis

Purified His-tagged RGS4 proteins were filtered by the 10 K MWCO centrifuge filter, buffer exchanged with the digestion buffer containing 50 mM Tris (pH 7.4) and 0.05% RG. Trypsin was added to the protein solution at a 1:50 enzyme/protein ratio and the digestion was performed at 37 °C for 3 hr. The digest was acidified with 0.5% TFA at room temperature for 10 min and dried down in a speed vac. The digest was then resuspended in 20% ACN/0.1% TFA and loaded into POROS R1 50 resin followed by 3 washes and sequential elution with 40% ACN/0.1% TFA, 60% ACN/0.1% TFA, and 80% ACN/0.1% TFA. A small portion of the digest and its eluents were crystallized with DHB and analyzed on an ultrafleXtreme^{TM} MALDI-TOF/TOF mass spectrometer with 40~45% laser power. A typical MALDI-TOF mass spectrum was acquired by signal averaging over 4000 laser shots from a Smartbeam-II^{TM} Nd:YAG laser operating at 355

nm and a repetition rate of 2 kHz. The spectra were analyzed using the FlexAnalysis 3.4 software.

6.2.5 LC-MS/MS Analysis of the Enriched Hydrophobic Peptides

The LC-MS/MS analysis was performed on a C4-nanoACQUITY UPLC connected to an LTQ-Orbitrap XL mass spectrometer as described in Chapter 3. Mobile phase A consisted of 95:5 water/ACN with 0.1% FA and mobile phase B consisted of 95:5 ACN/water with 0.1% FA. The 60% ACN/0.1%TFA eluent of the RGS4 digest was dried down and loaded into the nanoACQUITY UPLC with 40% B. The flow rate was kept at 1.5 µL/min for the first 2 mins, ramped down to 0.5 µL/min during the next minute, and kept constant at 0.5 µL/min for the rest of the HPLC run. The gradient was held at 40% B for 4 mins, and increased to 100% B over 30 mins. It was then held at 100% B for 5 mins, followed by a ramp to 40% B over 2 mins, and maintained at 40% B for 29 mins for column re-equilibration. The eluted peptides were subjected to MS analysis on the LTQ-Orbitrap XL and the instrument setup was the same as described in Chapter 3.

6.3 Results and Discussion

6.3.1 Production and Analysis of the Palmitoyl-RGS4 Standard

There are 11 cysteine residues on RGS4 and in-solution tryptic digestion covered all cysteines as shown in the previous chapter. Successful mapping of all *in vivo* palmitoylation sites requires our method for palmitoyl peptide preparation and LC-MS analysis to work properly for all cysteine-containing tryptic peptides from RGS4. In order

to test this, it is necessary to produce a palmitoyl RGS4 standard (RGS4-palm-std), ideally with all 11 cysteines palmitoylated. This was achieved by incubating purified RGS4 with 1 mM palmitoyl-CoA, as a concentration sufficiently high to produce universal palmitoylation at all accessible sites. The palmitoyl RGS4 standard was subsequently subjected to tryptic digestion in 50 mM Tris (pH 7.4)/0.05% RapiGest^{TM} to preserve palmitoylation. An aliquot of the tryptic digest was fractionated by POROS R1 50 based on the peptide hydrophobicity. Figure 6.2 shows the MALDI-TOF mass spectra of the tryptic digest of RGS4-palm-std and its eluents with 40% ACN/0.1% TFA, 60% ACN/0.1% TFA, and 80% ACN/0.1% TFA. These three eluents showed very different peptide distributions. Further analysis revealed that the most palmitoyl-peptides were recovered in the 60% ACN/0.1% TFA eluent , which contained few unmodified peptides. Thus, the palmitoyl-peptides were successfully enriched in the 60% ACN/0.1% TFA eluent which was subjected to LC-MS/MS analysis. With the optimized LC conditions developed in Chapter 3, enriched palmitoyl-peptides could bind to and elute from the column properly (Figure 6.3). Furthermore, with MS/MS sequencing, all cysteine residues were found to be palmitoylated (Figure 6.4a). Figure 6.5 shows the CID spectra of several palmitoyl peptides including $GHHHHHHMC_{palm}K^{3}$, $^{4}GLAGLPASC_{palm}LR^{14}$, and $^{82}SEYSEENIDFWISC_{palm}EEYKK^{100}$. Near-complete sequence coverage was obtained and, in each case, the palmitoyl group could be unambiguously localized to a specific cysteine residue. Note that the cysteine residues on these three peptides are Cys2, Cys12, and Cys95, which have been identified as *in vivo* palmitoylation sites by the radioactive labeling method previously.

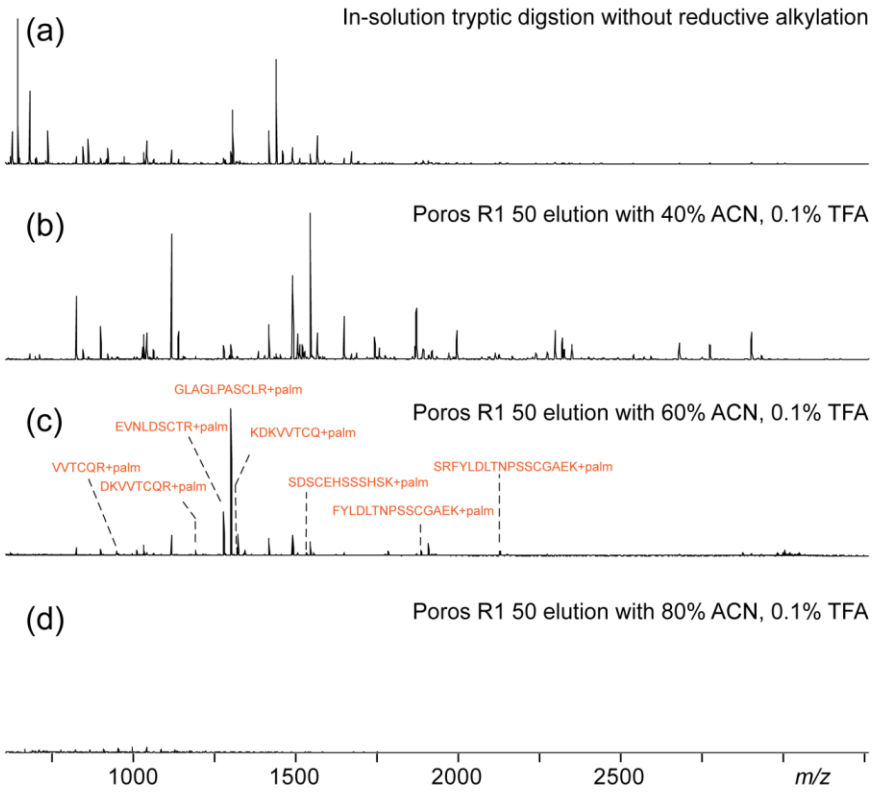

Figure 6.2 MALDI-TOF mass spectra of tryptic digests of RGS4-palm-std (a) and its sequential eluents from the Poros R1 50 resin (b-d).

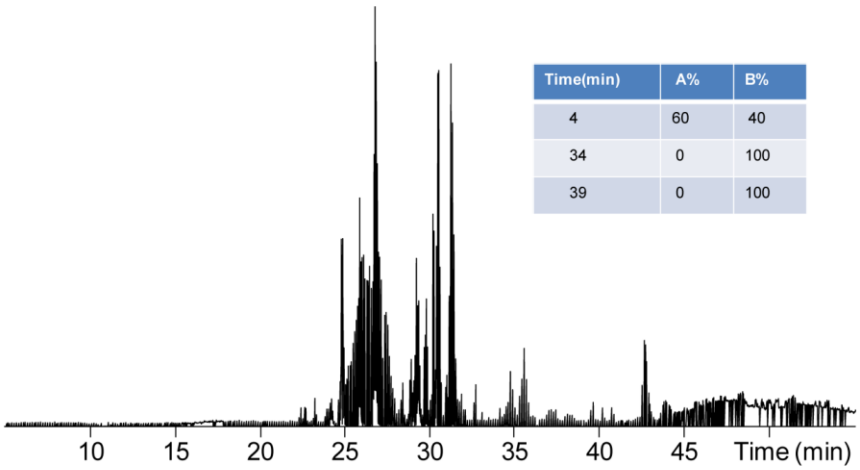

Figure 6.3 The TIC of the 60% ACN/0.1% TFA eluent of the RGS4-palm-std digest.

Figure 6.4 Sequence coverage maps and identified palmitoylation sites obtained from the LC-MS/MS analysis of the tryptic digests of RGS4 pre-incubated with 1 mM palmitoyl-CoA (a), RGS4 from *in vivo* metabolic labeling (b), and RGS4 pre-incubated with 100 µM palmitoyl-CoA (c).

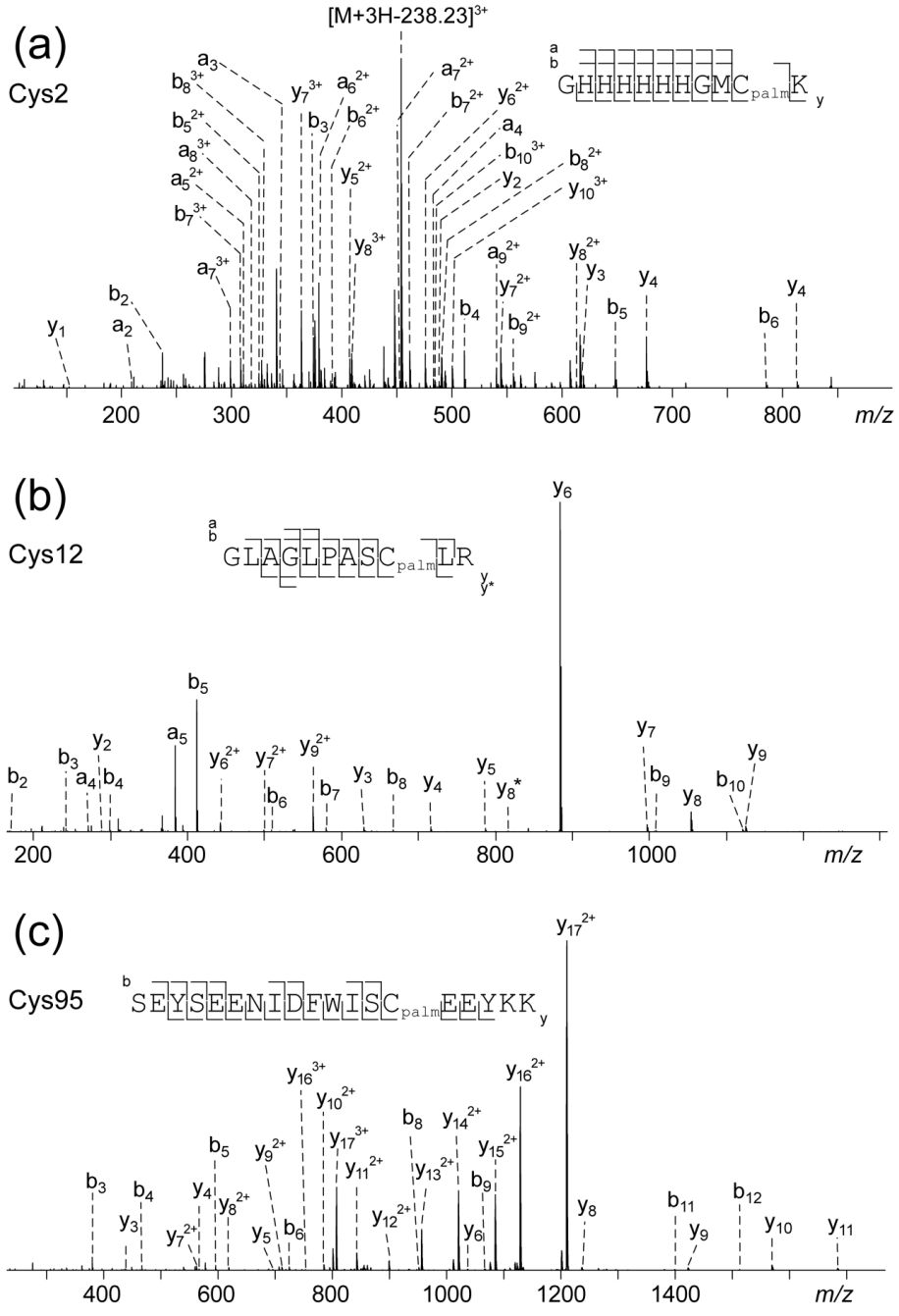

Figure 6.5 The CID spectra of GHHHHHHMC$_{palm}$K (a), GLAGLPASC$_{palm}$LR (b), and SEYSEENIDFWISC$_{palm}$EEYKK (c) extracted from the LC-MS/MS analysis of the RGS4-palm-std tryptic digest.

6.3.2 LC-MS/MS Analysis of *in vitro* Palmitoylated RGS4 and RGS4 Obtained from Sf9 Cell with or without Palmitate Labeling

As described above, our established LC-MS/MS method has the capability to detect palmitoylation at every site on RGS4 if it is present. However, when native RGS4 was prepared and tested under the same conditions, no palmitoylation was identified at any cysteine residue. Although acyl-biotin switch assay identified a single palmitoylation site at Cys12, it may be a false positive due to the incomplete blockage of free thiols. Since both MS-based methods failed to detect palmitoylation in RGS4 expressed under basal conditions, we decided to re-investigate the previously reported results. In a typical *in vivo* metabolic labeling experiment, approximately 1~2 mCi/mL [^{3}H]palmitate is added to the cell culture medium [240, 241], which is equal to about 30~60 μM according to the manufacturer's information sheet ([^{3}H]palmitate specific activity: 32 Ci/mmol) [241]. It is necessary to investigate whether at such concentration, the exogenous palmitate could change the profile of fatty acid metabolites, especially the level of *in vivo* palmitoyl-CoA.

To further evaluate the results obtained by radioactive metabolic labeling, an additional experiment was performed by analyzing RGS4 purified from Sf9 cells treated with palmitate (RGS4-palm-in-vivo), under the same conditions as were used in the early study by Tu and co-workers [61]. With palmitate added to the cell culture, three palmitoyl-containing peptides, ^{4}GLAGLPASC$_{palm}$LR^{14}, ^{140}NMLEPTITC$_{palm}$FDEAQKKIFNLMEK^{162}, and ^{173}FYLDLTNPSSC$_{palm}$GAEK^{187} were identified by LC-MS/MS analysis. Figure 6.6 shows the CID spectra of

^{140}NMLEPTITC$_{palm}$FDEAQKKIFNLMEK^{162} and ^{173}FYLDLTNPSSC$_{palm}$GAEK^{187}, whereas the CID spectrum of ^{4}GLAGLPASC$_{palm}$LR^{14} is the same as that shown in Figure 6.5b.

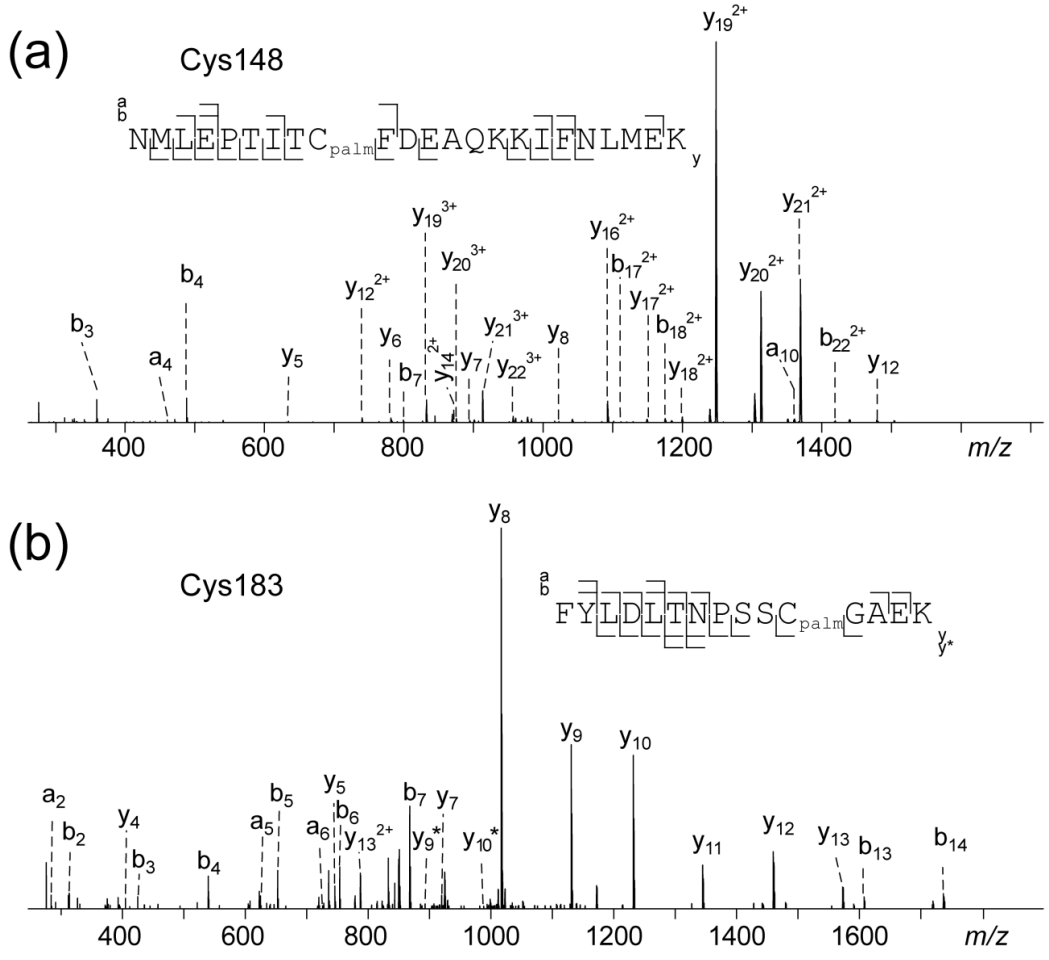

Figure 6.6 The CID spectra of NMLEPTITC$_{palm}$FDEAQKKIFNLMEK (a), and FYLDLTNPSSC$_{palm}$GAEK (b) extracted from the LC-MS/MS analysis of RGS4 from Sf9 cells treated with palmitate.

The previous study by Tu *et al.* also claimed that *in vitro* auto palmitoylation of purified RGS4 under proper conditions targeted the same cysteine residues that underwent palmitoylation *in vivo*. Here, we reproduced that experiment by incubating RGS4 with 100 µM palmitoyl-CoA under the same conditions and analyzed the resultant protein (RGS4-palm-in-vitro) by LC-MS/MS. Besides Cys12, Cys148, and Cys183, the three palmitoylation sites identified by LC-MS/MS analysis of RGS4-palm-in-vivo, two additional palmitoylation sites, Cys71 and Cys132, have been detected in RGS4-palm-in-vitro. Figure 6.4b-c shows a comparison of palmitoylation maps produced by LC-MS/MS analysis of RGS4-palm-in-vivo and RGS4-palm-in-vitro.

6.3.3 Re-evaluation of the Previous Radioactive Labeling Results

Several studies reported that RGS4 underwent *in vivo* palmitoylation [61, 242-244]. Deletion of the first thirty three amino acid residues or double mutation at Cys2 and Cys12 eliminated the [^{3}H]palmitate incorporation both *in vivo* and *in vitro*, indicating that palmitoylation occurred at Cys2 and/or Cys12 [61, 242]. Tu and co-workers suggested Cys95 as an additional palmitoylation site, and Figure 6.7, adapted from their original paper, provides information on the palmitoyl localization. In that study, RGS4-palm-in-vitro and RGS4-palm-in-vivo were treated with CNBr, which specifically cleaves the peptide bond at the C-terminus of a methionine residue. Since there are four methionine residues (Met1, Met19, Met141, and Met160) in RGS4, CNBr treatment of RGS4 could theoretically produce five peptide fragments: His tag-Met^{1} (1 kDa), Cys^{12}-Met^{19} (1.8 kDa), Lys^{20}-Met^{141} (14 kDa), Leu^{142}-Met^{160} (2.2 kDa), and Glu^{161}-Ala^{205} (5 kDa). SDS-PAGE of RGS4-palm-in-vitro and RGS4-palm-in-vivo after the CNBr cleavage both

showed two major radioactive bands at ~2 kDa and 14~20 kDa (Figure 6.7). The ~2 kDa band was assigned as Cys^{12}-Met^{19} (1.8 kDa) based on the Cys2/Cys12 mutation result, whereas the band between 14 and 20 kDa could only be assigned to Lys^{20}-Met^{141} (14 kDa) based on the molecular weight. However, the actual palmitoylation site(s) could not be determined because there are five cysteines (Cys33, Cys48, Cys71, Cys95, and Cys132) residing on the peptide fragment Lys^{20}-Met^{141}. Because it would be laborious and time-consuming to mutate every cysteine residue, Cys95 was chosen because it is a conserved cysteine among all RGS family members, and the authors speculated that its palmitoylation might be biologically significant. Pleasingly, their speculation was supported by the experimental observation that Cys95 mutant showed little palmitate incorporation to fragment Lys^{20}-Met^{141} at 14 kDa (Figure 6.7). Figure 6.8 summarizes their results.

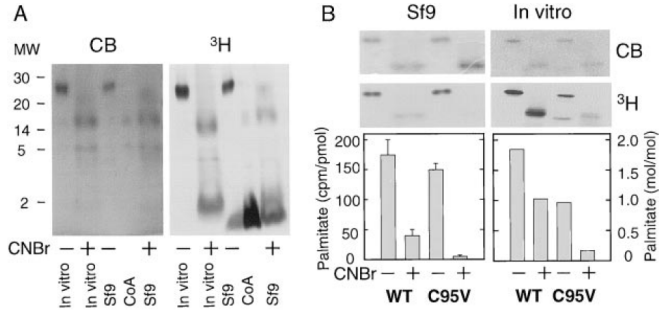

FIG. 2. **Localization of [^{3}H]palmitoylation sites on RGS4.** *A*, CNBr peptide mapping. [^{3}H]Palmitoylated RGS4 was either prepared by autopalmitoylation *in vitro* or purified from Sf9 cells grown with [^{3}H]palmitate as described in the legend to Fig. 1. Samples (20–40 pmol) were analyzed by SDS-PAGE either without further treatment or after cleavage by CNBr as described under "Experimental Procedures," as shown. The gel was stained with Coomassie Blue (*left panel*) and then subjected to fluorography (*right panel*) for 72 h. The *fourth lane* contained 10^5 cpm of free [^{3}H]Pal-CoA to indicate its migration in the gel. *B*, labeling of C95V RGS4. RGS4, wild-type or C95V, was either metabolically labeled in Sf9 cells and then purified (*left panels*) or was labeled with [^{3}H]palmitate by autopalmitoylation *in vitro* (*right panels*). Samples, either untreated (25 pmol) or CNBr-treated (50 pmol), were analyzed by SDS-PAGE. The gel was stained with Coomassie Blue (*CB*) and then subjected to fluorography (^{3}H) for 40 h. Radioactive bands were then cut out, hydrolyzed with H_2O_2, and counted. [^{3}H]Palmitate incorporation is expressed either as cpm/pmol (*left*) or as mol of palmitate/mol of RGS4 (*right*).

Figure 6.7 Localization of the palmitoylation site at Cys95 on RGS4, adapted from reference [61]

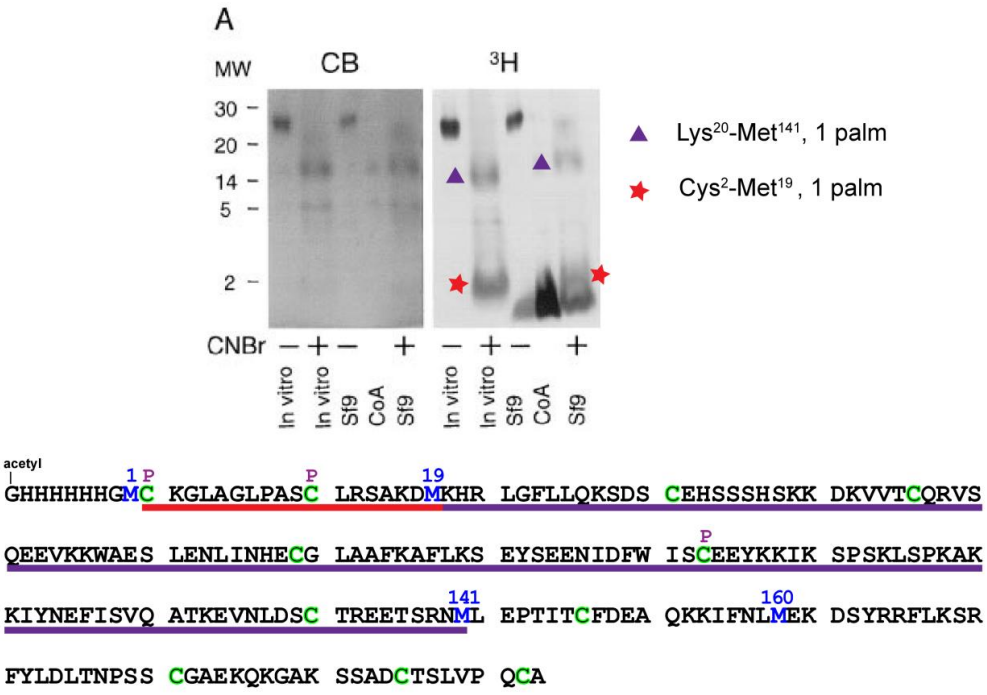

Figure 6.8 RGS4 palmitoylation map produced by radioactive labeling combined with the CNBr cleavage, based on the result from Figure 6.7.

However, the data obtained by the LC-MS/MS analysis did not completely agree with the previous result produced by radioactive labeling and site mutation. LC-MS/MS analysis failed to identify native palmitoylation on RGS4, and this might be due to the very low level of RGS4 palmitoylation under basal conditions. In contrast, when RGS4 was purified from Sf9 cells treated with palmitate, under the same conditions as used in the metabolic labeling experiment, palmitoylation at several cysteine sites was identified without much difficulty. This result underlined a caveat that is associated with the metabolic labeling approach: addition of [^{3}H]palmitate, and potentially the palmitic acid

analogue, 17-ODYA, may artificially boost the *in vivo* palmitoylation process, possibly by increasing the *in vivo* palmitoyl-CoA concentration. Furthermore, the biological role of *in vivo* palmitoylation on RGS4 is still elusive. A functional study reported by Srinivasa and co-workers showed that RGS4 failed to target the plasma membrane when its N-terminal thirty three amino acid residues were deleted. However, mutation of Cys2 and Cys12, although resulting in the failure of palmitate incorporation, did not affect the protein localization, suggesting that palmitoylation at these residues may not be responsible for RGS4 anchoring and trafficking [242]. Thus, results produced by metabolic palmitate labeling may not be a true reflection of the status of *in vivo* palmitoylation on RGS4 and it remains unclear whether RGS4 is naturally palmitoylated.

Moreover, even with addition of palmitate to the cell culture medium, the palmitoylation sites identified by LC-MS/MS (RGS4-palm-in-vivo: Cys12, Cys148, and Cys183; RGS4-palm-in-vitro: Cys12, Cys71, Cys132, Cys148, and Cys183) still differ from those assigned after radioactive labeling (Cys2/Cys12, and Cys95). Whereas palmitoylation on Cys95 appeared to be very convincing based on the results obtained by experiments combining the metabolic labeling, CNBr cleavage, and site mutation, several fine points in Figure 6.7, might have been neglected, potentially leading to inaccurate identification. Firstly, the bands between 14 and 20 kDa from RGS4-palm-in-vitro (marked by purple square) and RGS4-palm-in-vivo (marked by purple triangle) by the CNBr cleavage appeared to be different upon close examination (Figure 6.9a). Band triangle (*in vivo*) migrated more slowly than band square (*in vitro*), and had a lower relative radioactive intensity. Whereas the CNBr cleavage of both RGS4-palm-in-vitro

and RGS4-palm-in-vivo should produce the same fragments in terms of their length and amount, the observed differences between the *in vivo* and *in vitro* labeling samples can only be attributed to the number of palmitoyl groups on the peptide fragments. It is well known that a palmitoylated protein or peptide migrated faster in SDS-PAGE than its unmodified counterpart [244]. Thus, we speculate that the peptide in band square (*in vitro*) potentially carried more palmitoyl groups than the peptide in band triangle (*in vivo*) based on its faster migration rate and higher radioactivity. This speculation is further supported by the LC-MS/MS data that RGS4-palm-in-vitro contained two additional palmitoylation sites, Cys71, and Cys132, which reside in the peptide fragment Lys^{20}-Met^{141}. Secondly, because the vast majority of RGS4 was unmodified, the bands showing on the Coomassie Blue (CB) staining (Figure 6.9a, left panel) should mainly represent the unmodified RGS4 and its fragments, whereas the bands showing on the radioautograph (Figure 6.9a, right panel) should represent their palmitoylated counterparts. The previous assignment of band triangle (*in vivo*) in the radioautograph to the peptide Lys^{20}-Met^{141} with a palmitoyl group is inconsistent with the fact it showed up at a position well above its unmodified counterpart in the CB staining (14 kDa, marked with purple hexagon). Thus, the peptide that gave rise to band triangle likely contained more amino acid residues than previously speculated. As methionine undergoes oxidation easily during sample preparation and CNBr cannot cleave after an oxidized methionine, miscleavage could occur, producing larger peptide fragments than expected. If CNBr failed to cleave after Met141, the peptide Lys^{20}-Met^{160} would be produced. With a theoretical mass of 16297 Da, this peptide would migrate to the location of band triangle (*in vivo*). In support

of this, we did identify oxidized Met141 by LC-MS/MS: the CID spectrum of the tryptic peptide $^{140}NM_{ox}LEPTITC_{palm}FDEAQKKIFNLMEK^{162}$ from RGS4-palm-in-vivo is shown in Figure 6.9b. Thus, by careful examination of the results from both the radioactive labeling/CNBr cleavage experiment and LC-MS/MS analysis, we suggest that both band triangle (*in vivo*) and band square (*in vitro*) were the peptide fragment Lys^{20}-Met^{160} instead of Lys^{20}-Met^{141} as previously reported. This could explain the controversy on the palmitoylation status of Cys95. Because the LC-MS/MS analysis provided direct and unambiguous evidence on the palmitoylation sites, we believe that the radioactive signal showing between 14 and 20 kDa originated mainly from palmitoyl Cys148 on the peptide fragment Lys^{20}-Met^{160}, but not from palmitoyl Cys95 on Lys^{20}-Met^{141}. We further note that the abolishment of the signal between 14 and 20 kDa following Cys95 mutation is not a direct evidence of Cys95 palmitoylation. It only suggests that Cys95 is important for the palmitate incorporation to that peptide fragment. One possibility is that mutation of Cys95 induced protein conformational change making Cys148 inaccessible to palmitoyl-CoA. Actually, this may be a common caveat for PTM localization by amino acid mutation, which highlights the need for validation using MS-based, direct detection method. Lastly, besides the two major radioactive bands from RGS4 following the CNBr cleavage, there was another band, with low radioactivity but still observable, located at ~5 kDa, marked by a green cycle in Figure 6.9a. It could be assigned as fragment Glu^{161}-Ala^{205}, which is consistent with our finding of palmitoylation at Cys183.

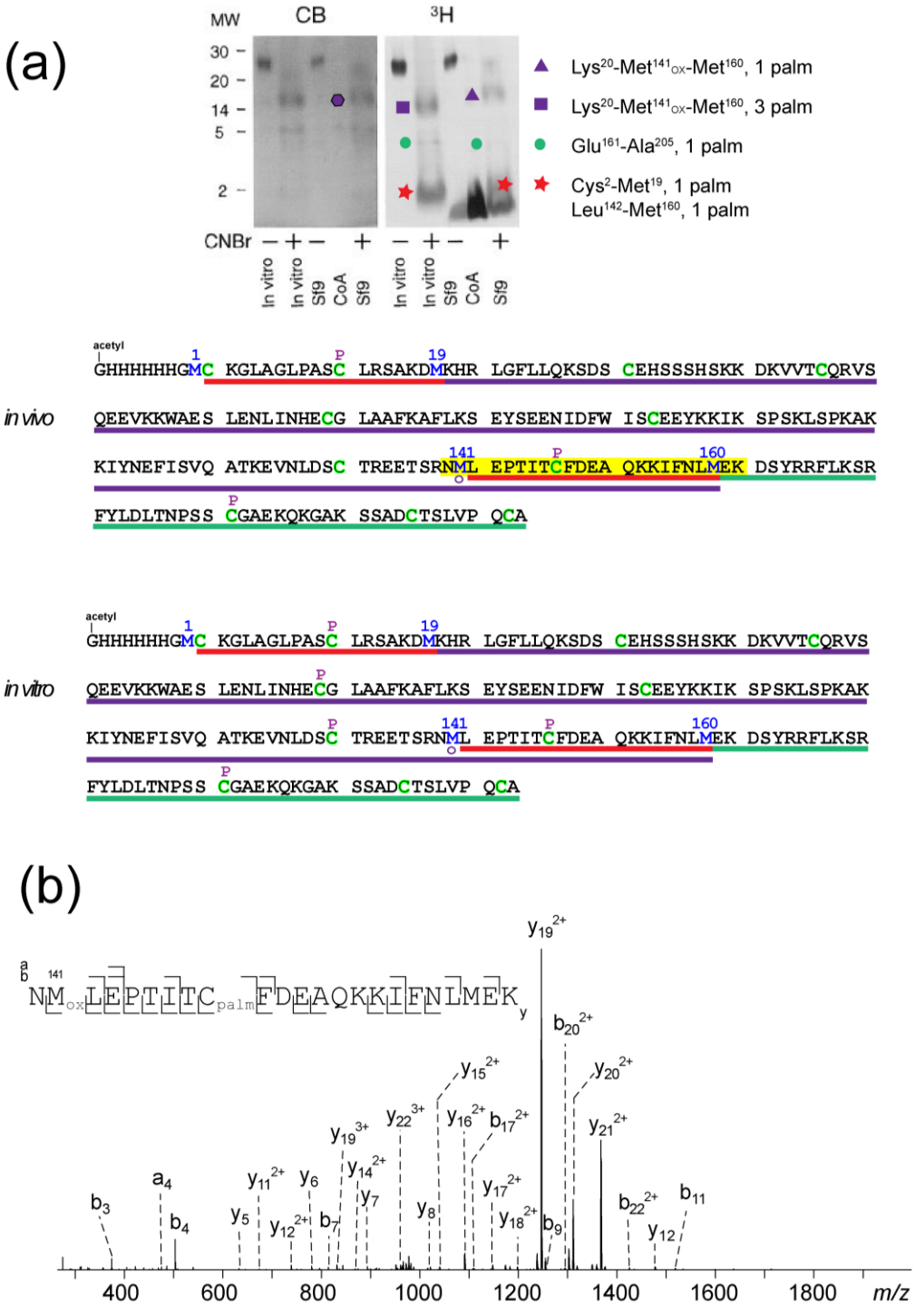

Figure 6.9 Evaluation of the previous radioactive labeling results by LC-MS/MS. (a) Re-assignment of CNBr-derived fragments produced from RGS4-palm-in-vitro and RGS4-

palm-in-vivo, (b) The CID spectrum of the tryptic peptide $NM_{ox}LEPTITC_{palm}FDEAQKKIFNLMEK$.

6.4 Conclusion

In this chapter, the established LC-MS/MS method was applied to analyze RGS4 which has been shown to undergo *in vivo* palmitoylation. By comparing the LC-MS/MS data to the classic metabolic labeling results, we discovered that addition of palmitate to the cell culture medium in a metabolic labeling experiment increased the extent of protein palmitoylation, which could potentially lead to false discovery of new palmitoylation targets as well as inaccuracy in relative palmitoyl quantification. When combined with protein cleavage and cysteine mutation, radioactive metabolic labeling can provide useful information for localization of palmitoylation site(s). However, it is laborious and the results are sometimes deceiving due to the sample complexity. On the other hand, MS can be used to analyze proteins obtained from cells grown in a culture medium without addition of palmitate, providing information on palmitoylation under basal conditions. Moreover, LC-MS/MS is a high-throughput method that can provide direct information on modification sites, and is thus capable of identifying multiple palmitoylation sites in a single run with little ambiguity. Therefore, we believe that our established LC-MS/MS method would constitute a more powerful alternative for characterization of *in vivo* palmitoylation.

Chapter 7: General Conclusion and Future Perspectives

7.1 General Conclusion

As a powerful proteomics tool, MS is capable of analyzing complex samples, providing both qualitative and quantitative information on PTMs in a single run. Although MS has been extensively used to study a variety of PTMs, it has seldom been applied to detect protein palmitoylation in its native form. In addition, our early attempts to identify *S*-palmitoylation on H-Ras were largely unsuccessful, underlying the difficulty of such a task. In Chapter 3, using several palmitoyl peptide standards as the model system, we developed a comprehensive strategy, including sample preparation, LC-MS and tandem MS analysis, for direct detection and quantification of *S*-palmitoyl peptides.

In Chapter 4 and Chapter 5, we further unveiled the complexity of sample preparation when a detergent is used. Whereas detergents are routinely used to improve bottom-up MS results by facilitating protein solubilization, this thesis provided the first evidence that they can also stabilize protein *S*-palmitoylation by preventing its hydrolysis and DTT-induced cleavage. However, one must be careful with the choice of detergent for palmitoyl studies, as ProteaseMAX ^{TM}, a commonly used MS-compatible detergent, can induce artifactual protein lipid modifications that interfere with palmitoyl detection. Meanwhile, RapiGest^{TM} did not produce any artifacts.

Because a palmitoyl peptide can be considered as a detergent-like molecule with the palmitoyl group as its hydrophobic tail and the peptide chain as its hydrophilic head, it is reasonable to expect the aggregation of palmitoyl peptides in aqueous solutions.

When studying a palmitoyl peptide standard GC_{palm}LGNAK, we found that aggregation of palmitoyl peptides could induce intermolecular palmitoyl transfer from the cysteine residue to the peptide N-terminus or the lysine side chain. Addition of RapiGest^{TM} inhibited palmitoyl peptide aggregation and dramatically slowed down the intermolecular palmitoyl transfer. On the other hand, a small amount of palmitoyl peptides still underwent intramolecular palmitoyl migration in the presence of RapiGest^{TM}. Thus, *N*-palmitoylation can potentially arise from *S*-palmitoylation during proteomic sample preparation, and this possibility needs be examined when identifying *in vivo N*-palmitoylation. Considering the major benefit of the use of RapiGest^{TM} to preserve *S*-palmitoylation, and the very slow rate of intramolecular palmitoyl transfer, RapiGest^{TM} is recommended during sample preparation for direct detection of *S*-palmitoylation.

In Chapter 6 we applied our established method to analyze biological samples, specifically, the RGS4 protein extracted from Sf9 cells. By comparing the LC-MS/MS results with those obtained by traditional radioactive labeling method, we concluded that addition of exogenous palmitate to the cell culture could artificially increase the level of protein palmitoylation, and does not reflect the true level of palmitoylation *in vivo*. Moreover, radioactive labeling, even when combined with specific site mutation, can still misidentify the palmitoylation sites due to sample complexity.

The information provided in this thesis should benefit researchers who are interested in the study of protein palmitoylation. We believe that the LC-MS/MS method developed here provided a fast, sensitive and reliable alternative for characterization of protein palmitoylation and will become widely accepted in the future.

7.2 Future Perspectives

Future work will mainly focus on the application of the established LC-MS/MS method to various biological samples. For example, in Chapter 6, we still failed to identify *S*-palmitoylation on RGS4 under basal conditions. It is possible that native *S*-palmitoylation is present at a very low level, so that we will need to scale up the sample amount or use a mass spectrometer with higher sensitivity (*e.g.* a Q-Exactive Plus instrument instead of the outdated LTQ-Orbitrap XL) to improve the chance of palmitoyl identification. In parallel, the ABE method will be performed as a positive control. Regarding the conflicting results on palmitoyl localization by LC-MS/MS and radioactive labeling methods, we proposed that, although Cys95 does not undergo palmitoylation, its mutation can prevent palmitoylation on Cys148. To test this hypothesis, the RGS4 C95V mutant needs to be examined by LC-MS/MS. Another challenging task is to analyze the PTMs on the C-terminus of H-Ras under both physiological and pathological conditions. The C-terminus of H-Ras is extensively modified: Cys181 and Cys184 are palmitoylated, and Cys186 is farnesylated. These lipid modifications are responsible for the anchoring of H-Ras to the inner surface of the plasma membrane where it relays extracellular signals to modulate cell growth and survival. Our previous data indicated that in bovine aortic endothelial cells, oxidative PTMs resulting from high fat high glucose treatment can compete with palmitoylation at Cys181 and Cys184 on H-Ras, leading to the shedding of H-Ras from the plasma membrane and a decrease in survival signaling [79]. It is thus of interest to map and compare PTMs on the C-terminus of H-Ras under normal conditions and under oxidative stress using our established LC-MS/MS method.

Another future direction would be to develop a method for top-down analysis of protein *S*-palmitoylation. The top-down approach is complementary to the bottom-up analysis, and is especially useful when the protein digests poorly. Furthermore, the top-down method can also be used to study the combinatorial effect of various PTMs on an individual protein molecule. This project will be initiated with examination of the RGS10 protein. There are only two cysteines on RGS10 which are both shown to be potential target for palmitoylation. The palmitoyl-RGS10 standard will be produced by incubation of the overexpressed RGS10 with palmitoyl-CoA. The method development including the optimization of palmitoyl protein isolation, LC-MS, and different fragmentation methods, will be performed in the future.

BIBLIOGRAPHY

1. Schmidt MFG, Schlesinger MJ: Fatty acid binding to vesicular stomatitis virus glycoprotein: a new type of post-translational modification of the viral glycoprotein. *Cell* 1979, 17(4):813-819.

2. Schmidt MF, Schlesinger MJ: Relation of fatty acid attachment to the translation and maturation of vesicular stomatitis and Sindbis virus membrane glycoproteins. *Journal of Biological Chemistry* 1980, 255(8):3334-3339.

3. Magee AI, Gutierrez L, McKay IA, Marshall CJ, Hall A: Dynamic fatty acylation of p21N-ras. *The EMBO Journal* 1987, 6(11):3353-3357.

4. Magee AI, Koyama AH, Malfer C, Wen D, Schlesinger MJ: Release of fatty acids from virus glycoproteins by hydroxylamine. *Biochimica et Biophysica Acta (BBA) - General Subjects* 1984, 798(2):156-166.

5. Veit M: Palmitoylation of virus proteins. *Biology of the Cell* 2012, 104(9):493-515.

6. Hemsley PA, Grierson CS: Multiple roles for protein palmitoylation in plants. *Trends in Plant Science* 2008, 13(6):295-302.

7. Bartels DJ, Mitchell DA, Dong X, Deschenes RJ: Erf2, a novel gene product that affects the localization and palmitoylation of Ras2 in saccharomyces cerevisiae. *Molecular and Cellular Biology* 1999, 19(10):6775-6787.

8. Roth AF, Wan J, Bailey AO, Sun B, Kuchar JA, Green WN, Phinney BS, Yates Iii JR, Davis NG: Global analysis of protein palmitoylation in yeast. *Cell* 2006, 125(5):1003-1013.

9. Schlesinger MJ, Magee AI, Schmidt MF: Fatty acid acylation of proteins in cultured cells. *Journal of Biological Chemistry* 1980, 255(21):10021-10024.

10. Shipston MJ: Ion channel regulation by protein palmitoylation. *Journal of Biological Chemistry* 2011, 286(11):8709-8716.

11. Goddard A, Watts A: Regulation of G protein-coupled receptors by palmitoylation and cholesterol. *BMC Biology* 2012, 10(1):1-3.

12. Smotrys JE, Linder ME: Palmitoylation of intracellular signaling proteins: regulation and function. *Annual Review of Biochemistry* 2004, 73(1):559-587.

13. Dunphy JT, Linder ME: Signalling functions of protein palmitoylation. *Biochimica et Biophysica Acta (BBA) - Molecular and Cell Biology of Lipids* 1998, 1436(1–2):245-261.

14. Linder ME, Deschenes RJ: Palmitoylation: policing protein stability and traffic. *Nature Reviews Molecular Cell Biology* 2007, 8(1):74-84.

15. Salaun C, Greaves J, Chamberlain LH: The intracellular dynamic of protein palmitoylation. *The Journal of Cell Biology* 2010, 191(7):1229-1238.

16. Berger M, Schmidt MF: Identification of acyl donors and acceptor proteins for fatty acid acylation in BHK cells infected with Semliki Forest virus. *The EMBO Journal* 1984, 3(4):713-719.

17. Duncan JA, Gilman AG: Autoacylation of G protein α subunits. *Journal of Biological Chemistry* 1996, 271(38):23594-23600.

18. Veit M: Palmitoylation of the 25-kDa synaptosomal protein (SNAP-25) in vitro occurs in the absence of an enzyme, but is stimulated by binding to syntaxin. *Biochemical Journal* 2000, 345(1):145-151.

19. Bañó MC, Jackson CS, Magee AI: Pseudo-enzymatic S-acylation of a myristoylated yes protein tyrosine kinase peptide in vitro may reflect non-enzymatic S-acylation in vivo. *Biochemical Journal* 1998, 330(2):723-731.

20. O'Brien PJ, St Jules RS, Reddy TS, Bazan NG, Zatz M: Acylation of disc membrane rhodopsin may be nonenzymatic. *Journal of Biological Chemistry* 1987, 262(11):5210-5215.

21. Bharadwaj M, Bizzozero OA: Myelin P0 glycoprotein and a synthetic peptide containing the palmitoylation site are both autoacylated. *Journal of Neurochemistry* 1995, 65(4):1805-1815.

22. Bizzozero OA, McGarry JF, Lees MB: Autoacylation of myelin proteolipid protein with acyl coenzyme A. *Journal of Biological Chemistry* 1987, 262(28):13550-13557.

23. Quesnel S, Silvius JR: Cysteine-containing peptide sequences exhibit facile uncatalyzed transacylation and acyl-CoA-dependent acylation at the lipid bilayer interface. *Biochemistry* 1994, 33(45):13340-13348.

24. Bizzozero OA, Bixler HA, Pastuszyn A: Structural determinants influencing the reaction of cysteine-containing peptides with palmitoyl-coenzyme A and other

thioesters. *Biochimica et Biophysica Acta (BBA) - Protein Structure and Molecular Enzymology* 2001, 1545(1–2):278-288.

25. Zhang ZY, Dixon JE: Active site labeling of the Yersinia protein tyrosine phosphatase: the determination of the pKa of the active site cysteine and the function of the conserved histidine 402. *Biochemistry* 1993, 32(36):9340-9345.

26. Dietrich LEP, Ungermann C: On the mechanism of protein palmitoylation. *EMBO reports* 2004, 5(11):1053-1057.

27. Faergeman NJ, Knudsen J: Role of long-chain fatty acyl-CoA esters in the regulation of metabolism and in cell signalling. *Biochemical Journal* 1997, 323(1):1-12.

28. Leventis R, Juel G, Knudsen JK, Silvius JR: Acyl-CoA binding proteins inhibit the nonenzymic S-acylation of cysteinyl-containing peptide sequences by long-chain acyl-CoAs. *Biochemistry* 1997, 36(18):5546-5553.

29. Dunphy JT, Schroeder H, Leventis R, Greentree WK, Knudsen JK, Silvius JR, Linder ME: Differential effects of acyl-CoA binding protein on enzymatic and non-enzymatic thioacylation of protein and peptide substrates. *Biochimica et Biophysica Acta (BBA) - Molecular and Cell Biology of Lipids* 2000, 1485(2–3):185-198.

30. Berger M, Schmidt MF: Cell-free fatty acid acylation of Semliki Forest viral polypeptides with microsomal membranes from eukaryotic cells. *Journal of Biological Chemistry* 1984, 259(11):7245-7252.

31. Mitchell DA, Farh L, Marshall TK, Deschenes RJ: A polybasic domain allows nonprenylated Ras proteins to function in Saccharomyces cerevisiae. *Journal of Biological Chemistry* 1994, 269(34):21540-21546.

32. Mitchell DA, Mitchell G, Ling Y, Budde C, Deschenes RJ: Mutational analysis of saccharomyces cerevisiae Erf2 reveals a two-step reaction mechanism for protein palmitoylation by DHHC enzymes. *Journal of Biological Chemistry* 2010, 285(49):38104-38114.

33. Mitchell DA, Hamel LD, Ishizuka K, Mitchell G, Schaefer LM, Deschenes RJ: The Erf4 subunit of the yeast Ras palmitoyl acyl transferase is required for stability of the acyl-Erf2 intermediate and palmitoyl transfer to a Ras2 substrate. *Journal of Biological Chemistry* 2012.

34. Roth AF, Feng Y, Chen L, Davis NG: The yeast DHHC cysteine-rich domain protein Akr1p is a palmitoyl transferase. *The Journal of Cell Biology* 2002, 159(1):23-28.

35. Fukata M, Fukata Y, Adesnik H, Nicoll RA, Bredt DS: Identification of PSD-95 palmitoylating enzymes. *Neuron* 2004, 44(6):987-996.

36. Jennings BC, Linder ME: DHHC protein S-acyltransferases use similar ping-pong kinetic mechanisms but display different acyl-coA specificities. *Journal of Biological Chemistry* 2012, 287(10):7236-7245.

37. Dietrich LEP, Gurezka R, Veit M, Ungermann C: The SNARE Ykt6 mediates protein palmitoylation during an early stage of homotypic vacuole fusion. *The EMBO journal* 2004, 23(1):45-53.

38. Mann RK, Beachy PA: Novel lipid modifications of secreted protein signals. *Annual Review of Biochemistry* 2004, 73(1):891-923.

39. Schweizer A, Kornfeld S, Rohrer J: Cysteine34 of the cytoplasmic tail of the cation-dependent mannose 6-phosphate receptor is reversibly palmitoylated and required for normal trafficking and lysosomal enzyme sorting. *The Journal of Cell Biology* 1996, 132(4):577-584.

40. Wedegaertner PB, Bourne HR, von Zastrow M: Activation-induced subcellular redistribution of Gs alpha. *Molecular Biology of the Cell* 1996, 7(8):1225-1233.

41. El-Husseini AE-D, Schnell E, Dakoji S, Sweeney N, Zhou Q, Prange O, Gauthier-Campbell C, Aguilera-Moreno A, Nicoll RA, Bredt DS: Synaptic strength regulated by palmitate cycling on PSD-95. *Cell* 2002, 108(6):849-863.

42. Robinson LJ, Busconi L, Michel T: Agonist-modulated Palmitoylation of Endothelial Nitric Oxide Synthase. *Journal of Biological Chemistry* 1995, 270(3):995-998.

43. Zeidman R, Jackson CS, Magee AI: Protein acyl thioesterases (Review). *Molecular Membrane Biology* 2009, 26(1-2):32-41.

44. Verkruyse LA, Hofmann SL: Lysosomal targeting of palmitoyl-protein thioesterase. *Journal of Biological Chemistry* 1996, 271(26):15831-15836.

45. Kong E, Peng S, Chandra G, Sarkar C, Zhang Z, Bagh MB, Mukherjee AB: Dynamic palmitoylation links cytosol-membrane shuttling of acyl-protein thioesterase-1 and acyl-protein thioesterase-2 with that of proto-oncogene H-Ras

product and growth-associated Protein-43. *Journal of Biological Chemistry* 2013, 288(13):9112-9125.

46. Hancock JF: Ras proteins: different signals from different locations. *Nature Reviews Molecular Cell Biology* 2003, 4(5):373-385.

47. Swarthout JT, Lobo S, Farh L, Croke MR, Greentree WK, Deschenes RJ, Linder ME: DHHC9 and GCP16 constitute a human protein fatty acyltransferase with specificity for H- and N-Ras. *Journal of Biological Chemistry* 2005, 280(35):31141-31148.

48. Apolloni A, Prior IA, Lindsay M, Parton RG, Hancock JF: H-ras but not K-ras traffics to the plasma membrane through the exocytic pathway. *Molecular and Cellular Biology* 2000, 20(7):2475-2487.

49. Rocks O, Peyker A, Kahms M, Verveer PJ, Koerner C, Lumbierres M, Kuhlmann J, Waldmann H, Wittinghofer A, Bastiaens PI: An acylation cycle regulates localization and activity of palmitoylated Ras isoforms. *Science* 2005, 307(5716):1746-1752.

50. Goodwin JS, Drake KR, Rogers C, Wright L, Lippincott-Schwartz J, Philips MR, Kenworthy AK: Depalmitoylated Ras traffics to and from the Golgi complex via a nonvesicular pathway. *The Journal of Cell Biology* 2005, 170(2):261-272.

51. Sato I, Obata Y, Kasahara K, Nakayama Y, Fukumoto Y, Yamasaki T, Yokoyama KK, Saito T, Yamaguchi N: Differential trafficking of Src, Lyn, Yes and Fyn is specified by the state of palmitoylation in the SH4 domain. *Journal of Cell Science* 2009, 122(7):965-975.

52. Oess S, Icking A, Fulton D, Govers R, Müller-esterl W: Subcellular targeting and trafficking of nitric oxide synthases. *The Biochemical Journal* 2006, 396(3):401-409.

53. Baekkeskov S, Kanaani J: Palmitoylation cycles and regulation of protein function (Review). *Molecular Membrane Biology* 2009, 26(1-2):42-54.

54. Aicart-Ramos C, Valero RA, Rodriguez-Crespo I: Protein palmitoylation and subcellular trafficking. *Biochimica et Biophysica Acta (BBA) - Biomembranes* 2011, 1808(12):2981-2994.

55. Rocks O, Gerauer M, Vartak N, Koch S, Huang Z-P, Pechlivanis M, Kuhlmann J, Brunsveld L, Chandra A, Ellinger B *et al*: The palmitoylation machinery is a spatially organizing system for peripheral membrane proteins. *Cell*, 141(3):458-471.

56. Shipston MJ: Ion channel regulation by protein S-acylation. *The Journal of General Physiology* 2014, 143(6):659-678.

57. Tian L, Jeffries O, McClafferty H, Molyvdas A, Rowe ICM, Saleem F, Chen L, Greaves J, Chamberlain LH, Knaus H-G *et al*: Palmitoylation gates phosphorylation-dependent regulation of BK potassium channels. *Proceedings of the National Academy of Sciences* 2008, 105(52):21006-21011.

58. Hayashi T, Thomas GM, Huganir RL: Dual palmitoylation of NR2 subunits regulates NMDA receptor trafficking. *Neuron* 2009, 64(2):213-226.

59. Moffett S, Mouillac B, Bonin H, Bouvier M: Altered phosphorylation and desensitization patterns of a human beta 2-adrenergic receptor lacking the palmitoylated Cys341. *The EMBO Journal* 1993, 12(1):349-356.

60. Baker TL, Booden MA, Buss JE: S-nitrosocysteine increases palmitate turnover on Ha-Ras in NIH 3T3 cells. *Journal of Biological Chemistry* 2000, 275(29):22037-22047.

61. Tu Y, Popov S, Slaughter C, Ross EM: Palmitoylation of a conserved cysteine in the regulator of G protein signaling (RGS) domain modulates the GTPase-activating activity of RGS4 and RGS10. *Journal of Biological Chemistry* 1999, 274(53):38260-38267.

62. Hiol A, Davey PC, Osterhout JL, Waheed AA, Fischer ER, Chen C-K, Milligan G, Druey KM, Jones TLZ: Palmitoylation regulates regulators of G-protein signaling (RGS)16 function: I. mutation of amino-terminal cysteine residues on RGS16 prevents its targeting to lipid rafts and palmitoylation of an internal cysteine residue. *Journal of Biological Chemistry* 2003, 278(21):19301-19308.

63. Calder PC, Yaqoob P: Lipid rafts—composition, characterization, and controversies. *The Journal of Nutrition* 2007, 137(3):545-547.

64. Brown DA: Lipid rafts, detergent-resistant membranes, and raft targeting signals. *Physiology* 2006, 21(6):430-439.

65. Yang X, Claas C, Kraeft S-K, Chen LB, Wang Z, Kreidberg JA, Hemler ME: Palmitoylation of tetraspanin proteins: modulation of CD151 lateral interactions, subcellular distribution, and integrin-dependent cell morphology. *Molecular Biology of the Cell* 2002, 13(3):767-781.

66. Rocha-Perugini V, González-Granado JM, Tejera E, López-Martín S, Yañez-Mó M, Sánchez-Madrid F: Tetraspanins CD9 and CD151 at the immune synapse

support T-cell integrin signaling. *European Journal of Immunology* 2014, 44(7):1967-1975.

67. Yu G-Y, Lee K-J, Gao L, Lai MMC: Palmitoylation and polymerization of hepatitis C virus NS4B protein. *Journal of Virology* 2006, 80(12):6013-6023.

68. Tu Y, Wang J, Ross EM: Inhibition of brain Gz GAP and other RGS proteins by palmitoylation of G protein α subunits. *Science* 1997, 278(5340):1132-1135.

69. El-Husseini AE-D, Bredt DS: Protein palmitoylation: a regulator of neuronal development and function. *Nature Reviews Neuroscience* 2002, 3(10):791-802.

70. Kostiuk MA, Keller BO, Berthiaume LG: Palmitoylation of ketogenic enzyme HMGCS2 enhances its interaction with PPARα and transcription at the Hmgcs2 PPRE. *The FASEB Journal* 2010, 24(6):1914-1924.

71. Gao Z, Ni Y, Szabo G, Linden J: Palmitoylation of the recombinant human A1 adenosine receptor: enhanced proteolysis of palmitoylation-deficient mutant receptors. *Biochemical Journal* 1999, 342(2):387-395.

72. Percherancier Y, Planchenault T, Valenzuela-Fernandez A, Virelizier J-L, Arenzana-Seisdedos F, Bachelerie F: Palmitoylation-dependent control of degradation, life span, and membrane expression of the CCR5 receptor. *Journal of Biological Chemistry* 2001, 276(34):31936-31944.

73. Ochsenbauer-Jambor C, Miller DC, Roberts CR, Rhee SS, Hunter E: Palmitoylation of the Rous sarcoma virus transmembrane glycoprotein is required for protein stability and virus infectivity. *Journal of Virology* 2001, 75(23):11544-11554.

74. Valdez-Taubas J, Pelham H: Swf1-dependent palmitoylation of the SNARE Tlg1 prevents its ubiquitination and degradation. *The EMBO Journal* 2005, 24(14):2524-2532.

75. Griendling KK, FitzGerald GA: Oxidative stress and cardiovascular injury: part I: Basic mechanisms and in vivo monitoring of ROS. *Circulation* 2003, 108(16):1912-1916.

76. Rodríguez-Capote K, Manzanares D, Haines T, Possmayer F: Reactive oxygen species inactivation of surfactant involves structural and functional alterations to surfactant proteins SP-B and SP-C. *Biophysical Journal* 2006, 90(8):2808-2821.

77. Parat M-O, Stachowicz RZ, Fox PL: Oxidative stress inhibits caveolin-1 palmitoylation and trafficking in endothelial cells. *Biochemical Journal* 2002, 361(3):681-688.

78. Clark KL, Oelke A, Johnson ME, Eilert KD, Simpson PC, Todd SC: CD81 associates with 14-3-3 in a redox-regulated palmitoylation-dependent manner. *Journal of Biological Chemistry* 2004, 279(19):19401-19406.

79. Burgoyne JR, Haeussler DJ, Kumar V, Ji Y, Pimental DR, Zee RS, Costello CE, Lin C, McComb ME, Cohen RA *et al*: Oxidation of HRas cysteine thiols by metabolic stress prevents palmitoylation in vivo and contributes to endothelial cell apoptosis. *The FASEB Journal* 2012, 26(2):832-841.

80. Mukai J, Liu H, Burt RA, Swor DE, Lai W-S, Karayiorgou M, Gogos JA: Evidence that the gene encoding ZDHHC8 contributes to the risk of schizophrenia. *Nature Genetics* 2004, 36(7):725-731.

81. Chen W-Y, Shi Y-Y, Zheng Y-L, Zhao X-Z, Zhang G-J, Chen S-Q, Yang P-D, He L: Case–control study and transmission disequilibrium test provide consistent evidence for association between schizophrenia and genetic variation in the 22q11 gene ZDHHC8. *Human Molecular Genetics* 2004, 13(23):2991-2995.

82. Yanai A, Huang K, Kang R, Singaraja RR, Arstikaitis P, Gan L, Orban PC, Mullard A, Cowan CM, Raymond LA *et al*: Palmitoylation of huntingtin by HIP14is essential for its trafficking and function. *Nature Neuroscience* 2006, 9(6):824-831.

83. Saleem AN, Chen Y-H, Baek HJ, Hsiao Y-W, Huang H-W, Kao H-J, Liu K-M, Shen L-F, Song Iw, Tu C-PD *et al*: Mice with alopecia, osteoporosis, and systemic amyloidosis due to mutation in *Zdhhc13*, a gene coding for palmitoyl acyltransferase. *PLoS Genetics* 2010, 6(6):e1000985.

84. Greaves J, Chamberlain LH: New links between S-acylation and cancer. *The Journal of Pathology* 2014, 233(1):4-6.

85. Yeste-Velasco M, Mao X, Grose R, Kudahetti SC, Lin D, Marzec J, Vasiljević N, Chaplin T, Xue L, Xu M *et al*: Identification of ZDHHC14 as a novel human tumour suppressor gene. *The Journal of Pathology* 2014, 232(5):566-577.

86. Yamamoto Y, Chochi Y, Matsuyama H, Eguchi S, Kawauchi S, Furuya T, Oga A, Kang JJ, Naito K, Sasaki K: Gain of 5p15.33 is associated with progression of bladder cancer. *Oncology* 2007, 72(1-2):132-138.

87. Mansilla F, Birkenkamp-Demtroder K, Kruhoffer M, Sorensen FB, Andersen CL, Laiho P, Aaltonen LA, Verspaget HW, Orntoft TF: Differential expression of DHHC9 in microsatellite stable and instable human colorectal cancer subgroups. *British Journal of Cancer* 2007, 96(12):1896-1903.

88. Yan S-M, Tang J-J, Huang C-Y, Xi S-Y, Huang M-Y, Liang J-Z, Jiang Y-X, Li Y-H, Zhou Z-W, Ernberg I *et al*: Reduced expression of ZDHHC2 is associated with lymph node metastasis and poor prognosis in gastric adenocarcinoma. *PLoS ONE* 2013, 8(2):e56366.

89. Hornemann T: Palmitoylation and depalmitoylation defects. *Journal of Inherited Metabolic Disease* 2014:1-8.

90. Korycka J, Łach A, Heger E, Bogusławska DM, Wolny M, Toporkiewicz M, Augoff K, Korzeniewski J, Sikorski AF: Human DHHC proteins: A spotlight on the hidden player of palmitoylation. *European Journal of Cell Biology* 2012, 91(2):107-117.

91. Kuhajda FP: Fatty acid synthase and cancer: New application of an old pathway. *Cancer Research* 2006, 66(12):5977-5980.

92. Postic C, Girard J: Contribution of de novo fatty acid synthesis to hepatic steatosis and insulin resistance: lessons from genetically engineered mice. *The Journal of Clinical Investigation* 2008, 118(3):829-838.

93. Sul HS, Wang D: Nutritional and hormonal regulation of enzymes in fat synthesis: studies of fatty acid synthase and mitochondrial glycerol-3-phosphate acyltransferase gene transcription. *Annual Review of Nutrition* 1998, 18(1):331-351.

94. Fiorentino M, Zadra G, Palescandolo E, Fedele G, Bailey D, Fiore C, Nguyen PL, Migita T, Zamponi R, Di Vizio D *et al*: Overexpression of fatty acid synthase is associated with palmitoylation of Wnt1 and cytoplasmic stabilization of [beta]-catenin in prostate cancer. *Laboratory Investigation* 2008, 88(12):1340-1348.

95. Wei X, Schneider JG, Shenouda SM, Lee A, Towler DA, Chakravarthy MV, Vita JA, Semenkovich CF: De novo lipogenesis maintains vascular homeostasis through endothelial nitric-oxide synthase (eNOS) palmitoylation. *Journal of Biological Chemistry* 2011, 286(4):2933-2945.

96. Wei X, Yang Z, Rey Federico E, Ridaura Vanessa K, Davidson Nicholas O, Gordon Jeffrey I, Semenkovich Clay F: Fatty acid synthase modulates intestinal barrier function through palmitoylation of Mucin 2. *Cell Host & Microbe* 2012, 11(2):140-152.

97. Veit M, Ponimaskin E, Schmidt MG: Analysis of S-acylation of proteins. In: *Post-translational Modifications of Proteins.* Edited by Kannicht C, vol. 446: Humana Press; 2008: 163-182.

98. Berthiaume L, Peseckis SM, Resh MD: [34] Synthesis and use of iodo-fatty acid analogs. In: *Methods in Enzymology.* Edited by Patrick J. Casey JEB, vol. Volume 250: Academic Press; 1995: 454-466.

99. Singaraja RR, Kang MH, Vaid K, Sanders SS, Vilas GL, Arstikaitis P, Coutinho J, Drisdel RC, El-Husseini AED, Green WN *et al*: Palmitoylation of ATP-binding cassette transporter A1 is essential for its trafficking and function. *Circulation Research* 2009, 105(2):138-147.

100. Resh MD: Use of analogs and inhibitors to study the functional significance of protein palmitoylation. *Methods* 2006, 40(2):191-197.

101. Staufenbiel M: Ankyrin-bound fatty acid turns over rapidly at the erythrocyte plasma membrane. *Molecular and Cellular Biology* 1987, 7(8):2981-2984.

102. Degtyarev MY, Spiegel AM, Jones TL: Palmitoylation of a G protein alpha i subunit requires membrane localization not myristoylation. *Journal of Biological Chemistry* 1994, 269(49):30898-30903.

103. Kennedy ME, Limbird LE: Palmitoylation of the alpha 2A-adrenergic receptor. Analysis of the sequence requirements for and the dynamic properties of alpha 2A-adrenergic receptor palmitoylation. *Journal of Biological Chemistry* 1994, 269(50):31915-31922.

104. Baker TL, Zheng H, Walker J, Coloff JL, Buss JE: Distinct rates of palmitate turnover on membrane-bound cellular and oncogenic H-Ras. *Journal of Biological Chemistry* 2003, 278(21):19292-19300.

105. Qanbar R, Bouvier M: Determination of protein-bound palmitate turnover rates using a three-compartment model that formally incorporates [^{3}H]palmitate Recycling. *Biochemistry* 2004, 43(38):12275-12288.

106. O'Dowd BF, Hnatowich M, Caron MG, Lefkowitz RJ, Bouvier M: Palmitoylation of the human beta 2-adrenergic receptor. Mutation of Cys341 in the carboxyl tail leads to an uncoupled nonpalmitoylated form of the receptor. *Journal of Biological Chemistry* 1989, 264(13):7564-7569.

107. Veit M, Kretzschmar E, Kuroda K, Garten W, Schmidt MF, Klenk HD, Rott R: Site-specific mutagenesis identifies three cysteine residues in the cytoplasmic tail

as acylation sites of influenza virus hemagglutinin. *Journal of Virology* 1991, 65(5):2491-2500.

108. Linder ME, Middleton P, Hepler JR, Taussig R, Gilman AG, Mumby SM: Lipid modifications of G proteins: alpha subunits are palmitoylated. *Proceedings of the National Academy of Sciences* 1993, 90(8):3675-3679.

109. Drisdel RC, Green WN: Labeling and quantifying sites of protein palmitoylation. *BioTechniques* 2004, 36(2):276-285.

110. Wan J, Roth AF, Bailey AO, Davis NG: Palmitoylated proteins: purification and identification. *Nature Protocols* 2007, 2(7):1573-1584.

111. Kolb HC, Finn MG, Sharpless KB: Click chemistry: diverse chemical function from a few good reactions. *Angewandte Chemie International Edition* 2001, 40(11):2004-2021.

112. Martin BR, Cravatt BF: Large-scale profiling of protein palmitoylation in mammalian cells. *Nature Methods* 2009, 6(2):135-138.

113. Ong S-E, Mann M: A practical recipe for stable isotope labeling by amino acids in cell culture (SILAC). *Nature Protocols* 2007, 1(6):2650-2660.

114. Martin BR, Wang C, Adibekian A, Tully SE, Cravatt BF: Global profiling of dynamic protein palmitoylation. *Nature Methods* 2012, 9(1):84-89.

115. Gross ER, Nithipatikom K, Hsu AK, Peart JN, Falck JR, Campbell WB, Gross GJ: Cytochrome P450 ω-hydroxylase inhibition reduces infarct size during reperfusion via the sarcolemmal KATP channel. *Journal of Molecular and Cellular Cardiology* 2004, 37(6):1245-1249.

116. Hardwick JP: Cytochrome P450 omega hydroxylase (CYP4) function in fatty acid metabolism and metabolic diseases. *Biochemical Pharmacology* 2008, 75(12):2263-2275.

117. Martin BR: Chemical approaches for profiling dynamic palmitoylation. *Biochemical Society transactions* 2013, 41(1):43-49.

118. Tom CTMB, Martin BR: Fat chance! Getting a grip on a slippery modification. *ACS Chemical Biology* 2012, 8(1):46-57.

119. Yates JR, Ruse CI, Nakorchevsky A: Proteomics by mass spectrometry: approaches, advances, and applications. *Annual Review of Biomedical Engineering* 2009, 11(1):49-79.

120. Karas M, Bachmann D, Hillenkamp F: Influence of the wavelength in high-irradiance ultraviolet laser desorption mass spectrometry of organic molecules. *Analytical Chemistry* 1985, 57(14):2935-2939.

121. Lewis JK, Wei J, Siuzdak G: Matrix-assisted laser desorption/ionization mass spectrometry in peptide and protein analysis. In: *Encyclopedia of Analytical Chemistry*. John Wiley & Sons, Ltd; 2006.

122. Hoffmann E, Stroobant V: Mass spectrometry: principles and applications, 3rd edition: John Wiley & Sons, Ltd; 2007.

123. Pappin DC: Peptide mass fingerprinting using MALDI-TOF mass spectrometry. In: *Protein Sequencing Protocols*. Edited by Smith B, vol. 64: Humana Press; 1997: 165-173.

124. Yamashita M, Fenn JB: Electrospray ion source. Another variation on the free-jet theme. *The Journal of Physical Chemistry* 1984, 88(20):4451-4459.

125. Fenn J, Mann M, Meng C, Wong S, Whitehouse C: Electrospray ionization for mass spectrometry of large biomolecules. *Science* 1989, 246(4926):64-71.

126. Aleksandrov M, Gall L, Krasnov N, Nikolayev V, Pavlenko V, Shkurov V: Extraction of ions from solutions at atmospheric pressure, mass spectrometric analysis of bioorganic substances. *Doklady Akademii Nauk SSSR (in Russian)* 1984, 277(2):379-383.

127. Gaskell SJ: Electrospray: principles and practice. *Journal of Mass Spectrometry* 1997, 32(7):677-688.

128. Banerjee S, Mazumdar S: Electrospray ionization mass spectrometry: a technique to access the information beyond the molecular weight of the analyte. *International Journal of Analytical Chemistry* 2012, 2012:40.

129. Brown RS, Lennon JJ: Mass resolution improvement by incorporation of pulsed ion extraction in a matrix-assisted laser desorption/ionization linear time-of-flight mass spectrometer. *Analytical Chemistry* 1995, 67(13):1998-2003.

130. Gross ML, Chen G, Pramanik B: Protein and peptide mass spectrometry in drug discovery: John Wiley & Sons; 2011.

131. Gross JH: Mass spectrometry: a textbook: Springer; 2004.

132. March RE: An introduction to quadrupole ion trap mass spectrometry. *Journal of Mass Spectrometry* 1997, 32(4):351-369.

133. Schwartz JC, Senko MW, Syka JEP: A two-dimensional quadrupole ion trap mass spectrometer. *Journal of the American Society for Mass Spectrometry* 2002, 13(6):659-669.

134. Scigelova M, Hornshaw M, Giannakopulos A, Makarov A: Fourier transform mass spectrometry. *Molecular & Cellular Proteomics* 2011, 10(7).

135. Makarov A, Scigelova M: Coupling liquid chromatography to Orbitrap mass spectrometry. *Journal of Chromatography A* 2010, 1217(25):3938-3945.

136. Roepstorff P, Fohlman J: Letter to the editors. *Biological Mass Spectrometry* 1984, 11(11):601-601.

137. Roepstorff P, Fohlman J: Proposal for a common nomenclature for sequence ions in mass spectra of peptides. *Biomedical Mass Spectrometry* 1984, 11(11):601.

138. Mitchell Wells J, McLuckey SA: Collision induced dissociation (CID) of peptides and proteins. In: *Methods in Enzymology.* Edited by Burlingame AL, vol. Volume 402: Academic Press; 2005: 148-185.

139. Johnson RS, Martin SA, Biemann K, Stults JT, Watson JT: Novel fragmentation process of peptides by collision-induced decomposition in a tandem mass spectrometer: differentiation of leucine and isoleucine. *Analytical Chemistry* 1987, 59(21):2621-2625.

140. Wysocki VH, Tsaprailis G, Smith LL, Breci LA: Mobile and localized protons: a framework for understanding peptide dissociation. *Journal of Mass Spectrometry* 2000, 35(12):1399-1406.

141. Paizs B, Suhai S: Fragmentation pathways of protonated peptides. *Mass Spectrometry Reviews* 2005, 24(4):508-548.

142. McLuckey SA, Goeringer DE: Special feature:tutorial slow heating methods in tandem mass spectrometry. *Journal of Mass Spectrometry* 1997, 32(5):461-474.

143. Zubarev RA, Kelleher NL, McLafferty FW: Electron capture dissociation of multiply charged protein cations. A nonergodic process. *Journal of the American Chemical Society* 1998, 120(13):3265-3266.

144. Zubarev RA: Reactions of polypeptide ions with electrons in the gas phase. *Mass Spectrometry Reviews* 2003, 22(1):57-77.

145. Zubarev RA, Kruger NA, Fridriksson EK, Lewis MA, Horn DM, Carpenter BK, McLafferty FW: Electron capture dissociation of gaseous multiply-charged proteins is favored at disulfide bonds and other sites of high hydrogen atom affinity. *Journal of the American Chemical Society* 1999, 121(12):2857-2862.

146. O'Connor PB, Cournoyer JJ, Pitteri SJ, Chrisman PA, McLuckey SA: Differentiation of aspartic and isoaspartic acids using electron transfer dissociation. *Journal of the American Society for Mass Spectrometry* 2006, 17(1):15-19.

147. Anusiewicz I, Skurski P, Simons J: Refinements to the Utah–Washington Mechanism of Electron Capture Dissociation. *The Journal of Physical Chemistry B* 2014, 118(28):7892-7901.

148. Simons J: Mechanisms for S–S and N–Cα bond cleavage in peptide ECD and ETD mass spectrometry. *Chemical Physics Letters* 2010, 484(4–6):81-95.

149. Syka JEP, Coon JJ, Schroeder MJ, Shabanowitz J, Hunt DF: Peptide and protein sequence analysis by electron transfer dissociation mass spectrometry. *Proceedings of the National Academy of Sciences of the United States of America* 2004, 101(26):9528-9533.

150. Kanshin E, Michnick S, Thibault P: Sample preparation and analytical strategies for large-scale phosphoproteomics experiments. *Seminars in Cell & Developmental Biology* 2012, 23(8):843-853.

151. Shevchenko A, Tomas H, Havlis J, Olsen JV, Mann M: In-gel digestion for mass spectrometric characterization of proteins and proteomes. *Nature Protocols* 2007, 1(6):2856-2860.

152. Washburn MP, Wolters D, Yates JR: Large-scale analysis of the yeast proteome by multidimensional protein identification technology. *Nature Biotechnology* 2001, 19(3):242-247.

153. Swartz ME: Ultra performance liquid chromatography (UPLC): an introduction. *Separation Science Re-Defined, LCGC Supplement* 2005, 8.

154. Mann M, Ong S-E, Grønborg M, Steen H, Jensen ON, Pandey A: Analysis of protein phosphorylation using mass spectrometry: deciphering the phosphoproteome. *Trends in Biotechnology* 2002, 20(6):261-268.

155. Zhang K, Williams KE, Huang L, Yau P, Siino JS, Bradbury EM, Jones PR, Minch MJ, Burlingame AL: Histone acetylation and deacetylation: identification

of acetylation and methylation sites of HeLa histone H4 by mass spectrometry. *Molecular & Cellular Proteomics* 2002, 1(7):500-508.

156. Cournoyer JJ, Lin C, O'Connor PB: Detecting deamidation products in proteins by electron capture dissociation. *Analytical Chemistry* 2005, 78(4):1264-1271.

157. Udeshi ND, Mertins P, Svinkina T, Carr SA: Large-scale identification of ubiquitination sites by mass spectrometry. *Nature Protocols* 2013, 8(10):1950-1960.

158. Silva AMN, Vitorino R, Domingues MRM, Spickett CM, Domingues P: Post-translational modifications and mass spectrometry detection. *Free Radical Biology and Medicine* 2013, 65(0):925-941.

159. Witze ES, Old WM, Resing KA, Ahn NG: Mapping protein post-translational modifications with mass spectrometry. *Nature Methods* 2007, 4(10):798-806.

160. Hensel J, Hintz M, Karas M, Linder D, Stahl B, Geyer R: Localization of the palmitoylation site in the transmembrane protein p12E of Friend murine leukaemia virus. *European Journal of Biochemistry* 1995, 232(2):373-380.

161. Liang X, Lu Y, Neubert TA, Resh MD: Mass spectrometric analysis of GAP-43/neuromodulin reveals the presence of a variety of fatty acylated species. *Journal of Biological Chemistry* 2002, 277(36):33032-33040.

162. Bizzozero OA, Malkoski SP, Mobarak C, Bixler HA, Evans JE: Mass-spectrometric analysis of myelin proteolipids reveals new features of this family of palmitoylated membrane proteins. *Journal of Neurochemistry* 2002, 81(3):636-645.

163. Roos M, Soskic V, Poznanovic S, Godovac-Zimmermann J: Post-translational modifications of endothelin receptor B from bovine lungs analyzed by mass spectrometry. *Journal of Biological Chemistry* 1998, 273(2):924-931.

164. Kordyukova LV, Serebryakova MV, Baratova LA, Veit M: S-acylation of the hemagglutinin of influenza viruses: mass spectrometry reveals site-specific attachment of stearic acid to a transmembrane cysteine. *Journal of Virology* 2008, 82(18):9288-9292.

165. Xue L, Gollapalli DR, Maiti P, Jahng WJ, Rando RR: A palmitoylation switch mechanism in the regulation of the visual cycle. *Cell* 2004, 117(6):761-771.

166. McClure M, DeLucas LJ, Wilson L, Ray M, Rowe SM, Wu X, Dai Q, Hong JS, Sorscher EJ, Kappes JC *et al*: Purification of CFTR for mass spectrometry

analysis: identification of palmitoylation and other post-translational modifications. *Protein Engineering Design and Selection* 2012, 25(1):7-14.

167. Yousefi-Salakdeh E, Johansson J, Strömberg R: A method for S- and O-palmitoylation of peptides: synthesis of pulmonary surfactant protein-C models. *Biochemical Journal* 1999, 343(3):557-562.

168. Ying W, Perlman DH, Li L, Théberge R, Costello CE, McComb ME: Highly efficient and selective enrichment of peptide subsets combining fluorous chemistry with reversed-phase chromatography. *Rapid Communications in Mass Spectrometry* 2009, 23(24):4019-4030.

169. Koegl M, Zlatkine P, Ley SC, Courtneidge SA, Magee AI: Palmitoylation of multiple Src-family kinases at a homologous N-terminal motif. *Biochemical Journal* 1994, 303(3):749-753.

170. Soghomonian J-J, Martin DL: Two isoforms of glutamate decarboxylase: why? *Trends in Pharmacological Sciences* 1998, 19(12):500-505.

171. Rüegg UT, Rudinger J: [10] Reductive cleavage of cystine disulfides with tributylphosphine. *Methods in Enzymology* 1977, Volume 47:111-116.

172. Burns JA, Butler JC, Moran J, Whitesides GM: Selective reduction of disulfides by tris(2-carboxyethyl)phosphine. *The Journal of Organic Chemistry* 1991, 56(8):2648-2650.

173. Grandier-Vazeille X, Tetaert D: Methodology for purification of large hydrophobic peptides by high-performance liquid chromatography. *Journal of Chromatography A* 1984, 296(0):301-308.

174. Kwok Y, Sung W-C, Lin AL-H, Liu H-H, Chou FA-H, Hsieh SS-Y, Leng C-H, Chong P: Rapid isolation and characterization of bacterial lipopeptides using liquid chromatography and mass spectrometry analysis. *Proteomics* 2011, 11(13):2620-2627.

175. Gustafsson M, Curstedt T, Jörnvall H, Johansson J: Reverse-phase HPLC of the hydrophobic pulmonary surfactant proteins: detection of a surfactant protein C isoform containing Nepsilon-palmitoyl-lysine. *Biochemical Journal* 1997, 326(3):799-806.

176. Hoffman MD, Kast J: Mass spectrometric characterization of lipid-modified peptides for the analysis of acylated proteins. *Journal of Mass Spectrometry* 2006, 41(2):229-241.

177. Guan Z: Identification and localization of the fatty acid modification in ghrelin by electron capture dissociation. *Journal of the American Society for Mass Spectrometry* 2002, 13(12):1443-1447.

178. Kaczorowska M, Cooper H: Electron capture dissociation and collision induced dissociation of S-dipalmitoylated peptides. *Journal of the American Society for Mass Spectrometry* 2013, 24(8):1224-1227.

179. Leymarie N, Costello CE, O'Connor PB: Electron capture dissociation initiates a free radical reaction cascade. *Journal of the American Chemical Society* 2003, 125(29):8949-8958.

180. Li X, Lin C, Han L, Costello C, O'Connor P: Charge remote fragmentation in electron capture and electron transfer dissociation. *Journal of the American Society for Mass Spectrometry* 2010, 21(4):646-656.

181. Moore BN, Ly T, Julian RR: Radical conversion and migration in electron capture dissociation. *Journal of the American Chemical Society* 2011, 133(18):6997-7006.

182. Fung YME, Chan TWD: Experimental and theoretical investigations of the loss of amino acid side chains in electron capture dissociation of model peptides. *Journal of the American Society for Mass Spectrometry* 2005, 16(9):1523-1535.

183. Olsen KEP, Andersen KB: Palmitoylation of the intracytoplasmic R peptide of the transmembrane envelope protein in moloney Murine leukemia virus. *Journal of Virology* 1999, 73(11):8975-8981.

184. Hackett M, Guo L, Shabanowitz J, Hunt D, Hewlett E: Internal lysine palmitoylation in adenylate cyclase toxin from Bordetella pertussis. *Science* 1994, 266(5184):433-435.

185. Fong KP, Tang HY, Brown AC, Kieba IR, Speicher DW, Boesze-Battaglia K, Lally ET: Aggregatibacter actinomycetemcomitans leukotoxin is post-translationally modified by addition of either saturated or hydroxylated fatty acyl chains. *Molecular Oral Microbiology* 2011, 26(4):262-276.

186. Pepinsky RB, Zeng C, Wen D, Rayhorn P, Baker DP, Williams KP, Bixler SA, Ambrose CM, Garber EA, Miatkowski K *et al*: Identification of a palmitic acid-modified form of human Sonic hedgehog. *Journal of Biological Chemistry* 1998, 273(22):14037-14045.

187. Chen M-H, Li Y-J, Kawakami T, Xu S-M, Chuang P-T: Palmitoylation is required for the production of a soluble multimeric Hedgehog protein complex

and long-range signaling in vertebrates. *Genes & Development* 2004, 18(6):641-659.

188. Taylor FR, Wen D, Garber EA, Carmillo AN, Baker DP, Arduini RM, Williams KP, Weinreb PH, Rayhorn P, Hronowski X *et al*: Enhanced potency of human Sonic Hedgehog by hydrophobic modification. *Biochemistry* 2001, 40(14):4359-4371.

189. Miura GI, Buglino J, Alvarado D, Lemmon MA, Resh MD, Treisman JE: Palmitoylation of the EGFR ligand Spitz by Rasp increases Spitz activity by restricting its diffusion. *Developmental Cell* 2006, 10(2):167-176.

190. Kleuss C, Krause E: Gαs is palmitoylated at the N-terminal glycine. *The EMBO journal* 2003, 22(4):826-832.

191. Ingham PW, McMahon AP: Hedgehog signaling in animal development: paradigms and principles. *Genes & Development* 2001, 15(23):3059-3087.

192. Buglino JA, Resh MD: Hhat is a palmitoylacyltransferase with specificity for N-palmitoylation of Sonic Hedgehog. *Journal of Biological Chemistry* 2008, 283(32):22076-22088.

193. Wieland T, Hornig H: S- acylspaltung bei S- acetyl- ω- aminomercaptanen verschiedener Kettenlänge. *Justus Liebigs Annalen der Chemie* 1956, 600(1):12-22.

194. Martin RB, Hedrick RI: Intramolecular S-O and S-N acetyl transfer reactions. *Journal of the American Chemical Society* 1962, 84(1):106-110.

195. Barnett RE, Jencks WP: Diffusion-controlled proton transfer in intramolecular thiol ester aminolysis and thiazoline hydrolysis. *Journal of the American Chemical Society* 1969, 91(9):2358-2369.

196. Cuccovia IM, Schroeter EH, De Baptista RC, Chaimovich H: Effect of detergents on the S- to N-acyl transfer of S-acyl-.beta.-mercaptoethylamines. *The Journal of Organic Chemistry* 1977, 42(21):3400-3403.

197. Dawson P, Muir T, Clark-Lewis I, Kent S: Synthesis of proteins by native chemical ligation. *Science* 1994, 266(5186):776-779.

198. Monbaliu J-CM, Katritzky AR: Recent trends in Cys-and Ser/Thr-based synthetic strategies for the elaboration of peptide constructs. *Chemical Communications* 2012, 48(95):11601-11622.

199. Mouls L, Subra G, Enjalbal C, Martinez J, Aubagnac JL: O–N-acyl migration in N-terminal serine-containing peptides: mass spectrometric elucidation and subsequent development of site-directed acylation protocols. *Tetrahedron Letters* 2004, 45(6):1173-1178.

200. Ji Y, Leymarie N, Haeussler DJ, Bachschmid MM, Costello CE, Lin C: Direct detection of S-palmitoylation by mass spectrometry. *Analytical Chemistry* 2013, 85(24):11952-11959.

201. Levental I, Lingwood D, Grzybek M, Coskun Ü, Simons K: Palmitoylation regulates raft affinity for the majority of integral raft proteins. *Proceedings of the National Academy of Sciences* 2010, 107(51):22050-22054.

202. Resh MD: Targeting protein lipidation in disease. *Trends in Molecular Medicine* 2012, 18(4):206-214.

203. Edelson-Averbukh M, Shevchenko A, Pipkorn R, Lehmann WD: Gas-phase intramolecular phosphate shift in phosphotyrosine-containing peptide monoanions. *Analytical Chemistry* 2009, 81(11):4369-4381.

204. Mischerikow N, Altelaar AFM, Navarro JD, Mohammed S, Heck A: Comparative assessment of site assignments in CID and ETD spectra of phosphopeptides discloses limited relocation of phosphate groups. *Molecular & Cellular Proteomics* 2010.

205. Xia Q, Lee M, Rose C, Marsh A, Hubler S, Wenger C, Coon J: Characterization and diagnostic value of amino acid side chain neutral losses following electron-transfer dissociation. *Journal of the American Society for Mass Spectrometry* 2011, 22(2):255-264.

206. Gygi SP, Corthals GL, Zhang Y, Rochon Y, Aebersold R: Evaluation of two-dimensional gel electrophoresis-based proteome analysis technology. *Proceedings of the National Academy of Sciences* 2000, 97(17):9390-9395.

207. Aebersold R, Goodlett DR: Mass spectrometry in proteomics. *Chemical Reviews* 2001, 101(2):269-296.

208. Aebersold R, Mann M: Mass spectrometry-based proteomics. *Nature* 2003, 422(6928):198-207.

209. Bantscheff M, Lemeer S, Savitski MM, Kuster B: Quantitative mass spectrometry in proteomics: critical review update from 2007 to the present. *Analytical and bioanalytical chemistry* 2012, 404(4):939-965.

210. Zhang Y, Fonslow BR, Shan B, Baek M-C, Yates III JR: Protein analysis by shotgun/bottom-up proteomics. *Chemical Reviews* 2013, 113(4):2343-2394.

211. Yu Y-Q, Gilar M, Lee PJ, Bouvier ESP, Gebler JC: Enzyme-friendly, mass spectrometry-compatible surfactant for in-solution enzymatic digestion of proteins. *Analytical Chemistry* 2003, 75(21):6023-6028.

212. Chen EI, Cociorva D, Norris JL, Yates JR: Optimization of mass spectrometry-compatible surfactants for shotgun proteomics. *Journal of Proteome Research* 2007, 6(7):2529-2538.

213. Saveliev SV, Woodroofe CC, Sabat G, Adams CM, Klaubert D, Wood K, Urh M: Mass spectrometry compatible surfactant for optimized in-gel protein digestion. *Analytical Chemistry* 2012, 85(2):907-914.

214. Karty JA, Ireland MM, Brun YV, Reilly JP: Artifacts and unassigned masses encountered in peptide mass mapping. *Journal of Chromatography B* 2002, 782(1):363-383.

215. Lubec G, Afjehi-Sadat L: Limitations and pitfalls in protein identification by mass spectrometry. *Chemical Reviews* 2007, 107(8):3568-3584.

216. Beck F, Lewandrowski U, Wiltfang M, Feldmann I, Geiger J, Sickmann A, Zahedi RP: The good, the bad, the ugly: validating the mass spectrometric analysis of modified peptides. *PROTEOMICS* 2011, 11(6):1099-1109.

217. Li X, Cournoyer JJ, Lin C, O'Connor PB: Use of ^{18}O labels to monitor deamidation during protein and peptide sample processing. *Journal of the American Society for Mass Spectrometry* 2008, 19(6):855-864.

218. Palmisano G, Melo-Braga MN, Engholm-Keller K, Parker BL, Larsen MR: Chemical deamidation: a common pitfall in large-scale N-linked glycoproteomic mass spectrometry-based analyses. *Journal of Proteome Research* 2012, 11(3):1949-1957.

219. Hunyadi-Gulyás É, Medzihradszky KF: Factors that contribute to the complexity of protein digests. *Drug Discovery Today: TARGETS* 2004, 3(2, Supplement):3-10.

220. Perdivara I, Deterding LJ, Przybylski M, Tomer KB: Mass spectrometric identification of oxidative modifications of tryptophan residues in proteins: chemical artifact or post-translational modification? *Journal of the American Society for Mass Spectrometry* 2010, 21(7):1114-1117.

221. Auclair JR, Salisbury JP, Johnson JL, Petsko GA, Ringe D, Bosco DA, Agar NYR, Santagata S, Durham HD, Agar JN: Artifacts to avoid while taking advantage of top-down mass spectrometry based detection of protein S-thiolation. *PROTEOMICS* 2014, 14(10):1152-1157.

222. Chiari M, Righetti PG, Negri A, Ceciliani F, Ronchi S: Preincubation with cysteine prevents modification of sulfhydryl groups in proteins by unreacted acrylamide in a gel. *Electrophoresis* 1992, 13(1):882-884.

223. Sechi S, Chait BT: Modification of cysteine residues by alkylation. A tool in peptide mapping and protein identification. *Analytical Chemistry* 1998, 70(24):5150-5158.

224. Hamdan M, Galvani M, Righetti PG: Monitoring 2-D gel-induced modifications of proteins by MALDI-TOF mass spectrometry. *Mass Spectrometry Reviews* 2001, 20(3):121-141.

225. Lippincott J, Apostol I: Carbamylation of cysteine: a potential artifact in peptide mapping of hemoglobins in the presence of urea. *Analytical Biochemistry* 1999, 267(1):57-64.

226. McCarthy J, Hopwood F, Oxley D, Laver M, Castagna A, Righetti PG, Williams K, Herbert B: Carbamylation of proteins in 2-D electrophoresis-Myth or Reality? *Journal of Proteome Research* 2003, 2(3):239-242.

227. Gharib M, Marcantonio M, Lehmann SG, Courcelles M, Meloche S, Verreault A, Thibault P: Artifactual sulfation of silver-stained proteins implications for the assignment of phosphorylation and sulfation sites. *Molecular & Cellular Proteomics* 2009, 8(3):506-518.

228. Nielsen ML, Vermeulen M, Bonaldi T, Cox J, Moroder L, Mann M: Iodoacetamide-induced artifact mimics ubiquitination in mass spectrometry. *Nature Methods* 2008, 5(6):459-460.

229. The QIAexpressionist™ [http://web.mnstate.edu/provost/QiaExpressionist.pdf]

230. ProteaseMAX™ Surfactant, Trypsin Enhancer Technical Bulletin [https://www.promega.com/resources/protocols/technical-bulletins/101/proteasemax-surfactant-trypsin-enhancer-protocol/]

231. Ruse CI, Willard B, Jin JP, Haas T, Kinter M, Bond M: Quantitative dynamics of site-specific protein phosphorylation determined using liquid chromatography electrospray ionization mass spectrometry. *Analytical Chemistry* 2002, 74(7):1658-1664.

232. Nomoto S, Adachi K, Yang L-X, Hirata Y, Muraguchi S, Kiuchi K: Distribution of RGS4 mRNA in mouse brain shown by in situ hybridization. *Biochemical and Biophysical Research Communications* 1997, 241(2):281-287.

233. Ross EM, Wilkie TM: GTPase-activating proteins for heterotrimeric G proteins: regulators of G protein signaling (RGS) and RGS-like proteins. *Annual Review of Biochemistry* 2000, 69(1):795-827.

234. Yan Y, Chi PP, Bourne HR: RGS4 inhibits Gq-mediated activation of mitogen-activated protein kinase and phosphoinositide synthesis. *Journal of Biological Chemistry* 1997, 272(18):11924-11927.

235. Saugstad JA, Marino MJ, Folk JA, Hepler JR, Conn PJ: RGS4 inhibits signaling by group I metabotropic glutamate receptors. *The Journal of Neuroscience* 1998, 18(3):905-913.

236. Beyer CE, Ghavami A, Lin Q, Sung A, Rhodes KJ, Dawson LA, Schechter LE, Young KH: Regulators of G-protein signaling 4: modulation of 5-HT1A-mediated neurotransmitter release in vivo. *Brain Research* 2004, 1022(1–2):214-220.

237. Grillet N, Pattyn A, Contet C, Kieffer BL, Goridis C, Brunet J-F: Generation and characterization of Rgs4 mutant mice. *Molecular and Cellular Biology* 2005, 25(10):4221-4228.

238. Mirnics K, Middleton FA, Stanwood GD, Lewis DA, Levitt P: Disease-specific changes in regulator of G-protein signaling 4 (RGS4) expression in schizophrenia. *Molecular Psychiatry* 2001, 6(3):293-301.

239. Stewart A, Huang J, Fisher RA: RGS proteins in heart: brakes on the vagus. In: *Frontiers in Physiology.* vol. 3; 2012: 95.

240. Rose JJ, Taylor JB, Shi J, Cockett MI, Jones PG, Hepler JR: RGS7 is palmitoylated and exists as biochemically distinct forms. *Journal of Neurochemistry* 2000, 75(5):2103-2112.

241. Bernstein L, Linder M, Hepler J: Analysis of RGS protein palmitoylation. In: *G Protein Signaling.* Edited by Smrcka A, vol. 237: Humana Press; 2004: 195-204.

242. Srinivasa SP, Bernstein LS, Blumer KJ, Linder ME: Plasma membrane localization is required for RGS4 function in Saccharomyces cerevisiae. *Proceedings of the National Academy of Sciences* 1998, 95(10):5584-5589.

243. Druey KM, Ugur O, Caron JM, Chen C-K, Backlund PS, Jones TLZ: Amino-terminal cysteine residues of RGS16 are required for palmitoylation and modulation of Gi- and Gq-mediated signaling. *Journal of Biological Chemistry* 1999, 274(26):18836-18842.

244. Wang J, Xie Y, Wolff DW, Abel PW, Tu Y: DHHC protein-dependent palmitoylation protects regulator of G-protein signaling 4 from proteasome degradation. *FEBS Letters* 2010, 584(22):4570-4574.

CURRICULUM VITAE

JI, YUHUAN
Email: jiyuhuan@bu.edu
Mass Spectrometry Resources, Boston University School of Medicine
670 Albany St, Rm504, Boston, MA
Year of Birth: 1981

Education

Ph.D., Biochemistry May 2015
Boston University School of Medicine, Boston, MA
Thesis title: Mass Spectrometry Analysis of Protein/Peptide *S*-Palmitoylation

M. Sc., Neurobiology September 2007
Harbin Medical University, Harbin, China
Thesis title: Astrocytic Differentiation of C6 Glioma Cells Induced by Bone Mesenchymal Stem Cells

Publications

Ji, Y., Leymarie, N., Haeussler, D.J., Bachschmid, M.M., Costello, C.E. & Lin, C.: Direct Detection of S-Palmitoylation by Mass Spectrometry. *Analytical Chemistry*. 85, 11952-11959 (2013)

Burgoyne, J.R., Haeussler, D.J., Kumar, V., Ji, Y., Pimental, D.R., Zee, R.S., Costello, C.E., Lin, C., McComb, M.E., Cohen, R.A. & Bachschmid, M.M.: Oxidation of HRas Cysteine Thiols by Metabolic Stress Prevents Palmitoylation in vivo and Contributes to Endothelial Cell Apoptosis. *The FASEB Journal*. 26, 832-841 (2012)

Wang, Q., Sun, B., Wang, D., Ji, Y., Kong, Q., Wang, G., Wang, J., Zhao, W., Jin, L. & Li, H.: Murine Bone Marrow Mesenchymal Stem Cells Cause Mature Dendritic Cells to Promote T-Cell Tolerance. *Scandinavian Journal of Immunology*. 68, 607-615 (2008)

Ji, Y., Li, H., Wang, D., Sun, B., Mu, L. & Wang, J.: Effects of Simulated Microgravity on the Morphology and Growth of Neurons. *Space Medicine & Medical Engineering* (in Chinese) 20, 327-331 (2007)

Wang, J., Sun, B., Wang, G., Ji, Y., Mu, L., Jin, L. & Li, H.: The Initial Establishment of Neurons Model in vitro Cultivation under the Condition of Simulated Microgravity. *Journal of Aerospace Medicine* (in Chinese) 17, 213-215 (2006)

Dong, X., Wang, J., Song, C., Ji, Y., Mu, L., Jin, L. & Li, H.: Effect of Weightlessness on Mouse NK Cell Bioactivity in vitro. *Journal of Microbiology* (in Chinese) 26, 40-43 (2006)

Ji, Y., Meng, X., Shi, W. & WANG, J.: Role of Focal Adhesion Kinase (FAK) for Metastasis of Lung Cancer. *Journal of Harbin Medical University* (in Chinese) 38, 13-16 (2004)

Selected Presentations

- *Oral Presentations:*
  Characterization of lipid modifications on regulator of G protein signaling 4 (RGS4) from Sf9 cells by mass spectrometry
  62nd ASMS conference, 2014, Baltimore, MD

  Mass spectrometry analysis of protein/peptide palmitoylation
  Biochemistry Seminar, 2012, Boston University School of Medicine, Boston, MA

- *Poster Presentations*
  Identification of H-Ras Post-translational Modifications under Oxidative Stress
  58th ASMS conference, 2010, Salt Lake City, UT

  Mass spectrometry study of protein/peptide palmitoylation
  59th ASMS conference, 2011, Denver, CO

  Direct detection of S-palmitoylation by mass spectrometry
  11th HUPO conference, 2012, Boston, MA

  Relative quantification of palmitoyl peptides using hydrophobic alkyl tag
  60th ASMS conference, 2012, Vancouver, BC, Canada

  S- to *N*-palmitoyl migration during proteomic sample preparation
  61st ASMS conference, 2013, Minneapolis, MN